universität wien

DISSERTATION | DOCTORAL THESIS

Titel | Title

The spatiotemporal dynamics of microbial activity at a local root exudation hotspot

verfasst von | submitted by

Julia Hildegard Wiesenbauer BSc MSc

angestrebter akademischer Grad | in partial fulfilment of the requirements for the degree of

Doctor of Philosophy (PhD)

Wien | Vienna, 2024

Studienkennzahl lt. Studienblatt | Degree programme code as it appears on the student record sheet:	UA 794 685 437
Dissertationsgebiet lt. Studienblatt | Field of study as it appears on the student record sheet:	Biologie
Betreut von | Supervisor:	Assoz. Prof. Mag. Dr. Christina Kaiser

Table of Contents

Table of Contents **3**

Acknowledgements **5**

Abstract **7**

Zusammenfassung **9**

Overview of manuscripts **12**

CHAPTER 1

Introduction, thesis outline and main goals 14

CHAPTER 2

A pulse of simulated root exudation alters the composition and temporal dynamics of microbial metabolites in its immediate vicinity 38

CHAPTER 3

Preferential use of organic acids over sugars by soil microbes in simulated root exudation 52

CHAPTER 4

An integrative imaging approach for studying microbial assimilation of ^{13}C-labelled root exudates in soil at the microscale 104

CHAPTER 5

Summary and general learnings 146

Acknowledgements

First and foremost, I would like to express my gratitude to my supervisor, Christina Kaiser. Without your guidance and support, this thesis would not have been possible. Thank you, Tina, for the opportunity to pursue my PhD under your supervision. Your mentorship has not only guided me through numerous challenges but has also allowed me to grow both personally and professionally.

To all my colleagues at TER, this work could not have been accomplished without your support. Whether it was contributing manpower during my experiments, engaging in enriching discussions, or most importantly, through your friendships, which kept me grounded during the challenging phases of my PhD. I am immensely thankful for it all.

A very special thank you goes to my Space Team colleagues, Stefan and Alex. I couldn't have asked for better colleagues and friends by my side during those tough times. I fondly recall our shared coffee breaks and am grateful to know I can always count on you.

Over the years at TER, I have also made many close friends. A heartfelt thank you to Vicky, Erika, Bruna, and Joana for the joyful moments and wonderful times we shared together.

Zum Schluss möchte ich noch meiner Familie und meinen Freunden für ihre Unterstützung und Ermutigung danken.

Abstract

Root exudates comprise a diverse array of chemical compounds that play critical roles in shaping the rhizosphere's chemical landscape and microbial communities. Mediated by the microbial community, root exudates impact nutrient availability, soil organic matter decomposition, and soil structural integrity by altering biochemical processes within the soil. Despite the recognized importance of root exudates in ecological interactions within the rhizosphere, the detailed mechanisms through which microbes metabolize these exudates and subsequently affect soil organic matter dynamics remain poorly understood. This thesis addresses this gap by exploring the intricate dynamics of microbial activity and nutrient cycling in response to simulated root exudation and assessing how variation in root exudate composition influence microbial processes across different soil types. It employs advanced isotopic and microscale analytical techniques cross three comprehensive studies to investigate these fine-scale spatiotemporal dynamics.

The first paper investigates the immediate effects of a pulse of ^{13}C-labelled low-molecular-weight organic carbon compounds on soil microbial metabolism. The simulation of root exudation through reverse microdialysis in undisturbed soil caused significant changes in microbial respiration and soil metabolite dynamics. The concentration of short-chain fatty acids increased, indicative of anaerobic metabolism, likely occurring at anoxic microsites that had formed due to oxygen depletion by increased microbial respiration at the exudation site. Concurrently, a threefold increase in ammonium and elevated nitrate levels were observed, indicating enhanced mineralization of organic nitrogen near plant roots.

The second paper challenges traditional views by demonstrating the preferential microbial uptake and respiration of organic acids over sugars in both meadow and forest soils. This study elucidates the nuanced impacts of exudate composition on microbial processes and nutrient mobilization, suggesting a complex interplay between substrate availability and microbial metabolic pathways.

The third manuscript skilfully combined isotope imaging using nanoscale secondary ion mass spectrometry with fluorescence microscopy and scanning electron microscopy to visualize the microscale spatial distribution of microbial communities and their assimilation of the added ^{13}C-labelled substrates. Results indicate that microbial access to substrates was significantly influenced by soil microarchitecture and microbial traits, providing a spatial complement to previous temporal analyses.

Collectively, these studies provide profound insights into the spatial and temporal dynamics of microbial activity triggered by root exudates, highlighting the role of microscale interactions in shaping rhizosphere processes and their implications for plant nutrient availability. This thesis underscores the

importance of considering both the microbial community and physicochemical soil properties to fully understand the ecological functions of the rhizosphere.

Zusammenfassung

Wurzelexsudate bestehen aus einer Vielfalt chemischer Verbindungen, die eine entscheidende Rolle bei der Gestaltung der chemischen Landschaft der Rhizosphäre und der mikrobiellen Gemeinschaften spielen. Dabei ist mikrobielle Gemeinschaft Vermittler durch den die Wurzelexsudate die Verfügbarkeit von Nährstoffen, den Abbau organischer Bodensubstanz und die Bodenstruktur beeinflussen, indem sie biochemische Prozesse verändern. Trotz der Bedeutung von Wurzelexsudaten in ökologischen Interaktionen in der Rhizosphäre sind die Mechanismen, durch die Mikroben diese Exsudate metabolisieren und dadurch die Dynamik der organischen Bodensubstanz beeinflussen, noch nicht im Detail erforscht. Diese Dissertation untersucht die komplexen Dynamiken der mikrobiellen Aktivität und der Nährstoffkreisläufe in der Rhizosphäre als Reaktion auf künstliche Wurzelexsudation, und erforscht, wie Variationen in der Zusammensetzung der Wurzelexsudate mikrobielle Prozesse in verschiedenen Bodenarten beeinflussen. Unter Einsatz fortschrittlicher Isotopenanalyse und Analysetechniken im Mikroskalabereich werden die feinskaligen räumlichen und zeitlichen Dynamiken in drei umfassenden Studien untersucht.

Die erste Publikation untersucht die unmittelbaren Auswirkungen eines Pulses von ^{13}C-markierten organischen Kohlenstoffverbindungen auf den mikrobiellen Stoffwechsel im Boden. Die Simulation der Wurzelexsudation durch ‚reverse' Mikrodialyse in ungestörtem Boden führte zu signifikanten Veränderungen in der mikrobiellen Atmung und der Dynamik der Bodenmetaboliten. Die Konzentration an kurzkettigen Fettsäuren stieg an, was auf einen anaeroben Stoffwechsel hindeutet, der wahrscheinlich an anoxischen mikroskopischen Stellen im Boden stattfand, die sich aufgrund des Sauerstoffmangels durch die gesteigerte mikrobielle Atmung am Exsudationsort gebildet hatten. Gleichzeitig wurde ein dreifacher Anstieg des Ammoniumgehalts sowie erhöhte Nitratwerte beobachtet, was auf eine stärkere Mineralisierung von organischem Stickstoff in der Nähe der Pflanzenwurzeln hindeutet.

Das zweite Manuskript demonstriert die bevorzugte mikrobielle Aufnahme und Veratmung von organischen Säuren gegenüber Zuckern in Wiesen- und Waldböden und stellt damit konventionelle Fachmeinungen in Frage. Diese Studie verdeutlicht die nuancierten Auswirkungen der Exsudatzusammensetzung auf mikrobielle Prozesse und die Mobilisierung von Nährstoffen, was auf ein komplexes Zusammenspiel zwischen Substratverfügbarkeit und mikrobiellen Stoffwechselwegen hinweist.

Das dritte Manuskript kombinierte geschickt Isotopenbildgebung mit der nanoskaligen Sekundärionen-Massenspektrometrie mit Fluoreszenzmikroskopie und Rasterelektronenmikroskopie, um die räumliche Verteilung der mikrobiellen Gemeinschaften und ihre Assimilation der zugesetzten ^{13}C-

markierten Substrate im mikroskaligen Bereich zu visualisieren. Die Ergebnisse zeigen, dass der mikrobielle Zugang zu Substraten signifikant durch die Mikroarchitektur des Bodens und mikrobielle Merkmale beeinflusst wurde und liefern eine räumliche Ergänzung zu vorherigen zeitlichen Analysen.

Zusammenfassend bieten diese Studien tiefgreifende Einblicke in die räumlichen und zeitlichen Dynamiken der durch Wurzelexsudate ausgelösten mikrobiellen Aktivität, unterstreichen die Rolle von mikroskaligen Interaktionen bei der Gestaltung der Rhizosphärenprozesse und deren Implikationen für die Nährstoffverfügbarkeit der Pflanzen. Diese Arbeit betont die Wichtigkeit der Berücksichtigung sowohl der mikrobiellen Gemeinschaft als auch der physikochemischen Bodeneigenschaften, um die ökologischen Funktionen der Rhizosphäre vollständig zu verstehen.

Overview of manuscripts

Chapter II

Manuscript title: A pulse of simulated root exudation alters the composition and temporal dynamics of microbial metabolites in its immediate vicinity

Author names: Julia Wiesenbauer, Alexander König, Stefan Gorka, Lilian Marchand, Naoise Nunan, Barbara Kitzler, Erich Inselsbacher, Christina Kaiser

Reference: Wiesenbauer, J., König, A., Gorka, S., Marchand, L., Nunan, N., Kitzler, B., Inselsbacher, E., Kaiser, C., 2024. A pulse of simulated root exudation alters the composition and temporal dynamics of microbial metabolites in its immediate vicinity. Soil Biology and Biochemistry 189, 109259. doi:10.1016/j.soilbio.2023.109259

Author contributions: CK conceived the study, with input by JW, SG, EI and NN. JW, SG and CK designed the experiment. JW, AK, SG, and LM did the experimental work, under supervision by CK. JW analysed the data and wrote the first draft of the manuscript with input by CK. All authors reviewed and edited the manuscript. JW revised the final version of the manuscript after assessment by two independent reviewers.

Chapter III

Manuscript title: Soil microbes prefer organic acids over sugars in simulated root exudation

Author names: Julia Wiesenbauer, Stefan Gorka, Kian Jenab, Raphael Schuster, Naresh Kumar, Cornelia Rottensteiner, Alexander König, Stephan Kraemer, Erich Inselsbacher, Christina Kaiser

Reference: *Soil Biology and Biochemistry,* revisions submitted;

Preprint*:* https://doi.org/10.1101/2024.12.03.626624

Author contributions: CK conceived the study, with input by JW, SG, EI and SK. JW, SG and CK designed the experiment. JW, SG, KJ, RS, CR, AK and NK did the experimental work, under supervision by CK. JW analysed the data and wrote the first draft of the manuscript with input by CK. All authors reviewed and edited the manuscript. JW revised the final version of the manuscript after assessment by two independent reviewers.

Chapter IV

Manuscript title: Correlative microscale imaging approach for mapping uptake of root exudates by soil microbes

Author names: Julia Wiesenbauer, Schmidt Hannes, Stefan Gorka, Arno Schintlmeister, Christina Kaiser

Reference: Draft

Author contributions: JW and CK conceived the study. CK oversaw the study. JW and SG sampled the soil and carried out the experiment. JW prepared the samples by resin embedding, as well as cutting and polished the embedded soil cores. JW visualized the samples using Laser Microdissection. JW and HS stained the samples and examined them with confocal laser scanning microscopy and were responsible for image capture and analysis. JW performed additional visualization with scanning electron microscopy. AS performed analysis by nanoscale secondary ion mass spectrometry (NanoSIMS). JW, SG, and CK conducted NanoSIMS image analysis with ImageJ. JW wrote the first version of the manuscript with contributions from SG and HS, and input by CK.

Chapter 1

Introduction, thesis outline and main goals

1. The rhizosphere: A crucial interface for root-microbe interactions

Soils store twice as much carbon (C) than the atmosphere or atmosphere and vegetation combined (Stockmann et al., 2013). Therefore, even small changes to organic C fluxes can have significant impacts on the atmospheric C concentrations and Earth's climate. The balance between C storage and C release from soil is determined by primary production (e.g., CO_2 fixed as plant biomass) and microbial decomposition of soil organic matter (SOM). Plant above- and belowground inputs contribute to long-term C storage as plant biomass is converted to SOM by microbial metabolic activity (Schimel and Schaeffer, 2012; Liang et al., 2017). Primarily microbial-derived C like necromass constitutes the SOM formed/ stabilized by 'entombing effects', resulting from a combination of physical and chemical protection of microbial C (Schmidt et al., 2011; Liang et al., 2017). In addition to their role in C sequestration, microorganisms promote the release of C by SOM decomposition. Accordingly, microorganisms are a key agent in soil C cycling. Therefore, it is important to better understand the (microbial) processes that control soil organic carbon (SOC) dynamics and their potential contribution to atmospheric CO_2 levels.

The rhizosphere, defined as the interface between plant roots and the surrounding soil (influenced by root activity), is of particular interest for advancing our understanding of the microbial processes. Rhizosphere processes are increasingly recognized to play a crucial role in soil organic matter (SOM) decomposition, nutrient release, and subsequent effects on terrestrial elemental cycles and global carbon (C) stocks (Finzi et al., 2015). Through rhizodeposition, roots provide soil microorganisms with compounds that serve as energy and nutrients, which drive high levels of high microbial activity (Marschner et al., 2012; Spohn and Kuzyakov, 2013; Blagodatskaya et al., 2014). The intricate interactions between roots and soil microbes, particularly through the microbial uptake and metabolism of C compounds, are pivotal in the SOC cycling.

The catalyst for these rhizosphere processes is the wide variety of C-rich compounds released by the roots into their immediate environment (Jones et al., 2009; Canarini et al., 2019). Broadly speaking, rhizodeposition encompasses all forms of organic C released by roots (Jones et al., 2004). This includes the shed off root cap and boarder cell, the death and lysis of cells, C transfer to root-associated symbionts such as mycorrhiza, gaseous losses, and active secretion of polymers like mucilage as well as passive root exudation (Jones et al., 2009). The exudates consist of low-molecular-weight

compounds such as amino acids, organic acids, and sugars (Badri and Vivanco, 2009; Vives-Peris et al., 2020). They are predominantly released at the root tips, either through passive diffusion or active exudation (Badri and Vivanco, 2009; Jones et al., 2009; Canarini et al., 2019). Fine roots and mycorrhizal hyphae move through the soil and release labile C compounds within a spatially and temporally constrained volume of soil ('hotspot')(Vogel et al., 2014; Kuzyakov and Blagodatskaya, 2015). This is attributed to, firstly, the root exudation being characterized by diurnal carbon release dynamics, with heightened exudation during daylight hours (Murray et al., 2004; Cardon and Gage, 2006; Garcia Arredondo et al., 2023), and secondly, the constant movement of growing roots through the soil. Consequently, root tips create distinct exudation hotspots of transiently high concentration of low-molecular-weight C compounds (Vogel et al., 2014). This results in a heterogeneous distribution of spots with dramatically increased C concentrations in soil (Vogel et al., 2014).

These root exudation 'hotspots' are characterised by high local C concentrations and strong concentration gradients (Kuzyakov and Razavi, 2019; Vetterlein et al., 2020), as opposed to the homogeneously distributed, moderately enhanced C availability throughout the soil that characterises the majority of substrate amendment experiments (e.g.: (Basiliko et al., 2012; Nottingham et al., 2012; Koranda et al., 2013; Girkin et al., 2018a; Jilling et al., 2021). The distribution of carbon (C) within the soil, whether as hotspots or homogeneously dispersed, significantly influences microbial activity. For instance, a recent mathematical analysis has shown that small-scale spatial heterogeneity of substrate distribution affects soil respiration in a way that cannot be subsumed by applying averaged homogenous conditions (Chakrawal et al., 2020). As the substrate diffuses away from the initial entry point, such as the root tip, the microbial density decreases, reducing the probability of substrate-decomposer encounters. In contrast, root exudation hotspots experience an increase in microbial activity driven by the concentrated substrate availability. However, this activity is time-limited because of the transient nature of exudation, giving rise to 'hot moments' (Kuzyakov and Blagodatskaya, 2015). These 'hot moments' are marked by rapid microbial responses to transient spikes in substrate availability (Kuzyakov and Blagodatskaya, 2015). This highlights how rhizosphere processes are critically dependent on the physicochemical and biotic micro-environment of the root exudation hotspot. Consequently, it is imperative to acknowledge the spatial scale and temporal framework within which rhizosphere processes unfold (Vetterlein et al., 2020).

1.1 Root exudates shape the environmental conditions

Root influence the chemical and physical properties of soil through the release of root exudates. For instance, certain plants have been observed to modify the pH of their rhizosphere to mobilize nutrients like phosphorus (Hinsinger et al., 2003; Khorassani et al., 2011; McKay Fletcher et al., 2021).

Additionally, as reported by Keiluweit *et al.* (2015), organic acid exudation can counteract the mineral protection of SOM, making it available to microbial decomposition. Moreover, roots and bacteria release mucilage and extracellular polymeric substances (EPS), respectively, which affect soil hydrology (Benard et al., 2019), and contribute to aggregate formation (Costa et al., 2018). Carbon inputs might also alter oxygen availability as a consequence of microbial O_2 consumption (Borer et al., 2018; Garcia Arredondo et al., 2023). Consequently, the microbial community in the rhizosphere experiences a rapidly changing microenvironment (Philippot et al., 2023). Hence, the ability to swiftly modulate metabolic pathways can mean the difference between surviving and thriving under dynamically changing conditions (Lecomte et al., 2018).

2. Dynamic response of microbial activity to root exudation

The dynamic interplay between root exudation and microbial activity in the rhizosphere is a critical driver of soil carbon (C) cycling, with profound implications for soil health, plant growth, and climate change dynamics (Finzi et al., 2015). Root exudates serve as central substrates for the rhizosphere microbial community and spark an array of metabolic pathways essential for SOM dynamics. Therefore, it is crucial to study the dynamics of microbial activity in response to root exudation.

2.1 Microbial uptake and metabolism of root exudates

Soil microbes are oftentimes carbon and energy limited, relying on root exudates as a prime carbon and energy source (Joergensen et al., 1990; Schmidt et al., 2011). Following the exudation, microbes rapidly take up and metabolize the exudates through different metabolic pathways. Small molecules can be directly taken up, while complex organic matter requires breakdown into smaller molecules by extracellular enzymes before uptake (Kirchman, 2018). Once inside the microbial cell, these compounds are typically funnelled into central metabolic pathways such as glycolysis, tricarboxylic acid cycle (TCA), the electron transport chain (ETC) and oxidative phosphorylation (Fuhrmann, 2021). These pathways break down compounds to produce energy carriers (e.g.: ATP, NADH) that fuel cellular processes. Apart from energy generation, these metabolic pathways also provide precursors for the synthesis of cellular components, including nucleic acids, proteins, lipids, contributing to the growth of microbial biomass (Fuhrmann, 2021). Additionally, enzymes may be produced that catalyse various metabolic pathways inside and outside the cell. In summary, root exudates are essential for the generation of energy, the synthesis of basic building blocks, and the overall maintenance of cellular functions.

Substrate preferences

The microbial community in the rhizosphere is significantly influenced by the composition of root exudates. From a nutrient perspective, the stoichiometry of exudates, especially the C:N ratio, can significantly affect the microbial metabolism and enzyme production, depending on prevailing nutrient limitations (Drake et al., 2013). The microbial community can tackle stoichiometric imbalances caused by substrate C:N by adapting their elemental use efficiencies and through production of extracellular enzymes to obtain limited nutrients (Craine et al., 2007; Mooshammer et al., 2014). For instance, it was shown that exudation of C increased extracellular enzyme activity and thereby N availability (Brzostek et al., 2013).

Moreover, from a purely carbon (centric) perspective, it has been shown that if the C input closely matches or falls below the microbial biomass, the microbial community is not efficiently activated, which inhibits biomass growth (Blagodatskaya et al., 2011). Moreover, microorganisms may exhibit preferences for different substrates based on the potential energy yield from metabolizing them, which depends on the oxidation status of the substance and the available electron acceptors (Bethke et al., 2011; Gunina et al., 2017). However, approaches that rank redox reactions according to their thermodynamic energy dissipation often fail to accurately predict microbial activities (Bethke et al., 2011). They assume that microbial communities will naturally select energy-rich substrates due to competitive dynamics, yet empirical observations frequently deviate from these predictions, indicating that additional factors may play a role (Bethke et al., 2011; Amenabar et al., 2017; Marquart et al., 2019).

Further, the fate of the C-compounds does not only depend on the C amount provided, but also on the identity of the substrates beyond the characterization of labile or 'recalcitrant' C. The utilization of compounds depends on their substrate class (e.g. sugar, organic acid, etc.), which determines their role in different metabolic pathways (Dijkstra et al., 2011; Apostel et al., 2013, 2015; Dippold and Kuzyakov, 2013; Gunina et al., 2014) and, consequently, significantly dictates the interaction between the microbial community and their environment. Research has shown that the addition of sugars, organic acids, amino acids, or phenolics as exudates all increased microbial biomass C, enzyme activity and SOC decomposition (Yan et al., 2023). While some compounds can be directly incorporated into the cells central C-cycle, others need to undergo some form of transformation first. Sugars, like glucose, enter the cell's central C-cycle through glycolysis (Stülke and Hillen, 2000), whereas organic acids, like acetate, must first be converted to intermediates of the TCA cycle, gluconeogenesis, and pentose phosphate pathway (Schilling et al., 2007). In terms of for N-containing compounds, glutamate serves as the central intermediate of N metabolism (Fisher, 1999). Sugars are utilized by soil microorganisms both as building blocks for various cellular components as well as an important energy

source (Gunina and Kuzyakov, 2015). Similarly, organic acids can be rapidly taken up by the soil microbial community, but they do also interact more readily with the soil solid phase through processes like sorption and desorption (Jones et al., 2003). Moreover, organic acids lower pH and contribute to the release of organic material previously bound by minerals (Keiluweit et al., 2015). Amino acids, serving as both C and N sources, are fundamental as building blocks for protein synthesis, promoting the production of N-containing molecules like enzymes, and thus play a role in the SOM cycling (Moe, 2013; Warren, 2014). That is why, due to their varied interactions with the soil environment and microbial community, root exudates of different compositions (e.g. substrate class, substrates physio-chemical properties) may translate to distinct patterns of microbial activity, SOM decomposition and soil chemistry.

2.2 Aerobic and anaerobic respiration in the rhizosphere

Following the root exudation, biotic and abiotic processes occur in the immediate vicinity of the exudation site. Among other things, an increased respiration attributed to increased microbial activity can often be observed. As part of their energy-producing metabolic processes, microbes convert substrate into carbon dioxide (CO_2), which is subsequently released. This CO_2 release is a critical component of the soil carbon cycle, contributing to the flux of C between the soil and the atmosphere (Bardgett et al., 2008; Singh et al., 2010; Finzi et al., 2015).

In the presence of oxygen (O_2), microbes perform **aerobic respiration**, efficiently breaking down organic substrates into CO_2 and H_2O, which releases significant amounts of energy. This energy is captured in energy carriers such as adenosine triphosphate (ATP), which microbes use to power the various cellular activities.

However, in densely populated microbial environments like the rhizosphere, where C inputs are frequent, microbes may encounter **anoxic conditions** that prevent aerobic respiration (Lecomte et al., 2018). These anoxic sites typically emerge due to high microbial activity in response to localized root exudation, where microbes use O_2 to reduce the C substrates. Driven by this O_2 consumption of microbes (and roots), anoxic hotpots arise, but only when the O_2 consumption exceeds the diffusive influx of O_2 (Uteau et al., 2015; Borer et al., 2018). Under such limited or no O_2 conditions, microbes perform anaerobic respiration like fermentation, which yields less energy than aerobic respiration but allows for continued energy production. While most energy can be obtained with O_2 as electron acceptor, in anaerobic respiration, the following alternative terminal electron acceptors (TEA) come into play, e.g., nitrate (NO_3^-), sulfate (SO_4^{2-}), sulfur (S), or metal ions (Fe^{3+}, Mn^{4+}) and inorganic electron acceptors (SeO_4^{2-}, AsO_4^{3-}, UO_2^{2+}). Organic compounds like organic acids (e.g.: fumarate) or humic substances may also serve as electron acceptors (Lecomte et al., 2018).

The degradation of complex organic compounds often requires the cooperation of multiple microbial species, a process known as syntrophy (McInerney et al., 2009; Morris et al., 2013). Syntrophic growth is particularly significant under anoxic conditions, where substrates are only partially oxidized during anaerobic respiration, leading to a release of intermediates (e.g., propionate, acetate, formate) from partially degraded compounds (Glissmann and Conrad, 2000; Lueders et al., 2004; Müller et al., 2010). These metabolic by-products can then be utilized by different members of the microbial community, fostering microbial synergy and syntrophic growth. Beyond syntrophic interactions, it has been observed that acetate, a byproduct of anaerobic respiration released during rapid microbial growth, is scavenged from the environment by the same microbial community, but only after the initial substrate has been depleted (Wolfe, 2005).

2.3 Degradation of organic matter - The rhizosphere priming effect

The presence of living roots can significantly influence SOM decomposition rates, potentially accelerating them by up to 380%, or, conversely, suppress them by half (Cheng et al., 2014). This stimulation of SOM decomposition by root activity (carbon input by rhizodeposition e.g. root exudates) is called 'rhizosphere priming effect' (RPE) (Kuzyakov, 2002, 2010; Dijkstra et al., 2013; Haichar et al., 2014; Huo et al., 2017). The RPE refers to the phenomenon in which labile, low-molecular weight C (LMWC) compounds accelerate the microbial decomposition of SOM, which facilitates the releases of CO_2 from SOM. The RPE thus links primary production and microbial decomposition. This rhizosphere priming effect has been reported across a variety of soil and vegetation types, and its intensity was found to differ depending on plant types and soil texture (Huo et al., 2017). Interestingly, the accelerated SOM decomposition can persist for days to weeks, extending well beyond the duration of the root exudation itself (Blagodatsky et al., 2010; Kuzyakov, 2010), even when the supply of exudate C is depleted.

Experimentally, the priming effect (PE) is usually measured as the difference between the SOM-derived CO_2 released from substrate-amended soils and control soils over time, resulting in a 'positive' PE or, less frequently, a 'negative' PE (Kuzyakov et al., 2000). The PE typically unfolds through a sequence of events that influence the source and dynamics of CO_2. Initially, the respiration is primarily attributed to the respiration of the supplied C-substrate (e.g. exudate-derived CO_2), with increased turnover of microbial biomass also contribute to respiration, collectively referred to as 'apparent' priming (Kuzyakov, 2010). This is followed by accelerated mineralization of SOM, which characterizes 'real' positive priming. Conversely, the **'negative' PE**, characterized by reduced SOM decomposition rates, occurs through mechanisms such as 'preferential substrate utilization' by microbes (Kaiser et al., 2014). Specifically, **'apparent' PE**, in contrast to real positive priming, occurs when the measured CO_2

is derived from a replacement of microbial cell C by added substrate C. Such apparent priming has been reported as a result of microbial activation or a 'tiggering effect' induced by labile substrate addition (De Nobili et al., 2001; Blagodatskaya and Kuzyakov, 2008). Finally, the **real positive PE**, i.e. the accelerated decomposition of SOM, has been attributed to several processes.

Despite extensive research, uncertainties regarding the mechanisms and controls governing the RPE remain subject of ongoing investigation (Bernard et al., 2022). Several explanations have been proposed to explain the RPE and its ecological implications.

Proposed mechanisms underlying the rhizosphere priming effect

A common explanation for the occurrence of RPE suggests that an input of labile carbon compounds **alleviates microbial carbon and energy constraints**. These constraints arise from a physical disconnection of the microbes from their substrates due to low soil organic carbon (SOC) concentrations (Schmidt et al., 2011), particularly in mineral soil. While microbes are restricted to the pore network they inhabit, organic matter (OM) might be located in (physically) inaccessible microsites or be physically protected (Schimel and Schaeffer, 2012). Moreover, for microbes to take up the complex high-molecular weight SOM, they must first break it down into smaller molecules outside the cell, which requires the energy-costly production of enzymes (Schimel and Weintraub, 2003). Further, the 'return on investment' is not always positive for the microbes, as the release of extracellular enzymes brings with it the risk of breakdown products not diffusing back to the cell (Schimel and Weintraub, 2003). Consequently, the release of easily assimilable organic compounds by plant roots can strongly stimulate SOM decomposition by activating dormant microorganisms ('triggering effect') (De Nobili et al., 2001) and by providing them with the necessary energy and carbon to grow and synthesize extracellular enzymes for SOM decomposition (Fontaine et al., 2003; Blagodatskaya and Kuzyakov, 2008; Kuzyakov, 2010; Dijkstra et al., 2013). This can, however, not fully explain why an accelerated microbial decomposition of complex SOM persists long after the labile C is depleted (Blagodatsky et al., 2010; Kuzyakov, 2010).

Alternatively, the RPE may arise due to a succession of functional microbial groups (Fontaine et al., 2003; Kuzyakov, 2010). According to this mechanism, the plant-derived labile C inputs are first rapidly metabolized by fast-growing bacteria ('r-strategists'). This initial stimulation of microbial activity leads to a release of CO_2 from increased microbial biomass turnover ('apparent' PE) (Kuzyakov, 2010). Subsequently, as the soluble compounds are exhausted, slow-growing bacteria and fungi ('K-strategists') that produce **extracellular enzymes** capitalize on the emerging bacterial necromass. Through **co-metabolism** they efficiently decompose more complex SOM, thereby contribution to the observed (real) PE (Fontaine et al., 2003; Blagodatskaya and Kuzyakov, 2008). The produced enzyme's efficiency to co-metabolise native SOM depends on the biochemical similarities between SOM and

carbon input (the fresh OM or necromass) (Fontaine et al., 2003). This explains why the input of complex C inputs (e.g. cellulose, lignocellulose) may elicit more pronounced PE compared to the addition of simple sugars like glucose (Koranda et al., 2013). These mechanisms are taking place when N is not limiting, however, under nutrient-limited conditions, alternative mechanisms come into play.

Thus, another possible explanation for the occurrence of RPE can be attributed to the microbial community mining for nitrogen (N), as suggested by the '**N-mining hypothesis'** (Chen et al., 2014). The labile C input stimulates the microbial biomass growth and leads to an increased microbial nitrogen demand in the rhizosphere, which is met through increased decomposition of SOM ('N-mining hypothesis') (Craine et al., 2007; Fontaine et al., 2011; Dijkstra et al., 2013). Nevertheless, this hypothesis does not adequately explain how microbes use the added C for biomass growth (Elser et al., 2000) or how they produce N-rich extracellular enzymes under N limitation (Drake et al., 2013). However, studies have demonstrated that incorporating N into substrate additions can alter both the direction and magnitude of the PE (Craine et al., 2007; Drake et al., 2013; Koranda et al., 2014; Wild et al., 2014), suggesting a mechanistically relevant role for nitrogen availability.

More recently, increased attention has been paid to abiotic mechanisms which could significantly contribute to priming effects (Keiluweit et al., 2015; Jilling et al., 2021). It has been shown that organic acids, commonly exuded by roots, liberate organic compounds from organo-mineral associations, thereby facilitating their degradation by microbes (Keiluweit et al., 2015; Jilling et al., 2021).

Although these concepts contribute to the mechanistic understanding of the rhizosphere priming effect (RPE), many lack experimental evidence, and a comprehensive, unifying concept of priming remains elusive.

Recently, a new possible explanation for the priming effect has been suggested that can only be understood in a microscale spatial context (Kaiser et al., 2017). It was proposed that an input of labile substrate, such as root exudates, cause an initial growth of microbial colonies. Since the extracellular enzyme production required to degrade SOM is too carbon and energy costly (Schimel and Weintraub, 2003) the initially formed colonies often collapse after the labile substrate (root exudate) is depleted. In some cases, however, if a colony grows beyond a certain threshold size it continues to grow even after the labile substrate is exhausted. This is the case because with the size of a colony its enzyme production efficiency increases. The more microbes are in close proximity to each other, the less products of enzymatic activity are lost by diffusion. Therefore, colony growth becomes self-sustaining if it reaches a certain threshold sized at which the collective 'return on investment' of enzyme production is positive. As a consequence, also SOM decomposition rates are increased in the long-term (priming effect). So far, this new explanation has only been shown in an individual-based computer

model (Kaiser et al., 2017). Nevertheless, it underlines the importance of considering the microscale spatial context when it comes to better understanding the priming effect. Hence, a highly concentrated hotspot of labile substrate, similar to a root exudation hotspot, may be required for a priming effect to occur. Subsequent microbial activities and priming processes would also take place in the vicinity of these hotspots and not throughout the bulk soil. So far, spatial dynamics of microbes at the µm-scale have not been investigated systematically as potential drivers of the priming effect. Considering both spatial and temporal dynamics could significantly enhance our understanding on the governing mechanisms involved. Studying the dynamics of soil metabolites that emerged in response to root exudation could provide valuable clues as to the nature of the metabolic processes and the timeframe and persistence of the rhizosphere priming effect.

3. Exploring spatiotemporal dynamics of microbial and soil processes at the microscale

Exploring the complex interactions within the rhizosphere soil environments requires innovative methods that can capture the dynamic nature of soil chemistry and microbial activity. Advances in soil technologies could provide deeper insights into these complex microbial processes.

3.1 Recent advances in microdialysis technique

The development and application of microdialysis in soil science represent a significant advancement in our ability to study the temporal dynamics and chemistry of soil solutions, which aids our exploration of rhizosphere processes. Originally developed for biomedical research, its potential for environmental research became soon apparent and microdialysis was established in soil (Miró and Frenzel, 2005; Sulyok et al., 2005; Inselsbacher et al., 2011; Inselsbacher and Näsholm, 2012; Inselsbacher, 2014; Oyewole et al., 2014).

Microdialysis is a technique that collects solutes from the soil solution (‘dialysate’) via a diffusion gradient across a permeable membrane (fine polyarylethersulphone membrane, e.g.: 10 mm length, 500 µm outer diameter, 20 kDa molecular weight cut-off) (Fig. 1). Using microdialysis aims to overcome several limitations linked to traditional sampling techniques, including destructive soil sampling and alteration of samples through handling (Miró and Frenzel, 2005; Rousk and Jones, 2010; Inselsbacher, 2014). A major advantage of microdialysis is its low invasiveness, since apart from the initial introduction of the microdialysis probe into the soil, the soil structure remains undisturbed. Microdialysis prioritizes measuring bioavailability of solutes within small spatial scales relevant to plant and microbes in undisturbed soil and allows to calculate diffusive fluxes from dialysate concentrations

(Inselsbacher et al., 2011; Oyewole et al., 2014; Brackin et al., 2015; Demand et al., 2017). This makes microdialysis probes instrumental in investigating biotic and abiotic rhizosphere processes at the microscale, as it offers high temporal and spatial resolution while preserving the integrity of the soil's physical structure.

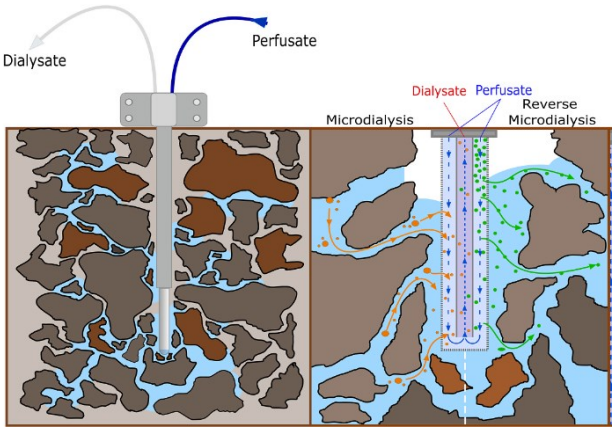


Figure 1. Classical and reverse microdialysis approach. Figure adapted from (König et al., 2022). The left panel depicts the microdialysis probe in the soil. The middle panel compares the classical microdialysis and reverse microdialysis approach. The classical microdialysis application is used to capture soil water solutes (orange particles), while reverse microdialysis introduces compounds (orange particles) into the surrounding soil. These processes are based on diffusion of compounds. The perfusate is pumped through the microdialysis probe (blue arrows), and diffusion of compounds occurs along the permeable membrane due to concentration gradients. After the perfusate has passed along the membrane, it is pumped out of the probe (dialysate, red) and collected for further analysis.

In its **classic application**, the technique has been used to sample a wide array of soil constituents, including nitrogen, root nutrients, phosphate, amino acids, and soil enzymes (Brackin et al., 2017; Buckley et al., 2017, 2019; Demand et al., 2017; Hill et al., 2019; McKay Fletcher et al., 2021). The recent establishment of a **'reverse' microdialysis** approach, also known as retrodialysis in biomedical research (Clément et al., 1998), further enhances its utility by allowing for the controlled release of low-molecular-weight (LMW) compounds into the soil, effectively mimicking root exudation patterns (Demand et al., 2017; König et al., 2022). This can be achieved by providing a higher concentration of compounds in the solution inside the microdialysis probes ('perfusate'), which then leads to a passive diffusion of compounds out of the microdialysis probe (i.e. reversing the concentration gradient). This reversed gradient facilitates the creation of localized hotspots of carbon concentration, enabling detailed studies of microbial activity and soil chemistry in response to the addition of organic compounds. This approach is well suited to simulating root exudation, since labile substances are transported into soil by passive diffusion, similar to living roots. This dual capability to both release and collect compounds makes 'reverse' microdialysis exceptionally versatile, offering insights into soil

metabolic processes with minimal disturbance to the soil structure. So far, the 'reverse' microdialysis approach has been used to study e.g., the effect of citric acid exudation on phosphate concentrations (Demand et al., 2017; Schack-Kirchner et al., 2020; McKay Fletcher et al., 2021), or the effect of sucrose exudation on nitrogen availability (Buckley et al., 2022).

The application of reverse microdialysis, combined with the use of ^{13}C-labelled organic compounds and stable isotope tracing, allows for an unprecedented examination of the spatial and temporal dynamics of microbial metabolism and soil chemistry in response to simulated root exudation (König et al., 2022). By creating discrete, mm-sized locations of enhanced carbon concentration, researchers can trace microbial respiration and uptake of exuded compounds with fine-scale precision. This approach not only simulates the natural process of root exudation but also provides valuable insights into the microbial activity and chemical changes (metabolite production and soil solution chemistry) within the soil, especially in the context of simulated root exudation.

In summary, microdialysis represents a pivotal tool in soil science, enabling the detailed study of soil solution chemistry and microbial dynamics with minimal disturbance to the native soil structure. Through both its classic and reverse applications, it offers a unique lens through which the complex interactions between roots and soil microorganisms can be explored, shedding light on the intricate processes that govern soil health and nutrient cycling.

3.2 Advanced imaging techniques for spatial analysis

The rhizosphere environment differs greatly at the microscale, and these variations across microhabitats affect the spatial distribution and activity of microorganisms (Chenu et al., 2001; Raynaud and Nunan, 2014; Kim et al., 2015; Juyal et al., 2021). Consequently, it is important to investigate the microscale spatial factors that influence microbial processes in the rhizosphere, alongside the temporal dynamics. However, traditional approaches such as bulk soil extraction or soil solution sampling through microsuction cups or Rhizon samplers (Puschenreiter et al., 2005; Dessureault-Rompré et al., 2006; Baumert et al., 2018) disturb the soil matrix and fail to capture the heterogeneity and inherent dynamics in natural soil environments (Moran and McGrath, 2021).

To address these challenges, advanced imaging techniques are of interest, which can visualize the microbial distribution, the soil microarchitecture and elemental composition, and the microbial activity at high spatial resolutions (Védère et al., 2022). Fluorescence microscopy, for example, enables the assessment of the microbial community distribution and plant-microbe interactions by using fluorochrome staining or targeted fluorescence *in situ* hybridization (FISH) (Eickhorst and Tippkötter, 2008; Cardinale, 2014; Schmidt et al., 2018). Nanoscale secondary ion mass spectrometry (NanoSIMS)

is a valuable tool for mapping the distribution of elements (Herrmann et al., 2007; Mueller et al., 2012). When integrating NanoSIMS with isotope labelling (i.e. 'nanoSIP'), it can elucidate the microscale spatial distribution of microorganisms and provide detailed insights into soil chemistry and SOM dynamics (Clode et al., 2009; Mueller et al., 2012; Pett-Ridge and Firestone, 2017). Moreover, combining nanoSIP with FISH has proven effective for linking microbial identity to isotopic enrichment (Li et al., 2008; Musat et al., 2014).

These techniques enable the study of soil chemistry and microbial interactions *in situ*, preserving the integrity of the soil's physical structure and capturing the transient and localized nature of microbial processes. By mitigating the limitations associated with more invasive sampling methods, such approaches offer a more accurate reflection of the complex interactions between roots and soil microorganisms, crucial for advancing our understanding of nutrient cycling in the context of rhizosphere dynamics.

This underscores the necessity of innovative approaches that can elucidate the spatial and temporal patterns of microbial activity and their responses to root exudates within undisturbed soil systems, addressing a gap that has long been neglected in soil microbial ecology.

4. Thesis outline and main goal

The interaction between plant roots and soil microbes is a fundamental aspect of soil carbon cycling. Organic carbon (C) released by the roots serves as a source of energy and nutrients to the soil microbes. These microbes may utilize the C to form new microbial biomass, which ultimately form soil organic matter (SOM) and contributes to C sequestration (CO_2 sink). Alternatively, the C input may accelerate SOM decomposition (i.e., rhizosphere priming effect), or the microbes may respire the C, converting it to CO_2. Both of these outcomes contribute to the C flux between the soil and the atmosphere. A thorough understanding of microbial utilization of root exudates and SOM, along with the microbial activity and metabolic processes occurring at root exudation sites, is essential. However, the complex microbial processes and mechanisms transpiring at these hotspots remain poorly understood.

The primary goal of my thesis was to unravel the fine-scale spatiotemporal dynamics of microbial activity that occur at root exudation sites and investigate the mechanisms that cause accelerated soil organic matter (SOM) degradation rates (i.e. priming) and its persistence long after the exudates have been depleted. Additionally, we wanted to explore how these dynamics are influenced by the composition of root exudates in different soil types. The foundational approach across the studies in this thesis was to release organic compounds into undisturbed soil using 'reverse' microdialysis, which closely mimics passive root exudate release and allowed for a detailed investigation of its immediate effects.

The **second chapter** of my thesis is dedicated to unravelling the fine-scale temporal dynamics of microbial activity and soil metabolite profiles following a simulated root exudation event by reverse microdialysis into undisturbed soil from a beech forest. The artificial root exudate was comprised of sugars and organic acids reflective of compounds commonly found in root exudates. Our study revealed that simulated root exudation with labile C-compounds in undisturbed soil significantly altered microbial metabolism and enhanced nutrient availability near the exudation site. Our experiment revealed a three-stage microbial response to artificial root exudation in undisturbed soil: Starting with an initial rapid substrate respiration potentially leading to oxygen depletion within hours, followed by (anaerobic) metabolism and the release of fermentation byproduct and N-compounds within a day, culminating in an accelerated SOM respiration by day three. These findings highlight the dynamic shifts in microbial metabolism and nutrient availability at the exudation site and advance our comprehension of the processes that contribute to rhizosphere priming.

The **third chapter** of my thesis explores the differential impact of sugars and organic acids, key components of root exudates, on microbial activity, soil metabolite production and priming effects in

different soil types. We simulate root exudation of only sugars, only organic acids, or their combination into intact meadow and forest, to clarify the impact of each compound class. We assessed substrate-induced microbial respiration, SOM mineralization, metabolite concentrations, and substrate incorporation into microbial lipid-derived fatty acids. Our findings reveal a distinct microbial preference for organic acids over sugars. Organic acids were rapidly removed from the exudation site and preferentially respired by the microbial community. Additionally, organic acids led to increased concentrations of microbial metabolic byproducts and cations near the exudation spot. In contrast, sugar alone had negligible effects on microbial activity, and when combined with organic acids, did not alter the outcomes observed with organic acids alone. This chapter elucidates how the composition of root exudates influences microbial dynamics and soil chemistry, highlighting the complex interplay between root exudate and soil microbial communities.

The **fourth chapter** aimed to establish an integrative imaging approach that leverages advanced imaging techniques, stable isotope probing, and reverse microdialysis to investigate the microscale spatial dynamics of microbial communities in the rhizosphere. We closely mimicked root exudation by utilizing reverse microdialysis to introduce ^{13}C-labelled substrates, causing only minimal disturbance to the soil structure. We integrated several imaging techniques to monitor the spatial distribution and assimilation of these substrates by soil microbes. Employing confocal laser scanning microscopy (CLSM), we visualized the spatial distribution of fluorescently labelled microbial cells in resin-embedded soil cores. Nanoscale secondary ion mass spectrometry (NanoSIMS) provided detailed isotopic and elemental analyses, mapping the distribution of ^{13}C alongside elements associated with organic compounds (C, N) and mineral particles (Si, Al). Scanning electron microscopy (SEM) complemented this by providing a structural context by visualized the soil microstructure surrounding the exudation site. By correlating structural data with chemical signatures, our approach allowed for the precise localization and characterization of microbial cells involved in the substrate assimilation. This integrated imaging approach provided a comprehensive view of the microbial assimilation patterns and the surrounding soil chemistry, revealing a varied microbial response to substrate availability. This chapter highlight the usefulness of combining these imaging methods to elucidate the spatial dynamics of microbial activity, such as substrate utilization, at the microscale, laying the foundation for understanding the microscale root-soil-microbe interactions in the rhizosphere.

References

Amenabar, M.J., Shock, E.L., Roden, E.E., Peters, J.W., Boyd, E.S., 2017. Microbial substrate preference dictated by energy demand rather than supply. Nature Geoscience 10, 577–581. doi:10.1038/ngeo2978

Apostel, C., Dippold, M., Glaser, B., Kuzyakov, Y., 2013. Biochemical pathways of amino acids in soil: Assessment by position-specific labeling and 13C-PLFA analysis. Soil Biology and Biochemistry 67, 31–40. doi:10.1016/j.soilbio.2013.08.005

Apostel, C., Dippold, M., Kuzyakov, Y., 2015. Biochemistry of hexose and pentose transformations in soil analyzed by position-specific labeling and 13C-PLFA. Soil Biology and Biochemistry 80, 199–208. doi:10.1016/j.soilbio.2014.09.005

Badri, D.V., Vivanco, J.M., 2009. Regulation and function of root exudates. Plant, Cell and Environment 32, 666–681. doi:10.1111/j.1365-3040.2009.01926.x

Bardgett, R.D., Freeman, C., Ostle, N.J., 2008. Microbial contributions to climate change through carbon cycle feedbacks. The ISME Journal 2, 805–814. doi:10.1038/ismej.2008.58

Basiliko, N., Stewart, H., Roulet, N.T., Moore, T.R., 2012. Do Root Exudates Enhance Peat Decomposition? Geomicrobiology Journal 29, 374–378. doi:10.1080/01490451.2011.568272

Baumert, V.L., Vasilyeva, N.A., Vladimirov, A.A., Meier, I.C., Kögel-Knabner, I., Mueller, C.W., 2018. Root Exudates Induce Soil Macroaggregation Facilitated by Fungi in Subsoil. Frontiers in Environmental Science 6. doi:10.3389/fenvs.2018.00140

Benard, P., Zarebanadkouki, M., Brax, M., Kaltenbach, R., Jerjen, I., Marone, F., Couradeau, E., Felde, V.J.M.N.L., Kaestner, A., Carminati, A., 2019. Microhydrological Niches in Soils: How Mucilage and EPS Alter the Biophysical Properties of the Rhizosphere and Other Biological Hotspots. Vadose Zone Journal 18, 180211. doi:10.2136/vzj2018.12.0211

Bernard, L., Basile-Doelsch, I., Derrien, D., Fanin, N., Fontaine, S., Guenet, B., Karimi, B., Marsden, C., Maron, P.A., 2022. Advancing the mechanistic understanding of the priming effect on soil organic matter mineralisation. Functional Ecology 36, 1355–1377. doi:10.1111/1365-2435.14038

Bethke, C.M., Sanford, R.A., Kirk, M.F., Jin, Q., Flynn, T.M., 2011. The thermodynamic ladder in geomicrobiology. American Journal of Science 311, 183–210. doi:10.2475/03.2011.01

Blagodatskaya, E., Blagodatsky, S., Anderson, T.-H.H., Kuzyakov, Y., 2014. Microbial Growth and Carbon Use Efficiency in the Rhizosphere and Root-Free Soil. PLoS ONE 9, e93282. doi:10.1371/journal.pone.0093282

Blagodatskaya, E., Kuzyakov, Y., 2008. Mechanisms of real and apparent priming effects and their dependence on soil microbial biomass and community structure: Critical review. Biology and Fertility of Soils 45, 115–131. doi:10.1007/s00374-008-0334-y

Blagodatskaya, E., Yuyukina, T., Blagodatsky, S., Kuzyakov, Y., Blagodatskaya, E., Yuyukina, T., Blagodatsky, S., Kuzyakov, Y., 2011. Three-source-partitioning of microbial biomass and of CO2 efflux from soil to evaluate mechanisms of priming effects. Soil Biology and Biochemistry 43, 778–786. doi:10.1016/j.soilbio.2010.12.011

Blagodatsky, S., Blagodatskaya, E., Yuyukina, T., Kuzyakov, Y., 2010. Model of apparent and real priming effects: Linking microbial activity with soil organic matter decomposition. Soil Biology and Biochemistry 42, 1275–1283. doi:10.1016/j.soilbio.2010.04.005

Borer, B., Tecon, R., Or, D., 2018. Spatial organization of bacterial populations in response to oxygen and carbon counter-gradients in pore networks. Nature Communications 9, 769. doi:10.1038/s41467-018-03187-y

Brackin, R., Atkinson, B.S., Sturrock, C.J., Rasmussen, A., 2017. Roots-eye view: Using microdialysis and microCT to non-destructively map root nutrient depletion and accumulation zones. Plant Cell and Environment 40, 3135–3142. doi:10.1111/pce.13072

Brackin, R., Näsholm, T., Robinson, N., Guillou, S., Vinall, K., Lakshmanan, P., Schmidt, S., Inselsbacher, E., 2015. Nitrogen fluxes at the root-soil interface show a mismatch of nitrogen fertilizer supply and sugarcane root uptake capacity. Scientific Reports 5, 15727. doi:10.1038/srep15727

Brzostek, E.R., Greco, A., Drake, J.E., Finzi, A.C., 2013. Root carbon inputs to the rhizosphere stimulate extracellular enzyme activity and increase nitrogen availability in temperate forest soils. Biogeochemistry 115, 65–76. doi:10.1007/s10533-012-9818-9

Buckley, S., Allen, D., Brackin, R., Jämtgård, S., Näsholm, T., Schmidt, S., 2019. Microdialysis as an in situ technique for sampling soil enzymes. Soil Biology and Biochemistry 135, 20–27. doi:10.1016/j.soilbio.2019.04.007

Buckley, S., Brackin, R., Näsholm, T., Schmidt, S., Jämtgård, S., 2022. The influence of sucrose on soil nitrogen availability – A root exudate simulation using microdialysis. Geoderma 409. doi:10.1016/j.geoderma.2021.115645

Buckley, S., Brackin, R., Näsholm, T., Schmidt, S., Jämtgård, S., 2017. Improving in situ recovery of soil nitrogen using the microdialysis technique. Soil Biology and Biochemistry 114, 93–103. doi:10.1016/j.soilbio.2017.07.009

Canarini, A., Kaiser, C., Merchant, A., Richter, A., Wanek, W., 2019. Root Exudation of Primary Metabolites: Mechanisms and Their Roles in Plant Responses to Environmental Stimuli. Frontiers in Plant Science 10. doi:10.3389/fpls.2019.00157

Cardinale, M., 2014. Scanning a microhabitat: plant-microbe interactions revealed by confocal laser microscopy. Frontiers in Microbiology 5. doi:10.3389/fmicb.2014.00094

Cardon, Z.G., Gage, D.J., 2006. Resource Exchange in the Rhizosphere: Molecular Tools and the Microbial Perspective. Annual Review of Ecology, Evolution, and Systematics 37, 459–488. doi:10.1146/annurev.ecolsys.37.091305.110207

Chakrawal, A., Herrmann, A.M., Koestel, J., Jarsjö, J., Nunan, N., Kätterer, T., Manzoni, S., 2020. Dynamic upscaling of decomposition kinetics for carbon cycling models. Geoscientific Model Development 13, 1399–1429. doi:10.5194/gmd-13-1399-2020

Chen, R., Senbayram, M., Blagodatsky, S., Myachina, O., Dittert, K., Lin, X., Blagodatskaya, E., Kuzyakov, Y., Blagodatskaya, E., Kuzyakov, Y., 2014. Soil C and N availability determine the priming effect: Microbial N mining and stoichiometric decomposition theories. Global Change Biology 20, 2356–2367. doi:10.1111/gcb.12475

Cheng, W., Parton, W.J., Gonzalez-Meler, M.A., Phillips, R., Asao, S., Mcnickle, G.G., Brzostek, E., Jastrow, J.D., 2014. Synthesis and modeling perspectives of rhizosphere priming. New Phytologist 201, 31–44. doi:10.1111/nph.12440

Chenu, C., Hassink, J., Bloem, J., 2001. Short-term changes in the spatial distribution of microorganisms in soil aggregates as affected by glucose addition. Biology and Fertility of Soils 34, 349–356. doi:10.1007/s003740100419

Clément, R., Malinovsky, J.-M., Dollo, G., Le Corre, P., Chevanne, F., Le Verge, R., 1998. In vitro and in vivo microdialysis calibration using retrodialysis for the study of the cerebrospinal distribution of bupivacaine. Journal of Pharmaceutical and Biomedical Analysis 17, 665–670. doi:10.1016/S0731-7085(97)00274-4

Clode, P.L., Kilburn, M.R., Jones, D.L., Stockdale, E.A., Cliff, J.B., Herrmann, A.M., Murphy, D.V., 2009. In Situ Mapping of Nutrient Uptake in the Rhizosphere Using Nanoscale Secondary Ion Mass Spectrometry. Plant Physiology 151, 1751–1757. doi:10.1104/pp.109.141499

Costa, O.Y.A., Raaijmakers, J.M., Kuramae, E.E., 2018. Microbial Extracellular Polymeric Substances: Ecological Function and Impact on Soil Aggregation. Frontiers in Microbiology 9. doi:10.3389/fmicb.2018.01636

Craine, J.M., Morrow, C., Fierer, N., 2007. MICROBIAL NITROGEN LIMITATION INCREASES DECOMPOSITION. Ecology 88, 2105–2113. doi:10.1890/06-1847.1

De Nobili, M., Contin, M., Mondini, C., Brookes, P.C., 2001. Soil microbial biomass is triggered into activity by trace amounts of substrate. Soil Biology and Biochemistry 33, 1163–1170. doi:10.1016/S0038-0717(01)00020-7

Demand, D., Schack-Kirchner, H., Lang, F., 2017. Assessment of diffusive phosphate supply in soils by microdialysis. Journal of Plant Nutrition and Soil Science 180, 220–230. doi:10.1002/jpln.201600412

Dessureault-Rompré, J., Nowack, B., Schulin, R., Luster, J., 2006. Modified micro suction cup/rhizobox approach for the in-situ detection of organic acids in rhizosphere soil solution. Plant and Soil 286, 99–107. doi:10.1007/s11104-006-9029-z

Dijkstra, F.A., Carrillo, Y., Pendall, E., Morgan, J.A., 2013. Rhizosphere priming: a nutrient perspective. Frontiers in Microbiology 4. doi:10.3389/fmicb.2013.00216

Dijkstra, P., Dalder, J.J., Selmants, P.C., Hart, S.C., Koch, G.W., Schwartz, E., Hungate, B.A., 2011. Modeling soil metabolic processes using isotopologue pairs of position-specific 13C-labeled glucose and pyruvate. Soil Biology and Biochemistry, 19th International Symposium on Environmental Biogeochemistry 43, 1848–1857. doi:10.1016/j.soilbio.2011.05.001

Dippold, M.A., Kuzyakov, Y., 2013. Biogeochemical transformations of amino acids in soil assessed by position-specific labelling. Plant and Soil 373, 385–401. doi:10.1007/s11104-013-1764-3

Drake, J.E., Darby, B.A., Giasson, M.A., Kramer, M.A., Phillips, R.P., Finzi, A.C., 2013. Stoichiometry constrains microbial response to root exudation-insights from a model and a field experiment in a temperate forest. Biogeosciences 10, 821–838. doi:10.5194/bg-10-821-2013

Eickhorst, T., Tippkötter, R., 2008. Detection of microorganisms in undisturbed soil by combining fluorescence in situ hybridization (FISH) and micropedological methods. Soil Biology and Biochemistry 40, 1284–1293. doi:10.1016/j.soilbio.2007.06.019

Elser, J.J., Fagan, W.F., Denno, R.F., Dobberfuhl, D.R., Folarin, A., Huberty, A., Interlandi, S., Kilham, S.S., McCauley, E., Schulz, K.L., Siemann, E.H., Sterner, R.W., 2000. Nutritional constraints in terrestrial and freshwater food webs. Nature 408, 578–580. doi:10.1038/35046058

Finzi, A.C., Abramoff, R.Z., Spiller, K.S., Brzostek, E.R., Darby, B.A., Kramer, M.A., Phillips, R.P., 2015. Rhizosphere processes are quantitatively important components of terrestrial carbon and nutrient cycles. Global Change Biology 21, 2082–2094. doi:10.1111/gcb.12816

Fisher, S.H., 1999. Regulation of nitrogen metabolism in Bacillus subtilis: vive la différence! Molecular Microbiology 32, 223–232. doi:10.1046/j.1365-2958.1999.01333.x

Fontaine, S., Henault, C., Aamor, A., Bdioui, N., Bloor, J.M.G., Maire, V., Mary, B., Revaillot, S., Maron, P.A., 2011. Fungi mediate long term sequestration of carbon and nitrogen in soil through their priming effect. Soil Biology and Biochemistry 43, 86–96. doi:10.1016/j.soilbio.2010.09.017

Fontaine, S., Mariotti, A., Abbadie, L., 2003. The priming effect of organic matter: a question of microbial competition? Soil Biology and Biochemistry 35, 837–843. doi:10.1016/S0038-0717(03)00123-8

Fuhrmann, J.J., 2021. 3 - Microbial metabolism, in: Gentry, T.J., Fuhrmann, J.J., Zuberer, D.A. (Eds.), Principles and Applications of Soil Microbiology (Third Edition). Elsevier, pp. 57–87. doi:10.1016/B978-0-12-820202-9.00003-4

Garcia Arredondo, M., Fang, Y., Jones, M., Yabusaki, S., Cardon, Z., Keiluweit, M., 2023. Resolving dynamic mineral-organic interactions in the rhizosphere by combining in-situ microsensors with plant-soil reactive transport modeling. Soil Biology and Biochemistry 184, 109097. doi:10.1016/j.soilbio.2023.109097

Girkin, N.T., Turner, B.L., Ostle, N., Craigon, J., Sjögersten, S., 2018. Root exudate analogues accelerate CO2 and CH4 production in tropical peat. Soil Biology and Biochemistry 117, 48–55. doi:10.1016/j.soilbio.2017.11.008

Glissmann, K., Conrad, R., 2000. Fermentation pattern of methanogenic degradation of rice straw in anoxic paddy soil. FEMS Microbiology Ecology 31, 117–126. doi:10.1111/j.1574-6941.2000.tb00677.x

Gunina, A., Dippold, M.A., Glaser, B., Kuzyakov, Y., 2014. Fate of low molecular weight organic substances in an arable soil: From microbial uptake to utilisation and stabilisation. Soil Biology and Biochemistry 77, 304–313. doi:10.1016/j.soilbio.2014.06.029

Gunina, A., Kuzyakov, Y., 2015. Sugars in soil and sweets for microorganisms: Review of origin, content, composition and fate. Soil Biology and Biochemistry 90, 87–100. doi:10.1016/j.soilbio.2015.07.021

Gunina, A., Smith, A.R., Kuzyakov, Y., Jones, D.L., 2017. Microbial uptake and utilization of low molecular weight organic substrates in soil depend on carbon oxidation state. Biogeochemistry 133, 89–100. doi:10.1007/s10533-017-0313-1

Haichar, F. el Z., Santaella, C., Heulin, T., Achouak, W., 2014. Root exudates mediated interactions belowground. Soil Biology and Biochemistry 77, 69–80. doi:10.1016/j.soilbio.2014.06.017

Herrmann, A.M., Ritz, K., Nunan, N., Clode, P.L., Pett-Ridge, J., Kilburn, M.R., Murphy, D.V., O'Donnell, A.G., Stockdale, E.A., 2007. Nano-scale secondary ion mass spectrometry — A new analytical tool in biogeochemistry and soil ecology: A review article. Soil Biology and Biochemistry 39, 1835–1850. doi:10.1016/j.soilbio.2007.03.011

Hill, E.J., Jones, D.L., Paterson, E., Hill, P.W., 2019. Hotspots and hot moments of amino acid N in soil: Real-time insights using continuous microdialysis sampling. Soil Biology and Biochemistry 131, 40–43. doi:10.1016/j.soilbio.2018.12.026

Hinsinger, P., Plassard, C., Tang, C., Jaillard, B., 2003. Origins of root-mediated pH changes in the rhizosphere and their responses to environmental constraints: A review. Plant and Soil 248, 43–59. doi:10.1023/A:1022371130939

Huo, C., Luo, Y., Cheng, W., 2017. Rhizosphere priming effect: A meta-analysis. Soil Biology and Biochemistry 111, 78–84. doi:10.1016/j.soilbio.2017.04.003

Inselsbacher, E., 2014. Recovery of individual soil nitrogen forms after sieving and extraction. Soil Biology and Biochemistry 71, 76–86. doi:10.1016/j.soilbio.2014.01.009

Inselsbacher, E., Näsholm, T., 2012. A novel method to measure the effect of temperature on diffusion of plant-available nitrogen in soil. Plant and Soil 354, 251–257. doi:10.1007/s11104-011-1061-y

Inselsbacher, E., Öhlund, J., Jämtgård, S., Huss-Danell, K., Näsholm, T., 2011. The potential of microdialysis to monitor organic and inorganic nitrogen compounds in soil. Soil Biology and Biochemistry 43, 1321–1332. doi:10.1016/j.soilbio.2011.03.003

Jilling, A., Keiluweit, M., Gutknecht, J.L.M., Grandy, A.S., 2021. Priming mechanisms providing plants and microbes access to mineral-associated organic matter. Soil Biology and Biochemistry 158, 108265. doi:10.1016/j.soilbio.2021.108265

Joergensen, R.G., Brookes, P.C., Jenkinson, D.S., 1990. Survival of the soil microbial biomass at elevated temperatures. Soil Biology and Biochemistry 22, 1129–1136. doi:10.1016/0038-0717(90)90039-3

Jones, D.L., Dennis, P.G., Owen, A.G., Van Hees, P.A.W., 2003. Organic acid behavior in soils - misconceptions and knowledge gaps. Plant and Soil 248, 31–41. doi:10.1023/A

Jones, D.L., Hodge, A., Kuzyakov, Y., 2004. Plant and mycorrhizal regulation of rhizodeposition. New Phytologist 163, 459–480. doi:10.1111/j.1469-8137.2004.01130.x

Jones, D.L., Nguyen, C., Finlay, R.D., 2009. Carbon flow in the rhizosphere: carbon trading at the soil–root interface. Plant and Soil 321, 5–33. doi:10.1007/s11104-009-9925-0

Juyal, A., Otten, W., Baveye, P.C., Eickhorst, T., 2021. Influence of soil structure on the spread of Pseudomonas fluorescens in soil at microscale. European Journal of Soil Science 72, 141–153. doi:10.1111/ejss.12975

Kaiser, C., Dieckmann, U., Franklin, O., 2017. The rhizosphere priming effect explained by microscale interactions among enzyme producing microbes. Presented at the Geophysical Research Abstracts, p. EGU 2017-19214.

Kaiser, C., Franklin, O., Dieckmann, U., Richter, A., 2014. Microbial community dynamics alleviate stoichiometric constraints during litter decay. Ecology Letters 17, 680–690. doi:10.1111/ele.12269

Keiluweit, M., Bougoure, J.J., Nico, P.S., Pett-Ridge, J., Weber, P.K., Kleber, M., 2015. Mineral protection of soil carbon counteracted by root exudates. Nature Climate Change 5, 588–595. doi:10.1038/nclimate2580

Khorassani, R., Hettwer, U., Ratzinger, A., Steingrobe, B., Karlovsky, P., Claassen, N., 2011. Citramalic acid and salicylic acid in sugar beet root exudates solubilize soil phosphorus. BMC Plant Biology 11, 121. doi:10.1186/1471-2229-11-121

Kim, H., Nunan, N., Dechesne, A., Juarez, S., Grundmann, G., 2015. The spatial distribution of exoenzyme activities across the soil micro-landscape, as measured in micro- and macro-aggregates, and ecosystem processes. Soil Biology and Biochemistry 91, 258–267. doi:10.1016/j.soilbio.2015.08.042

Kirchman, D.L., 2018. Degradation of organic matter, in: Kirchman, D.L. (Ed.), Processes in Microbial Ecology. Oxford University Press. doi:10.1093/oso/9780198789406.003.0007

König, A., Wiesenbauer, J., Gorka, S., Marchand, L., Kitzler, B., Inselsbacher, E., Kaiser, C., 2022. Reverse microdialysis: A window into root exudation hotspots. Soil Biology and Biochemistry 174, 108829. doi:10.1016/j.soilbio.2022.108829

Koranda, M., Kaiser, C., Fuchslueger, L., Kitzler, B., Sessitsch, A., Zechmeister-Boltenstern, S., Richter, A., 2014. Fungal and bacterial utilization of organic substrates depends on substrate complexity and N availability. FEMS Microbiology Ecology 87, 142–152. doi:10.1111/1574-6941.12214

Koranda, M., Kaiser, C., Fuchslueger, L., Kitzler, B., Sessitsch, A., Zechmeister-Boltenstern, S., Richter, A., 2013. Seasonal variation in functional properties of microbial communities in beech forest soil. Soil Biology and Biochemistry 60, 95–104. doi:10.1016/j.soilbio.2013.01.025

Kuzyakov, Y., 2010. Priming effects: Interactions between living and dead organic matter. Soil Biology and Biochemistry 42, 1363–1371. doi:10.1016/j.soilbio.2010.04.003

Kuzyakov, Y., 2002. Review : Factors affecting rhizosphere priming effects. Journal of Plant Nurition and Soil Science 165, 382–396.

Kuzyakov, Y., Blagodatskaya, E., 2015. Microbial hotspots and hot moments in soil: Concept & review. Soil Biology and Biochemistry 83, 184–199. doi:10.1016/j.soilbio.2015.01.025

Kuzyakov, Y., Friedel, J.K., Stahr, K., 2000. Review of mechanisms and quantification of priming effects. Soil Biology & Biochemistry 32, 1485–1498. doi:10.1016/S0038-0717(00)00084-5

Kuzyakov, Y., Razavi, B.S., 2019. Rhizosphere size and shape: Temporal dynamics and spatial stationarity. Soil Biology and Biochemistry 135, 343–360. doi:10.1016/j.soilbio.2019.05.011

Lecomte, S.M., Achouak, W., Abrouk, D., Heulin, T., Nesme, X., Haichar, F.E.Z., 2018. Diversifying Anaerobic Respiration Strategies to Compete in the Rhizosphere. Frontiers in Environmental Science 6, 139. doi:10.3389/fenvs.2018.00139

Li, T., Wu, T.-D., Mazéas, L., Toffin, L., Guerquin-Kern, J.-L., Leblon, G., Bouchez, T., 2008. Simultaneous analysis of microbial identity and function using NanoSIMS. Environmental Microbiology 10, 580–588.

Liang, C., Schimel, J.P., Jastrow, J.D., 2017. The importance of anabolism in microbial control over soil carbon storage. Nature Microbiology 2, 1–6. doi:10.1038/nmicrobiol.2017.105

Lueders, T., Pommerenke, B., Friedrich, M.W., 2004. Stable-Isotope Probing of Microorganisms Thriving at Thermodynamic Limits: Syntrophic Propionate Oxidation in Flooded Soil. Applied and Environmental Microbiology 70, 5778–5786. doi:10.1128/AEM.70.10.5778-5786.2004

Marquart, K.A., Haller, B.R., Paper, J.M., Flynn, T.M., Boyanov, M.I., Shodunke, G., Gura, C., Jin, Q., Kirk, M.F., 2019. Influence of pH on the balance between methanogenesis and iron reduction. Geobiology 17, 185–198. doi:10.1111/gbi.12320

Marschner, P., Marhan, S., Kandeler, E., 2012. Microscale distribution and function of soil microorganisms in the interface between rhizosphere and detritusphere. Soil Biology and Biochemistry 49, 174–183. doi:10.1016/j.soilbio.2012.01.033

McInerney, M.J., Sieber, J.R., Gunsalus, R.P., 2009. Syntrophy in anaerobic global carbon cycles. Current Opinion in Biotechnology, Chemical biotechnology ● Pharmaceutical biotechnology 20, 623–632. doi:10.1016/j.copbio.2009.10.001

McKay Fletcher, D.M., Shaw, R., Sánchez-Rodríguez, A.R., Daly, K.R., van Veelen, A., Jones, D.L., Roose, T., 2021. Quantifying citrate-enhanced phosphate root uptake using microdialysis. Plant and Soil 461, 69–89. doi:10.1007/s11104-019-04376-4

Miró, M., Frenzel, W., 2005. The potential of microdialysis as an automatic sample-processing technique for environmental research. TrAC - Trends in Analytical Chemistry 24, 324–333. doi:10.1016/j.trac.2004.10.004

Moe, L.A., 2013. Amino acids in the rhizosphere: From plants to microbes. American Journal of Botany 100, 1692–1705. doi:10.3732/ajb.1300033

Mooshammer, M., Wanek, W., Zechmeister-Boltenstern, S., Richter, A.A., 2014. Stoichiometric imbalances between terrestrial decomposer communities and their resources: mechanisms and implications of microbial adaptations to their resources. Frontiers in Microbiology 5. doi:10.3389/fmicb.2014.00022

Moran, J., McGrath, C., 2021. Comparison of Methods for Mapping Rhizosphere Processes in the Context of Their Surrounding Root and Soil Environments. BioTechniques 71, 604–614. doi:10.2144/btn-2021-0021

Morris, B.E.L., Henneberger, R., Huber, H., Moissl-Eichinger, C., 2013. Microbial syntrophy: interaction for the common good. FEMS Microbiology Reviews 37, 384–406. doi:10.1111/1574-6976.12019

Mueller, C.W., Kölbl, A., Hoeschen, C., Hillion, F., Heister, K., Herrmann, A.M., Kögel-Knabner, I., 2012. Submicron scale imaging of soil organic matter dynamics using NanoSIMS – From single particles to intact aggregates. Organic Geochemistry, Organic Isotopes in Soil 42, 1476–1488. doi:10.1016/j.orggeochem.2011.06.003

Müller, N., Worm, P., Schink, B., Stams, A.J.M., Plugge, C.M., 2010. Syntrophic butyrate and propionate oxidation processes: from genomes to reaction mechanisms. Environmental Microbiology Reports 2, 489–499. doi:10.1111/j.1758-2229.2010.00147.x

Murray, P., Ostle, N., Kenny, C., Grant, H., 2004. Effect of defoliation on patterns of carbon exudation from Agrostis capillaris. Journal of Plant Nutrition and Soil Science 167, 487–493. doi:10.1002/jpln.200320371

Musat, N., Stryhanyuk, H., Bombach, P., Adrian, L., Audinot, J.N., Richnow, H.H., 2014. The effect of FISH and CARD-FISH on the isotopic composition of13C- and15N-labeled Pseudomonas putida cells measured by nanoSIMS. Systematic and Applied Microbiology 37, 267–276. doi:10.1016/j.syapm.2014.02.002

Nottingham, A.T., Turner, B.L., Chamberlain, P.M., Stott, A.W., Tanner, E.V.J., 2012. Priming and microbial nutrient limitation in lowland tropical forest soils of contrasting fertility. Biogeochemistry 111, 219–237.

Oyewole, O.A., Inselsbacher, E., Näsholm, T., 2014. Direct estimation of mass flow and diffusion of nitrogen compounds in solution and soil. New Phytologist 201, 1056–1064. doi:10.1111/nph.12553

Pett-Ridge, J., Firestone, M.K., 2017. Using stable isotopes to explore root-microbe-mineral interactions in soil. Rhizosphere, New Understanding of Rhizosphere Processes Enabled by Advances in Molecular and Spatially Resolved Techniques 3, 244–253. doi:10.1016/j.rhisph.2017.04.016

Philippot, L., Chenu, C., Kappler, A., Rillig, M.C., Fierer, N., 2023. The interplay between microbial communities and soil properties. Nature Reviews Microbiology 1–14. doi:10.1038/s41579-023-00980-5

Puschenreiter, M., Wenzel, W.W., Wieshammer, G., Fitz, W.J., Wieczorek, S., Kanitsar, K., Köllensperger, G., 2005. Novel micro–suction-cup design for sampling soil solution at defined distances from roots. Journal of Plant Nutrition and Soil Science 168, 386–391. doi:10.1002/jpln.200421681

Raynaud, X., Nunan, N., 2014. Spatial ecology of bacteria at the microscale in soil. PLoS ONE 9. doi:10.1371/journal.pone.0087217

Rousk, J., Jones, D.L., 2010. Loss of low molecular weight dissolved organic carbon (DOC) and nitrogen (DON) in H2O and 0.5 M K2SO4 soil extracts. Soil Biology and Biochemistry 42, 2331–2335. doi:10.1016/j.soilbio.2010.08.017

Schack-Kirchner, H., Loew, C.A., Lang, F., 2020. The Cumulative Amount of Exuded Citrate Controls Its Efficiency to Mobilize Soil Phosphorus. Frontiers in Forests and Global Change 3, 1–12. doi:10.3389/ffgc.2020.550884

Schilling, O., Frick, O., Herzberg, C., Ehrenreich, A., Heinzle, E., Wittmann, C., Stülke, J., 2007. Transcriptional and Metabolic Responses of Bacillus subtilis to the Availability of Organic Acids: Transcription Regulation Is Important but Not Sufficient To Account for Metabolic Adaptation. Applied and Environmental Microbiology 73, 499–507. doi:10.1128/AEM.02084-06

Schimel, J.P., Schaeffer, S.M., 2012. Microbial control over carbon cycling in soil. Frontiers in Microbiology 3, 1–11. doi:10.3389/fmicb.2012.00348

Schimel, J.P., Weintraub, M.N., 2003. The implications of exoenzyme activity on microbial carbon and nitrogen limitation in soil: a theoretical model. Soil Biology and Biochemistry 35, 549–563. doi:10.1016/S0038-0717(03)00015-4

Schmidt, H., Nunan, N., Höck, A., Eickhorst, T., Kaiser, C., Woebken, D., Raynaud, X., 2018. Recognizing patterns: Spatial analysis of observed microbial colonization on root surfaces. Frontiers in Environmental Science 6, 1–12. doi:10.3389/fenvs.2018.00061

Schmidt, M.W.I.I., Torn, M.S., Abiven, S., Dittmar, T., Guggenberger, G., Janssens, I.A., Kleber, M., Kögel-Knabner, I., Lehmann, J., Manning, D.A.C.C., Nannipieri, P., Rasse, D.P., Weiner, S., Trumbore, S.E., Kleber, M., Ko, I., 2011. Persistence of soil organic matter as an ecosystem property. Nature 478, 49–56. doi:10.1038/nature10386

Singh, B.K., Bardgett, R.D., Smith, P., Reay, D.S., 2010. Microorganisms and climate change: Terrestrial feedbacks and mitigation options. Nature Reviews Microbiology 8, 779–790. doi:10.1038/nrmicro2439

Spohn, M., Kuzyakov, Y., 2013. Distribution of microbial- and root-derived phosphatase activities in the rhizosphere depending on P availability and C allocation – Coupling soil zymography with 14C imaging. Soil Biology and Biochemistry 67, 106–113. doi:10.1016/j.soilbio.2013.08.015

Stockmann, U., Adams, M.A., Crawford, J.W., Field, D.J., Henakaarchchi, N., Jenkins, M., Minasny, B., McBratney, A.B., Courcelles, V. de R. de, Singh, K., Wheeler, I., Abbott, L., Angers, D.A., Baldock, J., Bird, M., Brookes, P.C., Chenu, C., Jastrow, J.D., Lal, R., Lehmann, J., O'Donnell, A.G., Parton, W.J., Whitehead, D., Zimmermann, M., 2013. The knowns, known unknowns and unknowns of sequestration of soil organic carbon. Agriculture, Ecosystems and Environment 164, 80–99. doi:10.1016/j.agee.2012.10.001

Stülke, J., Hillen, W., 2000. Regulation of Carbon Catabolism in Bacillus Species. Annual Review of Microbiology 54, 849–880. doi:10.1146/annurev.micro.54.1.849

Sulyok, M., Miró, M., Stingeder, G., Koellensperger, G., 2005. The potential of flow-through microdialysis for probing low-molecular weight organic anions in rhizosphere soil solution. Analytica Chimica Acta 546, 1–10. doi:10.1016/j.aca.2005.05.027

Uteau, D., Hafner, S., Pagenkemper, S.K., Peth, S., Wiesenberg, G.L.B., Kuzyakov, Y., Horn, R., 2015. Oxygen and redox potential gradients in the rhizosphere of alfalfa grown on a loamy soil. Journal of Plant Nutrition and Soil Science 178, 278–287. doi:10.1002/jpln.201300624

Védère, C., Vieublé Gonod, L., Nunan, N., Chenu, C., 2022. Opportunities and limits in imaging microorganisms and their activities in soil microhabitats. Soil Biology and Biochemistry 174, 108807. doi:10.1016/j.soilbio.2022.108807

Vetterlein, D., Carminati, A., Kögel-Knabner, I., Bienert, G.P., Smalla, K., Oburger, E., Schnepf, A., Banitz, T., Tarkka, M.T., Schlüter, S., 2020. Rhizosphere Spatiotemporal Organization–A Key to Rhizosphere Functions. Frontiers in Agronomy 2, 1–22. doi:10.3389/fagro.2020.00008

Vives-Peris, V., de Ollas, C., Gómez-Cadenas, A., Pérez-Clemente, R.M., 2020. Root exudates: from plant to rhizosphere and beyond. Plant Cell Reports 39, 3–17. doi:10.1007/s00299-019-02447-5

Vogel, C., Mueller, C.W., Höschen, C., Buegger, F., Heister, K., Schulz, S., Schloter, M., Kögel-Knabner, I., 2014. Submicron structures provide preferential spots for carbon and nitrogen sequestration in soils. Nature Communications 5, 1–7. doi:10.1038/ncomms3947

Warren, C.R., 2014. Organic N molecules in the soil solution: what is known, what is unknown and the path forwards. Plant and Soil 375, 1–19. doi:10.1007/s11104-013-1939-y

Wild, B., Schnecker, J., Alves, R.J.E., Barsukov, P., Bárta, J., Čapek, P., Gentsch, N., Gittel, A., Guggenberger, G., Lashchinskiy, N., Mikutta, R., Rusalimova, O., Šantrůčková, H., Shibistova, O., Urich, T., Watzka, M., Zrazhevskaya, G., Richter, A., 2014. Input of easily available organic C and N stimulates microbial decomposition of soil organic matter in arctic permafrost soil. Soil Biology and Biochemistry 75, 143–151. doi:10.1016/j.soilbio.2014.04.014

Wolfe, A.J., 2005. The Acetate Switch. Microbiology and Molecular Biology Reviews 69, 12–50. doi:10.1128/MMBR.69.1.12-50.2005

Yan, S., Yin, L., Dijkstra, F.A., Wang, P., Cheng, W., 2023. Priming effect on soil carbon decomposition by root exudate surrogates: A meta-analysis. Soil Biology and Biochemistry 178, 108955. doi:10.1016/j.soilbio.2023.108955

Chapter 2

A pulse of simulated root exudation alters the composition and temporal dynamics of microbial metabolites in its immediate vicinity

Soil Biology and Biochemistry 189 (2024) 109259

Contents lists available at ScienceDirect

Soil Biology and Biochemistry

journal homepage: www.elsevier.com/locate/soilbio

A pulse of simulated root exudation alters the composition and temporal dynamics of microbial metabolites in its immediate vicinity

Julia Wiesenbauer [a,b,*], Alexander König [a,c], Stefan Gorka [a,b], Lilian Marchand [d], Naoise Nunan [e,f], Barbara Kitzler [g], Erich Inselsbacher [c], Christina Kaiser [a,**]

[a] Division of Terrestrial Ecosystem Research, Centre for Microbiology and Environmental Systems Science, University of Vienna, Vienna, Austria, Djerassiplatz 1, A-1030, Wien, Austria
[b] Doctoral School in Microbiology and Environmental Science, University of Vienna, Vienna, Austria
[c] Institute of Soil Research, University of Natural Resources and Applied Life Sciences – BOKU, Peter-Jordan-Straße 82, 1190, Wien, Austria
[d] Institut Agro Rennes-Angers, France
[e] Sorbonne Université, CNRS, IRD, INRAE, P7, UPEC, Institute of Ecology and Environmental Sciences—Paris, 4 Place Jussieu, 75005, Paris, France
[f] Department of Soil & Environment, Swedish University of Agricultural Sciences, P.O. Box 7014, 75007, Uppsala, Sweden
[g] Department for Forest Ecology and Soil, Austrian Research Centre for Forests, Seckendorff-Gudent-Weg 8, 1131, Vienna, Austria

ARTICLE INFO

Keywords:
Reverse microdialysis
Root exudation
Short-chain fatty acids
Sugar metabolism
Rhizosphere priming effect
Oxygen depletion

ABSTRACT

Root exudation increases the concentration of readily available carbon (C) compounds in its immediate environment. This creates 'hotspots' of microbial activity characterized by accelerated soil organic matter turnover with direct implications for nutrient availability for plants. However, our knowledge of the microbial metabolic processes occurring in the immediate vicinity of roots during and after a root exudation event is still limited.

Using reverse microdialysis, we simulated root exudation by releasing a ^{13}C-labelled mix of low-molecular-weight organic C compounds at mm-sized locations in undisturbed soil. Combined with stable isotope tracing, we investigated the fine-scale temporal and spatial response of microbial metabolism, soil chemistry, and traced microbial respiration and uptake of exuded compounds.

Our results show that a 9-h simulated root exudation pulse leads to i) a large local respiration event and ii) alteration of the temporal dynamics of soil metabolites over the following 12 day at the exudation spot. Notably, we observed a threefold increase in ammonium concentrations at 12 h and increased nitrate concentrations five days after the pulse. Moreover, various short-chain fatty acids (acetate, propionate, formate) increased over the following days, indicating altered microbial metabolic pathways and activity. Phospholipid and neutral lipid fatty acids (PLFAs, NLFAs) of all major microbial groups were significantly ^{13}C-enriched within a 5 mm radius around the microdialysis probes, but not beyond. The highest relative ^{13}C enrichment was observed in fungal NLFAs, indicating that a significant proportion of the exuded compounds had been incorporated into fungal storage compounds.

Our findings indicate that the punctual release of low-molecular-weight organic C compounds into intact soil significantly changes microbial metabolism and activity in its immediate surroundings, enhancing mineralization of native organic nitrogen. This highlights the versatility of microbial metabolic pathways in response to rapidly changing C availability and their effectiveness in increasing nutrient availability near plant roots.

1. Introduction

Roots release a variety of C-rich compounds into their immediate environment (Jones et al., 2009; Canarini et al., 2019). These compounds consist of high-molecular weight compounds such as mucilage and proteins, and low-molecular-weight compounds such as amino acids, organic acids, and sugars (Badri and Vivanco, 2009; Vives-Peris et al., 2020). The latter are predominantly released at the

* Corresponding author. Division of Terrestrial Ecosystem Research, Centre for Microbiology and Environmental Systems Science, University of Vienna, Vienna, Austria, Djerassiplatz 1, A-1030, Wien, Austria.
** Corresponding author.
E-mail addresses: julia.wiesenbauer@univie.ac.at (J. Wiesenbauer), christina.kaiser@univie.ac.at (C. Kaiser).

https://doi.org/10.1016/j.soilbio.2023.109259
Received 18 July 2023; Received in revised form 17 November 2023; Accepted 23 November 2023
Available online 1 December 2023
0038-0717/© 2023 The Authors. Published by Elsevier Ltd. This is an open access article under the CC BY license (http://creativecommons.org/licenses/by/4.0/).

root tips, either through passive diffusion or active exudation (Badri and Vivanco, 2009; Jones et al., 2009; Canarini et al., 2019). Consequently, due to their constant movement through the soil, tips of growing roots create distinct 'exudation hotspots' of transiently high concentration of low-molecular-weight C compounds (Vogel et al., 2014).

Such pulses of easily available C are thought to stimulate the activity of previously partly starving and thus inactive microbes in the surrounding of the pulse (De Nobili et al., 2001; Mondini et al., 2006; Kuzyakov et al., 2015; Vetterlein et al., 2020). This process is marked by an immediate respiration of the assimilated C (Butler et al., 2004; Kaštovská and Šantrůčková, 2007), followed by an enhanced respiratory activity driven by increased microbial biomass turnover (Blagodatskaya and Kuzyakov, 2008), which is eventually followed by accelerated SOM decomposition - a phenomenon called the rhizosphere priming effect (Kuzyakov, 2002, 2010; Dijkstra et al., 2013; Haichar et al., 2014; Huo et al., 2017). While priming effects are observed in the majority of investigated cases, instances of no or 'negative' priming (i.e. retardation of SOM decomposition) have been reported (Kuzyakov, 2002; Dijkstra et al., 2013; Luo et al., 2016). These findings underscore the complexity of the rhizosphere C-cycling and variability of microbial interactions.

As a result of this accelerated microbial activity, a variety of microbial metabolites is released into the soil solution. Pulses of root exudation and their consequences for microbial activity are referred to as 'hot moments' in soil, implying that these changes in the process rates and metabolite levels last only for a short duration (Kuzyakov et al., 2015). The amount and composition of microbial metabolites released likely reflect the microbial processes occurring in response to the root exudation event but have not been previously measured at the hotspot. Moreover, the actual timeframe of accelerated or altered process rates at hotspots is uncertain and could range from minutes to days (Kuzyakov et al., 2015; Vetterlein et al., 2020). By studying the dynamics of soil metabolites that emerge in response to root exudation, valuable insights can be gained into the metabolic pathways involved in the degradation and transformation of exudate compounds, as well as the timeframe and persistence of the rhizosphere priming effect.

A substantial fraction of the C exuded by roots is incorporated into the rhizosphere microbial biomass (Butler et al., 2004; Denef et al., 2007). It was observed that exudates of young beech trees where preferentially utilized by gram-negative bacteria and fungi (Esperschütz et al., 2009), while gram-positive bacteria appeared to have little reliance on rhizodeposits but perhaps benefitted from later priming effects (Butler et al., 2003; Esperschütz et al., 2009; Balasooriya et al., 2013). Conversely, Cesarz et al. (2013) reported that beech roots did not affect bacterial biomass, but rather led to an increase in the fungi-to-bacteria ratio. This highlights how root exudates may be preferentially utilized by certain microbial groups and shape the microbial community composition (Zhalnina et al., 2018; Seitz et al., 2022), though the specific outcomes remain uncertain.

Researchers have employed various approaches, e.g. rhizoboxes (Wenzel et al., 2001; Chaignon et al., 2002; zu Schweinsberg-Mickan et al., 2010; Spohn et al., 2013) or planar optodes (Santner et al., 2015; Li et al., 2019), to study a range of root and rhizosphere processes, including spatial distribution of microbes, enzymes and chemical compounds. A common drawback of these tool is the limited capacity of time-points, spots, and analytes they can assess, and their struggle with the heterogeneous soil structure. Moreover, such *in situ* studies based on root exudates present their own unique challenges, as the composition and concentration of root exudates cannot be controlled, and the presence of root respiration further complicates the analysis.

Thus, various studies have added powders or solutions containing compounds found in exudates to sieved soil in an attempt to explore e.g. the mechanisms behind rhizosphere priming effects (Basiliko et al., 2012; Nottingham et al., 2012; Koranda et al., 2013; Wild et al., 2014; Girkin et al., 2018; Jilling et al., 2021) or changes in the microbial community (Shi et al., 2011; Mau et al., 2015; Papp et al., 2020). In contrast to root exudation which creates localized high C concentrations with strong concentration gradients (Kuzyakov and Razavi, 2019; Vetterlein et al., 2020), the substrate addition results in uniform distribution of moderately enhanced C availability throughout the whole soil volume, which may affect microbial responses to substrate input considerably. In addition, the intricate mechanisms underlying the rhizosphere priming effect critically depend on the physico-chemical and biotic micro-environment of the root exudation hotspot, which is likely disintegrated by the abovementioned approaches.

Microdialysis allows to release artificial root exudates at small spots into undisturbed soil while at the same time collecting metabolites from the surrounding soil solution. In its classic application, metabolites are collected from the soil solution via a diffusion gradient across a small semi-permeable membrane inserted into the soil (Inselsbacher et al., 2011; Oyewole et al., 2014). By reversing the concentration gradient, i.e. by pumping high levels of low-molecular-weight compounds along the inside of the membrane, compounds can be released via passive diffusion at distinct soil spots (Buckley et al., 2022; König et al., 2022). This way it is possible to create a hotspot of high C concentration, akin to passive root exudation. Compared to Rhizon samplers, which also allow to mimic root exudation by releasing a solution (Kuzyakov et al., 2007; Keiluweit et al., 2015; Baumert et al., 2018), microdialysis has the benefit of not generating a mass flow into the soil by relying exclusively on diffusion. Moreover, the 'reverse' microdialysis approach offers the unique advantage of combining the release of organic compounds with the simultaneous collection of (other) soil metabolites (as by 'classic' microdialysis) at high temporal resolution.

The aim of this study was the detailed analysis of the fine-scale temporal dynamics of microbial activity and soil chemistry in response to a simulated root exudation pulse right at the exudation spot in intact soil. Specifically, we addressed the following questions:

(1) Does a 'root exudation' pulse alter the dynamics of soil metabolites at the exudation hotspot?
(2) What is the timescale and pattern of substrate- and SOM-derived microbial respiration following a simulated root exudation pulse?
(3) Which microbial groups are involved in the metabolism of 'root exudates' in the days following the pulse?

To achieve this, we used reverse microdialysis to release a mixture of ^{13}C-labelled sugars (fructose, glucose) and organic acids (acetate, succinate) into undisturbed soil cores over a period of 9 h while simultaneously collecting metabolites from the soil solution for 12 days. Additionally, we assessed substrate-induced respiration and SOM mineralization, and the uptake of ^{13}C-labelled substrate into different microbial groups. We observed a sequence of microbial processes over time and their limitation in space around the artificial root, marked by long-lasting effects of simulated root exudation on soil biogeochemistry and microbial activity.

2. Material and methods

2.1. Soil sampling

Soil was sampled in a managed mature beech (*Fagus sylvatica*) forest (average tree age around 90 yrs) in Klausen-Leopoldsdorf, Austria (48°07′ N, 16° 03′ E, 510 m asl). The soil is a Dystric Cambisol (over flysch) with a pH of 4.16 ($CaCl_2$) and an organic C and total N content of 5.01% and 0.38%, respectively (Kitzler et al., 2006; Brandstätter et al., 2013; König et al., 2022). We sampled soil on June 6th, 2018 at five locations along a horizontal transect at a distance of 60 cm each. After removing the litter layer, we took triplicate soil cores (10 cm diameter × 6 cm depth) right next to each other from the uppermost soil at each of the five locations. From each triplicate, one soil core was sieved, and the gravimetric soil water content was determined, which ranged between 44 and 53%. Per site, one of the two remaining intact soil cores was used to set up the mesocosms for the experiment (the third soil core served as

a backup).

2.2. Experiment design and microdialysis setup

Paired mesocosms (one for pulse simulation and one for control) were set up for each of the five soil sampling sites by coring two smaller cores (2.8 cm diameter × 3 cm height) from one larger soil core. Intact mesocosm cores were carefully placed in modified polypropylene centrifuge tubes (Greiner Bio-One, 50 ml), which were cut off 4 cm below their screw caps and turned upside-down, so they stood in their closed screw caps (opening screw caps allowed easy collection of the soil at the end of the experiment). One of the two paired mesocosm received a labile substrate pulse (n = 5) while the second mesocosm acted as a control (n = 5), receiving only water.

In order to maximize the soil volume affected by microdialysis within each undisturbed soil core, two microdialysis probes (CMA 20, 20 kDa molecular weight cut-off, 1 cm membrane length, 0.5 mm outer diameter; CMA Microdialysis AB, Kista, Sweeden) were inserted into each mesocosm soil core. To avoid damaging the microdialysis probes, holes were pre-made with steel needles (0.5 mm diameter) to help guide the probes into the soil, which was then gently compressed around it. To ensure that only one sample per hour per mesocosm was collected, the tubes of the two microdialysis probes were joined with a T-connector (Micro T, CMA Microdialysis AB, Kista, Sweden) (Fig. S1). Microdialysis probes were perfused with ultrapure water (Milli-Q) containing low concentrations of KCl (3.848 μM) and MgSO4 (1.595 μM) (from now on called 'background solution') at a perfusion flow rate of 2.5 μl min^{-1} per microdialysis probe using syringe pumps (CMA 4004, CMA Microdialysis AB, Solna, Sweden). The purpose of adding KCl and $MgSO_4$ to the perfusate was to prevent the formation of an osmotic gradient between the perfusate and the soil solution (Demand et al., 2017; Warren, 2018). Samples (dialysates) were collected in refrigerated fraction collectors (CM4 470, CMA Microdialysis AB, Solna, Sweden) and subsequently stored at −20 °C until analysis.

During an initial 3-h period, all microdialysis membranes were perfused with the background solution. This was done to facilitate the formation of water bridges within the soil and to analyse initial concentrations of soil compounds collected in the dialysates. In the following 9 h, we implemented a pulse of labile substrate using reverse microdialysis to mimic root exudation, similar to the diurnal carbon release dynamics observed in natural hotspots with heightened exudation during daylight hours (Murray et al., 2004; Cardon and Gage, 2006). A labile substrate mixture consisting of ^{13}C-labelled acetate, succinate, fructose and glucose (each 125 μmol C l^{-1}, 98 at% ^{13}C, uniformly labelled, Sigma-Aldrich) was added to the background solutions of one mesocosms of each pair (n = 5). These compounds were selected based on their prevalence in natural root exudates of beech trees (Smith, 1976) and to represent a range of chemical structures (sugar, organic acid) commonly found in root exudates (Vives-Peris et al., 2020). We deliberately refrained from including nitrogen-containing compounds, despite acknowledging their significance within root exudate (Drake et al., 2013; Edwards et al., 2018; Chari and Taylor, 2022), in order to focus specifically on the impact of carbon alone - a key element in the root exudate-microbe-soil interaction.

After this pulse, the perfusate was switched back to pure background solution. Control mesocosms received background solution throughout the whole experimental as perfusate. For the first 3 days (72 h), microdialysis was kept running constantly in all mesocosms and dialysates were collected hourly. Subsequently, the pumps were turned off and only switched on for 4 h on day 5, 7, and 12 to collect additional dialysate samples. Throughout the experiment, we monitored the water content by weighing the mesocosms and adjusting it, if necessary, by pipetting Milli-Q onto the surface.

2.3. Microbial responses to simulated root exudation

2.3.1. CO_2 analysis – gas sampling and estimation of respiration rates

Mesocosms were placed in airtight jars fitted with septa for taking gas samples (see Fig. S1). The microdialysis tubing was inserted through the septa to allow simultaneous dialysate collection. We took headspace gas samples at multiple time points during the experiment: on day 1 (hours 2, 6, 7, 8, 9, 10, 13), on days 2 and 3 (twice), and once on days 5, 7 and 12. The ^{12}C–CO_2 and ^{13}C–CO_2 concentration of gas samples were measured by a headspace gas sampler (GasBench II, Thermo Fisher Scientific, Bremen, Germany) couple to a isotope ratio mass spectrometry (Delta V Advantage, Thermo Electron, Bremen, Germany). When taking gas samples, the mesocosm jars (105 ml volume) were closed airtight, the first gas sample (15 ml) was taken and the removed air was replaced with artificial air (200 ppm CO_2) to avoid sub-atmospheric pressure. The second gas sample was taken after 60 min incubation time and the mesocosm jars were opened. The CO_2 concentration and ^{13}C signature of the second sample was corrected for the added artificial air. The total respiration rate and its atom percent ^{13}C (at% ^{13}C) signature were calculated from ^{12}C- and ^{13}C–CO_2 concentration differences between the initial gas sample and the second, corrected, gas sample. The percentage and total amount of respiration originating from the added ^{13}C-labelled substrate and from the native SOM were calculated using a two-pool mixing model with the ^{13}C signature of the added substrate (98 at% ^{13}C) and natural abundance of ^{13}C in the respiration of the control mesocosms (1.08 at% ^{13}C) as end members. For a detailed outline of the calculations see the supplementary materials.

It should be noted that the mesocosms that were to receive the labile substrate pulse exhibited a lower average respiration per gram of mesocosm-soil prior to the substrate pulse and lower SOM-derived respiration persisted throughout the first part of the experiment (Fig. S2). We attribute this to an uneven distribution of stones and organic matter across the mesocosms observed during soil harvest, which we could not control for before the experiment as we did not sieve the soil. To account for this initial variability, we calculated a normalized SOM-derived respiration, in which all respiration measurements were put in relation to the initial respiration (% of initial respiration, Fig. 1). This allows a more accurate comparison of the effect of the labile substrate addition on respiration (Fig. 1). For the original data in nmol CO_2 g^{-1} soil $hour^{-1}$, we refer the reader to Supplementary Fig. S2.

Additionally, we estimated the 'background' SOM-derived respiration in the immediate surrounding of each microdialysis probe, with the assumption that SOM-derived respiration was not locally affected by the substrate input. We calculated the fraction of the SOM-derived respiration obtained per soil core around the microdialysis probe as a cylindrical volume as:

$$R_{background} = R_{SOM} \times DW_{mesocosm} \times \frac{V_{cylinder}}{V_{mesocosm}}$$

where $R_{background}$ is the SOM-derived respiration (nmol CO_2 h^{-1} $V_{cylinder}^{-1}$) within $V_{cylinder}$, the cylindrical soil volume around the microdialysis probe, R_{SOM} is the SOM-derived respiration of the mesocosm (nmol CO_2 h^{-1} g^{-1}), $DW_{mesocosm}$ is the soil dry weight of the mesocosm (g), and $V_{mesocosm}$ is the volume of the mesocosm (mm^3).

We selected a 1-mm radius for our calculations as we aimed to estimate substrate- and SOM-derived respiration over a short 9-h period during which substrate was released. This falls at the lower end of range observed in several studies, which have reported plant root exudates occurring between 0.2 and 2 mm away from the surface of the roots (Falchini et al., 2003; Herman et al., 2006; zu Schweinsberg-Mickan et al., 2010). Occasionally, however, studies have found exudates to disperse up to 5–12 mm (Sauer et al., 2006; Dessureault-Rompré et al., 2007; Finzi et al., 2015).

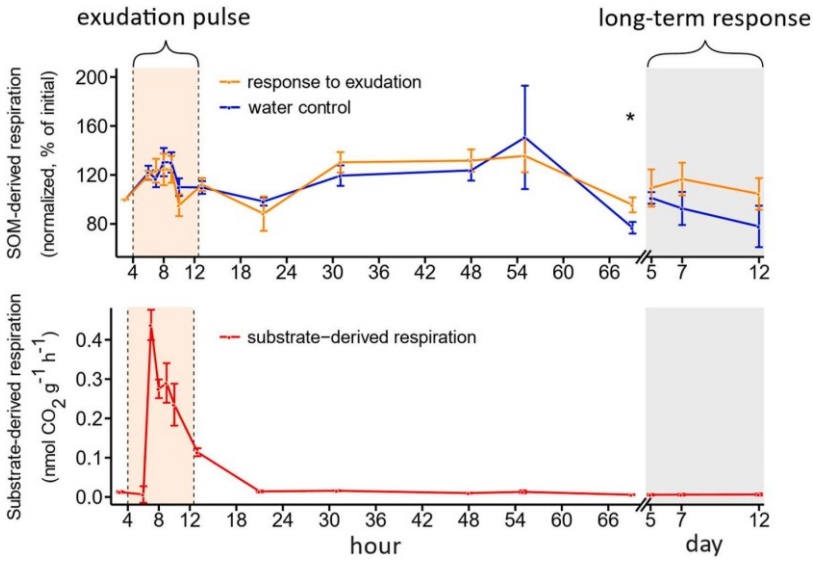


Fig. 1. Temporal dynamics of normalized SOM-derived respiration rate (percentage of initial respiration) and substrate-derived respiration rate. The time of the 9-h long pulse from labile substrate (4–12 h) is highlighted as an orange background and the long-term response (5–12 days) is highlighted as a grey background. The short-term response is depicted in hours and the long-term effects in days and are separated by an x-axis break at hour 72. Top: The normalized SOM-derived respiration rate normalized by dividing by the initial respiration rate in response to the exudation pulse (orange) compared to a water control (blue). Bottom: The respired labile substrate (nmol CO_2 g^{-1} h^{-1}) is shown in red. Depicted are the means and standard error of the mean (n = 5) with asterisks indicating significant differences in response to exudation pulse.

2.3.2. Dialysate analysis (soil chemistry & metabolites)

We measured organic and inorganic anions and sugars in the dialysates using HPLC (Dionex ICS 5000+, Thermo Fisher, Germany). To optimize the chromatographic analyses, we pooled the consecutive hourly dialysates and combined 2, 3 or 4 dialysates for periods 1–20 h, 21–29 h and remaining dialysates, respectively.

Anions were measured on a Dionex IonPac AS11-HC (2 × 250 mm) column with a Dionex IonPac AG11-HC (2 × 50 mm) guard column at a constant flow rate of 0.38 ml min^{-1} with a KOH solvent. We analysed acetate, propionate, formate, butyrate, chloride, nitrate, succinate, malate, sulfate, oxalate, phosphate, and citrate. The HPLC run started at 1 mM KOH (10 min), then increased to 15 mM (1 mM min^{-1}), then to 60 mM (5 mM/min) and kept at this concentration for 5 min and finally the run was ended with 7 min at 1 mM. Sugars (glucose, fructose, galactose, sucrose) were measured on a Thermo CarboPac PA20 (0.4 × 150 mm) column with a Thermo CarboPac PA20G (0.4 × 35 mm) guard column at a constant flow rate of 8 μl min^{-1} with a KOH solvent. We started the run with 10 min of 10 mM KOH, increased to 50 mM for 5 min, increased to 200 mM for 5 min and ended the run with 5 min at 20 mM. The ammonium concentration in dialysates was determined colorimetrically (Kandeler and Gerber, 1988; Hood-Nowotny et al., 2010).

2.3.3. PLFA and NLFA analyses

At the end of the experiment (day 12), we harvested the soil to investigate the ^{13}C enrichment of different microbial groups in soils that received labile ^{13}C-labelled substrate. We harvested soil in the surrounding (<5 mm) and distant (>5 mm, Fig. S3) radius of the microdialysis probes by coring the soil with a rectangular tube (1 cm × 1.5 cm) with the two microdialysis probes in the centre. Afterwards the soil was homogenised by mixing and stones were removed with a tweezer. To determine which microbial groups took up the substrate, we extracted the phospholipid and neutral lipid fatty acids (PLFAs, NLFAs) and used them as biomarkers for different microbial groups and fungal storage, respectively.

Lipids were extracted from lyophilized soils with a mixture of chloroform, methanol, and citrate buffer (v/v/v = 1:2:0.8; (Bligh and Dyer, 1959; Frostegård et al., 1991). Neutral lipids and phospholipids were consecutively eluted on silica solid phase extraction columns with chloroform and methanol, with an acetone washing step in-between. The extracts were subsequently derivatized via mild alkaline methanolysis. The resulting fatty acid methyl esters were analysed on a gas chromatograph (Trace GC Ultra, Thermo Scientific, Germany) coupled to a mass spectrometer (ISQ, Thermo Scientific, Germany) for fatty acid identification and quantification, and on a GC-Ultra (Thermo Fisher Scientific, Milan, Italy) coupled to an isotope ratio MS (Finnigan Delta-V, Thermo Fisher Scientific, Bremen, Germany) via a GC IsoLink (Thermo Fisher Scientific, Bremen, Germany) for determination of isotopic $^{13}C/^{12}C$ ratios. We used nonadecanoic acid methyl ester as an internal standard for quantification, and bacterial and fungal fatty acid methyl esters (BAME CP mix, Supelco; 37 Component FAME mix, Supelco) as qualitative external standards.

Fatty acids of the phospholipid and neutral lipid fractions were assigned to the same phylogenetic groups. Unless otherwise noted, fatty acids were assigned according to (Willers et al., 2015). We assigned the unsaturated fatty acids 14:0, 15:0, 16:0, 17:0 and 18:0 as general microbial markers (data not shown), the mono- and cyclopropyl-unsaturated fatty acids 16:1ω5 (Phillips et al., 2002), 16:1ω7, 17:1ω7, cy17:0 and cy19:0 as markers for gram-negative bacteria, the terminally branched fatty acids i15:0, a15:0, i16:0, i17:0 and a17:0 for gram-positive bacteria (excluding Actinobacteria) (Joergensen and Wichern, 2008), the methyl-branched fatty acids 10Me18:0 and 10Me19:0 for Actinobacteria, and the fatty acids 18:1ω9c, 18:1ω9t and 18:2ω6,9 for fungi. However, we must note that although the 18:1ω9t is reported as specific for fungi (Balser et al., 2005) it can also show patterns similar to gram-negative bacteria biomarkers.

We calculated isotopic enrichment in individual PLFAs and NLFAs as the difference in relative ^{13}C-enrichment of labelled samples to unlabelled control as at% ^{13}C excess (Kaiser et al., 2015). The relative ^{13}C content (μg ^{13}C excess) of individual PLFAs and NLFAs was calculated as relative ^{13}C-enrichment weighted by the mean abundance (in μg C in

FAs g^{-1} dry soil).

2.4. Statistical analysis

All statistical analysis were performed using R (R Core Team, 2022) and all graphs were plotted using ggplot2 (Wickham, 2016). We removed outliers that had values that were higher or lower three times the interquartile range. We tested the normality of the data using Shapiro-Wilk test, and homogeneity of variances using the Levene test.

We tested significant differences of compound concentrations per time point using Mann-Whitney *U* test (Table 1) since the data were neither normal distribution nor showed homogeneity of variances, regardless of data transformation. We log-transformed the respiration data (SOM-derived respiration and normalized SOM-derived respiration) and tested significant differences from control for each time point with Student's two sample *t*-test. The µg C and at% ^{13}C values of PLFA and NLFA biomarker groups were tested for differences between amended mesocosms receiving an exudation pulse compared to the water controls using a Student's two sample *t*-test (Table 2). Moreover, the µg C, µg ^{13}C excess and at% ^{13}C excess of fatty acid biomarker groups were tested for differences between PLFAs and NLFAs using a Student's two sample *t*-test or Mann-Whitney *U* test (Table 3).

3. Results

3.1. Transfer rates and retrieval rates of added labile substrate

The transfer rate of compounds i.e., the percentage of compounds in the perfusate that were actually released into the soil (König et al., 2022), were 31.84% (±0.87 se) for acetate, 15.06% (±1.08) for succinate, 9.15% (±1.21) for glucose and 5.65% (±1.7) for fructose, averaged over the 9-h pulse (Fig. 2: acetate, Fig. S4: succinate, glucose, fructose). This transfer rates correspond to an average 113.43 (±4.89 se) nmol C for acetate, 53.1 (±8.31) nmol C of succinate, 27.92 (±7.41) nmol C of glucose and 18.23 (±5.24) nmol C of fructose, or in sum 212.68 (±22.17) nmol C per mesocosm. The 'retrieval' rates i.e., the percentage of initially exuded compounds, which were retrieved back in the first 2 h after the pulse after switching back to background solution were 6.32% (±0.28 se) for acetate, 16.51% (±4.26) for succinate, 27.67% (±2.99) for glucose and 47.62% (±10.78) for fructose. This retrieval rates correspond to an average 7.14 (±0.33) nmol C acetate, 7.68 (±1.15) nmol C succinate, 9.38 (±0.36) nmol C glucose, and 9.63 (±0.88) nmol C fructose, or in sum 34.53 (±2.30) nmol C per mesocosm. Note that for sugars in particular, the transfer rates dropped to nearly zero percent after 4 h with simultaneously high retrieval rates (Fig. S4), indicating a saturation in sugars around the microdialysis probe after not being removed quickly enough by biological or physical processes.

3.2. Temporal pattern of several soil metabolites is altered after a pulse of labile C compounds over the following 2–12 days

Overall, we found that several soil metabolites, such as acetate, propionate, formate and ammonium, displayed distinct temporal patterns in the hours following the labile substrate pulse, but we also observed longer-term changes in acetate, formate, nitrate and sulfate concentrations several days later (Fig. 2, Table 1). The concentrations of certain small chain organic acids peaked about 24 h after the labile C input (Fig. 2, Table 1). Specifically, acetate concentrations increased significantly 9 h after the end of the input pulse (hour 20) and remained elevated for 34 h (i.e., until hour 53) (Fig. 2, Table 1). Similarly, in the same period, ammonium and propionate concentrations significantly increased compared to the control (hours 26–45 and hours 29–45, respectively). This increase in organic acids and ammonium was accompanied by a significant increase of sulfate during hours 29–33. Following the organic acid peak (acetate, ammonium, propionate) we detected a trend towards higher formate and sulfate concentration. We

Table 1
Statistics on changes in concentrations of compounds collected from soil solution by microdialysis (Fig. 2). Differences in soil metabolite concentration (µM) between soils that received a 9-h labile substrate pulse (n = 5) and a water control (n = 5) were tested by time period (2, 3, or 4 h pooled dialysate). The compounds acetate, succinate, fructose, and glucose were part of the 9-h labile substrate pulse (hour 4–12). The time points for the long-term response are given in days (day 5, 7 and 12). Empty cells indicate that the compound was not detected at the time point. Significant differences ($p < 0.05$) are indicated with asterisks next to an arrow indicating if concentrations were significantly higher (↑*) or lower (↓*) than the water control.

	hour	2	exudation pulse																	day				
			4	6	8	10	12	14	16	18	20	23	26	29	33	37	41	45	49	53	57	61	65	69	5	7	12
acetate		–	↑*	↑**	↑**	↑**	↑**	↑**	–	↓*	↑**	↑*	↑*	↑**	↑**	↑*	↑*	↑*	↑*	↑**	↑*	–	↑*	↑*	↑**	↑*	↑*	↑**
succinate		–	↑*	↑*	↑*	↑**	↑**	–							↑*	–	–	–	–	–							–
fructose			↑*	↑**	↑*	↑**	↑**	↑*																			
glucose			↑*	↑**	↑*	↑**	↑**	↑*																			
propionate		–	–	–	–	–	–	↓*	↓*	↓*	–	–	–	↑**	↑**	↑**	↑*	↑*	–	–	–	–	–	–	–	–	–
formate		–	–	↓*	–	–	–	↓**	↓**	↓**	↑*	–	–	–	–	–	–	–	–	–	–	–	–	–	–	–	↑**
ammonium		–	–	–	–	–	–	–	–	↓*	↓*	–	↑**	↑**	–	↑**	↑**	↑*	–	–	–	–	–	–	–	–	–
nitrate		–	–	–	–	–	–	–	–	–	–	–	–	–	–	–	–	–	–	–	–	–	–	–	–	–	↑**
sulfate		–	–	–	–	–	–	–	–	–	–	–	–	↑**	↑*	–	–	↑*	↑*	–	–	–	–	–	–	–	↑*
citrate		–	–	–	–	–	–	–	–	–	–	–	–	–			–										
oxalate		–	–	–	–	–	–	–	–	–	–	–	–	–	–	–	↑*	–	–	–	–	–	–	–	–	–	–

Mann-Whitney *U* test, p-value: >0.05 -, <0.05 *, <0.01 **, <0.001 ***.

Table 2
Response of phospholipid fatty acids (PLFAs) and neutral lipid fatty acids (NLFAs) in the proximity (<5 mm) of the microdialysis probe, 12 days after the simulated root exudation event. The differences of µg C and at% ^{13}C values (PLFA, NLFA) between exudation treatment (n = 5) and water control (n = 5) were tested. Depicted are p-values and asterisks for significant differences ($p < 0.05$).

data	biomarker	fungi			bacteria		
		18:2ω6,9	18:1ω9c	18:1ω9t	gram -	gram +	actino
µg C	PLFA	n.s.	n.s.	n.s.	n.s.	0.015 *	n.s.
	NLFA	n.s.	n.s.	n.s.	n.s.	n.s.	n.s.
at% ^{13}C	PLFA	n.s.	0.009 **	0.018 *	0.029 *	0.005 **	0.019 *
	NLFA	0.004 **	0.010 *	0.015 *	0.040 *	0.010 *	0.019 *

Student's *t*-test, p-value: >0.05 n.s., <0.05 *, <0.01 **, <0.001 ***.

Table 3
Differences between phospholipid fatty acids (PLFAs) and neutral lipid fatty acids (NLFAs) in the proximity (<5 mm) of the microdialysis probe, 12 days after the simulated root exudation event (n = 5). The differences between PLFA and NLFA for µg ^{13}C excess, µg C and at% excess were tested. Depicted are p-values and asterisks for significant differences ($p < 0.05$).

data	fungi			bacteria		
	18:2ω6,9	18:1ω9c	18:1ω9t	gram -	gram +	actino
µg C	n.s.	0.0 ***	0.0 ***	0.0 ***	0.0 ***	0.006 **
µg ^{13}C excess	n.s.	n.s.	0.032 *	n.s.	0.016 *	n.s.
at% ^{13}C excess	n.s.	0.021 *	n.s.	n.s.	n.s.	n.s.

Student's *t*-test (Mann-Whitney *U* test: µg ^{13}C excess), p-value: >0.05 n.s., <0.05 *, <0.01 **, <0.001 ***.

observed a slight increase in nitrate concentrations in the dialysates of all mesocosms over the first three days, but no significant differences between the ones that received an input pulse and the controls.

In the days 5–12, in a longer-term response to the labile substrate input, acetate levels again rose significantly on the third day and remained elevated until day 12. At the end of the experiment, the concentrations of acetate, formate, nitrate and sulfate were significantly higher in the dialysates of the samples that had received the input pulse compared to the control samples (Fig. 2). All other compounds (succinate, oxalate, citrate, glucose, and fructose) were detected in negligible amounts and were not clearly affected by the labile substrate input (Fig. S4). Butyrate, malate, phosphate, chloride, galactose and sucrose were not detected in our samples.

3.3. Rapid microbial respiration of labile substrate during the pulse precedes delayed changes in SOM respiration

Our measurements of ^{13}C concentration in the CO_2 produced during the incubation showed that the added mixture of ^{13}C-labelled C compounds was readily taken up and rapidly respired (Fig. 1). The substrate-derived respiration increased sharply 3 h after the start of the labile substrate pulse and remained elevated for the duration of the 9-h long substrate pulse. Out of the total substrate added, the microbes respired 34%, of which 45% was respired during the initial 2–3 h of the pulse (data published in: König et al., 2022). In the hours following the pulse the substrate-derived respiration levelled off (Fig. 1). In contrast, the SOM-derived respiration was unaffected initially (Fig. 1). On day 3, however, soils that received a labile substrate pulse respired significantly more SOM than the control soils (Welch's *t*-test, $t(6) = -2.52$, $p = 0.045$) when compared in % of their respective initial SOM respiration (Fig. 1). We observed a similar, albeit non-significant, trend of higher normalized SOM-respiration during later time points (day 5, 7, 12).

3.4. Estimated increase in CO_2 respiration at the exudation hotspot

In order to obtain a rough estimate on the magnitude of increase of

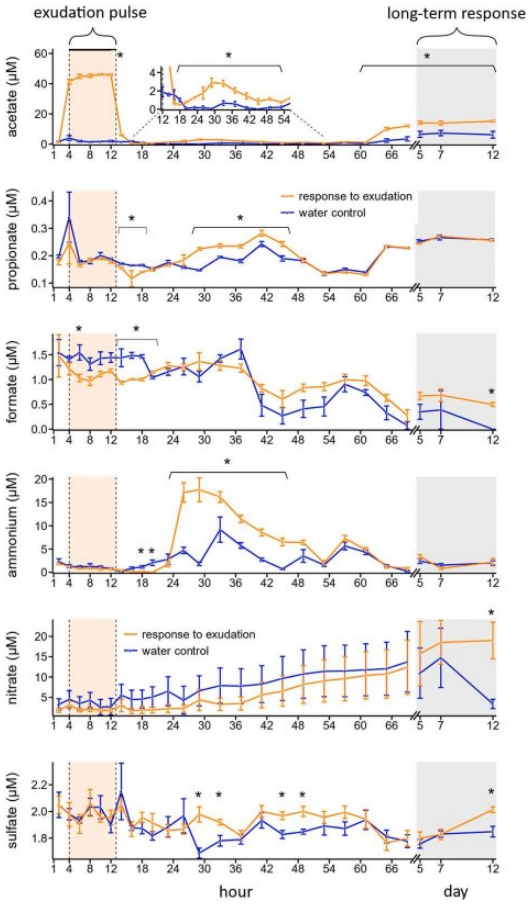


Fig. 2. Temporal dynamics of six soil metabolites (µM; acetate, propionate, formate, ammonium, nitrate, sulfate) in response to a 9-h long substrate pulse (orange) compared to a water control (blue). The time of the exudation pulse (4–12 h) is highlighted as an orange background and the long-term response (5–12 days) is highlighted as a grey background. The short-term response is depicted in hours and the long-term effects in days and are separated by an x-axis break at hour 72. Shown are the mean and standard error of the mean (n = 5) of concentrations in collected dialysate. Acetate was part of the labile substrate pulse and its initial concentration in perfusate is depicted as a black horizontal line. The difference between the black horizontal line and the acetate measurements in dialysates illustrate the net transfer into the soil. Asterisks indicate that the response to labile substrate significantly differs from the water control. Detailed statistics are shown in Table 1. For net transfers and temporal dynamics of succinate, glucose and fructose, as well as temporal dynamics of citrate and oxalate (n.s.) see Fig. S4.

microbial respiration right at the exudation hotspot, we calculated SOM-derived and substrate-derived respiration for a volume within a 1 mm radius around the microdialysis probes, which we assume to be directly affected by the substrate input. We calculated the fraction of the SOM-derived respiration obtained per soil core that occurred in a cylindrical volume of 1 mm radius and 10 mm height, with the aim to estimate the 'background' SOM-derived respiration in the immediate surrounding of each microdialysis probe. We then calculated the cumulative respiration within the hypothetical 1 mm diameter, consisting of the calculated SOM-derived respiration and the measured ^{13}C-substrate-derived respiration (Fig. 3), which we assumed to occur to 100% in the surrounding of the probes (Fig. 4). Based on these assumptions, during the second half of the pulse (hour 7–10), an average additional 10.15 nmol CO_2 (±1.7 se, n = 5) were respired from the added substrate in the immediate surrounding of each microdialysis probe, approximately doubling the respiration within this volume relative to the 'background' SOM-derived respiration (9.36 ± 1.46 se nmol CO_2) (Fig. 3). These calculations rely on our assumption that root exudates would not go beyond a 1 mm radius within 9 h, and that there is no local increase in SOM-derived respiration triggered by the released C compounds. If we would vary the assumed range of root exudates to 0.5, 2 or 5 mm radius within which 2.34, 37.45 and 234.06 nmol CO_2 would be respired from SOM, substrate-derived respiration would increase CO_2 production in this volume by 434, 27 and 4 %, respectively. If there was a local increase in SOM-derived respiration within the chosen radius (which we were unable to measure), we would underestimate the increase in respiration due to the added substrate, as our calculation only includes the substrate-derived respiration plus a volume-based aliquot of the total SOM-derived respiration of the core.

3.5. *Phospholipid and neutral lipid fatty acids were ^{13}C enriched in vicinity of the exudation hotspot*

All PLFA and NLFA biomarkers, except for the fungi-specific PLFA 18:2ω6,9, were significantly ^{13}C enriched in response to the labile substrate pulse within a 5 mm radius around the microdialysis membranes (at% ^{13}C: Fig. S5, Table 2). There was no significant enrichment in ^{13}C in biomarkers in the soil sampled further away i.e., between 5 and 10 mm around the membranes (Fig. S3). Within the 5 mm radius, the NLFA fungal biomarker 18:1ω9c showed the highest relative ^{13}C enrichment compared to the natural abundance control and was also significantly higher compared to its corresponding PLFA biomarker (at% ^{13}C excess: Fig. 4). The at% ^{13}C excess of the PLFAs and NLFAs from other microbial groups showed no significant differences (Table 3, Fig. 4).

When comparing absolute amounts of μg ^{13}C excess of PLFAs and NLFAs, we found significantly more ^{13}C in PLFA than in NLFA of 18:1ω9t (fungi), gram-positive bacteria, and gram-negative bacteria (not significant), while the fungal marker 18:1ω9c had a tendency (albeit not significant) for higher amounts of ^{13}C excess in NLFAs compared to PLFAs (μg ^{13}C excess: Fig. 4, Table 3). Since we did not find differences in the relative ^{13}C enrichments (at% ^{13}C excess) between PLFAs and NLFAs for 18:1ω9t, gram-negative and gram-positive bacteria, the observed differences in absolute ^{13}C enrichments need to be attributed to the higher absolute amounts (μg C) of PLFAs compared to NLFAs (μg C: Fig. S5).

The labile substrate input significantly increased the microbial biomass (i.e., μg C in PLFAs) of the gram-positive bacteria, but did not affect the biomass of any of the other groups. It also did not affect NLFAs of any microbial group (μg C: Fig. S5). NLFA concentrations were lower compared to PLFA concentrations for all groups except for the fungal biomarker 18:2ω6,9.

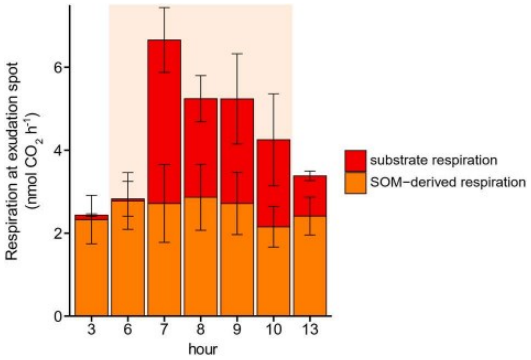


Fig. 3. In this hypothetical calculation, we depict the potential increase in microbial respiration within a 1-mm radius around the microdialysis probes before, during, and after a 9-h long release of readily available C substrates (succinate, acetate, glucose, fructose). The base of the stacked bars represents the aliquot of SOM-derived respiration for a cylindrical soil volume of 10 mm length and 1 mm radius, aiming to represent the immediate surrounding of the microdialysis probes (orange). Note that this calculation assumes that the SOM-derived respiration was homogenously distributed within the core, and not locally affected by the substrate input in the surroundings of the probes. The top of the stacked bars (red) shows the total amount of substrate-derived respiration in each soil core (divided by two), assuming that the released substrate was respired no further than 1 mm from each of the two microdialysis probes per core. Depicted are the means of 5 replicate cores and the standard error of the mean as error bars. The x-axis shows the hours of the experiment with each bar representing a 1-h long respiration measurement. Shaded area indicates the time period in which the substrate was released (4–12 h).

4. Discussion

Our results show that a pulse of organic C compounds released via micro-diffusion at discrete locations in intact soil alters the temporal dynamics of soil metabolites right at these spots over the following hours and days. Interestingly, the concentration of several small-chain fatty acids increased in response to the C input, indicating changes in microbial metabolic pathways. This went along with a strong increase of ammonium availability, indicating microbial mineralization of soil organic N. Our measurements thus support the widely observed phenomenon that labile C compounds exuded by roots lead to enhanced nutrient availability in the rhizosphere (Zhu et al., 2014; Murphy et al., 2015).

4.1. *Impact of labile C pulse on microbial activity*

Soil microbes respired the released substrate with a 2–3 h delay, which might reflect a physiological lag phase, caused by the need to adapt their internal cellular machinery to the availability of a new substrate (Bertrand, 2019). Had the delayed respiration of the added substrate been due to a slow diffusion of the substrate, we would have seen a steady increase in substrate-derived respiration and no lag phase followed by the very high respiration rates observed (Fig. 1, bottom). It was hypothesized that soil microbes, whose activity is often constrained by C and energy limitations (Blagodatskaya and Kuzyakov, 2013), maintain a state of 'metabolic alertness' to quickly utilize infrequently arriving resources in an otherwise scarce environment (De Nobili et al., 2001; Mondini et al., 2006). The observed 2–3 h delay is consistent with our previous study in which reverse microdialysis was performed with various organic C compounds in different soils (König et al., 2022). There, we observed – after a quick initial transfer – a rapid decline of transfer rates of all compounds into the soil. This indicates (as transfer rates depend on the concentration gradient between the perfusate and the soil), that the released substances accumulated in the soil solution outside the membrane. Transfer rates abruptly increased 3 h later, implying a sudden uptake of the accumulated compounds by microbes after a time delay. These findings, along with the here observed delay in microbial respiration, collectively suggest that microbes in intact soil

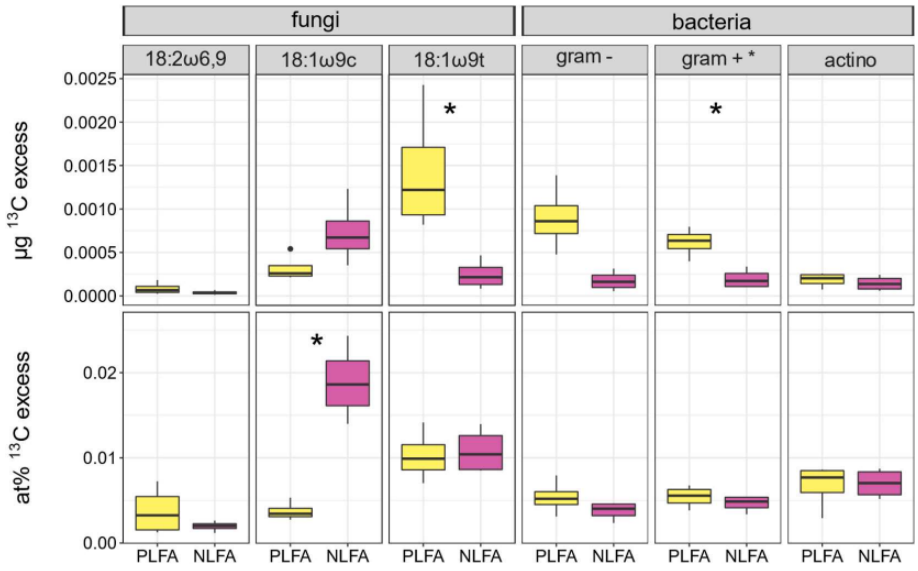


Fig. 4. Enrichment in labile-substrate derived ^{13}C in phospholipid fatty acids (PLFAs, yellow) and neutral lipid fatty acids (NLFAs, pink) in close proximity (<5 mm radius) to the microdialysis probe 12 days after a 9-h pulse of ^{13}C-labelled substrate (n = 5). Due to the significant enrichment observed in all PLFA and NLFA biomarkers (at% ^{13}C: Fig. 3S), except for 18:2ω6,9 PLFA, we have opted to exclusively present the ^{13}C excess data here (µg ^{13}C excess, at% ^{13}C excess). The fungi-specific fatty acid biomarkers 18:1ω9c, 18:1ω9t and 18:2ω6,9 are depicted ungrouped. The remaining fatty acids were grouped into gram-negative bacteria, gram-positive bacteria (*excluding *Actinobacteria*) and *Actinobacteria*. Asterisks indicate significant differences ($p < 0.05$) between PLFA and NLFA for µg ^{13}C excess and at % ^{13}C excess. Detailed statistics are shown in Table 2 and Table 3.

environments undergo a lag phase before taking up and respiring a new substrate.

Organic acids, in contrast to sugars, exhibited higher transfer rates (substrate release) during the pulse and lower back-retrieval rates afterwards, consistent with our previous study in which transfer and retrieval rates were negatively correlated (König et al., 2022). This suggests that sugars accumulated around the membrane after their initial release and were not effectively removed by biotic or abiotic processes like microbial uptake or adsorption to soil surfaces (Jones et al., 2003). Sugars, while widely regarded as ubiquitous substrates that undergo intensive recycling in microbial biomass (Apostel et al., 2015), appeared to be metabolised to a lesser extent by soil microbes compared to organic acids. The relatively quicker removal of organic acids from the membrane surrounding, as indicated by their higher transfer and lower back-retrieval rates, might indicate a more rapid adsorption to soil minerals compared to sugars. However, low-molecular-weight organic substances like glucose and acetate were reported to be consumed within a few hours (Jones et al., 2009), faster than their physico-chemical sorption to the soil (Fischer et al., 2010). To understand the underlying causes for the different behaviour of sugars and organic acids, future experiments should examine each compound class separately. Especially since glucose and acetate may enter different metabolic pathways, such as glycolysis and gluconeogenesis, respectively (Schink et al., 2022).

4.2. Rhizosphere priming effect and nitrogen mineralization

While the strong substrate respiration on the first day did not coincide with an accelerated SOM mineralization, we observed a significant increase in SOM-derived respiration compared to the control starting at day 3 (Fig. 1, top). This 'rhizosphere` priming effect may be attributed to a gradual activation and increase in microbial biomass in response to the added substrate (De Nobili et al., 2001), leading to an increased production of extracellular enzymes that boosted SOM decomposition (Kuzyakov, 2010; Dijkstra et al., 2013). This was further reflected in the up-to-threefold increase in ammonium concentrations within 24 h of substrate input. This indicates N mineralization from SOM and hence accelerated SOM decomposition, which was not yet matched by an increase in SOM-derived respiration (Fig. 1).

Priming effects have been reported to increase N mineralization (Dijkstra et al., 2009; Murphy et al., 2015). Adding C-rich substrate without providing additional N may have induced N-limitation and prompted the microbial community to mine for N (Craine et al., 2007; Fontaine et al., 2011; Brzostek et al., 2013). In a separate microdialysis experiment, sucrose addition was proposed to increase the N demand of the microbial community by alleviating C limitations (Buckley et al., 2022). Consequently, the delayed onset of increased SOM-derived respiration (priming effect) by three days could be partially ascribed to the lack of N in our exudate, which is recognized for its pivotal role in enzyme production (Drake et al., 2013) and, thus, the degradation of SOM. The sequence of events, ranging from substrate respiration to the subsequent increased ammonium concentrations (N-mining) and accelerated SOM-derived respiration (priming effect), can be attributed to the time, energy and N resources required for enzyme production (Liu et al., 2019).

Alternatively, the increase in ammonium concentrations could result from a liberation of previously clay-bound ammonium through organo-mineral interactions with the released organic acids (Keiluweit et al., 2015). We think, however, that this is an unlikely explanation, as the steep ammonium peak occurred only 24 h after the release of organic acids, at a time when both acetate and succinate were only present at much smaller than initial (acetate) or even negligible (succinate) concentrations (Fig. 2). From day 5 onwards, the increased nitrate concentration compared to the controls indicates microbial nitrification, probably triggered by the high amounts of ammonium. Besides nitrate, the elevated levels of acetate (days 3–12), formate (day 12), and sulfate (day 12; Fig. 2, Table 1), imply long lasting changes in soils that received labile substrate.

It should be noted that our experimental design placed limitations on the measurement sensitivity of a spatially constrained priming event.

Specifically, the high background of SOM-derived respiration of the whole soil core may have masked the local increase of SOM-derived respiration within the small volume influenced around the two microdialysis membranes. However, this 294:1 vol ratio (assuming a 1 mm radius of influenced soil around the two membranes) implies that the actual priming effect at the exudation hotspot on the third day was likely considerably higher than our observation suggests.

4.3. Altered metabolic pathways in response to labile C

Simultaneous with the onset of the 24-h long ammonium peak, other organic and inorganic compounds increased: acetate concentrations increased 6 h prior, while propionate, sulfate, and formate concentrations increased 3, 3 and 15 h after the onset of the ammonium peak (Fig. 2), suggesting a complex interplay of metabolic pathways. The organic acids could be fermentation products, indicating potential anaerobic conditions. However, in high glucose environments, it has been shown that *E. coli* cultures favour fermentation over respiration, leading to the release of high concentrations of acetate, even when oxygen is available (Luli and Strohl, 1990; Chacón et al., 2018; Mori et al., 2019). Remarkably, many bacteria employ these respiro-fermentative overflow metabolism and still attain high growth rates (Wortel et al., 2018). For thermo-dynamical reasons, heterotrophic microbes face a trade-off between growth rate and yield (Pfeiffer et al., 2001; Kreft and Bonhoeffer, 2005), which becomes particularly relevant under conditions of abundant resource or limited oxygen supply. Under such conditions the ATP production rate of respiration saturates rapidly and microbes can maximize growth rate at the expense of yield by switching at least partly to incomplete metabolic pathways. In *E. coli*, the growth-rate dependent acetate overflow was explained by fermentation being favoured at high growth rates due to its lower biosynthesis cost relative to the electron transport chain (Basan et al., 2015). Alternatively, the membrane real estate hypothesis proposes that at high growth rates, cells increase in size, reducing their available membrane area for respiratory proteins, prompting a shift towards less efficient but faster ATP production through fermentation (Szenk et al., 2017). Additionally, it was suggested that under nutrient limitations excess C may be routed to overflow respiration or excreted, to accommodate the decomposers stoichiometric requirements (Schimel and Weintraub, 2003; Manzoni and Porporato, 2009).

Interestingly, this would also be a viable strategy for microbes under aerobe conditions, given that microbes face a surplus of sugars (Lipson, 2015). Incomplete metabolic pathways, such as fermentation, allow a higher substrate flux per unit of time but go along with the release of metabolic intermediates such as acetate (Pfeiffer and Bonhoeffer, 2003). The release of high glucose levels at local exudation hotspots could thus have created the right conditions for this glucose-mediated aerobe acidogenesis to take place. Moreover, nutrient limitations induced by the absence of N in the exudate could have resulted in the redirection of surplus C towards excretion or potentially overflow respiration to meet the decomposers stoichiometric requirements (Schimel and Weintraub, 2003; Manzoni and Porporato, 2009). The reduction in the organic acid peaks, e.g., acetate starting at hour 33, signifies a transition from a period of rapid growth with organic acid production to a slower growth phase involving the assimilation of the excreted organic acids. This switch is likely driven by the depletion of the organic acid-producing carbon sources (e.g., sugars) (Wolfe, 2005). Collectively, our findings suggest altered metabolic pathways and microbial activity in the days following the substrate input. Going forward, it should be taken into account that high concentrations of organic acids, like acetate and formate measured in the rhizosphere solution of beach trees (*Fagus sylvatica*) (Fender et al., 2013), might originate from microbial excretion just as likely as from root exudates, highlighting the need for careful interpretation in future studies.

4.4. Oxygen depletion at the exudation hotspot

It is, however, also possible that microbial respiration in the immediate vicinity of the exudation spot caused a temporary depletion of oxygen (O_2) at the spot due to the additional respiration of the released substances: If we assume a pore space of approx. 50% of the soil volume (Voltolini et al., 2017), the 1 mm cylinder around each microdialysis probe will contain a pore volume of 15.71 mm^3. We calculated that, based on oxygen saturation levels of 9.1 mg l^{-1} (20 °C) in water and a concentration of 20.95% O_2 in (atmospheric) air the total amount of available O_2 within such a cylinder would be around 75.7 nmol O_2 (assuming a 50% water saturation of the soil pores), with only 2.24 nmol O_2 being dissolved and thus immediately available in water-filled soil pores (Supplementary material). Comparing this potential O_2 availability with the estimated increased O_2 demand for respiration (SOM-derived plus substrate-derived) of around 19.52 nmol CO_2 (nmol O_2, hour 7–10) during the 9-h long labile substrate pulse (Fig. 3) suggests that a temporary depletion of O_2 concentrations in the vicinity of the substrate input is possible. While it is unknown whether the release of high concentrations of organic compounds leads to temporary oxygen depletion around roots, the formation of anoxic hotspots has been shown in an artificial pore system caused by increased bacterial oxygen consumption at locations with high C availability (Borer et al., 2018). If temporary oxygen depletion occurs around root exudation hotspots it would have consequences for microbial metabolism. Microbes could, for instance, switch to an anaerobic metabolism, which would also go along with shorter, incomplete catabolic pathways that lead to a release of intermediates, such as acetate (Kreft et al., 2020). Moreover, when oxygen concentrations are low, nitrate can serve as an alternative electron acceptor, to allow the oxidation of SOM to CO_2 (Nannipieri and Eldor, 2009; Song et al., 2023). In this case, nitrate is reduced to ammonium in a process called dissimilatory nitrate reduction (Takaya, 2002; Nannipieri and Eldor, 2009), which might also have contributed, to the increased ammonium concentrations we observed at around hour 26–45.

4.5. Substrate utilization by microbial groups and fungal strategies

All microbial groups were significantly ^{13}C enriched exclusively within a 5 mm radius of the exudation pulse (at% ^{13}C: Fig. S5, Table 2). This suggests that the volume of influence of the exudation pulse, and thus the uptake of the ^{13}C-labelled substrate, was limited to the immediate vicinity of the input. This is consistent with the observations that most methods find the rhizosphere to extend between 0.5 and 4 mm (Kuzyakov and Razavi, 2019). Notably, among the microbial groups investigated, only the biomass of gram-positive bacteria significantly increased in response to the labile substrate pulse (µg C: Fig. 4S and Table 2). This was surprising, as we would instead have expected a biomass increase in gram-negative bacteria biomass, which are believed to primarily rely on simple (plant-derived) C compounds (Butler et al., 2003; Kramer and Gleixner, 2008). For instance, in the rhizosphere of young beech trees exudates were preferentially utilized by gram-negative bacteria and fungi, with gram-positive bacteria exhibiting little reliance on rhizodeposits (Esperschütz et al., 2009). Gram-positive bacteria, thought to prefer more complex C forms, were proposed to utilize older soil organic carbon upon fresh root exudate inputs (Bird et al., 2011). Consequently, the increase in gram-positive biomass seen 12 days after the labile substrate pulse may be attributed to them benefitting from priming SOM degradation.

PLFAs and NLFAs of the microbial groups (except 18:1ω9c) did not differ in their relative ^{13}C enrichment (at% ^{13}C excess: Fig. 4, Table 3). Still, gram-negative bacteria and gram-positive bacteria incorporated more ^{13}C into PLFAs than NLFAs in absolute amounts (µg ^{13}C excess: Fig. 4) which can be attributed to their higher concentrations of PLFAs compared to NLFAs (µg C: Fig. S5). Given that the extraction of fatty acids occurred 12 days after the substrate pulse, the ^{13}C incorporation

does not discern groups that initially utilized ^{13}C; rather, it identifies microbial groups that benefitted directly (initial uptake) or indirectly (cross-feeding) from the added substrate over the experimental duration.

Interestingly, we found that the three fungal fatty acid biomarkers responded very differently to the labile substrate input. The fungi-specific biomarker 18:1ω9c exhibited significantly higher at% ^{13}C excess in NLFAs than PLFAs (Fig. 4). In contrast, the 18:1ω9t fungal biomarker did not differ in relative ^{13}C enrichment between PLFAs and NLFAs (Fig. 4, bottom), but had higher absolute amounts of ^{13}C (μg ^{13}C excess) in PLFAs (Fig. 4, top). The fungal biomarker 18:2ω6,9 was the least responsive to the labile substrate input, with overall low fatty acid biomass, no significant enrichment of ^{13}C in the PLFAs, and only little ^{13}C incorporated into NLFAs (Fig. 4, Fig. S5). Under the assumption that these fatty acids are representative for different fungal groups or species (Joergensen, 2022), our data may reflect different fungal strategies. While PLFA are part of cell membranes, NLFA originate form fungal storage compounds (Bååth, 2003). Some fungi (represented by 18:1ω9c) may thus have invested into storage compounds whereas others (represented by 18:1ω9t) could have invested into biomass growth (PLFA). Alternatively, it could also be that fungi use the 18:1ω9c NLFA as a storage compound and incorporate the 18:1ω9t PLFA into cell membranes.

5. Conclusion

Our experiment demonstrated the complex microbial response to a spatially constrained input of labile C compounds, i.e. simulating root exudation, in an undisturbed soil. Our findings suggest that such an input pulse has altered microbial metabolism and increased nutrient availability around the exudation spot, revealing the time frame in which this might occur. We were able to identify a three-stage microbial response to artificial root exudation: First, a rapid local substrate respiration (2–3 h), likely depleting oxygen at the exudation spot; secondly, the initiation of (anaerobic) metabolic pathways, accompanied by the production of fermentation byproducts like organic acids and the release of N-compounds (ammonium) (onset approx. 24 h); and thirdly, the accelerated respiration of organic matter (day 3). Regardless, there are several aspects of root exudation we could not capture with our experimental design, such as the release of a more complex mixture of chemical compounds (including N and P), or the presence of an already specialised rhizosphere community inhabiting the root's surface. Our results provide valuable insights into the potential cascade of effects following a substrate pulse, thereby advancing our understanding of the underlying mechanisms of rhizosphere priming.

CRediT authorship contribution statement

Julia Wiesenbauer: Formal analysis, Investigation, Methodology, Software, Validation, Visualization, Writing – original draft, Writing – review & editing. **Alexander König:** Investigation, Methodology, Software, Visualization. **Stefan Gorka:** Formal analysis, Investigation, Methodology, Software, Validation, Writing – original draft, Writing – review & editing. **Lilian Marchand:** Investigation, Methodology. **Naoise Nunan:** Writing – review & editing, Funding acquisition. **Barbara Kitzler:** Resources. **Erich Inselsbacher:** Methodology, Resources, Writing – review & editing, Funding acquisition. **Christina Kaiser:** Conceptualization, Funding acquisition, Methodology, Project administration, Resources, Supervision, Validation, Writing – review & editing, Writing – original draft.

Declaration of competing interest

The authors declare that they have no known competing financial interests or personal relationships that could have appeared to influence the work reported in this paper.

Data availability

Data to this article can be found online at https://doi.org/10.5281/zenodo.8109601.

Acknowledgements

This study was funded by the Austrian Science Fund (FWF, project P30339–B29) and the European Research Council (ERC) under the European Union's Horizon 2020 research and innovation programme (grant agreement No 819446). We thank Dagmar Woebken, Andreas Richter and Hannes Schmidt for valuable discussions on the experimental design and interpretation of the results, Ludwig Seidl and Margarete Watzka for technical support.

Appendix A. Supplementary data

Supplementary data to this article can be found online at https://doi.org/10.1016/j.soilbio.2023.109259.

References

Apostel, C., Dippold, M., Kuzyakov, Y., 2015. Biochemistry of hexose and pentose transformations in soil analyzed by position-specific labeling and 13C-PLFA. Soil Biology and Biochemistry 80, 199–208. https://doi.org/10.1016/j.soilbio.2014.09.005.

Bååth, E., 2003. The use of neutral lipid fatty acids to indicate the physiological conditions of soil fungi. Microbial Ecology 45, 373–383. https://doi.org/10.1007/s00248-003-2002-y.

Badri, D.V., Vivanco, J.M., 2009. Regulation and function of root exudates. Plant, Cell and Environment 32, 666–681. https://doi.org/10.1111/j.1365-3040.2009.01926.x.

Balasooriya, W.K., Huygens, D., Denef, K., Roobroeck, D., Verhoest, N.E.C., Boeckx, P., 2013. Temporal variation of rhizodeposit-C assimilating microbial communities in a natural wetland. Biology and Fertility of Soils 49, 333–341. https://doi.org/10.1007/s00374-012-0729-7.

Balser, T.C., Treseder, K.K., Ekenler, M., 2005. Using lipid analysis and hyphal length to quantify AM and saprotrophic fungal abundance along a soil chronosequence. Soil Biology and Biochemistry 37, 601–604. https://doi.org/10.1016/j.soilbio.2004.08.019.

Basan, M., Hui, S., Okano, H., Zhang, Z., Shen, Y., Williamson, J.R., Hwa, T., 2015. Overflow metabolism in Escherichia coli results from efficient proteome allocation. Nature 528, 99–104. https://doi.org/10.1038/nature15765.

Basiliko, N., Stewart, H., Roulet, N.T., Moore, T.R., 2012. Do root exudates enhance peat decomposition? Geomicrobiology Journal 29, 374–378. https://doi.org/10.1080/01490451.2011.568272.

Baumert, V.L., Vasilyeva, N.A., Vladimirov, A.A., Meier, I.C., Kögel-Knabner, I., Mueller, C.W., 2018. Root exudates induce soil macroaggregation facilitated by fungi in subsoil. Frontiers in Environmental Science 6. https://doi.org/10.3389/fenvs.2018.00140.

Bertrand, R.L., 2019. Lag Phase Is a Dynamic, Organized, Adaptive, and Evolvable Period that Prepares Bacteria for Cell Division.

Bird, J.A., Herman, D.J., Firestone, M.K., 2011. Rhizosphere priming of soil organic matter by bacterial groups in a grassland soil. Soil Biology and Biochemistry 43, 718–725. https://doi.org/10.1016/j.soilbio.2010.08.010.

Blagodatskaya, E., Kuzyakov, Y., 2008. Mechanisms of real and apparent priming effects and their dependence on soil microbial biomass and community structure: critical review. Biology and Fertility of Soils 45, 115–131. https://doi.org/10.1007/s00374-008-0334-y.

Blagodatskaya, E., Kuzyakov, Y., 2013. Soil Biology & Biochemistry Active microorganisms in soil : critical review of estimation criteria and approaches. Soil Biology and Biochemistry 67, 192–211. https://doi.org/10.1016/j.soilbio.2013.08.024.

Bligh, E.G., Dyer, W.J., 1959. A rapid method of total lipid extraction and purification. Canadian Journal of Philosophy 37, 911–917.

Borer, B., Tecon, R., Or, D., 2018. Spatial organization of bacterial populations in response to oxygen and carbon counter-gradients in pore networks. Nature Communications 9, 769. https://doi.org/10.1038/s41467-018-03187-y.

Brandstätter, C., Keiblinger, K., Wanek, W., Zechmeister-Boltenstern, S., 2013. A closeup study of early beech litter decomposition: potential drivers and microbial interactions on a changing substrate. Plant and Soil 371, 139–154. https://doi.org/10.1007/s11104-013-1671-7.

Brzostek, E.R., Greco, A., Drake, J.E., Finzi, A.C., 2013. Root carbon inputs to the rhizosphere stimulate extracellular enzyme activity and increase nitrogen availability in temperate forest soils. Biogeochemistry 115, 65–76. https://doi.org/10.1007/s10533-012-9818-9.

Buckley, S., Brackin, R., Näsholm, T., Schmidt, S., Jämtgård, S., 2022. The influence of sucrose on soil nitrogen availability – a root exudate simulation using microdialysis. Geoderma 409. https://doi.org/10.1016/j.geoderma.2021.115645.

Butler, J.L., Bottomley, P.J., Griffith, S.M., Myrold, D.D., 2004. Distribution and turnover of recently fixed photosynthate in ryegrass rhizospheres. Soil Biology and Biochemistry 36, 371–382. https://doi.org/10.1016/j.soilbio.2003.10.011.
Butler, J.L., Williams, M.A., Bottomley, P.J., Myrold, D.D., 2003. Microbial community dynamics associated with rhizosphere carbon flow. Applied and Environmental Microbiology 69, 6793–6800. https://doi.org/10.1128/AEM.69.11.6793-6800.2003.
Canarini, A., Kaiser, C., Merchant, A., Richter, A., Wanek, W., 2019. Root exudation of primary metabolites: mechanisms and their roles in plant responses to environmental stimuli. Frontiers in Plant Science 10. https://doi.org/10.3389/fpls.2019.00157.
Cardon, Z.G., Gage, D.J., 2006. Resource exchange in the rhizosphere: molecular tools and the microbial perspective. Annual Review of Ecology, Evolution, and Systematics 37, 459–488. https://doi.org/10.1146/annurev.ecolsys.37.091305.110207.
Cesarz, S., Fender, A.-C., Beyer, F., Valtanen, K., Pfeiffer, B., Gansert, D., Hertel, D., Polle, A., Daniel, R., Leuschner, C., Scheu, S., 2013. Roots from beech (Fagus sylvatica L.) and ash (Fraxinus excelsior L.) differentially affect soil microorganisms and carbon dynamics. Soil Biology and Biochemistry 61, 23–32. https://doi.org/10.1016/j.soilbio.2013.02.003.
Chacón, J.M., Möbius, W., Harcombe, W.R., 2018. The spatial and metabolic basis of colony size variation. ISME Journal 12, 669–680. https://doi.org/10.1038/s41396-017-0038-0.
Chaignon, V., Di Malta, D., Hinsinger, P., 2002. Fe-deficiency increases Cu acquisition by wheat cropped in a Cu-contaminated vineyard soil. New Phytologist 154, 121–130. https://doi.org/10.1046/j.1469-8137.2002.00349.x.
Chari, N.R., Taylor, B.N., 2022. Soil organic matter formation and loss are mediated by root exudates in a temperate forest. Nature Geoscience 15, 1011–1016. https://doi.org/10.1038/s41561-022-01079-x.
Craine, J.M., Morrow, C., Fierer, N., 2007. Microbial NITROGEN LIMITATION INCREASES DECOMPOSITION. Ecology 88, 2105–2113. https://doi.org/10.1890/06-1847.1.
De Nobili, M., Contin, M., Mondini, C., Brookes, P.C., 2001. Soil microbial biomass is triggered into activity by trace amounts of substrate. Soil Biology and Biochemistry 33, 1163–1170. https://doi.org/10.1016/S0038-0717(01)00020-7.
Demand, D., Schack-Kirchner, H., Lang, F., 2017. Assessment of diffusive phosphate supply in soils by microdialysis. Zeitschrift Fur Pflanzenernahrung Und Bodenkunde 180, 220–230. https://doi.org/10.1002/jpln.201600412.
Denef, K., Bubenheim, H., Lenhart, K., Vermeulen, J., Cleemput, O.V., Boeckx, P., 2007. Community Shifts and Carbon Translocation within Metabolically-Active Rhizosphere Microorganisms in Grasslands under Elevated CO2.
Dessureault-Rompré, J., Nowack, B., Schulin, R., Luster, J., 2007. Spatial and temporal variation in organic acid anion exudation and nutrient anion uptake in the rhizosphere of Lupinus albus L. Plant and Soil 301, 123–134. https://doi.org/10.1007/s11104-007-9427-x.
Dijkstra, F.A., Bader, N.E., Johnson, D.W., Cheng, W., 2009. Does accelerated soil organic matter decomposition in the presence of plants increase plant N availability? Soil Biology and Biochemistry 41, 1080–1087. https://doi.org/10.1016/j.soilbio.2009.02.013.
Dijkstra, F.A., Carrillo, Y., Pendall, E., Morgan, J.A., 2013. Rhizosphere priming: a nutrient perspective. Frontiers in Microbiology 4. https://doi.org/10.3389/fmicb.2013.00216.
Drake, J.E., Darby, B.A., Giasson, M.A., Kramer, M.A., Phillips, R.P., Finzi, A.C., 2013. Stoichiometry constrains microbial response to root exudation-insights from a model and a field experiment in a temperate forest. Biogeosciences 10, 821–838. https://doi.org/10.5194/bg-10-821-2013.
Edwards, K.R., Kaštovská, E., Borovec, J., Šantrůčková, H., Picek, T., 2018. Species effects and seasonal trends on plant efflux quantity and quality in a spruce swamp forest. Plant and Soil 426, 179–196. https://doi.org/10.1007/s11104-018-3610-0.
Esperschütz, J., Buegger, F., Winkler, J.B., Munch, J.C., Schloter, M., Gattinger, A., 2009. Microbial response to exudates in the rhizosphere of young beech trees (Fagus sylvatica L.) after dormancy. Soil Biology and Biochemistry 41, 1976–1985. https://doi.org/10.1016/j.soilbio.2009.07.002.
Falchini, L., Naumova, N., Kuikman, P.J., Bloem, J., Nannipieri, P., 2003. CO2 evolution and denaturing gradient gel electrophoresis profiles of bacterial communities in soil following addition of low molecular weight substrates to simulate root exudation. Soil Biology and Biochemistry 35, 775–782. https://doi.org/10.1016/S0038-0717(03)00105-6.
Fender, A.-C., Gansert, D., Jungkunst, H.F., Fiedler, S., Beyer, F., Schützenmeister, K., Thiele, B., Valtanen, K., Polle, A., Leuschner, C., 2013. Root-induced tree species effects on the source/sink strength for greenhouse gases (CH4, N2O and CO2) of a temperate deciduous forest soil. Soil Biology and Biochemistry 57, 587–597. https://doi.org/10.1016/j.soilbio.2012.08.004.
Finzi, A.C., Abramoff, R.Z., Spiller, K.S., Brzostek, E.R., Darby, B.A., Kramer, M.A., Phillips, R.P., 2015. Rhizosphere processes are quantitatively important components of terrestrial carbon and nutrient cycles. Global Change Biology 21, 2082–2094. https://doi.org/10.1111/gcb.12816.
Fischer, H., Ingwersen, J., Kuzyakov, Y., 2010. Microbial uptake of low-molecular-weight organic substances out-competes sorption in soil. European Journal of Soil Science 61, 504–513. https://doi.org/10.1111/j.1365-2389.2010.01244.x.
Fontaine, S., Henault, C., Aamor, A., Bdioui, N., Bloor, J.M.G., Maire, V., Mary, B., Revaillot, S., Maron, P.A., 2011. Fungi mediate long term sequestration of carbon and nitrogen in soil through their priming effect. Soil Biology and Biochemistry 43, 86–96. https://doi.org/10.1016/j.soilbio.2010.09.017.
Frostegård, Å., Tunlid, A., Bååth, E., 1991. Microbial biomass measured as total lipid phosphate in soils of different organic content. Journal of Microbiological Methods 14, 151–163. https://doi.org/10.1016/0167-7012(91)90018-L.
Girkin, N.T., Turner, B.L., Ostle, N., Craigon, J., Sjögersten, S., 2018. Root exudate analogues accelerate CO2 and CH4 production in tropical peat. Soil Biology and Biochemistry 117, 48–55. https://doi.org/10.1016/j.soilbio.2017.11.008.
Haichar, F. el Z., Santaella, C., Heulin, T., Achouak, W., 2014. Root exudates mediated interactions belowground. Soil Biology and Biochemistry 77, 69–80. https://doi.org/10.1016/j.soilbio.2014.06.017.
Herman, D.J., Johnson, K.K., Jaeger, C.H., Schwartz, E., Firestone, M.K., 2006. Root influence on nitrogen mineralization and nitrification in avena barbata rhizosphere soil. Soil Science Society of America Journal 70, 1504–1511. https://doi.org/10.2136/sssaj2005.0113.
Hood-Nowotny, R., Umana, N.H.-N., Inselbacher, E., Oswald- Lachouani, P., Wanek, W., 2010. Alternative methods for measuring inorganic, organic, and total dissolved nitrogen in soil. Soil Science Society of America Journal 74, 1018–1027. https://doi.org/10.2136/sssaj2009.0389.
Huo, C., Luo, Y., Cheng, W., 2017. Rhizosphere priming effect: a meta-analysis. Soil Biology and Biochemistry 111, 78–84. https://doi.org/10.1016/j.soilbio.2017.04.003.
Inselsbacher, E., Öhlund, J., Jämtgård, S., Huss-Danell, K., Näsholm, T., 2011. The potential of microdialysis to monitor organic and inorganic nitrogen compounds in soil. Soil Biology and Biochemistry 43, 1321–1332. https://doi.org/10.1016/j.soilbio.2011.03.003.
Jilling, A., Keiluweit, M., Gutknecht, J.L.M., Grandy, A.S., 2021. Priming mechanisms providing plants and microbes access to mineral-associated organic matter. Soil Biology and Biochemistry 158, 108265. https://doi.org/10.1016/j.soilbio.2021.108265.
Joergensen, R.G., 2022. Phospholipid fatty acids in soil—drawbacks and future prospects. Biology and Fertility of Soils 58, 1–6. https://doi.org/10.1007/s00374-021-01613-w.
Joergensen, R.G., Wichern, F., 2008. Quantitative assessment of the fungal contribution to microbial tissue in soil. Soil Biology and Biochemistry 40, 2977–2991. https://doi.org/10.1016/j.soilbio.2008.08.017.
Jones, D.L., Dennis, P.G., Owen, A.G., Van Hees, P.A.W., 2003. Organic acid behavior in soils - misconceptions and knowledge gaps. Journal of Intelligent and Robotic Systems: Theory and Applications 248, 31–41. https://doi.org/10.1023/A.
Jones, D.L., Nguyen, C., Finlay, R.D., 2009. Carbon flow in the rhizosphere: carbon trading at the soil-root interface. Plant and Soil 321, 5–33. https://doi.org/10.1007/s11104-009-9925-0.
Kaiser, C., Kilburn, M.R., Clode, P.L., Fuchslueger, L., Koranda, M., Cliff, J.B., Solaiman, Z.M., Murphy, D.V., 2015. Exploring the transfer of recent plant photosynthates to soil microbes: mycorrhizal pathway vs direct root exudation. New Phytologist 205, 1537–1551. https://doi.org/10.1111/nph.13138.
Kandeler, E., Gerber, H., 1988. Short-term assay of soil urease activity using colorimetric determination of ammonium. Biology and Fertility of Soils 6, 68–72. https://doi.org/10.1007/BF00257924.
Kaštovská, E., Šantrůčková, H., 2007. Fate and dynamics of recently fixed C in pasture plant–soil system under field conditions. Plant and Soil 300, 61–69. https://doi.org/10.1007/s11104-007-9388-0.
Keiluweit, M., Bougoure, J.J., Nico, P.S., Pett-Ridge, J., Weber, P.K., Kleber, M., 2015. Mineral protection of soil carbon counteracted by root exudates. Nature Climate Change 5, 588–595.
Kitzler, B., Zechmeister-Boltenstern, S., Holtermann, C., Skiba, U., Butterbach-Bahl, K., 2006. Nitrogen oxides emission from two beech forests subjected to different nitrogen loads. Biogeosciences 3, 293–310. https://doi.org/10.5194/bg-3-293-2006.
König, A., Wiesenbauer, J., Gorka, S., Marchand, L., Kitzler, B., Inselsbacher, E., Kaiser, C., 2022. Reverse microdialysis: a window into root exudation hotspots. Soil Biology and Biochemistry 174, 108829. https://doi.org/10.1016/j.soilbio.2022.108829.
Koranda, M., Kaiser, C., Fuchslueger, L., Kitzler, B., Sessitsch, A., Zechmeister-Boltenstern, S., Richter, A., 2013. Seasonal variation in functional properties of microbial communities in beech forest soil. Soil Biology and Biochemistry 60, 95–104. https://doi.org/10.1016/j.soilbio.2013.01.025.
Kramer, C., Gleixner, G., 2008. Soil organic matter in soil depth profiles: distinct carbon preferences of microbial groups during carbon transformation. Soil Biology and Biochemistry 40, 425–433. https://doi.org/10.1016/j.soilbio.2007.09.016.
Kreft, J.-U., Bonhoeffer, S., 2005. The evolution of groups of cooperating bacteria and the growth rate versus yield trade-off. Microbiology 151, 637–641. https://doi.org/10.1099/mic.0.27415-0.
Kreft, J.U., Griffin, B.M., González-Cabaleiro, R., 2020. Evolutionary causes and consequences of metabolic division of labour: why anaerobes do and aerobes don't. Current Opinion in Biotechnology 62, 80–87. https://doi.org/10.1016/j.copbio.2019.08.008.
Kuzyakov, Y., 2010. Priming effects: interactions between living and dead organic matter. Soil Biology and Biochemistry 42, 1363–1371. https://doi.org/10.1016/j.soilbio.2010.04.003.
Kuzyakov, Y., 2002. Review : factors affecting rhizosphere priming effects. Journal of Plant Nutrition and Soil Science 165, 382–396.
Kuzyakov, Y., Blagodatskaya, E., Blagodatskaya, E., 2015. Microbial hotspots and hot moments in soil: concept & review. Soil Biology and Biochemistry 83, 184–199. https://doi.org/10.1016/j.soilbio.2015.01.025.
Kuzyakov, Y., Hill, P.W., Jones, D.L., 2007. Root exudate components change litter decomposition in a simulated rhizosphere depending on temperature. Plant and Soil 290, 293–305. https://doi.org/10.1007/s11104-006-9162-8.

Kuzyakov, Y., Razavi, B.S., 2019. Rhizosphere size and shape: temporal dynamics and spatial stationarity. Soil Biology and Biochemistry 135, 343–360. https://doi.org/10.1016/j.soilbio.2019.05.011.
Li, C., Ding, S., Yang, L., Zhu, Q., Chen, M., Tsang, D.C.W., Cai, G., Feng, C., Wang, Y., Zhang, C., 2019. Planar optode: a two-dimensional imaging technique for studying spatial-temporal dynamics of solutes in sediment and soil. Earth-Science Reviews 197, 102916. https://doi.org/10.1016/j.earscirev.2019.102916.
Lipson, D.A., 2015. The complex relationship between microbial growth rate and yield and its implications for ecosystem processes. Frontiers in Microbiology 6. https://doi.org/10.3389/fmicb.2015.00615.
Liu, Q., Xu, X., Wang, H., Blagodatskaya, E., Kuzyakov, Y., 2019. Dominant extracellular enzymes in priming of SOM decomposition depend on temperature. Geoderma 343, 187–195. https://doi.org/10.1016/j.geoderma.2019.02.006.
Luli, G.W., Strohl, W.R., 1990. Comparison of growth, acetate production, and acetate inhibition of Escherichia coli strains in batch and fed-batch fermentations. Applied and Environmental Microbiology 56, 1004–1011. https://doi.org/10.1128/aem.56.4.1004-1011.1990.
Luo, Z., Wang, E., Sun, O.J., 2016. A meta-analysis of the temporal dynamics of priming soil carbon decomposition by fresh carbon inputs across ecosystems. Soil Biology and Biochemistry 101, 96–103. https://doi.org/10.1016/j.soilbio.2016.07.011.
Manzoni, S., Porporato, A., 2009. Soil carbon and nitrogen mineralization: theory and models across scales. Soil Biology and Biochemistry 41, 1355–1379. https://doi.org/10.1016/j.soilbio.2009.02.031.
Mau, R.L., Liu, C.M., Aziz, M., Schwartz, E., Dijkstra, P., Marks, J.C., Price, L.B., Keim, P., Hungate, B.A., 2015. Linking soil bacterial biodiversity and soil carbon stability. The ISME Journal 9, 1477–1480. https://doi.org/10.1038/ismej.2014.205.
Mondini, C., Cayuela, M.L., Sanchez-Monedero, M.A., Roig, A., Brookes, P.C., 2006. Soil microbial biomass activation by trace amounts of readily available substrate. Biology and Fertility of Soils 42, 542–549. https://doi.org/10.1007/s00374-005-0049-2.
Mori, M., Marinari, E., De Martino, A., 2019. A yield-cost tradeoff governs Escherichia coli's decision between fermentation and respiration in carbon-limited growth. Npj Systems Biology and Applications 5, 16. https://doi.org/10.1038/s41540-019-0093-4.
Murphy, C.J., Baggs, E.M., Morley, N., Wall, D.P., Paterson, E., 2015. Rhizosphere priming can promote mobilisation of N-rich compounds from soil organic matter. Soil Biology and Biochemistry 81, 236–243. https://doi.org/10.1016/j.soilbio.2014.11.027.
Murray, P., Ostle, N., Kenny, C., Grant, H., 2004. Effect of defoliation on patterns of carbon exudation from Agrostis capillaris. Journal of Plant Nutrition and Soil Science 167, 487–493. https://doi.org/10.1002/jpln.200320371.
Nannipieri, P., Eldor, P., 2009. The chemical and functional characterization of soil N and its biotic components. Soil Biology and Biochemistry 41, 2357–2369. https://doi.org/10.1016/j.soilbio.2009.07.013.
Nottingham, A.T., Turner, B.L., Chamberlain, P.M., Stott, A.W., Tanner, E.V.J., 2012. Priming and microbial nutrient limitation in lowland tropical forest soils of contrasting fertility. Biogeochemistry 111, 219–237.
Oyewole, O.A., Inselsbacher, E., Näsholm, T., 2014. Direct estimation of mass flow and diffusion of nitrogen compounds in solution and soil. New Phytologist 201, 1056–1064. https://doi.org/10.1111/nph.12553.
Papp, K., Hungate, B.A., Schwartz, E., 2020. Glucose triggers strong taxon-specific responses in microbial growth and activity: insights from DNA and RNA qSIP. Ecology 101, 1–12. https://doi.org/10.1002/ecy.2887.
Pfeiffer, T., Bonhoeffer, S., 2003. An evolutionary scenario for the transition to undifferentiated multicellularity. Proceedings of the National Academy of Sciences 100, 1095–1098. https://doi.org/10.1073/pnas.0335420100.
Pfeiffer, T., Schuster, S., Bonhoeffer, S., 2001. Cooperation and competition in the evolution of ATP-producing pathways. Science 292, 504–507. https://doi.org/10.1126/science.1058079.
Phillips, R.L., Zak, D.R., Holmes, W.E., White, D.C., 2002. Microbial community composition and function beneath temperate trees exposed to elevated atmospheric carbon dioxide and ozone. Oecologia 131, 236–244. https://doi.org/10.1007/s00442-002-0868-x.
R Core Team, 2022. R: A Language and Environment for Statistical Computing. R Foundation for Statistical Computing, Vienna, Austria [WWW Document]. URL. https://www.r-project.org/.
Santner, J., Larsen, M., Kreuzeder, A., Glud, R.N., 2015. Two decades of chemical imaging of solutes in sediments and soils – a review. Analytica Chimica Acta 878, 9–42. https://doi.org/10.1016/j.aca.2015.02.006.
Sauer, D., Kuzyakov, Y., Stahr, K., 2006. Spatial distribution of root exudates of five plant species as assessed by 14C labeling. Journal of Plant Nutrition and Soil Science 169, 360–362. https://doi.org/10.1002/jpln.200621974.
Schimel, J.P., Weintraub, M.N., 2003. The implications of exoenzyme activity on microbial carbon and nitrogen limitation in soil: a theoretical model. Soil Biology and Biochemistry 35, 549–563. https://doi.org/10.1016/S0038-0717(03)00015-4.
Schink, S.J., Christodoulou, D., Mukherjee, A., Athaide, E., Brunner, V., Fuhrer, T., Bradshaw, G.A., Sauer, U., Basan, M., 2022. Glycolysis/gluconeogenesis specialization in microbes is driven by biochemical constraints of flux sensing. Molecular Systems Biology 18. https://doi.org/10.15252/msb.202110704.
Seitz, V.A., McGivern, B.B., Daly, R.A., Chaparro, J.M., Borton, M.A., Sheflin, A.M., Kresovich, S., Shields, L., Schipanski, M.E., Wrighton, K.C., Prenni, J.E., 2022. Variation in root exudate composition influences soil microbiome membership and function. Applied and Environmental Microbiology 88. https://doi.org/10.1128/aem.00226-22.
Shi, S., Richardson, A.E., O'Callaghan, M., DeAngelis, K.M., Jones, E.E., Stewart, A., Firestone, M.K., Condron, L.M., 2011. Effects of selected root exudate components on soil bacterial communities. FEMS Microbiology Ecology 77, 600–610. https://doi.org/10.1111/j.1574-6941.2011.01150.x.
Smith, W.H., 1976. Character and significance of forest tree root exudates. Ecology 57, 324–331. https://doi.org/10.2307/1934820.
Song, W., Hu, C., Luo, Y., Clough, T.J., Wrage-Mönnig, N., Ge, T., Luo, J., Zhou, S., Qin, S., 2023. Nitrate as an alternative electron acceptor destabilizes the mineral associated organic carbon in moisturized deep soil depths. Frontiers in Microbiology 14. https://doi.org/10.3389/fmicb.2023.1120466.
Spohn, M., Carminati, A., Kuzyakov, Y., 2013. Soil zymography – a novel in situ method for mapping distribution of enzyme activity in soil. Soil Biology and Biochemistry 58, 275–280. https://doi.org/10.1016/j.soilbio.2012.12.004.
Szenk, M., Dill, K.A., De Graff, A.M.R., 2017. Why do fast-growing bacteria enter overflow metabolism? Testing the membrane real estate hypothesis. Cell Systems 5, 95–104. https://doi.org/10.1016/j.cels.2017.06.005.
Takaya, N., 2002. Dissimilatory nitrate reduction metabolisms and their control in fungi. Journal of Bioscience and Bioengineering 94, 506–510. https://doi.org/10.1016/S1389-1723(02)80187-6.
Vetterlein, D., Carminati, A., Kögel-Knabner, I., Bienert, G.P., Smalla, K., Oburger, E., Schnepf, A., Banitz, T., Tarkka, M.T., Schlüter, S., 2020. Rhizosphere spatiotemporal organization–A key to rhizosphere functions. Frontiers in Agronomy 2, 1–22. https://doi.org/10.3389/fagro.2020.00008.
Vives-Peris, V., de Ollas, C., Gómez-Cadenas, A., Pérez-Clemente, R.M., 2020. Root exudates: from plant to rhizosphere and beyond. Plant Cell Reports 39, 3–17. https://doi.org/10.1007/s00299-019-02447-5.
Vogel, C., Mueller, C.W., Höschen, C., Buegger, F., Heister, K., Schulz, S., Schloter, M., Kögel-Knabner, I., 2014. Submicron structures provide preferential spots for carbon and nitrogen sequestration in soils. Nature Communications 5, 1–7. https://doi.org/10.1038/ncomms3947.
Voltolini, M., Taş, N., Wang, S., Brodie, E.L., Ajo-Franklin, J.B., 2017. Quantitative characterization of soil micro-aggregates: new opportunities from sub-micron resolution synchrotron X-ray microtomography. Geoderma 305, 382–393. https://doi.org/10.1016/j.geoderma.2017.06.005.
Warren, C.R., 2018. Development of online microdialysis-mass spectrometry for continuous minimally invasive measurement of soil solution dynamics. Soil Biology and Biochemistry 123, 266–275. https://doi.org/10.1016/j.soilbio.2018.05.022.
Wenzel, W.W., Wieshammer, G., Fitz, W.J., Puschenreiter, M., 2001. Novel rhizobox design to assess rhizosphere characteristics at high spatial resolution. Plant and Soil 237, 37–45. https://doi.org/10.1023/A:1013395122730.
Wickham, H., 2016. ggplot2: Elegant Graphics for Data Analysis. Springer-Verlag, New York.
Wild, B., Schnecker, J., Alves, R.J.E., Barsukov, P., Bárta, J., Čapek, P., Gentsch, N., Gittel, A., Guggenberger, G., Lashchinskiy, N., Mikutta, R., Rusalimova, O., Šantrůčková, H., Shibistova, O., Urich, T., Watzka, M., Zrazhevskaya, G., Richter, A., 2014. Input of easily available organic C and N stimulates microbial decomposition of soil organic matter in arctic permafrost soil. Soil Biology and Biochemistry 75, 143–151. https://doi.org/10.1016/j.soilbio.2014.04.014.
Willers, C., Jansen van Rensburg, P.J., Claassens, S., 2015. Phospholipid fatty acid profiling of microbial communities-a review of interpretations and recent applications. Journal of Applied Microbiology 119, 1207–1218. https://doi.org/10.1111/jam.12902.
Wolfe, A.J., 2005. The acetate switch. Microbiology and Molecular Biology Reviews 69, 12–50. https://doi.org/10.1128/MMBR.69.1.12-50.2005.
Wortel, M.T., Noor, E., Ferris, M., Bruggeman, F.J., Liebermeister, W., 2018. Metabolic enzyme cost explains variable trade-offs between microbial growth rate and yield. PLoS Computational Biology 14, e1006010. https://doi.org/10.1371/journal.pcbi.1006010.
Zhalnina, K., Louie, K.B., Hao, Z., Mansoori, N., da Rocha, U.N., Shi, S., Cho, H., Karaoz, U., Loqué, D., Bowen, B.P., Firestone, M.K., Northen, T.R., Brodie, E.L., 2018. Dynamic root exudate chemistry and microbial substrate preferences drive patterns in rhizosphere microbial community assembly. Nature Microbiology 3, 470–480. https://doi.org/10.1038/s41564-018-0129-3.
Zhu, B., Gutknecht, J.L.M.M., Herman, D.J., Keck, D.C., Firestone, M.K., Cheng, W., 2014. Rhizosphere priming effects on soil carbon and nitrogen mineralization. Soil Biology and Biochemistry 76, 183–192. https://doi.org/10.1016/j.soilbio.2014.04.033.
zu Schweinsberg-Mickan, M.S., Joergensen, R.G., Müller, T., 2010. Fate of 13C- and 15N-labelled rhizodeposition of Lolium perenne as function of the distance to the root surface. Soil Biology and Biochemistry 42, 910–918. https://doi.org/10.1016/j.soilbio.2010.02.007.

Chapter 3

Preferential use of organic acids over sugars by soil microbes in simulated root exudation

Preferential use of organic acids over sugars by soil microbes in simulated root exudation

Julia Wiesenbauer [a,b], Stefan Gorka [a,b], Kian Jenab [a,b], Raphael Schuster [a], Naresh Kumar [c], Cornelia Rottensteiner [a], Alexander König [a,d], Stephan Kraemer [e], Erich Inselsbacher [d], Christina Kaiser [a]

Correspondence author: Christina Kaiser, christina.kaiser@univie.ac.at, Julia Wiesenbauer, Julia.wiesenbauer@univie.ac.at

[a] Division of Terrestrial Ecosystem Research, Centre for Microbiology and Environmental Systems Science, University of Vienna, Vienna, Austria, Djerassiplatz 1, A-1030, Wien, Austria

[b] Doctoral School in Microbiology and Environmental Science, University of Vienna, Vienna, Austria

[c] Soil Chemistry, Wageningen University and Research, Wageningen, The Netherlands

[d] University of Natural Resources and Applied Life Sciences Vienna, Department of Forest and Soil Sciences, Institute of Soil Research, Vienna, Austria

[e] Department of Environmental Geosciences, Centre for Microbiology and Environmental Systems Science, University of Vienna, Vienna, Austria

Abstract

Sugars and organic acids, primary components in plant root exudates, are thought to enhance microbial decomposition of organic matter in the rhizosphere. However, their specific impacts on microbial activity and nutrient mobilisation remain poorly understood. Here, we simulated passive root exudation to investigate the distinct effects of sugars and organic acids on microbial metabolism in the rhizosphere. We released ^{13}C-labelled sugars and/or organic acids via reverse microdialysis into intact meadow and forest soils over 6-hours. We measured substrate-induced microbial respiration, soil organic matter mineralization, metabolite concentrations, and substrate incorporation into lipid-derived fatty acids. Our results reveal a pronounced microbial preference for organic acids over sugars, with organic acids being removed faster from the exudation spot and preferentially respired by microbes. Unlike sugars, organic acids increased concentrations of microbial metabolic byproducts and cations (K, Ca, Mg) near the exudation spot. Our results challenge the prevailing assumption that sugars are the most readily available and rapidly consumed substrates for soil microbes. Microbial preference for organic acids indicates a trade-off between rapid biomass growth and ATP yield. Our findings underscore the significant role of exudate composition in influencing microbial dynamics and nutrient availability, and emphasize the importance of biotic and abiotic feedback mechanisms in the rhizosphere in regulating root exudation.

Key words:

Artificial root exudate, rhizosphere processes, biogeochemical feedback, cation mobilization, short-chain fatty acids, microbial metabolites, growth yield trade-off

1. Introduction

Plants release a considerable fraction of recently photo-assimilated carbon (C) as low-molecular weight compounds, such as sugars, organic acids and amino acids, via their fine roots (Badri and Vivanco, 2009; Jones et al., 2009; Canarini et al., 2019; Vives-Peris et al., 2020). These root exudates trigger a cascade of biotic and abiotic interactions in the rhizosphere. They facilitate the release of organic matter from mineral surfaces, and enhance its decomposition by soil microbes, thereby increasing nutrient availability in the soil immediately surrounding the roots (Brzostek et al., 2013; Drake et al., 2013; Kuzyakov and Blagodatskaya, 2015; Mommer et al., 2016; Lu et al., 2019). Root exudation rates, which are linked to plant photosynthesis rates, appear to be increasing due to increasing atmospheric CO_2 concentrations, with repercussions for soil organic matter turnover in the rhizosphere (Phillips et al., 2011; Meier et al., 2015; Calvo et al., 2017; Gargallo-Garriga et al., 2018; Dong et al., 2021).

Beyond just the quantity of root exudates, the chemical identity of exudates is expected to influence rhizosphere processes. Sugars and organic acids, two of the main compound classes in root exudates (Smith, 1976; Fender et al., 2013), are expected to affect the abiotic and biotic soil environment differently (Jones et al., 2003; Oburger et al., 2009; Steinauer et al., 2016). In contrast to sugars, organic acids are charged, and so they are more likely to be sorbed to the soil mineral phase, becoming unavailable to microbes until desorption (Jones and Edwards, 1998). Moreover, organic acids liberate organic compounds from mineral-organic associations, facilitating their subsequent decomposition by soil microbes (Keiluweit et al., 2015; Jilling et al., 2021). At the same time, they solubilise or desorb mineral-associated nutrients and metals through acidification, chelation, and exchange reactions (Keiluweit et al., 2015; Adeleke et al., 2017; Jilling et al., 2021). Sugars, on the other hand, are thought to be primarily and rapidly taken up and metabolised by microorganisms, with sorption, leaching and plant uptake playing a much smaller role (Gunina and Kuzyakov, 2015). When artificial root exudates were added to low fertility grassland soils, sugars increased respiration and dissolved organic C (DOC) more strongly than did organic acids (Liu et al., 2022). Additionally, an experiment applying different root exudate compounds to woodland soils showed that glucose was more strongly retained in microbial biomass than oxalic acid (Oldfield et al., 2018). Conversely, it is thought that organic acids cause stronger changes to the microbial community composition than sugars, as they are likely metabolised by specialised microorganisms, whereas sugars are utilised by a broader range of microbes (Landi et al., 2006; Eilers et al., 2010; Shi et al., 2011; Macias-Benitez et al., 2020).

Microbial growth on organic acids requires different metabolic pathways than those used when growing on sugars. Organic acids, such as short chain fatty acids, need to be transformed by specific enzymes into acetyl-coenzyme A, which is then fed into the Tricarboxylic Acid (TCA) cycle to obtain energy (Pavoncello et al., 2022). The production of precursors necessary for cellular biosynthesis requires: i) a 'glyoxylate bypass' in the TCA cycle to produce, e.g., amino acid precursors (Wolfe, 2005; Pavoncello et al., 2022) and ii) gluconeogenesis for the synthesis of glucose from non-carbohydrate precursors. The latter pathway runs in the opposite direction to glycolysis (breakdown of glucose to pyruvate) (Schink et al., 2022). Microbes may switch between sugar and organic acid metabolization, but the reversal of the central C flux direction, from glycolysis to gluconeogenesis, and vice versa, involves a lag phase of minutes to hours (Basan et al., 2020). On the one hand, a switch to gluconeogenesis can occur after the depletion of sugars that were initially metabolised by glycolysis. For example, *E. coli* excretes acetate during overflow metabolism as a strategy to maximise growth on glucose (Basan et al., 2015), and may later switch to utilizing this acetate once glucose is depleted (Wolfe, 2005). However, it has also been shown that *E. coli* co-consumes acetate and glucose when glucose is present in excess (Enjalbert et al., 2017). On the other hand, both metabolic pathways could run side by side, carried out by different parts of the microbial community specialised in the utilization of different substrates (cross-feeding), which would allow for a more resource-efficient utilization of available substrates within the microbial community. It is therefore unsurprising that substrate identity affects microbial community assembly (composition, diversity) and function (Shi et al., 2011; Steinauer et al., 2016; Zhalnina et al., 2018; Gu et al., 2020; Estrela et al., 2021).

To date, the magnitude and nature of the effects of root exudate composition on microbial activity is elusive. Little is known about the distinct effects of major compound classes, such as sugars or organic acids, on the dynamics of complex microbial communities in the rhizosphere. Although some studies have investigated the effect of different compound classes in artificial root exudates on rhizosphere processes, such as soil-mineral interactions (Keiluweit et al., 2015), soil organic C and nitrogen (N) turnover (Chari and Taylor, 2022; Liu et al., 2022) and greenhouse gas fluxes (Girkin et al., 2018a, 2018b), we still lack a deeper understanding of how rhizosphere communities utilise different compound classes within exudates.

Studying microbial processes in undisturbed soil is crucial for obtaining accurate and ecologically relevant insights, as biogeochemical and structural heterogeneities at the pore-scale govern soil processes and functions (Schlüter et al., 2020). Intact soil structure preserves the natural spatial distribution of resources and decomposers, significantly influencing microbial access to resources and thereby affecting microbial activity and decomposition processes (Nunan et al., 2020). Equally important is the accurate simulation of passive root exudation. Artificial 'root exudates' can be

introduced into the soil using various techniques beyond directly mixing substrates into the soil. Methods include the addition of 'exudates' with pipettes or needles (Luo et al., 2014; Steinauer et al., 2016; Liu et al., 2022), delivery through microporous capillaries (Baumert et al., 2018; Sokol and Bradford, 2019; X. Zhang et al., 2019; Chari and Taylor, 2022) or by an automated drip-tip system (ARES) (Lopez-Sangil et al., 2017). These so-called 'artificial roots' often combine exudate release with water flow. However, most root exudates are passively released (Canarini et al., 2019), thereby depending on diffusion gradients, which create a direct feedback between their removal by biotic and abiotic soil processes and exudate release rates. Conventional mass flow-based 'artificial roots' cannot account for this feedback, highlighting the need for methods that better simulate natural passive exudation.

By contrast, 'reverse microdialysis', which relies on passive diffusion through a small permeable membrane, enables the release of compounds from the microdialysis probe based on concentration gradients between the membrane's interior and the surrounding soil solution (Buckley et al., 2022; König et al., 2022; Wiesenbauer et al., 2024). This method provides a more realistic simulation of passive root exudation by modelling how rhizosphere processes affect compound release rates. Specifically, if these compounds are not removed from the soil solution by biotic or abiotic processes, their accumulation inhibits further diffusion, highlighting the dynamic feedback from the rhizosphere. Measuring this 'uptake' feedback not only offers insights into processes that selectively remove certain compounds from the rhizosphere but may also inform about the capacity for passive exudate release by plant roots under specific conditions.

Our previous work showed that organic acids were released more rapidly than sugars in soil, suggesting quicker removal from the rhizosphere compared to sugars (König et al., 2022; Wiesenbauer et al., 2024). We showed that this faster removal cannot be attributed to molecular size, which primarily governs diffusion in water. Instead, it may result from a more rapid adsorption to soil minerals or a microbial preference for metabolizing organic acids over sugars. This finding contradicts the general consensus that simple sugars are more rapidly metabolised by soil microbes due to their high energy yield (Gunina and Kuzyakov, 2015; Schink et al., 2022). To determine whether abiotic processes or microbial preferences for metabolising organic acids drive these differences in the rhizosphere, it is necessary to measure microbial utilisation of different compound classes individually. This approach would enhance our understanding of how different compound classes within root exudates contribute to nutrient mobilisation and C turnover in the rhizosphere.

The aim of this study was to analyse the distinct effects of sugars and organic acids, primary components of plant root exudates, on fine-scale temporal dynamics of microbial activity and soil

chemistry at root exudation hotspots in intact soil. Specifically, we aimed to differentiate the impact of these compound classes on microbial and abiotic rhizosphere processes at root exudation hotspots using two distinctly different soil types—beech forest soil and extensively managed meadow soil—allowing for a broader perspective. To investigate this, we utilized reverse microdialysis to release ^{13}C-labelled sugars and organic acids, both individually and in combination, into intact soil cores over a 6-hour period while simultaneously collecting metabolites from the soil solution for 18 days. In addition to analysing the temporal metabolite dynamics, we measured substrate-induced respiration and soil organic matter (SOM) mineralization, and the incorporation of substrates into microbial biomass, using lipid-derived fatty acids.

We hypothesize that:

a) Sugars, being the most readily available substrate to the broader microbial community, will elicit stronger microbial responses than organic acids.
b) A combination of sugars and organic acids in artificial root exudates will produce additive effects, increasing respiration rates and diversifying the spectrum of produced metabolites, compared to when these substrates are provided separately, as each compound class stimulates different microbial groups and metabolic pathways.
c) The impact of artificial root exudates on microbial activity will show consistent patterns across different soil types, suggesting that microbial responses are primarily determined by the type of exudates rather than by soil properties.

2. Materials and Methods

2.1 Soil sampling

Soil samples were collected from an extensively managed meadow (Gumpenstein, Austria, 47° 29' N, 14° 06' E, 732 m asl.) on 11th July, 2019, which was a Cambisol with loamy sand texture (Reinthaler et al., 2021), and a mature beech (*Fagus sylvatica*) forest (Klausen-Leopoldsdorf, Austria, 48° 07' N, 16° 03' E, 510 m asl.) on 23rd July, 2019, which was a Dystric Cambisol with silty clay texture (König et al., 2022) (Tab. 1). For both sites, the upper 6 cm of soil was sampled after removing the above-ground biomass and the litter layer. Samples were taken at five spots along an 8 m transect in the meadow soil and five random spots within a 5 x 5 m plot in the beech forest, using large soil cores (10 cm diameter, 6 cm height).

Table 1. Soil properties of forest and meadow soils.

Soil properties	(a) Forest	(b) Meadow
Soil type	Dystric Cambisol	Cambisol
Texture	3% sand, 51% silt, 46% clay (silty clay)	44.2% sand, 47.6% silt, 8.3% clay (loamy sand)
pH (H_2O)	4.27 ± 0.17	5.74 ± 0.17
DOC (mg g^{-1})	0.16 ± 0.02	0.27 ± 0.03
TN (mg g^{-1})	0.04 ± 0.0	0.04 ± 0.0
C_{mic} (mg g^{-1})	0.97 ± 0.16	1.78 ± 0.28
N_{mic} (mg g^{-1})	0.09 ± 0.01	0.42 ± 0.04
$C:N_{mic}$	10.78 ± 0.5	4.15 ± 0.28
Al (mg g^{-1})	12.44 ± 0.23	14.03 ± 0.13
Ca (mg g^{-1})	1.77 ± 0.38	3.09 ± 0.23
Cr (mg g^{-1})	0.03 ± 0	0.05 ± 0
Cu (mg g^{-1})	0.03 ± 0	0.04 ± 0
Fe (mg g^{-1})	24.73 ± 0.66	30.47 ± 0.3
Mg (mg g^{-1})	2.68 ± 0.11	9.2 ± 0.13
Mn (mg g^{-1})	1.11 ± 0.11	0.55 ± 0.01
Na (mg g^{-1})	0.06 ± 0	0.04 ± 0
Ni (mg g^{-1})	0.03 ± 0	0.04 ± 0
Zn (mg g^{-1})	0.07 ± 0	0.1 ± 0.01

The pH, dissolved organic C (DOC), total N (TN), microbial C and N, microbial C:N ratio, and elemental concentrations of (a) forest and (b) meadow soil. All values are mean ± SE, n = 5. Exceptions include DOC, C_{mic}, $C:N_{mic}$ for forest soil, for which n=3.

Initial soil analyses were conducted on samples sieved to 2 mm, collected adjacent to the soil cores used for the microdialysis experiment. These analyses included measurements of pH in soil slurries (water), and dissolved organic C, total N, microbial C and N by chloroform fumigation extraction (Tab. 1, Methods S1). Total element concentration (Al, Ca, Cr, Cu, Fe, Mg, Mn, Na, Ni, Zn) of acid-digested (Aqua regia), finely ground, lyophilised soils was measured by inductively coupled plasma optical emission spectroscopy (ICP-OES, 5110, Agilent Technologies, USA) (Tab. 1).

We determined gravimetric water content of soils sampled with a small soil corer (1 cm diameter, 3 cm height) from larger cores. After removing roots, stones and organic material with tweezers, the soil was dried overnight in a drying oven. Initial gravimetric water content was 19 ± 3% (mean ± SD) in meadow and 12 ± 3% in forest soils. The gravimetric water content of the large soil cores was adjusted to 30% during the 2-3 days post-sampling while the soils were incubated at field temperature (12 °C; until experiment). Water was added incrementally using a pipette to ensure even distribution across

the soil surface: 5 ml was pipetted onto each core on the first and second days, and on the third day, the remaining volume (< 5 ml) necessary to achieve the target 30% gravimetric water content was added. This adjustment was critical to ensure the effective microdialysis performance, as the soil water content is essential for facilitating compound diffusion, particularly at the slow flow rates used in our experiments (Buckley et al., 2020; Müller et al., 2023).

2.2 Experimental design

To investigate the response of rhizosphere processes to simulated root exudate input in intact soil, we designed a microdialysis experiment using the large soil cores that preserved the natural soil structure. Three days after collection, eight smaller soil cores (1 cm diameter) were extracted from each large soil core using stainless-steel pipes fashioned into corers. These corers had an inner diameter of 0.95 cm and a wall thickness of 0.25 cm and were cut into 3 cm length. Subsampling was performed to ensure even distribution of the eight 1-cm diameter cores within each large core. From these, pair of cores – twin cores – were formed, assigning one pair to each of four experimental treatments. This resulted in a total of 40 twin cores, i.e., 40 pairs of small soil cores, with five replicates per treatment across two different soils. These twin cores were treated as a single analytical unit and placed in a customised setup, termed a 'mesocosm', to ensure unified measurements of respiration, collection of analytes ('dialysates') and soil harvesting.

The twin-core approach was a modification from our previous study, which used a single large core (2.8 x 3 cm) (König et al., 2022; Wiesenbauer et al., 2024). In that experiment, we determined that the microdialysis probe's influence was limited to a smaller volume around the probe (< 0.5 cm radius) than initially expected (Wiesenbauer et al., 2024). Consequently, in our current study, we adopted smaller soil cores to ensure the entire soil was affected by the microdialysis probe. This adjustment also ensures that changes in SOM-derived respiration in response to artificial root exudates are more effectively captured, enhancing the sensitivity and accuracy of our respiration measurements.

For the mesocosm assembly, we used 50 ml Falcon tubes, modified by turning them on their lid and cutting them off at 4 cm height, with a Styrofoam placed into the lid to securely hold the twin soil cores in their stainless-steel corers (Fig. S1). Into the centre of each small soil core, a microdialysis probe (CMA 20, CMA Microdialysis AB, Kista, Sweden) with a membrane length of 10 mm and a molecular weight cut-off of 20 kDa was inserted.

The microdialysis probes were connected to syringe pumps (CMA 4004, CMA Microdialysis AB, Solna, Sweden), set to perfuse at a rate of 2.5 µl min^{-1} per membrane (the liquid is called perfusate).

Each pair of cores within a mesocosm was connected via a Y-connector (CMA Microdialysis AB) to one syringe that delivered equal volume to both cores, ensuring homogeneous perfusion across twin cores. Additionally, the microdialysis probes were connected to cooled (6 °C) fraction collectors (CM4 470, CMA Microdialysis AB, Solna, Sweden), which collected dialysate samples (i.e., the liquid containing the analytes collected through passive diffusion from the soil solution) in fractions of 45 min (112.5 µl). The dialysates from each pair were pooled, reflecting a combined response from the twin cores, which allowed for a comprehensive assessment of nutrient dynamics within the mesocosm.

2.3 Simulation of root exudation using microdialysis

On day 1 of our 18-day long microdialysis experiment, we simulated a 6-hour long root exudation using the 'reverse' microdialysis approach (König et al., 2022). To investigate the effect of different root exudate compositions on soil metabolite dynamics, we utilised three artificial exudates (i.e., perfusates): pure sugar, pure organic acids, a combination of both, alongside a water-only control for comparison. Specifically, sugar-only exudates consisted of glucose and fructose, organic acid-only exudates contained acetic and succinic acid, and the mixed exudate was comprised of all four compounds, each uniformly labelled with 99 atom% ^{13}C (Sigma-Aldrich). A C concentration of 500 µmol C l^{-1} per compound was maintained in each exudate treatment. This approach was chosen to facilitate direct comparisons and isolate the effects of compound type from those related to carbon concentration, allowing us to attribute variations in response specifically to the properties of the individual compounds themselves. Specifically, the sugar treatment comprised 500 µmol C l^{-1} each of glucose and fructose, totalling 1000 µmol C l^{-1}. The organic acid treatment contained 500 µmol C l^{-1} each of acetate and succinate, also totalling 1000 µmol C l^{-1}. For the mixed treatment, each of the four compounds (glucose, fructose, acetate, succinate) was included at 500 µmol C l^{-1}, totalling 2000 µmol C l^{-1}. These compounds, commonly found in root exudates (Smith, 1976), were selected to cover a range of chemical structures typical of root exudates (Vives-Peris et al., 2020). It is important to note that the ratio of sugars to organic acids in this study was not designed to replicate the composition found in natural root exudates, as this ratio varies widely across different plant species (Smith, 1976; Williams et al., 2022), growth phases (Gransee and Wittenmayer, 2000), and environmental conditions (Gargallo-Garriga et al., 2018).

Initially, all mesocosms were infused with ultrapure water for 3 hours to assess the initial state of soil solution chemistry. Subsequently, each mesocosm was infused with its respective perfusate, i.e., either artificial root exudate (sugars, organic acids, mixed) or ultrapure water for controls. Following the 6-hour exudate simulation, all treatments were continuously infused with ultrapure water for

three days, during which dialysates were collected to further explore soil metabolite dynamics. All dialysates were pooled in 3-hour fractions (four consecutive 45-minute dialysates) and stored at -20 °C until analysis. After this period, the pumps were turned off, and the membranes were left in the soils. Subsequently, on days 4, 5, 6 and 18, the pumps were turned on for 4.5 hours each day to collect additional dialysates.

2.4 Soil metabolite analysis

Concentrations of sugars, organic and inorganic anions, and cations in the dialysates were quantified using high-performance liquid chromatography (HPLC, Dionex ICS 5000+, Thermo Fisher, Germany). Sugars (supplements: glucose, fructose; not detectable: galactose, sucrose) were measured on a Thermo CarboPac PA20 (0.4 x 150 mm) column with a Thermo CarboPac PA20G (0.4 x 35 mm) guard column at a constant flow rate of 8 µl min^{-1} with a KOH solvent. Anions (butyrate, lactate, propionate; supplements: acetate, succinate; no significant response: citrate, formate, malate, nitrate, oxalate, phosphate, sulfate) were measured on a Dionex IonPac AS11-HC (2 x 250 mm) column with a Dionex IonPac AG11-HC (2 x 50 mm) guard column at a constant flow rate of 0.25 ml min^{-1} with a KOH solvent. Cations (ammonium, potassium, magnesium, calcium; not quantifiable: manganese) were measured on a Dionex IonPac CS16 (5 x 250 mm) column with a guard column at a constant flow rate of 1 ml min^{-1} with a methansulfonic acid as solvent. Further details on the HPLC methods are provided in supporting information (Methods S2, S3, S4). Sugars and anions were measured at 14 time points, while cations were measured at 8 time points throughout the experiment.

2.5 Transfer and retrieval rates

We determined the release of glucose, fructose, acetate and succinate into the soil as the percentage of the total concentration of each compound in the exudation solution that was passively released into the soil. We calculated these so-called 'transfer rates' based on the compound concentrations in the exudation solution before and after their passage through the microdialysis system (König et al., 2022).

$$Transfer\ rate\ (\%) = \left(\frac{C_{perfusate} - C_{dialysate}}{C_{perfusate}}\right) * 100 \quad (1)$$

where $C_{perfusate}$ is the concentration in the exudation solution before it was pumped through the microdialysis system ('perfusate') and $C_{dialysate}$ is the concentration in the exudation solution that was collected after it was pumped through the microdialysis system ('dialysate').

Additionally, 'retrieval rates' were calculated as the percentage of released compounds that were recovered from the soil surrounding the membrane over a 12-hour period following the exudation. During this period, all treatments were infused with ultra-pure water to collect compounds present in the soil solution around the membrane.

$$Retrieval\ rate\ (\%) = \frac{C_{retrieved}}{C_{released}} * 100 \quad (2)$$

Here, $C_{released}$ is the total amount of a compound released during the 6-hour exudation pulse and $C_{retrieved}$ is the amount recovered from soil within 12 hours.

The transfer rates reflect the efficiency with which compounds pass from the perfusate though the microdialysis membrane into the surrounding soil solution. In water, transfer rates are primarily governed by diffusive molecular properties like size and charge. In intact soils, however, transfer rates are significantly lower and predominantly determined by soil type, independent of molecular properties (König et al., 2022). This difference arises because the soil's physical structure confines the diffusible space for released molecules to a small volume around the membrane. Molecules that are not removed by biotic (e.g. microbial assimilation) or abiotic (e.g. adsorption to minerals) mechanisms quickly accumulate outside the membrane, restricting further diffusion. Determining transfer rates of certain molecules into a given soil will thus inform about how readily these compounds are removed from the surrounding of the exudation spot by abiotic or biotic mechanisms.

Retrieval rates also provide insight into the dynamics of compound removal following their release. Higher retrieval rate suggest that a larger proportion of the initially released compounds remained in the soil solution, not assimilated by microbes or removed by abiotic processes, and were therefore recoverable. Thus, retrieval rates measure the extent to which released compounds are either retained or processed in the soil environment post-release.

2.6 Respiration measurements

To measure microbial respiration, mesocosms were placed in airtight jars fitted with septa for gas sampling (Fig. S1). Microdialysis tubing was passed through the septa to enable continuous dialysate collection. Gas samples were taken before, during, and after the substrate pulse on day 1, with additional samples collected on subsequent days 2, 4, 6, and 18. For gas sampling, the jars were closed, the first gas sample was taken with a syringe (18 ml) and replaced with artificial air (200 ppm CO_2) to prevent negative atmospheric pressure. After incubation (~90 min on day 1 & 2; during exudation ~180 min for forest and ~130 min for meadow), a second gas sample was taken, and jars were opened. On days 4, 6, and 18, incubation lasted ~140 min, except ~180 min for meadow soils on day 8. We

measured CO_2 concentration and ^{13}C signature of gas samples using a headspace gas sampler (GasBench II, Thermo Fisher Scientific, Bremen, Germany) coupled to an isotope ratio mass spectrometer (Delta V Advantage, Thermo Electron, Bremen, Germany). The CO_2 concentration and ^{13}C signature of the second gas sample were corrected for added artificial air.

The respiration rate (nmol CO_2 g^{-1} dw h^{-1}) and its atom percent ^{13}C (at% ^{13}C) signature were calculated as the difference of ^{12}C-CO_2 and ^{13}C-CO_2 concentration between the first and second corrected gas sample. Using uniformly ^{13}C-labelled substrates allowed us to distinguish between substrate-derived and SOM-derived respiration using a two-pool mixing model, considering the ^{13}C signature of added substrate and natural ^{13}C abundance of control mesocosm respiration. Detailed calculations are provided in the supporting information (Methods S5).

2.7 Harvest

On day 18, we harvested the soil surrounding the microdialysis membrane from two distances: 'central' (≤ 2.5 mm radius) and 'surrounding' soil (> 2.5 mm radius). After pulling out the microdialysis probe, we used a 5 mm inner diameter stainless steel tube to collect the 'central' soil. Soil of twin cores were pooled for each mesocosm, and small stones and larger organic materials were removed using tweezers. Soils were lyophilised for 48 hours and stored at -20°C until further analysis. The 'surrounding' soil (> 2.5 mm from input) was used for lipid extraction, because the 'central' soil was used for another analysis, which unfortunately remained inconclusive and was thus not added to this manuscript. Consequently, the relatively low ^{13}C signal observed is a conservative estimate of lipid-derived fatty acid enrichment near the membrane, as we previously demonstrated that ^{13}C enrichment decreases significantly with distance from the microdialysis membrane (Wiesenbauer et al., 2024).

2.8 PLFA and NLFA analyses

To assess the incorporation of labile substrates into microbial biomass and their impact on microbial community structure, we extracted the phospholipid and neutral lipid fatty acids (PLFA, NLFA) from the lyophilised 'surrounding' soils (> 2.5 mm from input) as described in Gorka *et al.* (2023). For a complete description of the extraction procedure and fatty acid assignments see the supporting information (Methods S6). The extracted fatty acid methyl esters were analysed using gas chromatography (Trace GC Ultra, Thermo Scientific, Germany) coupled to a mass spectrometer (ISQ, Thermo Scientific, Germany) for fatty acid identification and quantification, as well as a GC-Ultra (Thermo Fisher Scientific, Milan, Italy) coupled to an isotope ratio mass spectrometer (IRMS; Finnigan Delta-V, Thermo Fisher Scientific, Bremen, Germany) for determination of isotopic $^{13}C/^{12}C$ ratios.

2.9 Statistical analysis

All statistical analyses were performed using R version 4.2.2 (R Core Team, 2022). We assessed differences between treatments for each time point in SOM-derived and substrate-derived respiration rates (nmol CO_2 g^{-1} dw h^{-1}), compound concentrations in dialysate (µmol l^{-1}), transfer and retrieval rates (%), and PLFAs and NLFAs (nmol C g^{-1} dw, at% ^{13}C). Since the data did not meet the assumptions of normality, we performed Kruskal-Wallis tests separately for each soil type to determine significant differences ($\alpha = 0.05$) between treatments. This was followed by Dunn's tests as post-hoc analysis (Bonferroni corrected p-values) to identify specific differences between treatments. The Kruskal-Wallis test statistics and Dunn's post-hoc test results of compound concentrations and substrate-derived respiration rates are presented in the supplement tables (Tab. S1, S2, S3). For compound concentrations released during the pulse, we also analysed differences between the first and second half of the exudation pulse using repeated measures ANOVA when assumptions of normality and variance homogeneity were met; otherwise, we used paired Wilcoxon signed-rank tests (Table S4). Figures were created using ggplot2 (Wickham, 2016).

3. Results

3.1 Microbes preferentially respired organic acids compared to sugars

Both forest and meadow soils exhibited higher respiration rates of organic acids compared to sugars (Fig. 1). Substrate addition did not significantly change SOM-derived respiration in either soil with SOM-derived respiration rates remaining similar to controls throughout the 18-day experiment (Fig. 1). Both soils exhibited the highest substrate-derived respiration rate during the exudation pulse, which decreased thereafter (Fig. 1). Substrate-derived respiration rates were about 4-8 times higher when organic acids were part of the exudate solution compared to when only sugars were present. There was a minor, non-significant difference in substrate-derived respiration rates between soils receiving sugars and organic acids combined and those receiving only organic acids, which was slightly more pronounced in the meadow soil (Fig. 1, Tab. S1). Substrate respiration was measured for a 3-hour period during the 6-hour input pulse. Extrapolating the measured values to 6 hours, and relating them to the measured C input, shows that about 8, 10 and 9% of the released C has been respired during the pulse in the sugar, organic acid and mixed treatment, respectively.

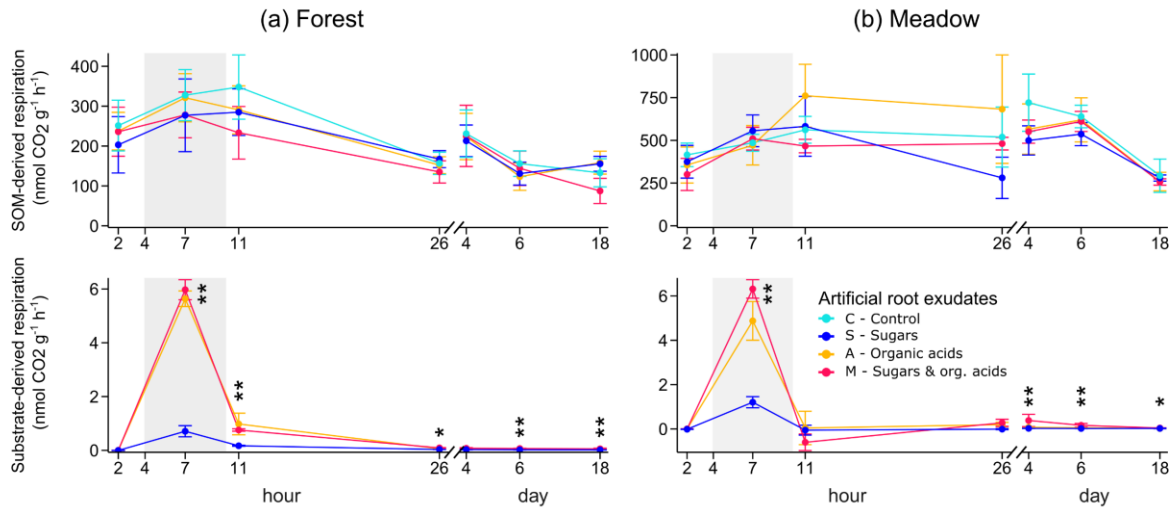


Figure 1. The SOM-derived and substrate-derived respiration rates (nmol CO_2 g^{-1} dw h^{-1}) for (**a**) forest and (**b**) meadow soils. The 6-hour long labile substrate pulse (hours 4-9) is indicated by a grey background. An x-axis break follows the initial 26-hour period, and subsequent measurements (days 4-18) are presented on a day-timescale. Data are presented as means ± SE (*n* = 5). Asterisks denote significant differences (Kruskal-Wallis test, * < 0.05, ** < 0.01, *** < 0.001) between soils that received an input of sugars (dark blue), organic acids (orange), sugars combined with organic acids (pink), and the control (light blue; only SOM-derived respiration). Kruskal-Wallis test statistics and Dunn's post-hoc test results of substrate-derived respiration are provided in Table S1.

3.2 Higher passive release for organic acids than sugars

We observed that the transfer rates - percentage of artificial root exudates that was passively released into the soil - were considerably higher for organic acids (55-67% acetate, 39-41% succinate) than for sugars (7-17% glucose, 14-23% fructose) (Fig. 2, forest: $\chi2(3) = 0.001$, $p < 0.001$, meadow: $\chi2(3) = 31.436$, $p < 0.001$). Additionally, several of the transfer rates were higher in the first half compared to the second half of the 6-hour long labile substrate pulse (Fig. S2, Tab. S4). Given that each compound was present at identical concentration (500 µmol C^{-1} l^{-1} per compound) in the perfusates, i.e. artificial root exudates, differences in transfer rates reflected differences in absolute amounts of C released. Over the 6-hour input period, on average 90-110 nmol C was released from the sugar-only perfusate, while 430-490 nmol C was released from the organic acids-only perfusate (Fig. 3). The mixed sugar and organic-acid treatment released about 550-660 nmol C, reflecting the combined sum of the C released in the sugar-only and organic acids-only treatments. There was no significant difference in the amount of each compound released, regardless of whether they were in a single-compound class treatment or the mixed treatment (Fig. 3).

In the hours after the labile substrate pulse had ended, less than 1% of the released compounds were back retrieved from the forest soil (Fig. 2). In the meadow soil, retrieval rates were varied for different compounds, i.e., less than 1% of acetate and about 6% of succinate were retrieved, while the retrieval rates of glucose and fructose were higher, at 28-42% and 21-25% respectively (Fig. 2, S3).

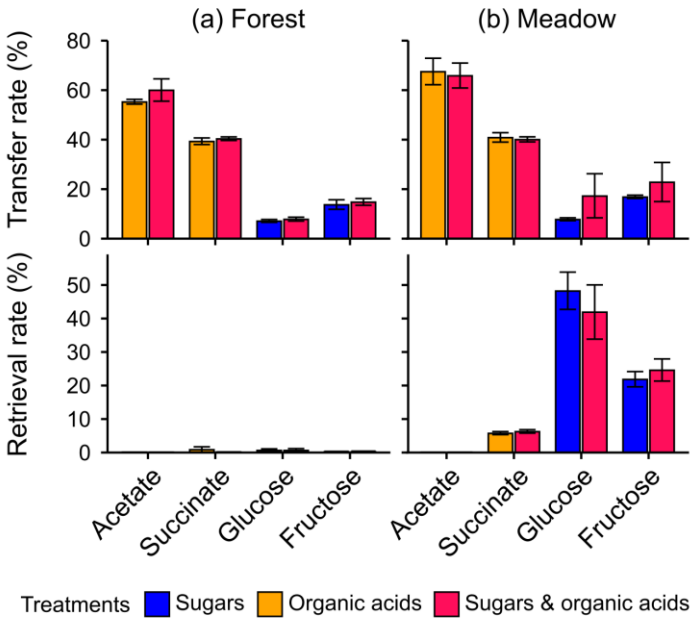


Figure 2. Transfer and retrieval rates (%) of substrates during and after a 6-hour artificial root exudate pulse in (**a**) forest and (**b**) meadow soils. The experiment included three labile substrate treatments ('exudates'): sugar-only (dark blue), containing glucose and fructose; organic acid-only (orange), containing acetate and succinate; and a mixed exudate (pink), containing all four compounds. Each compound was present at a concentration of 500 µmol C l^{-1} in the artificial root exudates. Transfer rates indicate the percentage of these compounds released during the 6-hour pulse, while retrieval rates indicate the percentage of initially transferred substrates recovered from the soil in the 12 hours following the pulse. Transfer and retrieval rates of individual compounds did not significantly differ between substrate treatments (Kruskal-Wallis test). Data are presented as means ± SE (*n* = 5).

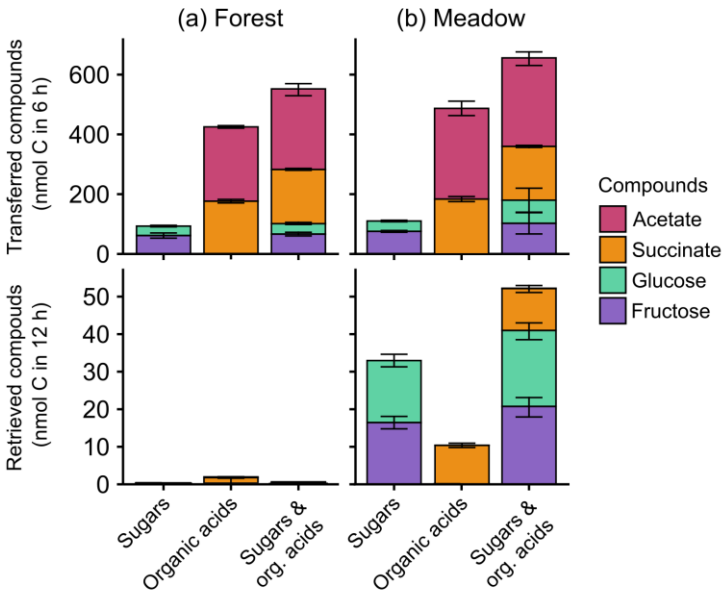


Figure 3. Substrate release and retrieval (nmol C) during and after a 6-hour artificial root exudate pulse in (**a**) forest and (**b**) meadow soils. The experiment included three labile substrate treatments ('exudates'): sugar-only, containing glucose and fructose; organic acid-only, containing acetate and succinate; and a mixture exudate, containing all four compounds. Transferred compounds refers to the amount of C released during the 6-hour pulse, while retrieved compounds quantify the amount of initially added C recovered from the soil in the 12 hours following the pulse. Data are presented as means ± SE (*n* = 5).

3.3 Organic acids, but not sugars, induced increased microbial metabolites and cations

The release of organic acids by reverse microdialysis (with or without sugars) led to a significant rise in the concentrations of the short-chain fatty acids (SCFAs) butyrate, lactate, and propionate during the second half of the simulated root exudation pulse (i.e., at about 3 hours after the start of the pulse) (Fig. 4, Tab. S2). Curiously, in the forest soil the increase in lactate levels was much more pronounced in response to the organic acids-only compared to the mixed exudate, with concentrations increasing 10-fold (Fig.4). In addition, organic acid release (with/ without sugars) significantly increased ammonium (NH_4), potassium (K), magnesium (Mg), and calcium (Ca) concentrations around the probe during the pulse (Fig. 5, Tab. S2). The release of sugars, on the contrary, did not elicit any discernible changes in the concentrations of SCFAs or cations compared to the control (Fig. 4, Fig. 5, Tab. S2). Providing sugars alongside organic acids did not affect the concentrations of metabolites or cations compared to organic acids-only treatment, except for the higher lactate levels in the latter (Fig.4). This pattern of organic acids inducing higher concentrations of metabolites and cations, while sugars did not, was largely consistent across both investigated soils.

In addition to the immediate effects following the simulated root exudation pulse, treatment-induced changes in metabolite and cation concentrations were also observed at later time points (day 2-18, Fig. 4, Fig. 5). They were, however, not consistent across soils or treatments. For instance, lactate concentration was increased after 18 days in the forest soil after mixed compound addition. Similarly, NH_4 was significantly increased in forest soils 6 days after having received organic acids. There was, however, no effect on NH_4 concentrations beyond the first 24 hours in the meadow treatment.

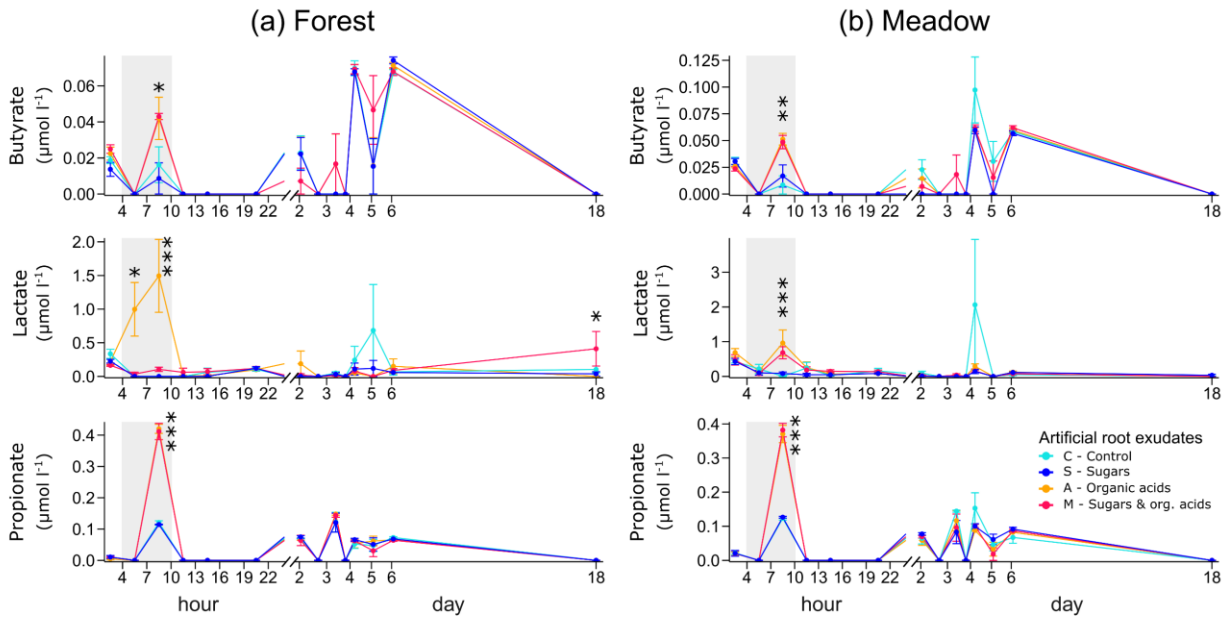


Figure 4. Concentration of butyrate, lactate, and propionate (µmol l^{-1}) in dialysates collected from (**a**) forest and (**b**) meadow soils before, during and after a 6-hour long labile substrate pulse. The period of simulated exudation (hours 4-9) is indicated by a grey background. An x-axis break follows the initial 24-hour period, and subsequent observations (days 2-18) are presented on a day-timescale. Asterisks denote significant differences (Kruskal-Wallis test, * < 0.05, ** < 0.01, *** < 0.001) between soils that received an input of sugars (dark blue), organic acids (orange), a mixture of sugars and organic acids (pink), and control (light blue). Data are presented as means ± SE (*n* = 5). Each data point represents the mean concentration measured in dialysates collected over a 3-hour period on day 1 and a 4.5-hour period on subsequent days, plotted at the midpoint of each collection period. Kruskal-Wallis test statistics and Dunn's post-hoc test results are provided in Table S2.

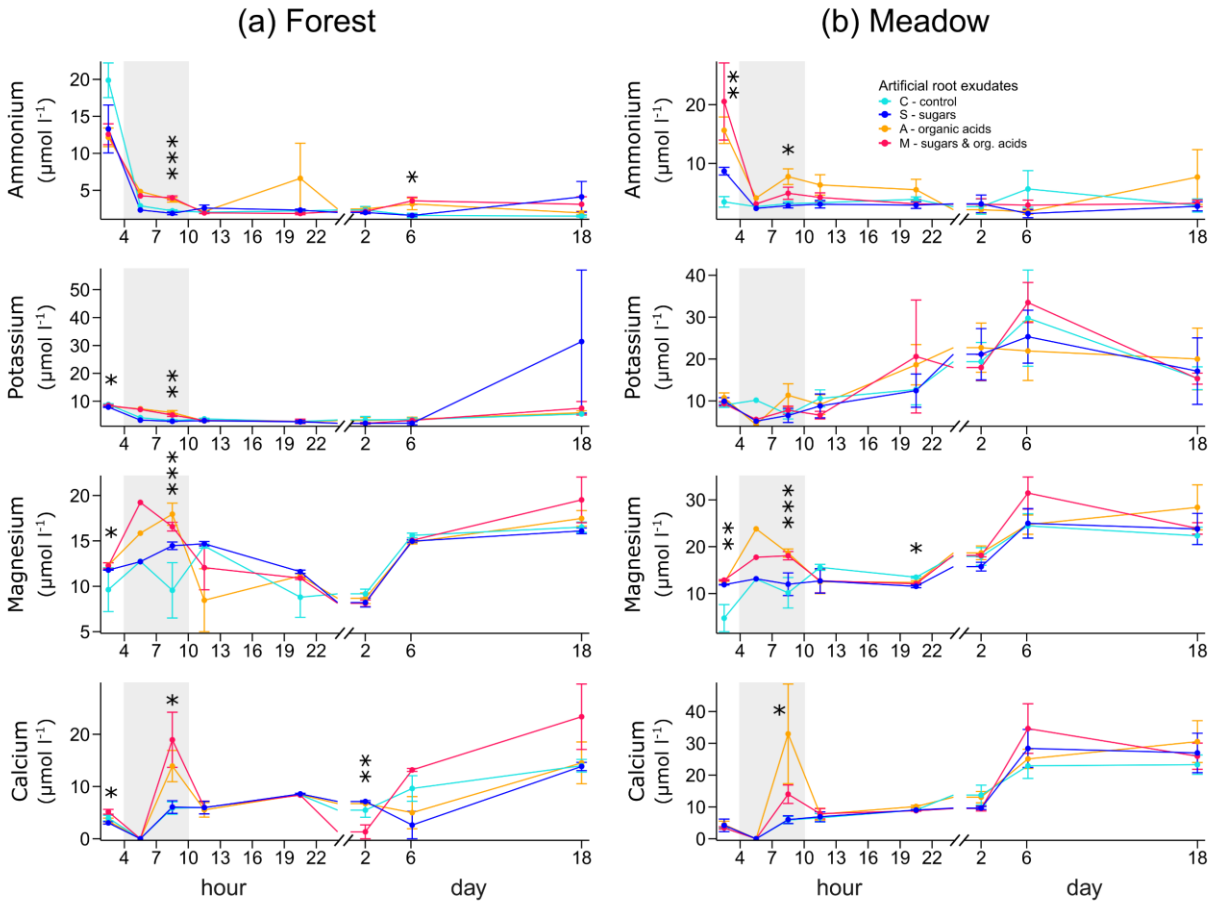


Figure 5. Concentrations of ammonium, potassium, magnesium, and calcium (µmol l^{-1}) in dialysates collected from (**a**) forest and (**b**) meadow soils before, during and after a 6-hour long labile substrate pulse. The period of simulated exudation (hours 4-9) is indicated by a grey background. An x-axis break follows the initial 24-hour period, and subsequent observations (days 2-18) are presented on a day-timescale. Asterisks denote significant differences (Kruskal-Wallis test, * < 0.05, ** < 0.01, *** < 0.001) between soils that received an input of sugars (dark blue), organic acids (orange), a mixture of sugars and organic acids (pink), and control (light blue). Data are presented as means ± SE (*n* = 5), except for hour 4 (*n* = 1). Each data point represents the mean concentration measured in dialysates collected over a 3-hour period on day 1 and a 4.5-hour period on subsequent day, plotted at the midpoint of each collection period. Kruskal-Wallis test statistics and Dunn's post-hoc test results are provided in Table S2.

3.4 Incorporation of combined sugars and organic acids into microbial biomass versus sugars-only into microbial storage

The sum of all microbial PLFAs (nmol C g^{-1} DW), which we used as a proxy for total microbial biomass, remained unaffected by simulated root exudation (>2.5 mm distance from membrane) across treatments (Fig. 6). Similarly, there was no increase in PLFA concentrations associated with any individual microbial group (gram-negative and gram-positive bacteria, fungi, actinobacteria) (Fig. S4). The sum of microbial NLFAs, which we use as a proxy for microbial storage compounds, significantly increased in meadow soils that had received a mix of organic acids and sugars (Fig. 6). This increase was primarily attributed to an increase in the general NLFA biomarkers, such as palmitic acid (16:0) (Fig. S6).

PLFAs were significantly enriched in ^{13}C in meadow soils in response to mixed labile substrate addition (at% ^{13}C: Fig. 6). A similar, though statistically non-significant, trend of ^{13}C incorporation in PLFAs was observed in forest soils following organic acid additions (with or without sugars). However, this trend was significant in forest soils when looking only at general and gram-negative PLFA biomarkers (Fig. S5). We observed a significant ^{13}C enrichment into NLFAs after sugar addition in meadow soils (Fig. 6). Again, this enrichment was mainly driven by incorporation of ^{13}C into general NLFA biomarkers, such as 16:0 (Fig S7).

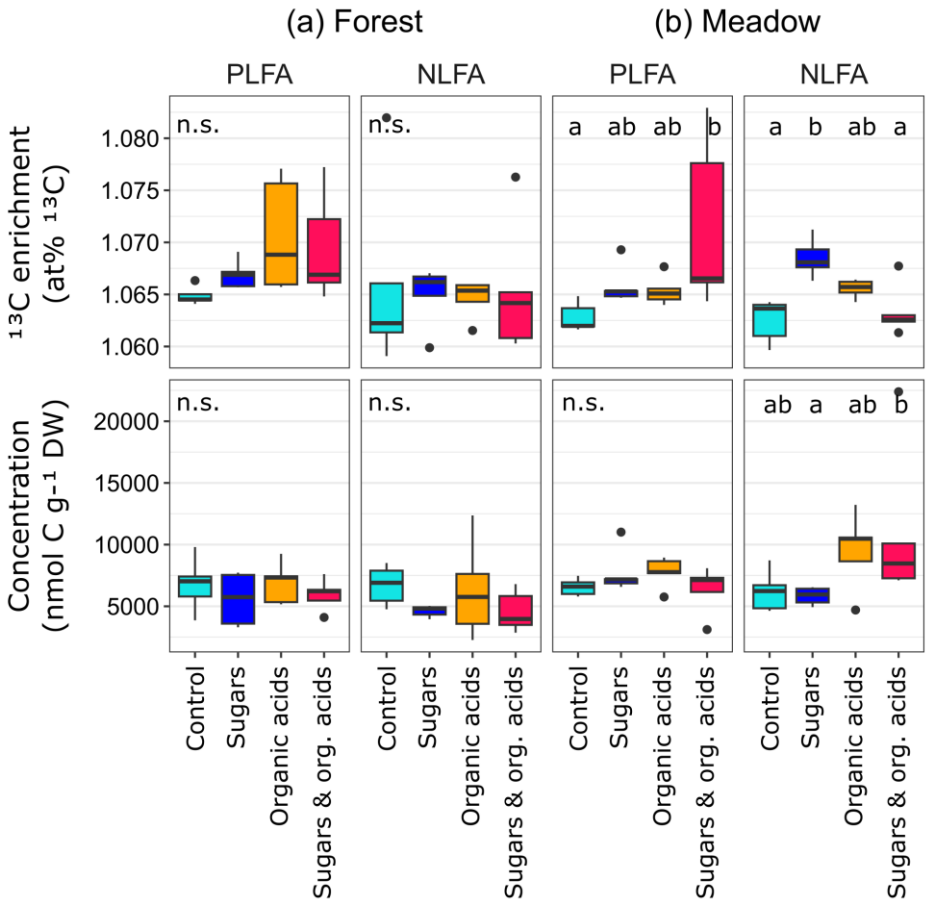


Figure 6. The concentration (nmol C g^{-1} dw) and ^{13}C enrichment (at% ^{13}C) of phospholipid fatty acids (PLFAs) and neutral lipid fatty acids (NLFA) in (**a**) forest and (**b**) meadow soils. Letters indicate significant difference between treatments (Kruskal-Wallis test, $p < 0.05$, Post-hoc test: Dunn's test) that received only sugars (dark blue), only organic acids (orange), a mixture of sugars and organic acids (pink), and a control (light blue) that did not receive a labile substrate pulse (n = 5). Note that our sampling excluded soil within a 2.5 mm radius of the microdialysis membrane, making the measurements a conservative estimate of lipid-derived fatty acids enrichment in the immediate vicinity of the membrane.

4. Discussion

Organic acids and sugars are two of the major compound classes exuded by plant roots. It has often been assumed that sugars act as a primary energy source for microbes, while organic acids play a key role in releasing nutrients from mineral and humic surfaces (Keiluweit et al., 2015). However, our findings extend these traditional views by demonstrating that organic acids in plant root exudates may also serve as an essential energy source for microbes, which are metabolised even faster and to a greater extent compared to sugars.

4.1 Disparity in sugar and organic acid release

Our results show considerably higher passive release rates of organic acids compared to sugars in both soils (Fig. 2, Fig. 3). The already low release rates of sugars dropped further in the second half of the pulse, indicating rapid saturation of sugars around the microdialysis membrane (Fig S2, Tab S4). Moreover, in the forest soil, lower sugar transfer rates were associated with high back retrieval rates after the substrate pulse ended (Fig. 2). We consistently observed this pattern across our previous studies involving various soil types (König et al., 2022; Wiesenbauer et al., 2024) suggesting that lower rates of passive sugar release into soil compared to organic acids might be a widespread phenomenon. Our previous research demonstrated that higher substrate diffusion through microdialysis into intact soil can only be attributed to higher rates of biotic or abiotic compound removal around the membrane, which supersedes effects of molecular size and charge (König et al., 2022). Higher removal rates of acetate and succinate may partly be attributed to their charged nature, which facilitates rapid adsorption to minerals (Jones et al., 2003). Nevertheless, the significantly higher respiration derived from organic acids suggests a more substantial microbial uptake and mineralization rate compared to sugars (Fig. 1), which may have contributed to the consistently high release of organic acids during the simulated root exudation (Fig. S2). Our findings imply a microbial preference for organic acids over sugars, challenging the established view that sugars (monosaccharides) are the preferred source of readily available substrates which are rapidly consumed (Jones and Murphy, 2007; Gunina and Kuzyakov, 2015).

4.2 Preferential utilization of organic acids over sugars

Why do microbial communities in both soils prefer to assimilate organic acids, even though catabolizing sugars typically yields more energy? The full oxidation of hexoses, such as glucose and fructose during aerobic respiration yields about 28-32 ATP (Romano and Conway, 1996; Pastor et al., 2019), while those of organic acids such as acetate only yields about 12 ATP.

Despite this, we found that microbes favoured acetate and succinate. These organic acids are often considered metabolic endproducts in bacteria due to their partial oxidation, yet they serve as vital sources of C and energy that offer distinct advantages. For instance, acetate can be metabolized through the formation of acetyl-coenzyme A (acetyl-CoA), employing a shorter pathway that bypasses the decarboxylation step of glucose to acetyl-CoA (S. Zhang et al., 2019; Hosmer et al., 2023). This acetyl-CoA then enters the TCA cycle and is linked to energy production through a series of reactions that efficiently generate ATP and other energy carriers. Under conditions of high substrate flux, shorter metabolic pathways result in higher rates of ATP production, albeit at a lower ATP yield per unit of metabolised substrate (Kreft et al., 2020).

The choice to metabolise organic acids over sugars suggests a strategic trade-off by microbes between maximizing rate of ATP production and thus biomass growth and optimizing ATP yield (Kreft and Bonhoeffer, 2005; Wortel et al., 2018; Kreft et al., 2020). In environments where rapid biomass accumulation is crucial and substrate is in excess, such as in the rhizosphere or the here investigated exudation hotspots, the fast but lower-yielding ATP production from organic acid catabolism may be more beneficial than pursuing the higher ATP yield from sugar metabolism.

In addition, sugars and organic acids fuel two major opposing pathways of the central C metabolism—glycolysis for energy production from glucose, and gluconeogenesis for synthesizing glucose from non-carbohydrate sources (Schink et al., 2022). Typically, microbes metabolize either glucose or organic acids, since both metabolic pathways run in opposite directions (Schink et al., 2022). Given their faster diffusion, an initially higher organic acid concentration in the mixed substrate treatment might have signalled the microbial cells to opt for gluconeogenesis as the primary pathway in their central C metabolism. Moreover, even as substrate availability changes, microbes cannot immediately switch between glycolytic (sugars) to gluconeogenic (organic acids) substrates, as this transition involves a lag phase (Basan et al., 2020). Furthermore, considering the notably lower ^{13}C respiration rates when only sugars were released, our results collectively suggest that gluconeogenesis, rather than glycolysis, may have been the default pathway in the majority of soil microbes. This aligns with the typical soil metabolic landscape, as a significant fraction of SOM is microbial necromass (i.e., proteins, storage and membrane lipids), whose breakdown products are gluconeogenic rather than glycolytic substrates.

4.3 Microbial incorporation of substrate-C into biomass

Our data indicates that microbes took up released exudates. The highest ^{13}C enrichment was found in the combined sugar and organic acid treatment in the meadow soil, which could be attributed to the higher release of substrate-C in mixed exudate soils (Fig. 3). Additionally, in forest soils, general

and gram-negative biomarkers showed significant ^{13}C incorporation into PLFAs in the organic acid treatment, while sugars lead to a significant enrichment in NLFA biomarkers in the meadow soil. Overall, we observed only a relatively low ^{13}C signal in PLFAs and NLFAs, which we attribute to our limitation of analysing soil only from beyond a >2.5 mm radius of the microdialysis membrane. Sampling soil from as close as possible to the membrane would yield clearer and more significant ^{13}C enrichment pattern, as we have demonstrated before (Wiesenbauer et al., 2024).

4.4 Organic acids input causes short-chain fatty acids production

Upon assimilation, the substrates were directed towards different catabolic and anabolic processes, including the production of metabolites. Organic acids, with or without sugars, promoted microbial activity (as evident from ^{13}C respiration measurements) and the production of short-chain fatty acids (SCFAs) such as butyrate, lactate, and propionate (Fig. 4). However, sugars alone did not induce metabolite production.

It remains unclear whether the butyrate, propionate and lactate we observed in the organic acid treatments originated from the breakdown of these organic acids (succinate) or from the induced breakdown of soil organic matter. SCFAs are commonly produced in anoxic environments as intermediates of organic matter degradation through fermentation. However, they can also occur as byproducts of high substrate turnover in aerobic conditions (Wolfe, 2005). Notably, SCFAs themselves are a non-fermentable C source and require a terminal electron-acceptor, such as O_2 in aerobic or NO_3 in anaerobic conditions, to be fully oxidized (Pavoncello et al., 2022). The anoxic sites conducive to fermentation may emerge at spots of high microbial activity, like (artificial) root exudation hotspots, where O_2 consumption due to substrate degradation exceeds the O_2 influx (Kreft et al., 2020). Indeed, it has been shown that O_2 concentrations decreases during times of active root exudations in the rhizosphere of *Vicia Faba* (Garcia Arredondo et al., 2023) and after the release of glucose, acetic acid, and oxalic acid near an artificial root (Keiluweit et al., 2015). Under these O_2-limited conditions, microbes perform shorter incomplete catabolic pathways such as fermentation, which support high growth rates due to higher ATP flux, despite their lower ATP yield compared to more yield-efficient pathways like aerobic respiration. This illustrates a trade-off between growth rate and yield (Kreft and Bonhoeffer, 2005; Wortel et al., 2018; Kreft et al., 2020).

Here, we assume that an O_2 depletion was caused by the respiration of added substrate (Wiesenbauer et al., 2024), specifically organic acids. While SOM decomposition prompted by substrate addition might have contributed to O_2 consumption, no significant changes in SOM-derived respiration were observed (Fig. 1). However, localised increases in SOM-derived respiration may have gone undetected.

Anaerobic respiration is increasingly recognised as a fundamental trait to colonise the rhizosphere (Lecomte et al., 2018). Until now, research on anaerobic metabolic processes has focussed on aqueous environments and paddy soils, leaving the rhizosphere of forest and meadow soil notably understudied (Lecomte et al., 2018). We observed butyrate, lactate, and propionate production in response to organic acid addition in our artificial rhizosphere (Fig. 4). While direct comparisons with rhizosphere studies are lacking, research on anaerobic metabolism in other environments provides context. For instance, in rice paddy soils, butyrate and propionate are common intermediary products of organic material decomposition (Rui et al., 2009). Similarly, in the gut, butyrate and propionate are commonly metabolised from complex carbohydrates like plant cell wall polysaccharides (Koh et al., 2016; Nogal et al., 2021), as well as from host-derived succinate by gut microbiota (Wei et al., 2023). In contrast to these environments, soils provide a wide array of alternative terminal electron acceptors in anaerobic conditions, such as NO_3, SO_2, or Fe (III), which would allow to feed intermediary fermentation products into anaerobic respiration (Keiluweit et al., 2017; Lecomte et al., 2018). One way to provide a more reliable evidence for anaerobic metabolism in the rhizosphere could be to monitor O_2 levels simultaneously when simulating root exudation (Garcia Arredondo et al., 2023).

4.5 Organic acid induced mobilization of cations

The mobilization of K (only forest), Ca, and Mg concentrations in both soils (Fig. 5) could be a consequence of abiotic interactions between organic acids and soil minerals. Organic acids can dissolve minerals through acidification, chelation, and exchange reactions (Adeleke et al., 2017), thereby making nutrients available for plant uptake (Giehl and von Wirén, 2014). Acidolysis occurs when protons from organic acids lower the pH, inducing the release of cations like Fe, K and Mg (Uroz et al., 2009; Adeleke et al., 2017). Moreover, organic acids form complexes with cations and mineral surfaces/metals in a process called chelation (Uroz et al., 2009), thereby increasing the solubility of nutrients like Ca, Mg, Fe, and Al (Golubev et al., 2006; Xu and Gao, 2008). Additionally, organic acids can displace cations through ligand exchange (Oburger et al., 2009; Keiluweit et al., 2015). Although acetate is a relatively weak complexing agent, it possible that the protons it released mobilized cations such as K, Ca, Mg, and NH_4 from clay minerals or organic matter via cation exchange reactions.

As our findings demonstrate (Fig. 4), various bacteria and fungi produce and release organic acids similar to those produced by plant roots, which can fulfil the same function of solubilizing elements (Banfield et al., 1999; Jones et al., 2003; van Schöll et al., 2008; Adeleke et al., 2010; Uroz et al., 2011; R. A. Adeleke et al., 2012; R. Adeleke et al., 2012). Consequently, the observed increase in nutrient concentrations (K, Ca, Mg) in response to both added and microbially produced organic acids highlights their pivotal role in mobilizing mineral-associated nutrients in the rhizosphere.

While our study demonstrates the role of organic acids in mobilizing soil nutrients within acidic soil, it is important to consider the potential variability of these processes in soils with different pH levels. Most nutrients are not uniformly available across the pH spectrum (Barrow and Hartemink, 2023). In low pH conditions, metal cations and protonated anions (e.g., Al^{3+}, Mn^{2+}, Fe^{2+}) are more soluble, while higher pH favour carbonate or hydroxyl complexes. The desorption of cations shifts dramatically across a narrow pH range, with small pH decreases leading to greater desorption (Barrow and Hartemink, 2023). Moreover, in alkaline-calcareous soils where phosphorus availability is typically limited, plants release organic acids to mobilizing phosphorus (Qetrani et al., 2024). This highlights the importance of considering soil pH when evaluating the ecological roles of organic acids in different soil types.

4.6 Implications of rhizosphere feedback on root exudation

Root exudation of primary metabolites, such as sugars, organic acids and amino acids, is thought to occur through passive transport along electrochemical and concentration gradients between rhizodermal cells and the soil environment (Canarini et al., 2019). These gradients are affected by the rate at which compounds are removed by microbial activity or interaction with soil surfaces. Our findings suggest that while organic acids are quickly removed by both biotic and abiotic processes, sugars are not. However, if sugars are not readily metabolised by soil microbes, this impairs the plant's ability to release photosynthates as sugars into the rhizosphere. Although it has been suggested that anions like organic acids tend to be released from roots more easily than sugars due to charge differences (Jones, 1998), our study is the first to demonstrate that soil microbes may contribute to this pattern by preferably taking up organic acids over sugars at root exudation hotspots.

Traditional root exudation measurements have reported sugars as a significant proportion of total root exudates (Farrar et al., 2003; Badri and Vivanco, 2009). However, these measurements typically involve removing surrounding soil and sampling root exudates hydroponically to avoid the alteration of exuded compounds by the surrounding soil matrix and microbes (Kuijken et al., 2015; Oburger and Schmidt, 2016). This approach, however, also eliminates soil microbial feedback on diffusional exudation rates, which may result in an overestimation of sugar exudation rates. Our research suggests that the exudation of sugars by roots may be impeded by low microbial metabolism of sugars in the rhizosphere, emphasising the importance of biotic and abiotic rhizosphere feedback mechanisms in regulating root exudation rates.

5. Conclusion

This study elucidates the distinct roles of sugars and organic acids in shaping microbial dynamics and soil chemistry within the rhizosphere at root exudation hotspots. Contrary to our initial hypothesis, our findings revealed a pronounced microbial preference for organic acids over sugars, indicating that organic acids are not merely agents for nutrient mobilization but also crucial substrates for microbial metabolism.

Moreover, our results challenge the conventional understanding that sugars, due to their supposed bioavailability, would elicit stronger microbial responses. Instead, we discovered that sugars were minimally utilized by the microbial community, even in the absence of alternative substrates. Due to this negligible impact of sugars on microbial activity, the combination of sugars and organic acids did not result in the anticipated additive effects. This outcome suggests a complex interplay of microbial preference that is not solely dictated by substrate availability but perhaps also influenced by the metabolic cost-benefit strategies employed by soil microbes in different environmental contexts.

Interestingly, the microbial and chemical response to these compound classes exhibited consistent patterns across different soil types, supporting our hypothesis that microbial responses are primarily driven by the nature of the exudates rather than the soil properties. This consistency across soil types emphasizes the fundamental roles of chemical composition of root exudates in shaping microbial ecology and biogeochemical cycles at the root-soil interface.

These insights expand our knowledge of microbial utilization of root exudates, highlighting the integral role of organic acids in rhizosphere dynamics. By demonstrating that organic acids, rather than sugars, primarily drive microbial activity, this study deepens our understanding of nutrient cycling and microbial energy strategies at the root-soil interface.

Acknowledgements

We would like to thank Joshua Schimel for his careful reading and constructive feedback, which improved this paper.

Data availability

Data to this article can be found online at https://doi.org/10.5281/zenodo.13338424.

Supporting Information

The following Supporting material is available for this article:

Fig. S1 Photographs of experimental setup

Fig. S2 Concentration of compounds released during the first and second half of the simulated exudation

Fig. S3 Compound concentrations of perfusate compounds during day 1

Fig. S4 Concentration of PLFAs for biomarker groups

Fig. S5 ^{13}C enrichment of PLFAs for biomarker groups

Fig. S6 Concentration of NLFAs for biomarker groups

Fig. S7 ^{13}C enrichment of NLFAs for biomarker groups

Table S1 Kruskal-Wallis test statistics and post-hoc test results of substrate-derived respiration

Table S2 Kruskal-Wallis test statistics and post-hoc test results of compound concentrations

Table S3 Kruskal-Wallis test statistics and post-hoc test results of perfusate compound concentrations

Table S4 Statistics testing difference between C release between first and second half of exudation pulse

Methods S1 Analysis of microbial biomass C and N

Methods S2 High-performance liquid chromatography of sugars

Methods S3 High-performance liquid chromatography of anions

Methods S4 High-performance liquid chromatography of cations

Methods S5 Calculation of respiration rates

Methods S6 Phospholipid and neutral lipid extraction and analysis



Figure S1 These photographs illustrate our experimental setup. (**A**) Each mesocosm (cut of 50 ml falcon tube) held two small undisturbed soil cores (1 cm diameter, 3 cm height). The two microdialysis probes, one per soil core, were kept stable in the soil by attaching them to an aluminium strip on top of the falcon. The dialysate of the two soil cores per mesocosm were always pooled. (**B**) During microdialysis the mesocosms were kept in airtight jars fitted with a septum through which the microdialysis tubing was passed through. This allowed for simultaneous collection of dialysates in fraction collectors (in the background of picture A and B) and gas sampling with closed jar lid. (**C**) Between measurements the mesocosms were placed in plastic containers with lids, with a wet paper towel on the bottom to reduce drying at room temperature. They were aired at least once a day and the weight of the mesocosms was tracked and water added on top of cores to adjust for water loss.

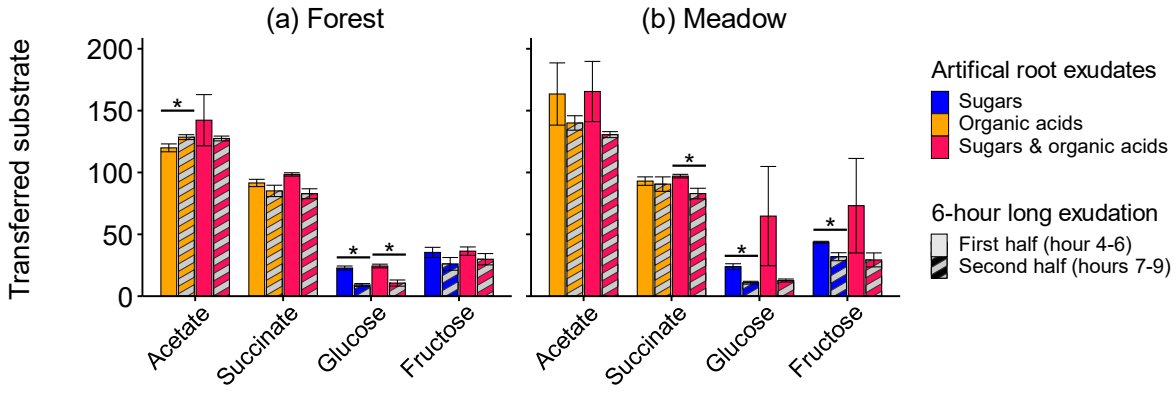


Figure S2 The concentration (nmol C) of compounds released into (**a**) forest and (**b**) meadow soil, given for the first (solid colour, hours 4-6) and second half (dashed colour, hours 7-9) of the 6-hour long input pulse. Transferred compound concentrations are given for the artificial root exudates composed of either only sugars (blue), only organic acids (orange) or a mixture of sugars and organic acids (pink). All measures are means ± SE (n = 5). Asterisks indicate significant differences (Table 4, repeated measures ANOVA, paired Wilcoxon signed-rank test) in released C between first and second half of input pulse.

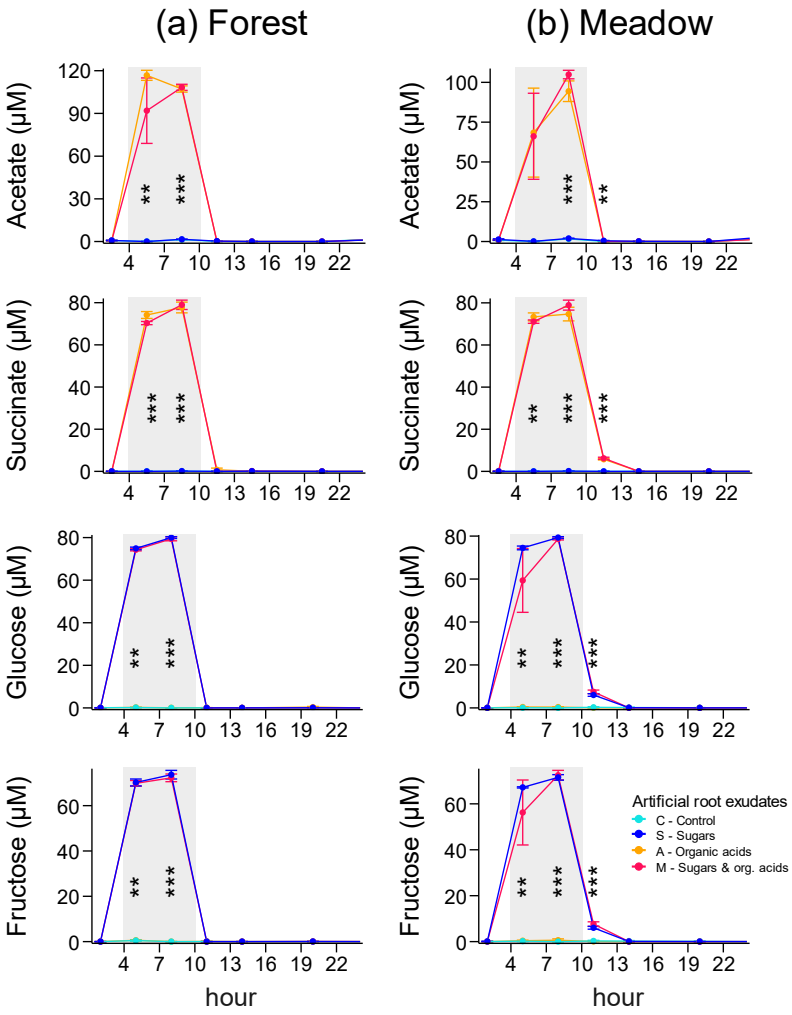


Figure S3 Compound concentration (µmol l^{-1}) of organic acids (acetate, succinate) and sugars (glucose, fructose) that made up the perfusate ("artificial root exudate"). Concentrations were measured in dialysates collected from (**a**) forest and (**b**) meadow soils before, during and after a 6-hour long labile substrate pulse, highlighted with a grey background. It should be noted that the concentrations depicted during the pulse (grey background) are concentrations in dialysate. Which means that only the difference to the perfusate concentration (equivalent to 250 µM acetate, 125 µM succinate, 83.3 µM glucose, 83.3 µM fructose: each 500 µmol C l^{-1}) was transferred into soil. All measures are mean ± SE (n = 5). Asterisks indicate significant differences (Kruskal-Wallis test, * < 0.05, ** < 0.01, *** < 0.001) between soils that received an input of sugars (S: dark blue), organic acids (A: orange), a mixture of sugars and organic acids (M: pink) or control (C: light blue). Post hoc test results can be found in Table S3 (Dunn's test). Each data point represents the mean concentration measured in dialysates collected over a 3-hour period, with the point plotted at the midpoint of this period.

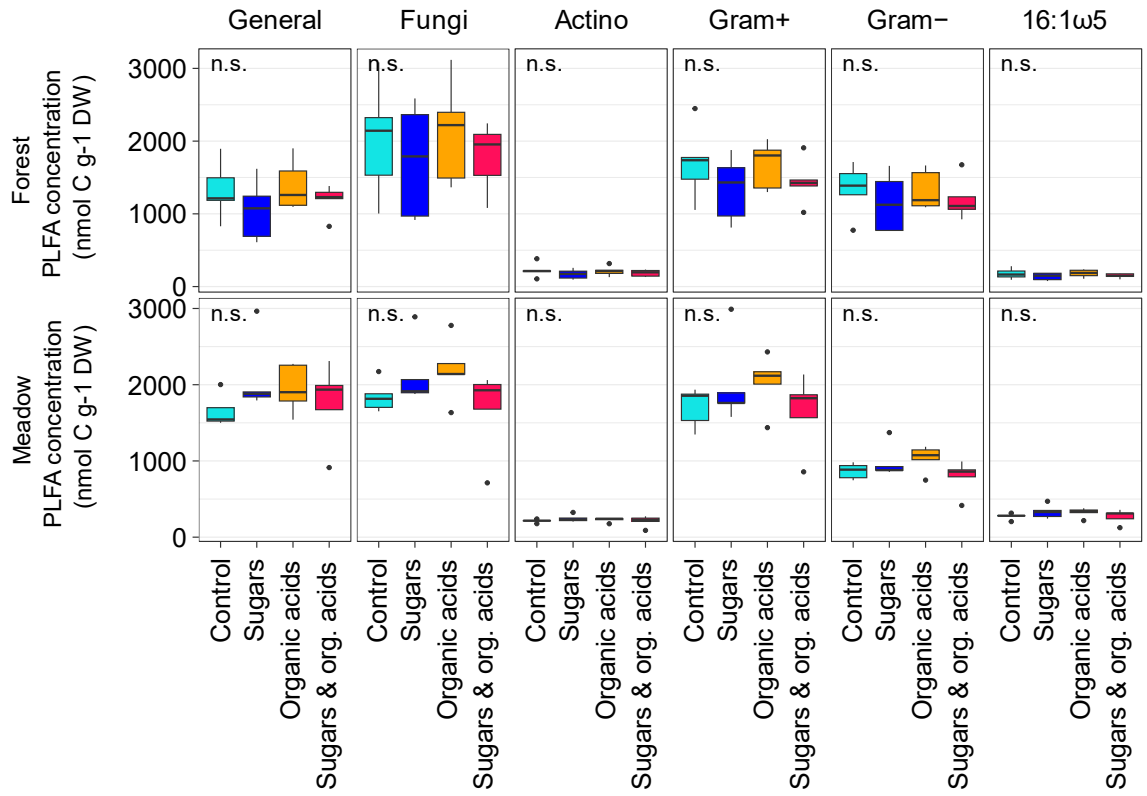


Figure S4 The concentration (nmol C g^{-1} dw) of phospholipid fatty acids (PLFAs) in forest and meadow soils. The fatty acids were grouped into general fatty acids, fungi, *Actinobacteria*, gram-positive bacteria (excluding *Actinobacteria*), gram-negative bacteria. The fatty acid 16:1ω5 was left ungrouped, because it is known to be a biomarker specific for arbuscular mycorrhiza fungi in meadow soil, but not in forest soil. Letters indicate significant difference between the treatments (Kruskal-Wallis test, $p < 0.05$, post-hoc test: Dunn's test) that received only sugars (dark blue), only organic acids (orange), a mixture of sugars and organic acids (pink) and a control (light blue) that did not receive a labile substrate pulse ($n = 5$).

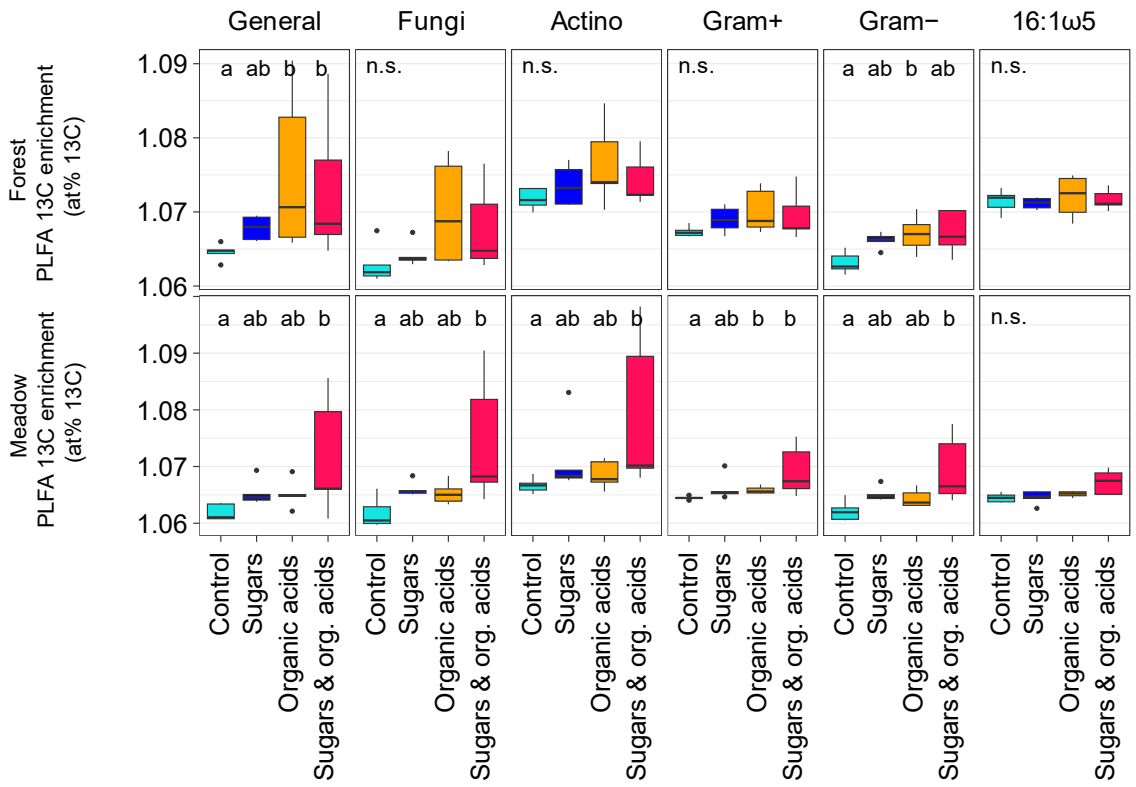


Figure S5 The ^{13}C enrichment (at% ^{13}C) of phospholipid fatty acids (PLFAs) in forest and meadow soils. The fatty acids were grouped into general fatty acids, fungi, *Actinobacteria*, gram-positive bacteria (excluding *Actinobacteria*), gram-negative bacteria. The fatty acid 16:1ω5 was left ungrouped, because it is known to be a biomarker specific for arbuscular mycorrhiza fungi in meadow soil, but not in forest soil. Letters indicate significant difference between the treatments (Kruskal-Wallis test, $p < 0.05$, post-hoc test: Dunn's test) that received only sugars (dark blue), only organic acids (orange), a mixture of sugars and organic acids (pink) and a control (light blue) that did not receive a labile substrate pulse ($n = 5$).

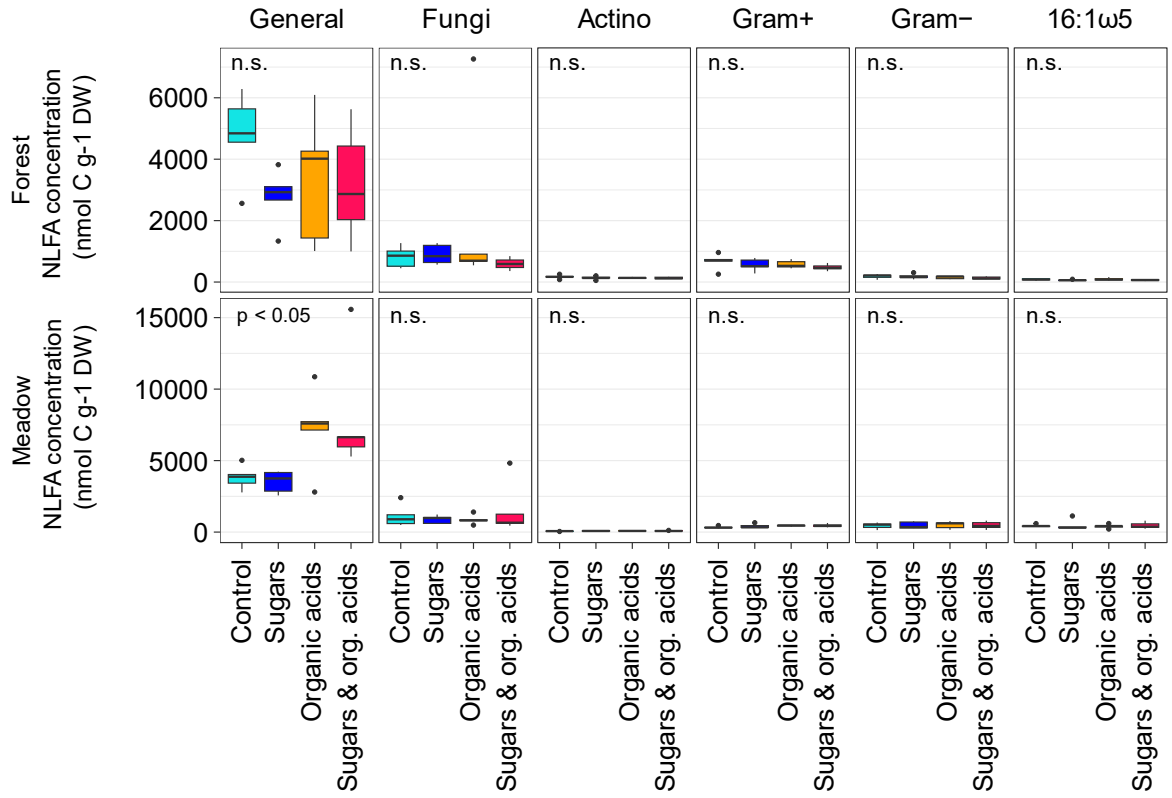


Figure S6 The concentration (nmol C g^{-1} dw) of neutral lipid fatty acids (NLFAs) in forest and meadow soils. The fatty acids were grouped into general fatty acids, fungi, *Actinobacteria*, gram-positive bacteria (excluding *Actinobacteria*), gram-negative bacteria. The fatty acid 16:1ω5 was left ungrouped, because it is known to be a biomarker specific for arbuscular mycorrhiza fungi in meadow soil, but not in forest soil. Letters indicate significant difference between the treatments (Kruskal-Wallis test, $p < 0.05$, post-hoc test: Dunn's test) that received only sugars (dark blue), only organic acids (orange), a mixture of sugars and organic acids (pink) and a control (light blue) that did not receive a labile substrate pulse ($n = 5$).

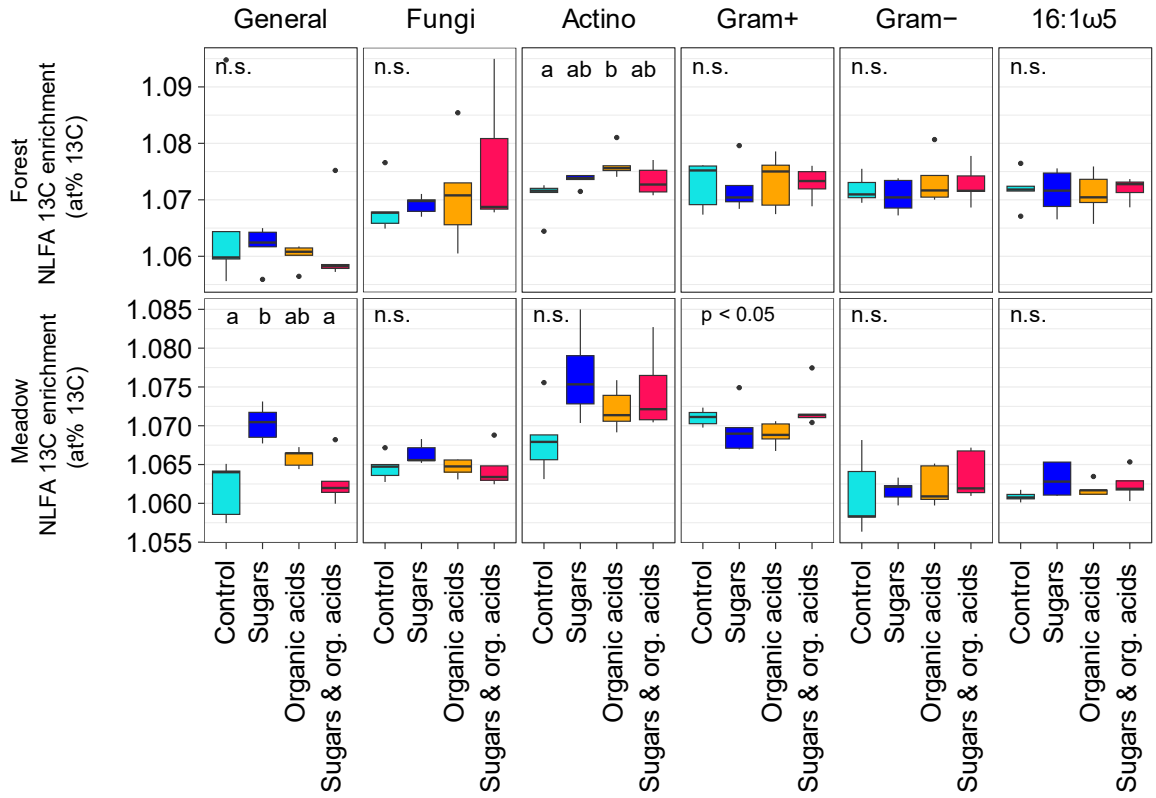


Figure S7 The ^{13}C enrichment (at% ^{13}C) of neutral lipid fatty acids (NLFAs) in forest and meadow soils. The fatty acids were grouped into general fatty acids, fungi, *Actinobacteria*, gram-positive bacteria (excluding *Actinobacteria*), gram-negative bacteria. The fatty acid 16:1ω5 was left ungrouped, because it is known to be a biomarker specific for arbuscular mycorrhiza fungi in meadow soil, but not in forest soil. Letters indicate significant difference between the treatments (Kruskal-Wallis test, $p < 0.05$, post-hoc test: Dunn's test) that received only sugars (dark blue), only organic acids (orange), a mixture of sugars and organic acids (pink) and a control (light blue) that did not receive a labile substrate pulse ($n = 5$).

Table S1 Kruskal-Wallis test statistics and Dunn's post-hoc test results of substrate-derived respiration rates across treatments (Fig. 1).

	Day	Hour	χ^2	df	p-value	Dunn's post-hoc	Asterisk
(a) Forest	1	6.5	9.62	2	0.008	S^a A^b M^b	**
	1	11	9.98	2	0.007	S^a A^b M^b	**
	2	26	8.852	2	0.012	S^a A^{ab} M^b	*
	6		9.757	2	0.008	S^a A^{ab} M^b	**
	18		9.471	2	0.009	S^a A^b M^b	**
(b) Meadow							
	1	6.5	10.5	2	0.005	S^a A^{ab} M^b	**
	4		12.5	2	0.002	S^a A^{ab} M^b	**
	6		11.1	2	0.004	S^a A^{ab} M^b	**
	18		6.339	2	0.042	S^a A^a M^b	*

Only significant differences are presented. Superscript letters indicate significant differences between treatments as determined by Dunn's post-hoc test following a Kruskal-Wallis test. These letters compare substrate-derived respiration rates among treatments that received sugars (**S**), organic acids (**A**), and sugars combined with organic acids (**M**) in (**a**) forest and (**b**) meadow soils.

Table S2 Kruskal-Wallis test statistics and Dunn's post-hoc test results of compound concentrations across treatments (Fig. 4, Fig. 5).

Soil	Compound	Day	Hour	χ^2	df	p-value	Dunn's post-hoc	Asterisk
(a) Forest	Butyrate	1	7	9.980	3	0.019	C^{ab} S^{a} A^{b} M^{ab}	*
	Lactate	1	4	11.211	3	0.011	C^{a} S^{a} A^{b} M^{ab}	*
	Lactate	1	7	18.634	3	0	C^{a} S^{a} A^{b} M^{ab}	***
	Lactate	18	432	7.922	3	0.048	C^{a} S^{b} A^{b} M^{a}	*
	Propionate	1	7	18.091	3	0	C^{a} S^{a} A^{b} M^{b}	***
	Ammonium	1	7	16.867	3	0.001	C^{ac} S^{a} A^{bc} M^{b}	***
	Ammonium	6	144	10.989	3	0.012	C^{a} S^{a} A^{b} M^{b}	*
	Potassium	1	1	10.520	3	0.015	C^{a} S^{b} A^{ab} M^{ab}	*
	Potassium	1	7	15.127	3	0.002	C^{a} S^{a} A^{b} M^{b}	**
	Magnesium	1	1	8.897	3	0.031	C^{ab} S^{a} A^{b} M^{ab}	*
	Magnesium	1	7	15.693	3	0.001	C^{a} S^{a} A^{b} M^{b}	***
	Calcium	1	1	8.520	3	0.036	C^{ab} S^{a} A^{ab} M^{b}	*
	Calcium	1	7	8.708	3	0.033	C^{a} S^{ab} A^{ab} M^{b}	*
	Calcium	2	40	11.957	3	0.008	C^{a} S^{a} A^{a} M^{b}	**
(b) Meadow	Butyrate	1	7	15.383	3	0.002	C^{a} S^{a} A^{b} M^{ab}	**
	Lactate	1	7	17.530	3	0.001	C^{a} S^{a} A^{b} M^{ab}	***
	Propionate	1	7	17.417	3	0.001	C^{a} S^{a} A^{b} M^{b}	***
	Ammonium	1	1	13.491	3	0.004	C^{a} S^{ab} A^{b} M^{b}	**
	Ammonium	1	7	10.327	3	0.016	C^{a} S^{a} A^{b} M^{ab}	*
	Magnesium	1	1	11.744	3	0.008	C^{a} S^{ab} A^{ab} M^{b}	**
	Magnesium	1	7	17.250	3	0.001	C^{a} S^{a} A^{b} M^{b}	***
	Magnesium	1	19	10.611	3	0.014	C^{a} S^{b} A^{ab} M^{ab}	*
	Calcium	1	7	8.828	3	0.032	C^{a} S^{ab} A^{b} M^{ab}	*

Only significant differences are presented. Superscript letters indicate significant differences between treatments as determined by Dunn's post-hoc test following a Kruskal-Wallis test. These letters compare compound concentrations among treatments that received sugars (**S**), organic acids (**A**), and sugars combined with organic acids (**M**) in (**a**) forest and (**b**) meadow soils.

Table S3 Kruskal-Wallis test statistics and Dunn's post-hoc test results of compound concentrations present in perfusate across treatments (Fig. S3).

Soil	Compound	Day	Hour	χ^2	df	p-value	Dunn's post-hoc	Asterisk
(a) Forest	Acetate	1	4	14.358	3	0.002	C^a S^a A^b M^{ab}	**
	Acetate	1	7	17.637	3	0.001	C^a S^a A^b M^b	***
	Succinate	1	4	15.664	3	0.001	C^a S^{ac} A^b M^{bc}	***
	Succinate	1	7	17.514	3	0.001	C^a S^a A^b M^b	***
	Glucose	1	4	15.136	3	0.002	C^a S^b A^{ac} M^{bc}	**
	Glucose	1	7	19.025	3	0	C^a S^b A^{ac} M^{bc}	***
	Fructose	1	4	14.533	3	0.002	C^a S^b A^a M^b	**
	Fructose	1	7	19.007	3	0	C^a S^b A^a M^b	***
	Fructose	5	120	9.113	3	0.028	C^a S^b A^b M^{ab}	***
(b) Meadow	Acetate	1	7	18.519	3	0	C^a S^{ac} A^{bc} M^b	***
	Acetate	1	10	12.861	3	0.005	C^{ab} S^a A^b M^b	**
	Succinate	1	4	14.508	3	0.002	C^a S^{ac} A^b M^{bc}	**
	Succinate	1	7	18.370	3	0	C^a S^{ac} A^{bc} M^b	***
	Succinate	1	10	19.761	3	0	C^a S^a A^b M^b	***
	Glucose	1	4	12.292	3	0.006	C^a S^b A^{ab} M^b	**
	Glucose	1	7	19.966	3	0	C^a S^b A^{ac} M^{bc}	***
	Glucose	1	10	19.217	3	0	C^a S^b A^a M^b	***
	Fructose	1	4	11.586	3	0.009	C^a S^b A^{ab} M^b	**
	Fructose	1	7	18.452	3	0	C^a S^b A^a M^b	***
	Fructose	1	10	19.354	3	0	C^a S^b A^a M^b	***
	Fructose	4	96	8.916	3	0.03	C^a S^{ab} A^b M^{ab}	*

Only significant differences are presented. Superscript letters indicate significant differences between treatments as determined by Dunn's post-hoc test following a Kruskal-Wallis test. These letters compare compound concentrations among treatments that received sugars (**S**), organic acids (**A**), and sugars combined with organic acids (**M**) in (**a**) forest and (**b**) meadow soils.

Table S4 Results of statistical tests evaluating significant differences in compound concentrations (nmol C) released into soils between the first half (hours 4–6) and the second half (hours 7–9) of the labile substrate pulse. (Fig. S2).

Soil	Compound	Treatment	p-value	Statistic	df	Asterisk	Test
(a) Forest	Acetate	Organic acids	0.046	8.138	1	*	repeated measures ANOVA
	Acetate	Mixed	0.625	5		n.s	paired Wilcoxon signed-rank test
	Succinate	Organic acids	0.255	1.766	1	n.s	repeated measures ANOVA
	Succinate	Mixed	0.125	14		n.s	paired Wilcoxon signed-rank test
	Glucose	Sugars	0	147.608	1	***	repeated measures ANOVA
	Glucose	Mixed	0.003	43.392	1	**	repeated measures ANOVA
	Fructose	Sugars	0.053	7.442	1	n.s	repeated measures ANOVA
	Fructose	Mixed	0.188	13		n.s	paired Wilcoxon signed-rank test
(b) Meadow	Acetate	Organic acids	0.812	9		n.s	paired Wilcoxon signed-rank test
	Acetate	Mixed	0.812	9		n.s	paired Wilcoxon signed-rank test
	Succinate	Organic acids	0.598	0.326	1	n.s	repeated measures ANOVA
	Succinate	Mixed	0.033	10.281	1	*	repeated measures ANOVA
	Glucose	Sugars	0.007	25.361	1	**	repeated measures ANOVA
	Glucose	Mixed	0.062	15		n.s	paired Wilcoxon signed-rank test
	Fructose	Sugars	0.03	10.787	1	*	repeated measures ANOVA
	Fructose	Mixed	0.312	12		n.s	paired Wilcoxon signed-rank test

The statistical comparisons were conducted using repeated measures ANOVA or paired Wilcoxon signed-rank tests, as appropriate. Significant differences are marked with asterisks in Figure S2.

Methods S1 Analysis of microbial biomass C and N

We analysed microbial biomass C by chloroform fumigation-extractions (Vance et al., 1987). Soils (2 g) were fumigated over chloroform for 24 h, and subsequently fumigated and non-fumigated soils were extracted with 15 ml KCl (1 M) for 30 min before filtering through ash-free cellulose filters (Whatman). KCl-extracts were measured with TOC/TN analyser (TOC-VCPH/TMN-1, Shimadzu, Japan), and microbial biomass C and N were calculated as the difference in dissolved organic carbon (DOC) and total nitrogen (TN) between fumigated non-fumigated soils. Two outlier values were removed from forest microbial biomass carbon. We used a conversion factor for microbial biomass C and N of 0.45 to take into account incomplete extraction (Joergensen, 1996). In forest soils, two outliers had to be removed from the microbial biomass C and C:N ratio.

Methods S2 High-performance liquid chromatography to measure sugars

We measured sugars in the dialysates using HPLC (Dionex ICS 5000+, Thermo Fisher, Germany). Sugars (glucose, fructose, galactose, sucrose) were measured on a Thermo CarboPac PA20 (0.4 x 150 mm) column with a Thermo CarboPac PA20G (0.4 x 35 mm) guard column at a constant flow rate of 8 µl min^{-1} with a KOH solvent. The run was 25 min long, starting at 8 mM for 12 min, then increasing to 200 mM over 5 min. We kept the concentration at 200 mM for 1 minute, then lowered the concentration to 8 mM over 1 minute, keeping the concentration at 8 mM for 5 min until the end of the 25-minute run. While the analytical setup for sugar measurements was capable of detecting fructose, galactose, glucose, and sucrose, only glucose and fructose were present in our samples.

Methods S3 High-performance liquid chromatography to measure anions

We measured organic and inorganic anions in the dialysates using HPLC (Dionex ICS 5000+, Thermo Fisher, Germany). We analysed acetate, butyrate, citrate, formate, lactate, malate, nitrate, oxalate, phosphate, propionate, succinate, and sulfate. The anions were measured on a Dionex IonPac AS11-HC (2 x 250 mm) column with a Dionex IonPac AG11-HC (2 x 50 mm) guard column at a constant flow rate of 0.25 ml min^{-1} with a KOH solvent. The 45 min HPLC run started at 1 mM for 10 min, then increased to 15 mM for 14 min (until min 24), then increased to 60 mM for 9 min (until min 33), where we kept it for 5 min at 60 mM (until min 38). Afterwards we lowered concentrations to 1 mM and kept it there until the end of the 45-minute run. While the analytical setup for anion measurement was capable of detecting acetate, butyrate, formate, lactate, malate, oxalate, propionate, succinate, citrate, nitrate, phosphate, and sulfate, only butyrate, lactate, and propionate concentrations showed significant responses to the simulated exudation and are presented in the paper.

Methods S4 High-performance liquid chromatography to measure cations

We measured cations in the dialysates using HPLC (Dionex ICS 5000+, Thermo Fisher, Germany). We analysed ammonium, potassium, magnesium, manganese, and calcium. The cations were measured on a Dionex IonPac CS16 (5 x 250 mm) column with a guard column at a constant flow rate of 1 ml min^{-1} with methanesulfonic acid as solvent. The dialysates from the first day were run with a short method and the remaining dialysates were measured with a longer method.

The shorter method was 35 minutes long, starting with 30 mM for 10 min, then increased to 60 mM over 5 min (until minute 15) at which concentration (60 mM) it remained for 10 min (until minute 25). Afterwards we decreased to 30 mM over 1 min (until min 26), at which concentration it remained until the end of the run at minute 35.

The longer method was 47 minutes long, starting with 30 mM for 22 min, then increased to 60 mM over 5 min (until minute 27) at which concentration (60 mM) it remained for 10 min (until minute 37). Afterwards we decreased to 30 mM over 1 min (until min 38), at which concentration it remained until the end of the run at minute 47. While the analytical setup for cation measurement detected ammonium, potassium, magnesium, calcium, and manganese, though manganese levels could not be reliably quantified.

Methods S5 Calculations of soil respiration rates and SOM- and substrate-derived respiration rates

The following equations were adopted from the supplements from König *et al.* (2022).
We used the following equations to calculate respiration rates and its ^{13}C signature:

$$CO_{2\ corrected\ t0} = \frac{CO_{2\ sample} \times \left(V_{jar} - V_{sample}\right) + CO_{2\ blank} \times V_{jar}}{V_{jar}} \quad (1)$$

where $CO_{2\ corrected\ t0}$ is the CO_2 concentration (ppm) at time 0, $CO_{2\ sample}$ and $CO_{2\ blank}$ refers to the measured CO_2 concentration (ppm) in sample or blank, V_{sample} and V_{jar} refers to the volume of the sampled gas and the glass jar.

$$^{13}CO_{2\ corrected\ t0} = \frac{CO_{2\ sample} \times \left(\frac{at\%\ ^{13}C_{sample}}{100}\right) \times \left(V_{jar} - V_{sample}\right) + CO_{2\ blank} \times \left(\frac{at\%\ ^{13}C_{blank}}{100}\right) \times V_{sample}}{V_{jar}} \quad (2)$$

where $^{13}CO_{2\ corrected\ t0}$ is the calculated concentration of $^{13}CO_2$ concentration (ppm) present in the jar after taking out sample t0 and replacement by the artificial air; at% $^{13}C_{sample}$ and at% $^{13}C_{blank}$ refers to the relative ^{13}C content (in at% ^{13}C) in the measured gas sample t0 and the artificial air (blank).

$$^{13}CO_{2\ sample\ t1} = CO_{2\ sample\ t1} \times \frac{at\%\ ^{13}C_{sample\ t1}}{100} \quad (3)$$

where $^{13}CO_{2\ sample\ t1}$ is the relative concentration of ^{13}C-CO_2 (ppm) in sample t1, $CO_{2\ sample\ t1}$ is the concentration of CO_2 at t1 (1 hour after t0).

$$CO_{2\ increase} = CO_{2\ sample\ t1} - CO_{2\ corrected\ t0} \quad (4)$$

$$^{13}CO_{2\ increase} = {}^{13}CO_{2\ sample\ t1} - {}^{13}CO_{2\ sample\ t0} \quad (5)$$

where $CO_{2\ increase}$ and $^{13}CO_{2\ increase}$ stand for the increase in total CO_2 and $^{13}CO_2$ (ppm), respectively, during the incubation time of 1 hour.

$$Respiration_{sample} = \left(\frac{\frac{CO_{2\ increase}}{10^6} \times V_{jar}}{Mol.Volume\ CO_2} \times 1000 \right) \Big/ gDW \quad (6)$$

where $Respiration_{sample}$ refers to the total respiration rate in the samples that received labelled substrates (treatment) or those which did not (control), expressed in nmol CO_2 h^{-1} g^{-1} dry soil. Mol.Volume CO_2 represents the molecular volume of CO_2 at normal atmospheric pressure and room temperature (24.465×10^{-3} ml µmol^{-1}).

$$at\%\ ^{13}C_{respiration} = \frac{^{13}CO_{2\ increase}}{CO_{2\ increase}} \times 100 \quad (7)$$

At% $^{13}C_{respiration}$ represents the relative ^{13}C content in respired CO_2 after substrate addition (in at% ^{13}C).

$$APE\ ^{13}C_{respiration} = at\%\ ^{13}C_{treatment} - at\%\ ^{13}C_{control} \quad (8)$$

where at% $^{13}C_{treatment}$ and at% $^{13}C_{control}$ refer to the at% ^{13}C of respired CO_2 (as calculated with the previous formula) in the sample which received ^{13}C-labelled substrate (treatment) and the corresponding one which did not (control).

$$Substrate\ Respiration = \frac{APE\ ^{13}C_{respiration}}{APE\ ^{13}C_{substrate}} \times Respiration_{treatment}$$

(9)

where Substrate Respiration represents the CO_2 production from the added substrate in nmol CO_2 h^{-1} g^{-1} dry soil. APE ^{13}C substrate stands for the ^{13}C enrichment of used substrate.

$$SOM\ Respiration_{treatment} = Respiration_{treatment} - Substrate\ Respiration$$

(10)

where SOM Respiration represents soil organic matter (SOM) derived respiration in nmol CO_2 h^{-1} g^{-1} dry soil.

Methods S6 Phospholipid and neutral lipid extraction and analysis

The lipids in the lyophilized "outer" soils (approx. 1 g dry weight soil) were extracted with a monophasic mixture of chloroform, methanol and citrate buffer (pH = 4) in a 1:2:0.8 volume ratio (Bligh and Dyer, 1959; Frostegård et al., 1991). After phase separation with addition of chloroform and citrate buffer, the lower phase containing the total lipids was collected. These were consequently fractionated with silica solid phase extraction columns (Phenomenex, Strata SI-1 Silica, 55 µm, 70 A) by eluting consecutively with a chloroform-ethanol mix (v:v = 98:2; Gorka *et al.*, 2023) yielding neutral lipids, pure acetone, and a chloroform-methanol-water mix (v:v:v = 5:5:1; Buyer & Sasser, 2012) yielding phospholipids. Phospho- and neutral lipids were derivatized to fatty acid methyl esters by mild alkaline methanolysis. The resulting PLFAs and NLFAs were analysed on a gas chromatograph (Trace GC Ultra, Thermo Scientific, Germany) coupled to a mass spectrometer (ISQ, Thermo Scientific, Germany) for fatty acid identification and quantification, and on a GC-Ultra (Thermo Fisher Scientific, Milan, Italy) coupled to an isotope ratio mass spectrometer (IRMS; Finnigan Delta-V, Thermo Fisher Scientific, Bremen, Germany) via a GC IsoLink (Thermo Fisher Scientific, Bremen, Germany) for determination of isotopic $^{13}C/^{12}C$ ratios. We used nonadecanoic acid (FAME 19:0) as an internal standard for quantification, and bacterial and fungal fatty acid methyl esters (BAME CP mix, Supelco; 37 Component FAME mix, Supelco) as qualitative external standards. Fatty acids with ≥20 carbon atoms and unidentified fatty acids were removed from the data.

Fatty acids were classified based on their taxonomic specificity into general microbial biomass (10:0, 14:0, 15:0, 16:0, 17:0, 18:0), fungi (18:1ω9c, 18:1ω9t, 18:2ω6,9, 18:3ω6,9,12), *Actinobacteria* (10Me17:0, 10Me18:0), gram-positive bacteria (i14:0, a15:0, i15:0, 16:0Me, i16:0, 17:0Me, a17:0, cy17:0, i17:0, i18:0), and gram-negative bacteria (14:1ω5, 15:1ω5, 15:1ω5c, 2OH 16:0, i16:1ω6, 16:1ω7, 16:1ω9, 16:2ω6,9, 17:1ω7, 17:1ω8, 18:1ω5, 18:1ω7, cy19:0, 19:1ω9)(Willers et al., 2015). The fatty acid 16:1ω5 was analysed separately as it is found in high abundances in spores of arbuscular-mycorrhizal fungi (particularly NLFAs) which we expected to be abundant in the meadow soil, but can also be found in gram-negative bacteria (Lekberg et al., 2022; Olsson and Lekberg, 2022).

Reference

Adeleke, R., Cloete, T.E., Khasa, D.P., 2012. Culturable microorganisms associated with Sishen iron ore and their potential roles in biobeneficiation. World Journal of Microbiology and Biotechnology 28, 1057–1070. doi:10.1007/s11274-011-0904-2

Adeleke, R., Nwangburuka, C., Oboirien, B., 2017. Origins, roles and fate of organic acids in soils: A review. South African Journal of Botany 108, 393–406. doi:10.1016/j.sajb.2016.09.002

Adeleke, R.A., Cloete, T.E., Bertrand, A., Khasa, D.P., 2012. Iron ore weathering potentials of ectomycorrhizal plants. Mycorrhiza 22, 535–544. doi:10.1007/s00572-012-0431-5

Adeleke, R.A., Cloete, T.E., Bertrand, A., Khasa, D.P., 2010. Mobilisation of potassium and phosphorus from iron ore by ectomycorrhizal fungi. World Journal of Microbiology and Biotechnology 26, 1901–1913. doi:10.1007/s11274-010-0372-0

Badri, D.V., Vivanco, J.M., 2009. Regulation and function of root exudates. Plant, Cell and Environment 32, 666–681. doi:10.1111/j.1365-3040.2009.01926.x

Banfield, J.F., Barker, W.W., Welch, S.A., Taunton, A., 1999. Biological impact on mineral dissolution: Application of the lichen model to understanding mineral weathering in the rhizosphere. Proceedings of the National Academy of Sciences 96, 3404–3411. doi:10.1073/pnas.96.7.3404

Barrow, N.J., Hartemink, A.E., 2023. The effects of pH on nutrient availability depend on both soils and plants. Plant and Soil 487, 21–37. doi:10.1007/s11104-023-05960-5

Basan, M., Honda, T., Christodoulou, D., Hörl, M., Chang, Y.-F., Leoncini, E., Mukherjee, A., Okano, H., Taylor, B.R., Silverman, J.M., Sanchez, C., Williamson, J.R., Paulsson, J., Hwa, T., Sauer, U., 2020. A universal trade-off between growth and lag in fluctuating environments. Nature 584, 470–474. doi:10.1038/s41586-020-2505-4

Basan, M., Hui, S., Okano, H., Zhang, Z., Shen, Y., Williamson, J.R., Hwa, T., 2015. Overflow metabolism in Escherichia coli results from efficient proteome allocation. Nature 528, 99–104. doi:10.1038/nature15765

Baumert, V.L., Vasilyeva, N.A., Vladimirov, A.A., Meier, I.C., Kögel-Knabner, I., Mueller, C.W., 2018. Root Exudates Induce Soil Macroaggregation Facilitated by Fungi in Subsoil. Frontiers in Environmental Science 6. doi:10.3389/fenvs.2018.00140

Bligh, E.G., Dyer, W.J., 1959. A rapid method of total lipid extraction and purification. Canadian Journal of Philosophy 37, 911–917.

Brzostek, E.R., Greco, A., Drake, J.E., Finzi, A.C., 2013. Root carbon inputs to the rhizosphere stimulate extracellular enzyme activity and increase nitrogen availability in temperate forest soils. Biogeochemistry 115, 65–76. doi:10.1007/s10533-012-9818-9

Buckley, S., Brackin, R., Jämtgård, S., Näsholm, T., Schmidt, S., 2020. Microdialysis in soil environments: Current practice and future perspectives. Soil Biology and Biochemistry 143. doi:10.1016/j.soilbio.2020.107743

Buckley, S., Brackin, R., Näsholm, T., Schmidt, S., Jämtgård, S., 2022. The influence of sucrose on soil nitrogen availability – A root exudate simulation using microdialysis. Geoderma 409. doi:10.1016/j.geoderma.2021.115645

Buyer, J.S., Sasser, M., 2012. High throughput phospholipid fatty acid analysis of soils. Applied Soil Ecology, Microorganisms and the Sustainable Management of Soil 61, 127–130. doi:10.1016/j.apsoil.2012.06.005

Calvo, O.C., Franzaring, J., Schmid, I., Müller, M., Brohon, N., Fangmeier, A., 2017. Atmospheric CO2 enrichment and drought stress modify root exudation of barley. Global Change Biology 23, 1292–1304. doi:10.1111/gcb.13503

Canarini, A., Kaiser, C., Merchant, A., Richter, A., Wanek, W., 2019. Root Exudation of Primary Metabolites: Mechanisms and Their Roles in Plant Responses to Environmental Stimuli. Frontiers in Plant Science 10. doi:10.3389/fpls.2019.00157

Chari, N.R., Taylor, B.N., 2022. Soil organic matter formation and loss are mediated by root exudates in a temperate forest. Nature Geoscience 15, 1011–1016. doi:10.1038/s41561-022-01079-x

Dong, J., Hunt, J., Delhaize, E., Zheng, S.J., Jin, C.W., Tang, C., 2021. Impacts of elevated CO2 on plant resistance to nutrient deficiency and toxic ions via root exudates: A review. Science of The Total Environment 754, 142434. doi:10.1016/j.scitotenv.2020.142434

Drake, J.E., Darby, B.A., Giasson, M.A., Kramer, M.A., Phillips, R.P., Finzi, A.C., 2013. Stoichiometry constrains microbial response to root exudation-insights from a model and a field experiment in a temperate forest. Biogeosciences 10, 821–838. doi:10.5194/bg-10-821-2013

Eilers, K.G., Lauber, C.L., Knight, R., Fierer, N., 2010. Shifts in bacterial community structure associated with inputs of low molecular weight carbon compounds to soil. Soil Biology and Biochemistry 42, 896–903. doi:10.1016/j.soilbio.2010.02.003

Enjalbert, B., Millard, P., Dinclaux, M., Portais, J.-C., Létisse, F., 2017. Acetate fluxes in Escherichia coli are determined by the thermodynamic control of the Pta-AckA pathway. Scientific Reports 7, 42135. doi:10.1038/srep42135

Estrela, S., Sanchez-Gorostiaga, A., Vila, J.C., Sanchez, A., 2021. Nutrient dominance governs the assembly of microbial communities in mixed nutrient environments. eLife 10, e65948. doi:10.7554/eLife.65948

Farrar, J., Hawes, M., Jones, D., Lindow, S., 2003. How roots control the flux of carbon to the rhizosphere. Ecology 84, 827–837. doi:10.1890/0012-9658(2003)084[0827:HRCTFO]2.0.CO;2

Fender, A.-C., Gansert, D., Jungkunst, H.F., Fiedler, S., Beyer, F., Schützenmeister, K., Thiele, B., Valtanen, K., Polle, A., Leuschner, C., 2013. Root-induced tree species effects on the source/sink strength for greenhouse gases (CH4, N2O and CO2) of a temperate deciduous forest soil. Soil Biology and Biochemistry 57, 587–597. doi:10.1016/j.soilbio.2012.08.004

Frostegård, Å., Tunlid, A., Bååth, E., 1991. Microbial biomass measured as total lipid phosphate in soils of different organic content. Journal of Microbiological Methods 14, 151–163. doi:10.1016/0167-7012(91)90018-L

Garcia Arredondo, M., Fang, Y., Jones, M., Yabusaki, S., Cardon, Z., Keiluweit, M., 2023. Resolving dynamic mineral-organic interactions in the rhizosphere by combining in-situ microsensors with plant-soil reactive transport modeling. Soil Biology and Biochemistry 184, 109097. doi:10.1016/j.soilbio.2023.109097

Gargallo-Garriga, A., Preece, C., Sardans, J., Oravec, M., Urban, O., Peñuelas, J., 2018. Root exudate metabolomes change under drought and show limited capacity for recovery. Scientific Reports 8, 1–15. doi:10.1038/s41598-018-30150-0

Giehl, R.F.H., von Wirén, N., 2014. Root Nutrient Foraging. Plant Physiology 166, 509–517. doi:10.1104/pp.114.245225

Girkin, N.T., Turner, B.L., Ostle, N., Craigon, J., Sjögersten, S., 2018a. Root exudate analogues accelerate CO2 and CH4 production in tropical peat. Soil Biology and Biochemistry 117, 48–55. doi:10.1016/j.soilbio.2017.11.008

Girkin, N.T., Turner, B.L., Ostle, N., Sjögersten, S., 2018b. Composition and concentration of root exudate analogues regulate greenhouse gas fluxes from tropical peat. Soil Biology and Biochemistry 127, 280–285. doi:10.1016/j.soilbio.2018.09.033

Golubev, S.V., Bauer, A., Pokrovsky, O.S., 2006. Effect of pH and organic ligands on the kinetics of smectite dissolution at 25°C. Geochimica et Cosmochimica Acta 70, 4436–4451. doi:10.1016/j.gca.2006.06.1557

Gorka, S., Darcy, S., Horak, J., Imai, B., Mohrlok, M., Salas, E., Richter, A., Schmidt, H., Wanek, W., Kaiser, C., Canarini, A., 2023. Beyond PLFA: Concurrent extraction of neutral and glycolipid fatty acids provides new insights into soil microbial communities. Soil Biology and Biochemistry 187, 109205. doi:10.1016/j.soilbio.2023.109205

Gransee, A., Wittenmayer, L., 2000. Qualitative and quantitative analysis of water-soluble root exudates in relation to plant species and development. Journal of Plant Nutrition and Soil Science 163, 381–385. doi:10.1002/1522-2624(200008)163:4<381::AID-JPLN381>3.0.CO;2-7

Gu, Y., Wang, X., Yang, T., Friman, V., Geisen, S., Wei, Z., Xu, Y., Jousset, A., Shen, Q., 2020. Chemical structure predicts the effect of plant-derived low-molecular weight compounds on soil microbiome structure and pathogen suppression. Functional Ecology 34, 2158–2169. doi:10.1111/1365-2435.13624

Gunina, A., Kuzyakov, Y., 2015. Sugars in soil and sweets for microorganisms: Review of origin, content, composition and fate. Soil Biology and Biochemistry 90, 87–100. doi:10.1016/j.soilbio.2015.07.021

Hosmer, J., McEwan, A.G., Kappler, U., 2023. Bacterial acetate metabolism and its influence on human epithelia. Emerging Topics in Life Sciences 8, 1–13. doi:10.1042/ETLS20220092

Jilling, A., Keiluweit, M., Gutknecht, J.L.M., Grandy, A.S., 2021. Priming mechanisms providing plants and microbes access to mineral-associated organic matter. Soil Biology and Biochemistry 158, 108265. doi:10.1016/j.soilbio.2021.108265

Joergensen, R.G., 1996. The fumigation-extraction method to estimate soil microbial biomass: Calibration of the *k*EC value. Soil Biology and Biochemistry 28, 25–31. doi:10.1016/0038-0717(95)00102-6

Jones, D.L., 1998. Organic acids in the rhizosphere – a critical review. Plant and Soil 25–44. doi:10.1023/A:1004356007312

Jones, D.L., Dennis, P.G., Owen, A.G., Van Hees, P.A.W., 2003. Organic acid behavior in soils - misconceptions and knowledge gaps. Plant and Soil 248, 31–41. doi:10.1023/A

Jones, D.L., Edwards, A.C., 1998. Influence of sorption on the biological utilization of two simple carbon substrates. Soil Biology and Biochemistry 30, 1895–1902. doi:10.1016/S0038-0717(98)00060-1

Jones, D.L., Murphy, D.V., 2007. Microbial response time to sugar and amino acid additions to soil. Soil Biology and Biochemistry 39, 2178–2182. doi:10.1016/j.soilbio.2007.03.017

Jones, D.L., Nguyen, C., Finlay, R.D., 2009. Carbon flow in the rhizosphere: carbon trading at the soil–root interface. Plant and Soil 321, 5–33. doi:10.1007/s11104-009-9925-0

Keiluweit, M., Bougoure, J.J., Nico, P.S., Pett-Ridge, J., Weber, P.K., Kleber, M., 2015. Mineral protection of soil carbon counteracted by root exudates. Nature Climate Change 5, 588–595. doi:10.1038/nclimate2580

Keiluweit, M., Wanzek, T., Kleber, M., Nico, P., Fendorf, S., 2017. Anaerobic microsites have an unaccounted role in soil carbon stabilization. Nature Communications 8, 1771. doi:10.1038/s41467-017-01406-6

Koh, A., Vadder, F.D., Kovatcheva-Datchary, P., Bäckhed, F., 2016. From Dietary Fiber to Host Physiology: Short-Chain Fatty Acids as Key Bacterial Metabolites. Cell 165, 1332–1345. doi:10.1016/j.cell.2016.05.041

König, A., Wiesenbauer, J., Gorka, S., Marchand, L., Kitzler, B., Inselsbacher, E., Kaiser, C., 2022. Reverse microdialysis: A window into root exudation hotspots. Soil Biology and Biochemistry 174, 108829. doi:10.1016/j.soilbio.2022.108829

Kreft, J.-U., Bonhoeffer, S., 2005. The evolution of groups of cooperating bacteria and the growth rate versus yield trade-off. Microbiology 151, 637–641. doi:10.1099/mic.0.27415-0

Kreft, J.U., Griffin, B.M., González-Cabaleiro, R., 2020. Evolutionary causes and consequences of metabolic division of labour: why anaerobes do and aerobes don't. Current Opinion in Biotechnology 62, 80–87. doi:10.1016/j.copbio.2019.08.008

Kuijken, R.C.P., Snel, J.F.H., Heddes, M.M., Bouwmeester, H.J., Marcelis, L.F.M., 2015. The importance of a sterile rhizosphere when phenotyping for root exudation. Plant and Soil 387, 131–142. doi:10.1007/s11104-014-2283-6

Kuzyakov, Y., Blagodatskaya, E., 2015. Microbial hotspots and hot moments in soil: Concept & review. Soil Biology and Biochemistry 83, 184–199. doi:10.1016/j.soilbio.2015.01.025

Landi, L., Valori, F., Ascher, J., Renella, G., Falchini, L., Nannipieri, P., 2006. Root exudate effects on the bacterial communities, CO2 evolution, nitrogen transformations and ATP content of rhizosphere and bulk soils. Soil Biology and Biochemistry 38, 509–516. doi:10.1016/j.soilbio.2005.05.021

Lecomte, S.M., Achouak, W., Abrouk, D., Heulin, T., Nesme, X., Haichar, F.E.Z., 2018. Diversifying Anaerobic Respiration Strategies to Compete in the Rhizosphere. Frontiers in Environmental Science 6, 139. doi:10.3389/fenvs.2018.00139

Lekberg, Y., Bååth, E., Frostegård, Å., Hammer, E., Hedlund, K., Jansa, J., Kaiser, C., Ramsey, P.W., Řezanka, T., Rousk, J., Wallander, H., Welc, M., Olsson, P.A., 2022. Fatty acid 16:1ω5 as a proxy for arbuscular mycorrhizal fungal biomass: current challenges and ways forward. Biology and Fertility of Soils 58, 835–842. doi:10.1007/s00374-022-01670-9

Liu, Y., Evans, S.E., Friesen, M.L., Tiemann, L.K., 2022. Root exudates shift how N mineralization and N fixation contribute to the plant-available N supply in low fertility soils. Soil Biology and Biochemistry 165, 108541. doi:10.1016/j.soilbio.2021.108541

Lopez-Sangil, L., George, C., Medina-Barcenas, E., Birkett, A.J., Baxendale, C., Bréchet, L.M., Estradera-Gumbau, E., Sayer, E.J., 2017. The Automated Root Exudate System (ARES): a method to apply solutes at regular intervals to soils in the field. Methods in Ecology and Evolution 8, 1042–1050. doi:10.1111/2041-210X.12764

Lu, J., Dijkstra, F.A., Wang, P., Cheng, W., 2019. Roots of non-woody perennials accelerated long-term soil organic matter decomposition through biological and physical mechanisms. Soil Biology and Biochemistry 134, 42–53. doi:10.1016/j.soilbio.2019.03.015

Luo, Y., Zhao, X., Andrén, O., Zhu, Y., Huang, W., 2014. Artificial root exudates and soil organic carbon mineralization in a degraded sandy grassland in northern China. Journal of Arid Land 6, 423–431. doi:10.1007/s40333-014-0063-z

Macias-Benitez, S., Garcia-Martinez, A.M., Caballero Jimenez, P., Gonzalez, J.M., Tejada Moral, M., Parrado Rubio, J., 2020. Rhizospheric Organic Acids as Biostimulants: Monitoring Feedbacks on Soil Microorganisms and Biochemical Properties. Frontiers in Plant Science 11, 633. doi:10.3389/fpls.2020.00633

Meier, I.C., Pritchard, S.G., Brzostek, E.R., McCormack, M.L., Phillips, R.P., 2015. The rhizosphere and hyphosphere differ in their impacts on carbon and nitrogen cycling in forests exposed to elevated CO2. New Phytologist 205, 1164–1174. doi:10.1111/nph.13122

Mommer, L., Hinsinger, P., Prigent-Combaret, C., Visser, E.J.W., 2016. Advances in the rhizosphere: stretching the interface of life. Plant and Soil 407, 1–8. doi:10.1007/s11104-016-3040-9

Müller, R., Peticzka, R., Inselsbacher, E., 2023. Applicability of the microdialysis technique in dry soils: Impact of soil water content depends on perfusion flow rate. Soil Biology and Biochemistry 177, 108903. doi:10.1016/j.soilbio.2022.108903

Nogal, A., Valdes, A.M., Menni, C., 2021. The role of short-chain fatty acids in the interplay between gut microbiota and diet in cardio-metabolic health. Gut Microbes 13, 1897212. doi:10.1080/19490976.2021.1897212

Nunan, N., Schmidt, H., Raynaud, X., 2020. The ecology of heterogeneity: soil bacterial communities and C dynamics. Philosophical Transactions of the Royal Society of London. Series B, Biological Sciences 375, 20190249. doi:10.1098/rstb.2019.0249

Oburger, E., Kirk, G.J.D., Wenzel, W.W., Puschenreiter, M., Jones, D.L., 2009. Interactive effects of organic acids in the rhizosphere. Soil Biology and Biochemistry 41, 449–457. doi:10.1016/j.soilbio.2008.10.034

Oburger, E., Schmidt, H., 2016. New Methods To Unravel Rhizosphere Processes. Trends in Plant Science 21, 243–255. doi:10.1016/j.tplants.2015.12.005

Oldfield, E.E., Crowther, T.W., Bradford, M.A., 2018. Substrate identity and amount overwhelm temperature effects on soil carbon formation. Soil Biology and Biochemistry 124, 218–226. doi:10.1016/j.soilbio.2018.06.014

Olsson, P.A., Lekberg, Y., 2022. A critical review of the use of lipid signature molecules for the quantification of arbuscular mycorrhiza fungi. Soil Biology and Biochemistry 166, 108574. doi:10.1016/j.soilbio.2022.108574

Pastor, J.M., Borges, N., Pagán, J.P., Castaño-Cerezo, S., Csonka, L.N., Goodner, B.W., Reynolds, K.A., Gonçalves, L.G., Argandoña, M., Nieto, J.J., Vargas, C., Bernal, V., Cánovas, M., 2019. Fructose metabolism in Chromohalobacter salexigens: interplay between the Embden–Meyerhof–Parnas and Entner–Doudoroff pathways. Microbial Cell Factories 18, 134. doi:10.1186/s12934-019-1178-x

Pavoncello, V., Barras, F., Bouveret, E., 2022. Degradation of Exogenous Fatty Acids in Escherichia coli. Biomolecules 12. doi:10.3390/biom12081019

Phillips, R.P., Finzi, A.C., Bernhardt, E.S., 2011. Enhanced root exudation induces microbial feedbacks to N cycling in a pine forest under long-term CO2 fumigation. Ecology Letters 14, 187–194. doi:10.1111/j.1461-0248.2010.01570.x

Qetrani, S., Bouray, M., Oukarroum, A., 2024. Phosphorus mobilization and acquisition in the alkaline-calcareous rhizosphere: A synthesis. Rhizosphere 30, 100907. doi:10.1016/j.rhisph.2024.100907

R Core Team, 2022. R: A language and environment for statistical computing. R Foundation for Statistical Computing, Vienna, Austria.

Reinthaler, D., Harris, E., Pötsch, E.M., Herndl, M., Richter, A., Wachter, H., Bahn, M., 2021. Responses of grassland soil CO2 production and fluxes to drought are shifted in a warmer climate under elevated CO2. Soil Biology and Biochemistry 163, 108436. doi:10.1016/j.soilbio.2021.108436

Romano, A.H., Conway, T., 1996. Evolution of carbohydrate metabolic pathways. Research in Microbiology 147, 448–455. doi:10.1016/0923-2508(96)83998-2

Rui, J., Peng, J., Lu, Y., 2009. Succession of Bacterial Populations during Plant Residue Decomposition in Rice Field Soil. Applied and Environmental Microbiology 75, 4879–4886. doi:10.1128/AEM.00702-09

Schink, S.J., Christodoulou, D., Mukherjee, A., Athaide, E., Brunner, V., Fuhrer, T., Bradshaw, G.A., Sauer, U., Basan, M., 2022. Glycolysis/gluconeogenesis specialization in microbes is driven by biochemical constraints of flux sensing. Molecular Systems Biology 18, e10704. doi:10.15252/msb.202110704

Schlüter, S., Sammartino, S., Koestel, J., 2020. Exploring the relationship between soil structure and soil functions via pore-scale imaging. Geoderma 370, 114370. doi:10.1016/j.geoderma.2020.114370

Shi, S., Richardson, A.E., O'Callaghan, M., DeAngelis, K.M., Jones, E.E., Stewart, A., Firestone, M.K., Condron, L.M., 2011. Effects of selected root exudate components on soil bacterial communities. FEMS Microbiology Ecology 77, 600–610. doi:10.1111/j.1574-6941.2011.01150.x

Smith, W.H., 1976. Character and Significance of Forest Tree Root Exudates. Ecology 57, 324–331. doi:10.2307/1934820

Sokol, N.W., Bradford, M.A., 2019. Microbial formation of stable soil carbon is more efficient from belowground than aboveground input. Nature Geoscience 12, 46–53. doi:10.1038/s41561-018-0258-6

Steinauer, K., Chatzinotas, A., Eisenhauer, N., 2016. Root exudate cocktails: the link between plant diversity and soil microorganisms? Ecology and Evolution 6, 7387–7396. doi:10.1002/ece3.2454

Uroz, S., Calvaruso, C., Turpault, M.-P., Frey-Klett, P., 2009. Mineral weathering by bacteria: ecology, actors and mechanisms. Trends in Microbiology 17, 378–387. doi:10.1016/j.tim.2009.05.004

Uroz, S., Oger, P., Lepleux, C., Collignon, C., Frey-Klett, P., Turpault, M.-P., 2011. Bacterial weathering and its contribution to nutrient cycling in temperate forest ecosystems. Research in Microbiology, Special issue on environmental microbiology 162, 820–831. doi:10.1016/j.resmic.2011.01.013

van Schöll, L., Kuyper, T.W., Smits, M.M., Landeweert, R., Hoffland, E., Breemen, N. van, 2008. Rock-eating mycorrhizas: their role in plant nutrition and biogeochemical cycles. Plant and Soil 303, 35–47. doi:10.1007/s11104-007-9513-0

Vance, E.D., Brookes, P.C., Jenkinson, D.S., 1987. Microbial biomass measurements in forest soils: The use of the chloroform fumigation-incubation method in strongly acid soils. Soil Biology and Biochemistry 19, 697–702. doi:10.1016/0038-0717(87)90051-4

Vives-Peris, V., de Ollas, C., Gómez-Cadenas, A., Pérez-Clemente, R.M., 2020. Root exudates: from plant to rhizosphere and beyond. Plant Cell Reports 39, 3–17. doi:10.1007/s00299-019-02447-5

Wei, Y., Ma, X., Zhao, J., Wang, X., Gao, C., 2023. Succinate metabolism and its regulation of host-microbe interactions. Gut Microbes 15, 2190300. doi:10.1080/19490976.2023.2190300

Wickham, H., 2016. ggplot2: Elegant Graphics for Data Analysis. Springer-Verlag New York.

Wiesenbauer, J., König, A., Gorka, S., Marchand, L., Nunan, N., Kitzler, B., Inselsbacher, E., Kaiser, C., 2024. A pulse of simulated root exudation alters the composition and temporal dynamics of microbial metabolites in its immediate vicinity. Soil Biology and Biochemistry 189, 109259. doi:10.1016/j.soilbio.2023.109259

Willers, C., Jansen van Rensburg, P.J.J., Claassens, S., 2015. Phospholipid fatty acid profiling of microbial communities-a review of interpretations and recent applications. Journal of Applied Microbiology 119, 1207–1218. doi:10.1111/jam.12902

Williams, A., Langridge, H., Straathof, A.L., Muhamadali, H., Hollywood, K.A., Goodacre, R., de Vries, F.T., 2022. Root functional traits explain root exudation rate and composition across a range of grassland species. Journal of Ecology 110, 21–33. doi:10.1111/1365-2745.13630

Wolfe, A.J., 2005. The Acetate Switch. Microbiology and Molecular Biology Reviews 69, 12–50. doi:10.1128/MMBR.69.1.12-50.2005

Wortel, M.T., Noor, E., Ferris, M., Bruggeman, F.J., Liebermeister, W., 2018. Metabolic enzyme cost explains variable trade-offs between microbial growth rate and yield. PLOS Computational Biology 14, e1006010. doi:10.1371/journal.pcbi.1006010

Xu, N., Gao, Y., 2008. Characterization of hematite dissolution affected by oxalate coating, kinetics and pH. Applied Geochemistry 23, 783–793. doi:10.1016/j.apgeochem.2007.12.026

Zhalnina, K., Louie, K.B., Hao, Z., Mansoori, N., da Rocha, U.N., Shi, S., Cho, H., Karaoz, U., Loqué, D., Bowen, B.P., Firestone, M.K., Northen, T.R., Brodie, E.L., 2018. Dynamic root exudate chemistry and microbial substrate preferences drive patterns in rhizosphere microbial community assembly. Nature Microbiology 3, 470–480. doi:10.1038/s41564-018-0129-3

Zhang, S., Yang, W., Chen, H., Liu, B., Lin, B., Tao, Y., 2019. Metabolic engineering for efficient supply of acetyl-CoA from different carbon sources in Escherichia coli. Microbial Cell Factories 18, 130. doi:10.1186/s12934-019-1177-y

Zhang, X., Dippold, M.A., Kuzyakov, Y., Razavi, B.S., 2019. Spatial pattern of enzyme activities depends on root exudate composition. Soil Biology and Biochemistry 133, 83–93. doi:10.1016/j.soilbio.2019.02.010

Chapter 4

An integrative imaging approach for studying microbial assimilation of ^{13}C-labelled root exudates in soil at the microscale

An integrative imaging approach for studying microbial assimilation of ^{13}C-labelled root exudates in soil at the microscale

Julia Wiesenbauer [a,b], Schmidt Hannes [a], Stefan Gorka [a,b], Schintlmeister Arno [c,d], Carsten Müller [e], Christina Kaiser [a]

[a] Division of Terrestrial Ecosystem Research, Centre for Microbiology and Environmental Systems Science, University of Vienna, Vienna, Austria, Djerassiplatz 1, A-1030, Wien, Austria

[b] Doctoral School in Microbiology and Environmental Science, University of Vienna, Vienna, Austria

[c] Department of Microbiology and Environmental Systems Science, Division of Microbial Ecology, University of Vienna, Vienna, Austria

[d] Large-Instrument Facility for Advanced Isotope Research, University of Vienna, Vienna, Austria

[e] Department of Ecology, Technical University of Berlin, Berlin, Germany.

Abstract

Understanding assimilation of root exudates by soil microorganisms is crucial for advancing our knowledge of carbon (C) and nutrient cycling in the rhizosphere. However, studying such interactions on the microbial scale poses significant challenges due to the complex soil matrix and transient nature of root exudation. This necessitates innovative approaches that can accurately simulate and observe these intricate biological processes in undisturbed soil systems. Our study introduces an integrated approach that combines stable isotope probing with high-resolution imaging techniques. We simulated root exudation of ^{13}C-labelled substrates using reverse microdialysis to minimize disturbance to the soil structure. We employed confocal laser scanning microscopy (CLSM) to visualize the spatial distribution of fluorescently labelled microbial cells and scanning electron microscopy (SEM) to provide detailed structural context of these areas. Nanoscale secondary ion mass spectrometry (NanoSIMS) was used to map the distribution of isotopic signature (^{13}C) alongside elements associated with organic compounds (C, N) and mineral particles (Si, Al). By integrating these techniques, we were able to correlate data on soil structure and microbial distribution with chemical signatures and to investigate the microbial assimilation of ^{13}C-labelled substrate close to the artificial root. We observed that some, but not all, of the microbial cells had assimilated substrate-derived ^{13}C, highlighting varied microbial response within the rhizosphere soil space. Our findings demonstrate the effectiveness of correlative approaches for elucidating the spatial dynamics of microbial activity and substrate utilization at the microscale. This approach lays the groundwork for more detailed investigations into the intricate microbial processes that influence rhizosphere dynamics.

1. Introduction

Interactions between soil microbes and plant roots are central to carbon (C) and nutrient cycling in terrestrial ecosystems (Blagodatskaya and Kuzyakov, 2008; Dijkstra et al., 2021). Plant roots exude a diverse array of organic compounds into the soil (Jones et al., 2009; Canarini et al., 2019), which serve as substrate for microbial communities, promoting increased microbial activity and stimulating nutrient mobilization (Blagodatskaya and Kuzyakov, 2008; Dijkstra et al., 2021). These exudates not only shape microbial communities (Haichar et al., 2008; Zhalnina et al., 2018) but also influence soil chemistry, e.g., by changing the pH (Hinsinger et al., 2003), and mobilizing nutrients like phosphorus or mineral-associated organic compounds (Khorassani et al., 2011; Keiluweit et al., 2015; Jilling et al., 2021). In turn, the microbial communities modify their soil environment through their activity and metabolism (Philippot et al., 2023), driving processes that releases C and other essential elements (Uroz et al., 2009; Wiesenbauer et al., 2024b, submitted). Additionally, root exudates and microbial products, such as mucilage and extracellular polymeric substances (EPS), respectively, affect soil hydrology (Benard et al., 2019) and are considered potential contributors of aggregate formation (Lehmann et al., 2017; Costa et al., 2018). Collectively, these biotic and abiotic processes determine nutrient availability for plants and microbes in the rhizosphere. However, studying these complex exudate-microbe-soil interactions in their natural spatial context poses significant challenges, as the intricate soil matrix and the dynamic nature of root exudation demand methods, which can accurately simulate and observe these biological processes at the microscale.

The complexity of the rhizosphere, with its opaque soil matrix and delicate microbial interactions, poses substantial challenges for direct observation and accurate simulation of microbial processes (Oburger and Schmidt, 2016; Védère et al., 2022). Microdialysis has emerged as a minimally invasive method to simulate passive root exudation and to study the microbial processes (e.g.: respiration, metabolite production) brought about at the exudation site at high temporal resolution (König et al., 2022; Wiesenbauer et al., 2024a, 2024b). Microdialysis membranes are inserted into the soil, and isotopically labelled substrates are released through diffusion, while simultaneously collect compounds from the soil solution (König et al., 2022). The simulation of root exudation through reverse microdialysis closely mimics natural interactions between microbes and root exudates, offering a more accurate reflection of in-situ dynamics. While these studies provided insights on microbial responses to artificial root exudation over time, they can't elucidate the spatial microscale context in which they happen**.**

Traditional methods for studying microbial activity in the rhizosphere, such as bulk soil sampling or the use of invasive instruments, often disrupt the soil matrix and fail to capture the complex

interplay of physical, chemical, and biological factors that characterize microbial dynamics at the microscale. These methods struggle to capture the spatial heterogeneity and functional diversity in undisturbed soil environments, overlooking the individual contributions of microorganisms and their localized interactions within the rhizosphere (Oburger and Schmidt, 2016; Moran and McGrath, 2021). Particularly, they do not account for the 'hot moments' and 'hotspots' areas of intense microbial activity driven by the localized, high concentration of root-derived carbon compounds (Kuzyakov and Blagodatskaya, 2015). This spatial and temporal variability is critical for understanding how microorganisms contribute to carbon cycling and nutrient availability in the rhizosphere. Consequently, there is a need to develop innovative, minimally invasive approaches that can accurately map and quantify these dynamic microbial responses, elucidating the spatial patterns of microbial activity in response to root exudates within undisturbed soil systems.

Various advanced imaging techniques can offer insight into the spatial aspect of microbial activity in the rhizosphere, each shedding light on different aspects of microbial interactions and environmental structure at micro to nano scales (Védère et al., 2022). For example, confocal laser scanning microscopy (CLSM) is used in identifying and localizing microbial cells and biomolecules using various fluorescent stains (Cardinale, 2014). On the other hand, scanning electron microscopy (SEM) provides high-resolution images of surface topography, offering detailed insights into soil microstructures and the presence of microorganisms (Witzgall et al., 2021). Furthermore, nanoscale secondary ion mass spectrometry (NanoSIMS) allows for detailed isotopic and elemental analysis at submicron scales, crucial for tracing nutrient and isotopes (e.g.: ^{13}C, ^{15}N) in microbial communities (Herrmann et al., 2007; Mueller et al., 2013). NanoSIMS in combination with stable isotope probing (SIP) can be used to gain insights into the microbial uptake and metabolism of nutrients linked to the spatial aspect (Musat et al., 2016). Moreover, many of these visualization techniques initially involve resin embedding of the soil after fixation of cells, to keep the soil structure intact, so that the spatial relationship of microbial populations and their micro-environment remains preserved. As each of these methods alone offers a unique but limited perspective, a holistic approach that integrates these techniques could provide significant advantages.

Recent studies have used combinations of imaging techniques to advance our understanding of spatial relationships in the rhizosphere. For instance, Schlüter et al. (2019) employed a combination of X-ray microtomography with fluorescence microscopy, SEM and NanoSIMS to explore how the spatial distribution of bacteria around decaying organic matter, i.e. substrate availability, relates to pore architecture. Lippold et al. (2023) established a correlative imaging workflow using X-ray CT and chemical analysis (micro-X-ray fluorescence spectroscopy, NanoSIMS, laser-ablation isotope ratio mass spectrometry) to map chemical gradients around 3D root segments, employing ^{13}C and ^{15}N isotopes to

traces C and N dynamics in the rhizosphere. Bandara et al. (2021) developed a comprehensive approach to simultaneous identify microbes and analysing the chemical environment at micro- to nano-meter resolution. Their technique integrates resin embedding and sectioning with a suite of analytical tools, including helium ion microscopy (HIM), catalysed reporter deposition-fluorescence in situ hybridization (CARD-FISH), scanning electron microscopy with energy-dispersive X-ray analysis (SEM-EDX), time-of-flight secondary ion mass spectrometry (ToF-SIMS), NanoSIMS, and confocal Raman spectroscopy (μ-Raman). This allows for precise spatial mapping of bacteria and detailed chemical profiling within the soil structure.

While these studies illustrate the potential of advanced imaging techniques to directly observe microbial processes at root exudation sites, none have integrated a minimally invasive method like reverse microdialysis to simulate root exudation. Reverse microdialysis allows precise control over both the quantity and composition of the substrate. By introducing stable isotope-labelled substrates and monitoring their assimilation by nearby microbial population using imaging techniques, this approach effectively bridges the gap between controlled laboratory experiments and the dynamic conditions of natural soil environments.

Building on the need for refined methodologies to study soil and microbial dynamics, this study presents an integrative approach that combines CLSM's ability to identify and localize microbial cells, SEM's imaging of soil microstructures, and NanoSIMS's precise elemental and isotopic analysis with stable isotope probing (SIP) to investigate the assimilation of artificial root exudates by the microbial communities in a spatial context in their native environment. Our primary objectives were to develop and test a methodological workflow which allows us to: (1) simulate root exudation in a minimally invasive manner using reverse microdialysis to best preserve the soil's native structure, (2) utilize fluorescent microscopy to map the spatial distribution of fluorescence-stained microbial cells in resin-embedded soil cores, (3) employ SEM, coupled with energy-dispersive X-ray spectroscopy (SEM-EDX), to analyse soil structure and elemental composition, and (4) apply NanoSIMS to precisely map the uptake of ^{13}C-labeled substrates by microbial communities and the spatial distribution of soil organic matter (SOM) and minerals.

This integrated approach provided a comprehensive view of microbial distribution relative to the soil structure and allowed for a precise localization and chemical characterization of microbial populations in their soil environment. The overlay of CLSM, SEM and NanoSIMS images emerged as a powerful means of linking structural information (fluorescence microscopy, SEM) with functional and isotopic data (NanoSIMS). This enabled the identification and characterization of microbial cells involved in substrate assimilation near the exudation sites, as well as the mapping of organic compounds (C, N) and mineral particles (e.g.: Si, Fe, Al). We observed that not all microbial populations

assimilated the ^{13}C-labelled substrate, but those that did were closely associated with microbial hotspots. These results highlight the nuanced dynamics of microbial activity and substrate utilization at the microscale in the rhizosphere. We believe this approach will prove to be a powerful tool to explore the spatial dynamics of soil nutrients and their assimilation by soil microbes, thus providing a more holistic view of microbial interactions within their native habitat.

2. Material & Methods

2.1 Collection of undisturbed soil cores

We collected undisturbed soil cores from an extensively managed meadow (Gumpenstein, Austria, 47° 29' N, 14° 06' E, 732 m asl.) on 11th July, 2019. The soil was a Cambisol with loamy sand texture (44.2% sand, 47.6% silt, 8.3% clay)(Reinthaler et al., 2021). After removing the above-ground biomass and the litter layer, we used large corers (10 cm diameter, 6 cm height) to take soil cores from five distinct locations within the meadow and transported them to the laboratory.

To determine gravimetric water content, we cored two small soil cores (1 cm diameter, 3 cm height) from each of the large cores. The soil from the two small cores was combined, and stones, roots and organic material were removed with tweezers. The soils were then dried overnight in a drying oven to determine the water content by comparing weights before and after the drying. The initial gravimetric water content was 19%. Over the following three days, the water content in the large soil cores was adjusted to 30% by pipetting autoclaved tap water onto their surfaces, ensuring optimal conditions to simulate root exudation using reverse microdialysis. The large soil cores were kept at field temperatures (12 °C) in an incubator.

2.2 Simulation of ^{13}C-labelled root exudation by reverse microdialysis

The samples for this study were specifically designed to investigate the spatial dynamics within the rhizosphere at the microscale. They were collected at the end of an experiment which mimicked passive root exudation (Wiesenbauer et al., 2024b, submitted). It involved releasing a 6-hour pulse of ^{13}C-labelled sugars and amino acids into undisturbed soil using reverse microdialysis. Subsequently, temporal dynamics of soil metabolites were monitored by collecting metabolites from the soil solution over an 18-day time period following the pulse release. The experimental setup is described in detail in Wiesenbauer et al. (2024b, submitted). Briefly, after adjusting the water content of the large soil cores to 30%, we cored eight smaller soil cores from each of the five large soil cores using stainless steel cylindrical corers (1 cm diameter, 3 cm height). The small soil cores were kept in their stainless-

steel corers to ensure minimal disturbance to soil structure. Always two small soil cores were paired and

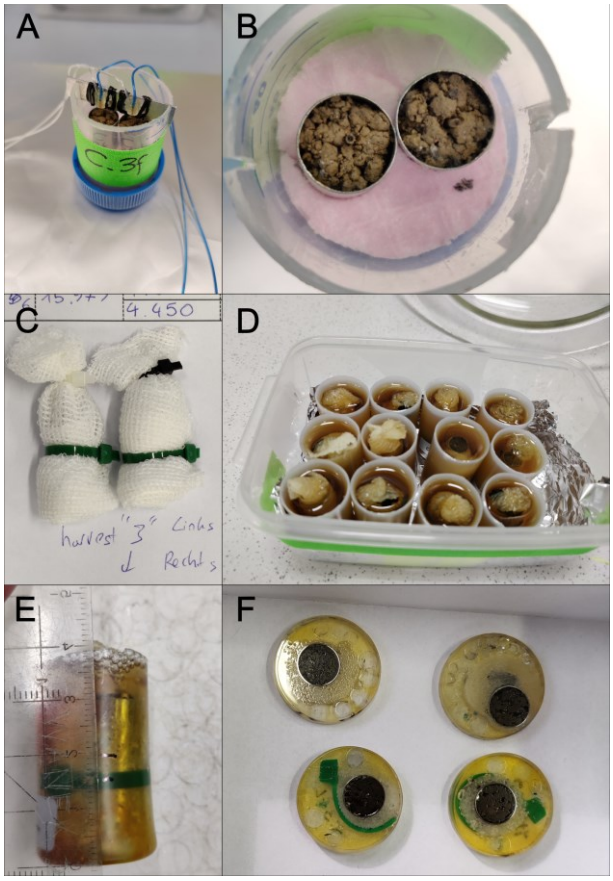


Figure 1. Overview of sample preparation and experimental setup for simulating root exudation in undisturbed soil cores. (**A**) Customised mesocosm setup assembled by modifying a 50 ml Falcon tube to hold two small soil cores (1 cm diameter, 3 cm height), each fitted with a microdialysis membrane secured to an aluminium strip with rubber bands to minimize soil disturbance. (**B**) Eighteen days after the simulated root exudation, soil cores were harvested. Microdialysis probes were carefully cut off, leaving the membranes in place to preserve soil structure. (**C**) The harvested soil cores were wrapped in gauze, which was secured with colour-coded cable ties for easy identification during sample preparation. (**D**) Gauze-wrapped cores were then embedded in epoxy resin in moulds. (**E**) After resin curing, cores were freed from moulds and a 5 mm disc was cut out carefully centering at the height of the microdialysis membrane. (**F**) The discs were polished to a surface finish of 1 µm for detailed imaging analyses.

placed in a customised setup, referred to as 'mesocosm'. These mesocosms consisted of 50 ml Falcon tubes, turned on their lid and cut off at 4 cm height, with Styrofoam placed into the lid to securely hold a pair of small soil cores within their stainless-steel corers (Fig. 1a). Into the centre of each core one microdialysis probe (CMA 20, CMA Microdialysis AB, Kista, Sweden) with a membrane length of 10 mm and a molecular weight cut-off of 20 kDa was inserted. To minimize the disturbance to the soil structure, the microdialysis probes were held in place by securing them to an aluminium strip with rubber bands (Fig. 1a). While each of the pairs of small soil cores was initially viewed as a single analytical unit for the purpose of the experiment, only one core of each pair was later embedded in resin.

We simulated a 6-hour long root exudation pulse by releasing an artificial root exudate composed of a mixture of glucose, fructose, acetate, succinate into the soil using reverse microdialysis (Wiesenbauer et al., 2024a). Each of the four compounds was uniformly labelled with 99 atom% ^{13}C (Sigma-Aldrich) and dissolved in MilliQ water, at a concentration of 500 µmol C l^{-1} per compound, totalling 2000 µmol C l^{-1}. The microdialysis probes were connected to syringe pumps (CMA 4004, CMA Microdialysis AB, Solna, Sweden) set to a flow rate of 2.5 µl min^{-1} per membrane.

The mesocosms were infused for 6 hours with either the ^{13}C-labelled artificial root exudate or with MilliQ water for control mesocosms. The ^{13}C-labelled substrate was released outside the permeable membrane through passive diffusion. During the 6-hour exudation pulse, 656 ± 207 nmol C (mean ± standard deviation) were released, of which 72.6% of nmol C were from organic acids and only 27.4% were from sugars (Wiesenbauer et al., 2024b, submitted). Since substrate release rates rely on diffusion gradients, there is a direct feedback between their removal from around the microdialysis membrane and the rates at which substrates are released. This suggests that the notably higher release of organic acids can be attributed to stronger removal forces in the vicinity of the microdialysis membrane, likely due to microbial uptake (Wiesenbauer et al., 2024b, submitted). The microdialysis probes remained in place throughout the 18-day experiment.

On day 18, at the conclusion of the experiment, the small soil cores were harvested, one of each pair was used to measure phospholipid fatty acids (PLFAs) and neutral lipid fatty acids (NLFAs) (Wiesenbauer et al., 2024b, submitted), while the other one was embedded in resin for imaging analysis. To maintain the integrity of the soil structure for the 'imaging' core, the microdialysis probes were carefully cut off, leaving the membranes inserted in the soil (Fig. 1b). The soil cores were then wrapped in gauze and secured with colour-coded cable ties for easy identification during subsequently resin embedding (Fig. 1c).

2.3 Fixation, dehydration and resin impregnation of soil cores

We chemically fixed the soil cores with 1% paraformaldehyde in autoclaved 1 x phosphate-buffered saline (PBS) for 48 hours at 4 °C: For this, we placed the gauze-wrapped soil cores upright in glass jars equipped with a spacer (metal grid on cryovial lids) at the bottom, ensuring that soil cores receiving the ^{13}C-labelled substrate and control soil cores were always kept in separate jars. The upright positioning of the soil cores was maintained throughout all processes (fixation, dehydration and resin impregnation) to ensure uniform treatment and effective drainage. We added the 1% paraformaldehyde solution to the jars in three increments until the cores were fully submerged. Between each addition, we allowed a 10-minute waiting period at 4 °C to ensure gradual saturation from the bottom, allowing air to escape from the soil cores. Finally, we closed the jars and kept them at 4 °C for 48 hours for fixation.

After 48 hours, we washed the soil cores with 1 × PBS: We first carefully removed the 1% paraformaldehyde solution from the jars to ensure its safe and correct disposal. Then, we placed the cores on paper towels to drain excess liquid. Once drained, the cores were returned to the emptied jars. We added 1× PBS in two increments until the cores were submerged, waiting 10 minutes after each addition. For the final step in the washing process, we removed the PBS and drained the cores on paper towels. We repeated this washing steps twice, for a total of three washes. Subsequently, we stored the soil cores in 3:2 EtOH:PBS (v:v) at -20 °C until further processing (19 days).

We performed a gradual acetone series to dehydrate the samples (50%, 70%, 90%, 3× 100%): We removed the EtOH-PBS solution and placed the cores on paper towels to drain excess liquid. We placed the cores in new glass jars fitted with a spacer at the bottom. We added 50% acetone in 3 increments until the cores were fully submerged, allowing a 10-minute pause between each addition to ensure gradual saturation. After the cores were submerged for 30 minutes, we emptied the 50% acetone and allowed the cores to drain excess liquid on paper towels. Once drained, the cores returned to the empty jars, and we continued the dehydration series with the next higher acetone concentration. We repeated the dehydration in 100% acetone three times, using a freshly opened acetone bottle and new glass jars that had not been in contact with water. After the final 100% acetone submersion, the cores were stored in 100% acetone overnight.

We impregnated the soil cores in a series of Araldite 502 resin and acetone mixtures, starting with a 1:3 ratio (v:v) and progressing to a 1:1 ratio, finishing with pure Araldite 502 epoxy resin: The Araldite 502 epoxy resin was prepared from three components, the resin Araldite 502 (Polyscience), the hardener Dodecenylsuccinylanhydrid (DDSA, Polyscience) and the accelerator N,N-Benzyldimethylamin (BDMA, Polyscience) at a ratio of 1:0.9231:0.05385 (Araldite 502:DDSA:BDMA).

On the first day, we prepared a 1:3 (v:v) Araldite 502:acetone mixture, using only the Araldite 502 resin and DDSA components (1:0.9231, Araldite 502:DDSA), specifically omitting the BDMA accelerator to prevent premature curing of the resin. First, we removed the acetone from the jars, placed the cores on paper towel to drain excess liquid, and then transferred them to new jars fitted with spacers at the bottom. We gradually saturated the cores with a 1:3 Araldite 502:acetone solution from the bottom in three increments until fully submerged, each addition followed by a 20-minute waiting period to allow air to escape from small soil pores and ensure full saturation with the mixture. We then incubated them at room temperature overnight.

On the second day, we removed the 1:3 Araldite 502:acetone solution and drained the excess solution from the cores by placing them on paper towels for several minutes. We prepared a 1:1 (v:v) Araldite 502:acetone solution, including BDMA accelerator with the resin components (1:0.9231:0.05385, Araldite 502:DDSA:BDMA). We placed the soil cores in jars and added Araldite 502:acetone (1:1) solution in three increments until fully submerged, waiting 20 min between each addition. To aid the penetration of the more viscous resin mixture into the smallest soil pores, we placed the jars in a desiccator and applied a gentle vacuum using a water pump. We monitored the vacuum level by placing a beaker containing acetone and boiling chips inside the desiccator. Boiling chips are small porous stones that promote steady boiling and prevent superheating by providing nucleation sites for bubble formation. This setup allowed us to visually check that the vacuum remained below the boiling point of acetone (no bubble formation on boiling chips), thus preventing any undesired boiling. After the vacuum was set, the desiccator was sealed, and the cores were left to incubate overnight.

On the third day, we prepared pure Araldite 502 resin (1:0.9231:0.05385, Araldite 502:DDSA:BDMA). We removed the 1:1 Araldite 502:acetone mixture and placed the soil cores on paper towels for several minutes to drain excess resin. The final moulds used for resin impregnation were 20 ml scintillation tubes (Fisher), modified by cutting off the bottleneck to create a 4.5 cm tall mould with 2.3 cm diameter opening. We positioned soil cores upright within their moulds, surrounded by glass beads to prevent tension-induced cracks during curing (Fig. 1d). We gradually added pure Araldite 502 resin to slowly saturate the soil cores from the bottom. Once submerged, the moulds were placed in a desiccator, and we applied a vacuum using a water pump, after which the desiccators were sealed to maintain the vacuum. The cores were incubated under these conditions for 3 days at room temperature, with the vacuum reapplied daily. After 3 days, the samples were cured at 65 °C for 5 days.

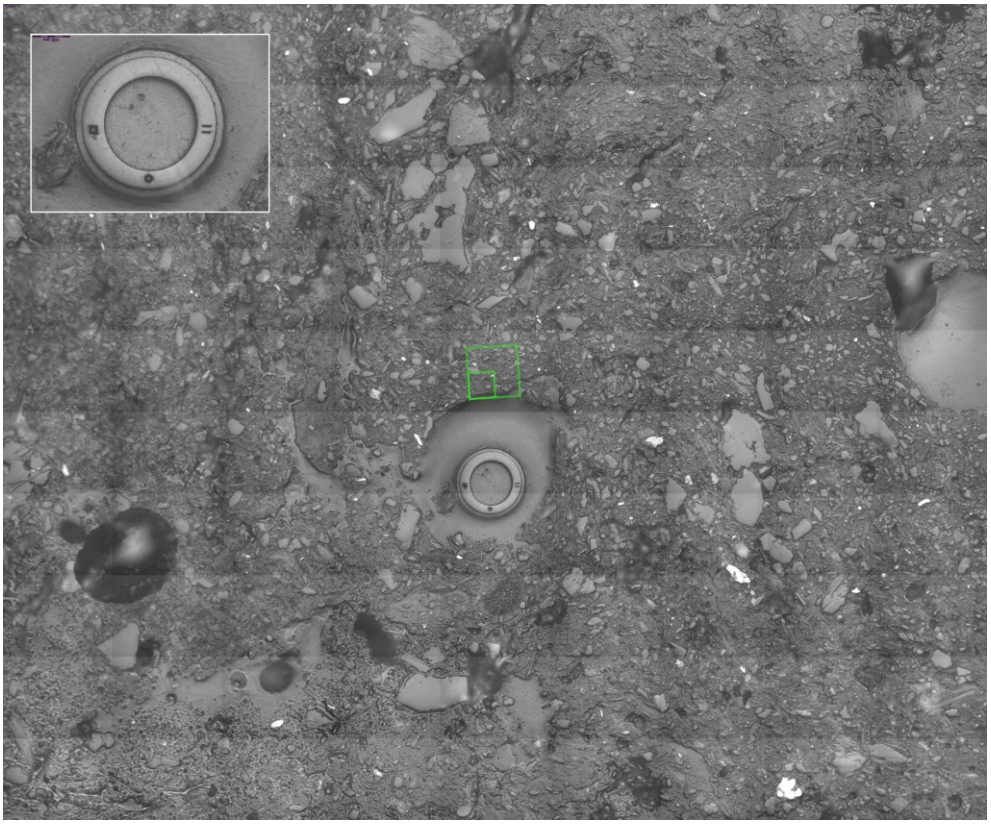


Figure 2. Comprehensive overview image of soil core cross-section with a microdialysis membrane at the centre. The figure presents a stitched overview image of the soil core's surface that received labile substrate, captured at 20× magnification using transmitted light – bright field (TL-BF) with a laser microdissection microscope (Leica LMD 7000, Germany). The zoomed-in section (top left corner) displays the microdialysis membrane. We used a laser to engrave markings onto the microdialysis membrane (0.5 mm diameter), facilitating navigation of the disc during subsequent microscopy analyses. Symbols include a circle to denote 'south', a square for 'west', and two parallel lines for 'east'. The green square indicates the area of CLSM image (Fig. 4) chosen for NanoSIMS analysis.

2.4 Cutting and polishing of discs

We cut a 5 mm slice from each resin-embedded soil core at a height of 1.5-2 cm from the bottom (Fig. 1e), which corresponds to the position of the microdialysis membrane within the cores (Discoplan-TS, Struers; PetroThin Thin Sectioning System, Buehler). The resulting discs, each with a diameter of 2.3 cm, were too small for the 1-inch (2.54 cm) holder required for NanoSIMS analysis. To accommodate this, we placed the discs in 1-inch diameter round moulds and filled the surrounding gap with additional Araldite 502 resin. If large non-resin filled soil pores were uncovered during cutting, we filled them with resin to ensure the structural integrity of the discs during polishing. Afterwards, the discs were cured at 65 °C for 24 hours. Finally, the 1-inch discs were polished using a manual polishing machine (LS 2, Remet, Italy) and MD-grinding discs (Struers) and SF1 polishing suspension (Logitech) to achieve a surface finish of 1 µm (Fig. 1f).

2.5 Laser microdissection microscopy

We used a laser microdissection (LMD) microscope (Leica LMD 7000, Germany) to engrave symbols on our round discs with the laser, which were essential for maintaining orientation during the subsequent microscopy. The settings for laser cutting were power 15, aperture 10, speed 8, specimen balance 0, heat current 80%, pulse frequency 1210 Hz. We engraved symbols into the resin just outside the soil core and directly into the microdialysis membrane at the centre of the disc: a circle to indicate the “south” direction, a square for “west”, and two parallel lines for “east”. We used transmitted light – bright field (TL-BF) to capture an overview image of each disc at 20× magnification with a CCD camera, using a 6.3x/0.13 dry objective, a light intensity of 42, an aperture of 22, a field diaphragm of 25. These images were stitched together from multiple individual pictures to create a comprehensive view of the entire disc surface (Fig. 2).

2.6 Confocal laser scanning microscopy

To visualize microbial cells in our soil cores we stained them with dsGreen (Lumiprobe, Germany), a fluorescent stain analogous to SYBR Green I, which has been shown to give strong fluorescent signals (Richter-Heitmann et al., 2016). Therefore, we pipetted 100 µl of a 50 × dsGreen solution in 1 × PBS evenly across the disc surface and incubated it at room temperature for 10 min in the dark. Afterwards, we removed excess stain with a pipette and tissue paper. We added a drop of mounting medium (CitiFluor) before covering the disc with a high-precision glass coverslip (Carl Roth).

Fluorescence microscopy was conducted using a confocal laser scanning microscope (CLSM; Leica TCS SP8X, Leica, Germany) equipped with a 63× glycerol objective and a white-light laser. The dsGreen was excited at a wavelength of 490 nm and recorded between 510 to 541 nm. Background

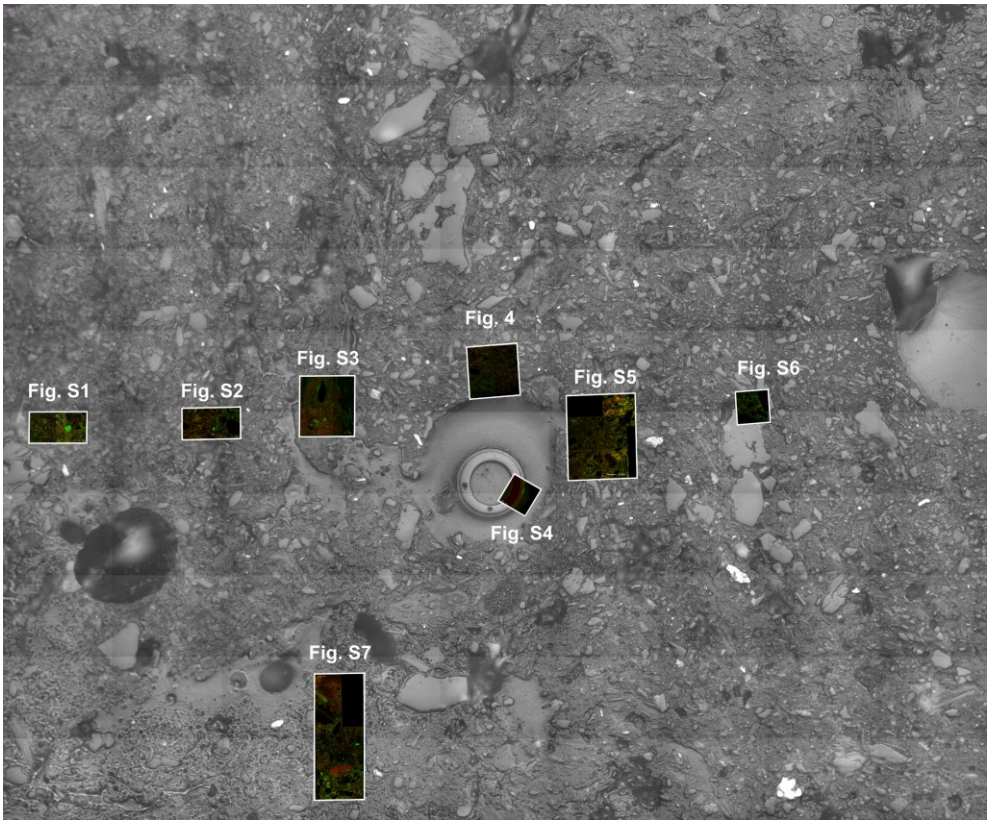


Figure 3. Overlay of CLSM fluorescence images on LMD overview image of soil core cross-section. A figure presents a comprehensive overview image of the soil core's surface that received labile substrate, captured at 20× magnification using a laser microdissection microscope. Fluorescence images from confocal laser scanning microscopy (CLSM), where microbes were stained with dsGreen, are superimposed on the LMD image, illustrating the microbial distribution along a transect that spans across the entire width of the soil core cross-section. The superimposed CLSM images are presented in Figure 4 and Figures S1 through S7 in the supplementary materials.

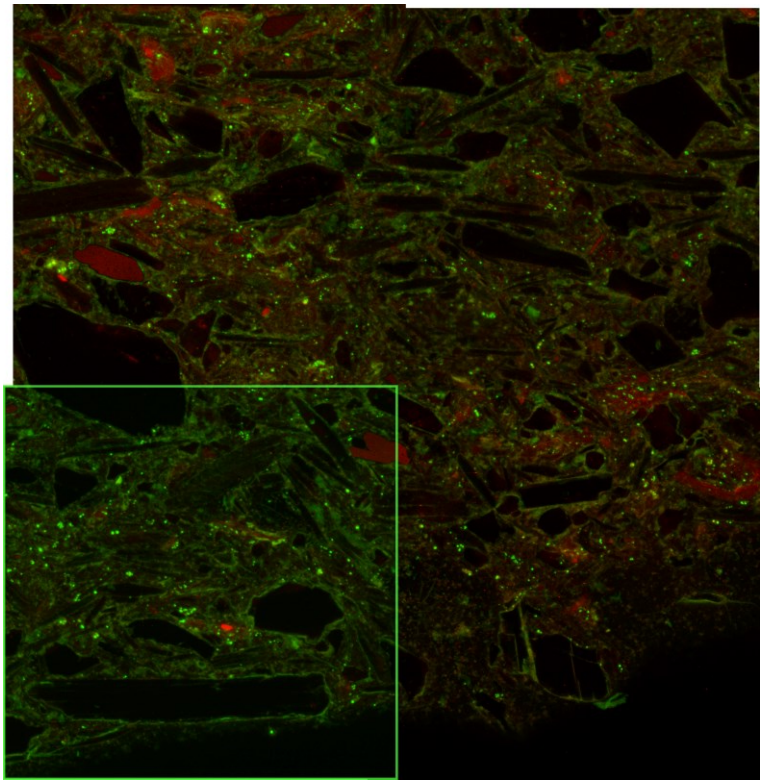


Figure 4. **Composite CLSM images of dsGreen stained microbial cells.** This composite image combines four CLSM images, each 184.5 × 184.5 µm, showcasing microbial cells stained with dsGreen. Red and green fluorescence channels were captured and overlaid to distinguish microbes (green) from organic matter and general background fluorescence (red). The bottom left image (green frame) in the composite was selected for subsequent NanoSIMS analysis.

autofluorescence, which provides addition spatial information, was captured through excitation at 561 nm and emission between 580 to 750 nm. The distinct excitation and emission wavelengths allowed us to capture separate signals for the fluorescence dye (green) and the autofluorescence (red) originating from background such as organic matter, enabling clear differentiation between microbial cells and the surrounding soil matrix (Cardinale, 2014; Schmidt et al., 2018). We acquired image stacks of varying depth and projected them into a single layer. The settings for each z-stack included an image size of 184.5 × 184.5 µm, an image resolution of 1024 ×1024 pixels, a bit depth of 8 per channel, a scan speed of 100 Hz, line averaging of 4, frame averaging of 1, a slice distance of 0.7 µm, a zoom factor of 1, and pinhole of 1 AU. Image stacks were stored as Leica ∗.lif files without post-processing.

We captured images at 8 locations along a west-to-east transect through the center of the ^{13}C-labelled soil core at the level of the microdialysis membrane (Fig. 3). At several locations, multiple images were taken and subsequently stitched together to form larger composite images (e.g. 1 × 2 or 2 × 2; Fig. 4). The composite CLSM images from the transect that were not selected for SEM or NanoSIMS analysis are included as supplementary figures S1 through S7. Additionally, we captured 9 images south of the microdialysis membrane, forming one large composite image (Fig. S8). Furthermore, a transect comprising 11 CLSM images of the control soil core was captured and assembled into one composite image (Fig. 6c, S8).

2.7 SEM

We acquired secondary electron images of regions where microbial cells were previously visualized using CLSM images. This step was crucial for our study as we aimed to perform NanoSIMS imaging on these regions, which requires high-resolution SEM images to accurately locate the target spots. Additionally, SEM imaging provides information on the microstructural properties of the soil, such as particle size distribution and pore space geometry. This high-resolution structural insight is useful to understand the physical context of microbial habitats, which can influence microbial accessibility to substrates and nutrient uptake. To prepare the discs for secondary electron microscopy (SEM), the discs were gold-palladium-coated (Au-Pd) using a sputter coater (Agar 108, Agar Scientific, Essex, UK). SEM was conducted using a JEOL IT 300 scanning electron microscope at the Core Facility Cell Imaging and Ultrastructure Research (CIUS) at the University of Vienna. SEM images were captured using a backscattered electron detector (BED-C) under high vacuum conditions, with an acceleration voltage of 15 kV and an image resolution of 5120 × 3840 pixels at 200× magnification (Fig. 5b), or 25 kV at 30x magnification (Fig. 5a). Additionally, an overview image at 50× magnification was captured from the control disc (which did not receive ^{13}C-labelled substrate), and the sample's elemental composition was analysed using SEM by means of energy dispersive X-ray analysis (SEM-EDX, Fig. 6).

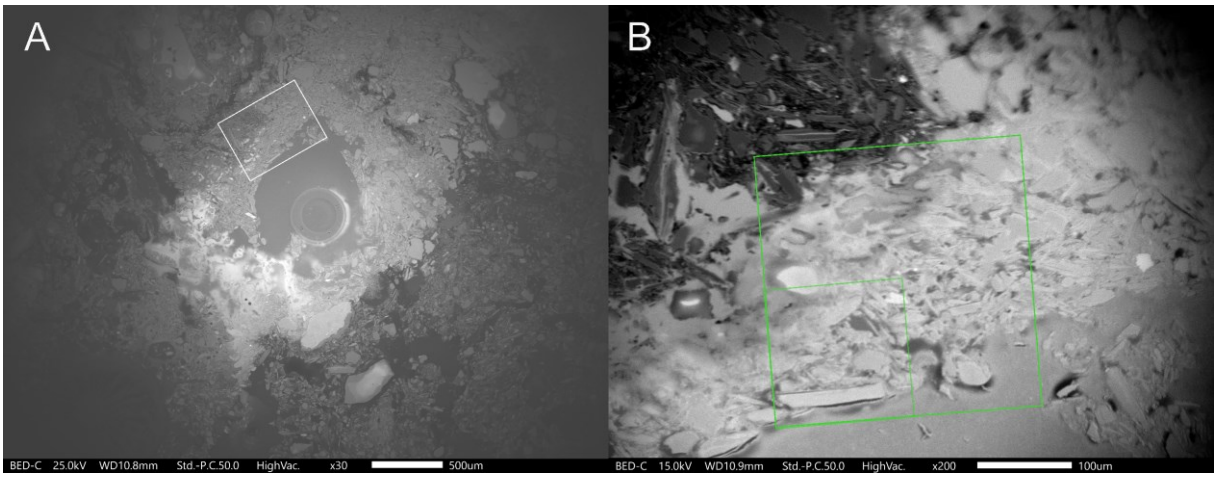


Figure 5. SEM images visualising the undisturbed soil structure around the microdialysis membrane. (**A**) A scanning electron microscopy (SEM) image captured at 30× magnification with a backscattered electron detector (BED-C) showing the area surrounding the microdialysis membrane at the centre of the soil core, where the ^{13}C-labelled substrate was introduced through diffusion ('reverse microdialysis'). This broad view contextualises the spatial relationship of the microdialysis membrane within the surrounding undisturbed soil. The white square references the area shown in (B). (**B**) A SEM image at 200× magnification captures the region where CLSM images were taken (indicated by the green square) and subsequent isotopic analysis was performed with NanoSIMS (smaller green square).

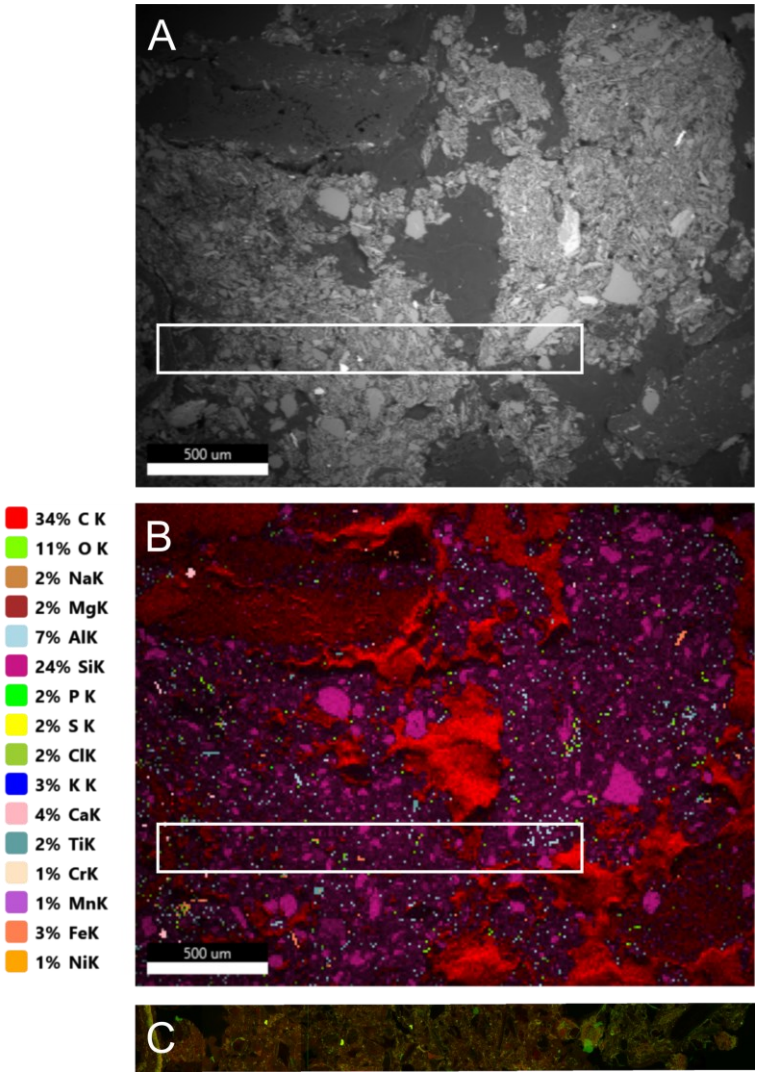


Figure 6. Elemental composition of control soil core analysed with SEM-EDX. This figure presents a comprehensive view of the control soil core, which did not receive any ^{13}C-labelled substrate. (**A**) shows the SEM image (50×) of the soil core, highlighting the undisturbed soil structure. (**B**) displays the energy dispersive X-ray (EDX) analysis. The EDX plot provides a detailed breakdown of the elemental composition, essential for selecting ions as proxy for soil minerals for subsequent NanoSIMS imaging. The elements silicon (Si) and aluminium (Al) were selected over iron (Fe) due to their prevalence, as shown in the analysis. (**C**) is a CLSM image displaying fluorescence-stained microbial cells from the same area of the soil core analysed in the EDX. A white rectangle in both the SEM and EDX plots marks the specific region corresponding to the CLSM image. The CLSM image is presented in supplementary Figure S8.

This analysis was instrumental in determining which ions to select for NanoSIMS imaging to represent the mineral structure; based on their prevalence, we opted for silicon (Si) and aluminium (Al) over iron (Fe). The alignment of the SEM with the CLSM images was facilitated by the LMD overview image (Fig. 2), which was essential for precisely locating the areas where fluorescently stained microbial cells were observed (Fig. 4).

2.8 Nanoscale secondary ion mass spectrometry

Elemental and isotope analyses were carried out using a NanoSIMS 50L instrument (Cameca, Gennevilliers, France) at the University of Vienna. The detailed elemental and isotopic maps generated by NanoSIMS provides us with information about the spatial distribution and uptake of ^{13}C-labelled substrate within microbial cells. The measurements were conducted with a 16 keV Cs^+ primary ion beam, allowing for the simultaneous detection of seven secondary ion species: $^{12}C^-$, $^{12}C^{13}C^-$, $^{12}C^{14}N^-$, $^{28}Si^-$, $^{31}P^-$, $^{32}S^-$, and $^{27}Al^{16}O^-$ as well as secondary electrons. Prior to image acquisition, additional pre-sputtering with a high-intensity primary beam was performed on the selected spot to prepare the sample surface for optimal imaging. One CLSM image, taken just below the microdialysis probe near the ^{13}C-labelled substrate input, was selected as the most promising area for NanoSIMS analysis (Fig. 2, 4). The resulting NanoSIMS image covered an area of 60 × 60 µm at an image resolution of 512 × 512 pixel (Fig. 7).

2.9 NanoSIMS image processing

NanoSIMS image data were processed using the OpenMIMS plugin (Center for Nano Imaging, https://nano.bwh.harvard.edu/MIMSsoftware) for the image analysis software Fiji (Schindelin et al., 2012). The carbon isotope composition image displaying the $^{13}C/(^{12}C+^{13}C)$ isotope fraction, designated at% ^{13}C, was inferred from the C_2^- secondary ion signal intensity distribution image via per-pixel calculation of $^{13}C^{12}C^-/(2*^{12}C^{12}C^-+^{13}C^{12}C^-)$ intensity ratios (Fig. 9a). Additionally, the N/C ratio image, displaying the $^{14}N/(^{12}C+^{13}C)$ fraction, was inferred from the N^- and C_2^- secondary ion signal intensity distribution image via per-pixel calculation of $^{12}C^{14}N^-/(2*^{12}C^{12}C^-+^{13}C^{12}C^-)$ intensity ratios (Fig. 9b). The N/C ratio image, which serves as a proxy for biomass, offers additional evidence for identifying microbial cells, complementing the cell identification provided by the CLSM image (Fig. 9b). The Si^- and $^{27}Al^{16}O^-$ secondar ion maps were crucial to visualize the soil structure, as they correspond to mineral particles (Mueller et al., 2013). The Si^- map, along with SEM image, provided important reference points for overlaying the CLSM and NanoSIMS images and aligning these datasets (Fig. 8).

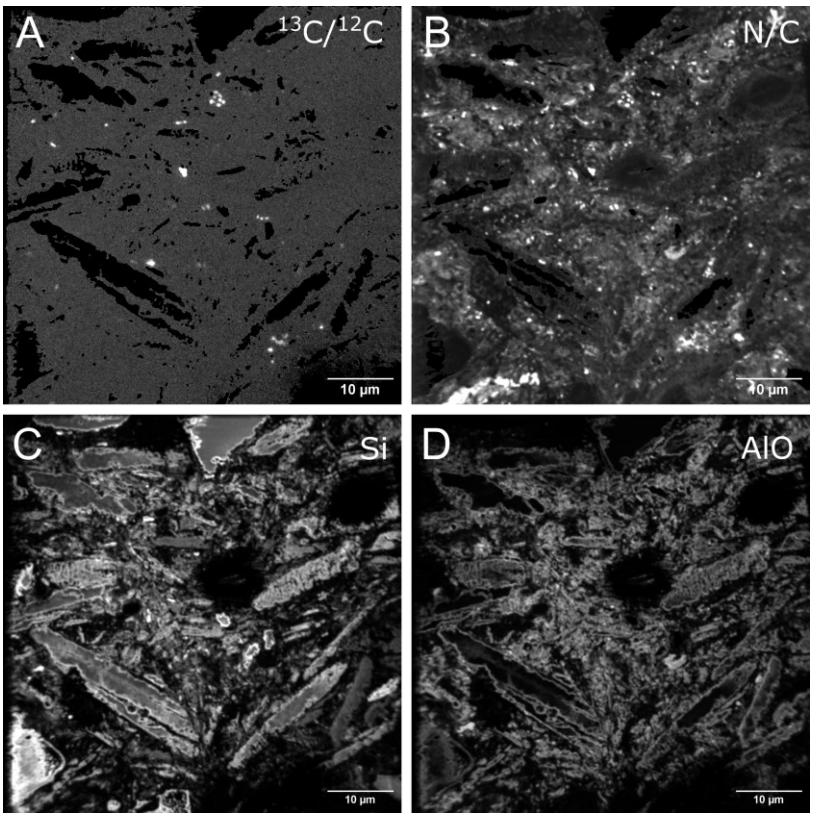


Figure 7. Comprehensive NanoSIMS analysis from soil near the microdialysis membrane. The nanoscale secondary ion mass spectrometry (NanoSIMS) images provide detailed elemental and isotopic insights into the soil sample, following 18 days after the introduction of ^{13}C-labelled substrate. The panels display (**A**) the at% ^{13}C calculated as $^{13}C^{12}C^-/(2*^{12}C^{12}C^-+^{13}C^{12}C^-)$, (**B**) the N/C ratio calculated as $^{12}C^{14}N^-/(2*^{12}C^{12}C^-+^{13}C^{12}C^-)$, (**C**) the secondary ion map of silicon ($^{28}Si^-$), and (**D**) the secondary ion map of aluminium oxide ($^{27}Al^{16}O^-$). The C/N ratio was used to help identify microbial cells, while Si and Al-oxide served as proxy for the soil's mineral structure, providing context for the microbial distribution within the undisturbed soil environment. The at% ^{13}C highlight the distribution of substrate derived ^{13}C.

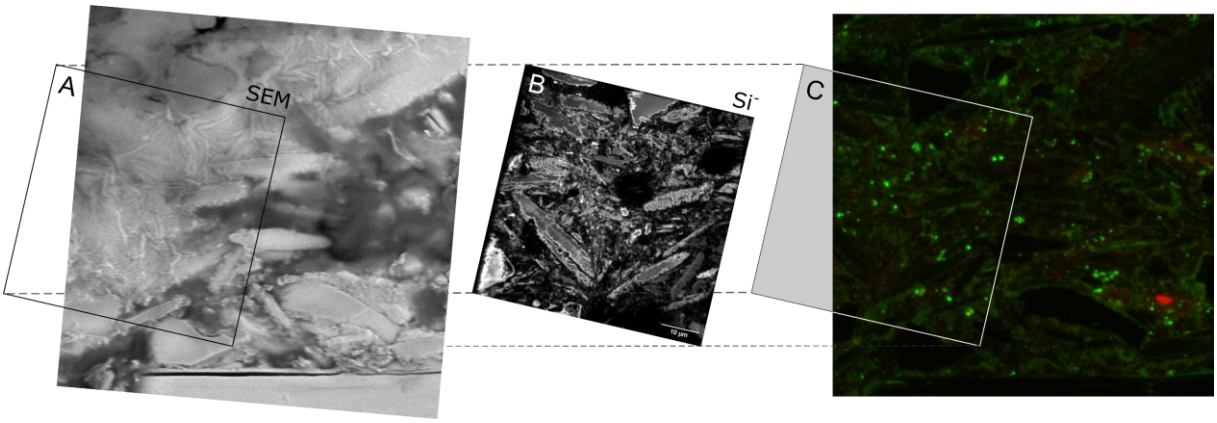


Figure 8. Integration of NanoSIMS and CLSM images using SEM and Si^- secondary ion map signals. This figure demonstrates the alignment process necessary to integrate CLSM and NanoSIMS data. The alignment was achieved through the use of (**A**) SEM images and (**B**) the Si^- secondary ion map obtained from NanoSIMS, which served as proxies for the soil's mineral structure. This provides the structural context needed for precise overlay the images and correlate them to (**C**) the CLMS image of fluorescence-stained microbial cells. This critical alignment step ensures precise localization of microbial cells in relation to the substrate-derived ^{13}C (NanoSIMS), enabling detailed spatial analysis of substrate assimilation by microbial communities.

2.10 Integration of CLSM and NanoSIMS data

To map the ^{13}C signal to microbial cells, the NanoSIMS image was superimposed onto the corresponding CLSM image. The alignment of these images was challenging and was achieved using the SEM image and the Si^- secondary ion map, which provided structural context for accurate overlay (Fig. 8). This alignment was done in Inkscape, which facilitated the precise positioning of layers. This integrated approach allowed for the spatial correlation of fluorescence-labelled spots in the CLSM image with regions high in $^{12}C^{14}N$ (e.g.: cellular biomass) and enriched in ^{13}C in the NanoSIMS image (Fig. 9).

Seventy-eight regions of interest (ROI) were defined across the NanoSIMS images and were annotated as potential microbial cells based on the CLSM image and the at% ^{13}C and N/C ratio images (Fig. 9). Average secondary ion signal intensities ($^{12}C^{12}C^-$, $^{13}C^{12}C^-$) were extracted from each ROI. ROI specific C isotope compositions were calculated from $^{12}C^{12}C^-$ and $^{12}C^{13}C^-$ secondary ion signals detected for each ROI (Fig. 10). Additionally, to determine the natural abundance levels of ^{13}C, C isotope compositions from five regions were selected, yielding 1.10 ± 0.01 at% ^{13}C (mean ± standard deviation). ROI were considered significantly enriched if their at% ^{13}C exceeded the natural abundance ^{13}C by more than two times its standard deviation, a threshold which was established as 1.12 at% ^{13}C. Based on this threshold, the 78 ROI were categorized into two groups according to their ^{13}C enrichment, 49 ^{13}C-enriched (> 1.12 at% ^{13}C) and 29 unlabelled ROI (Fig. 11).

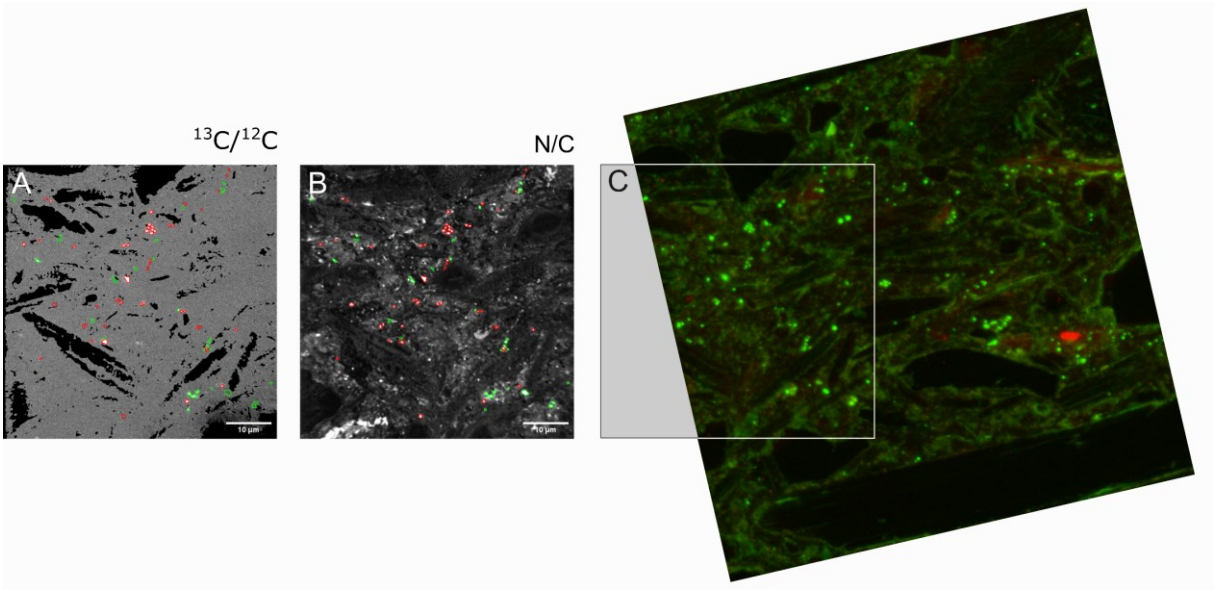


Figure 9: Spatial correlation of NanoSIMS and CLSM images showing ^{13}C-labelled substrate assimilation by microbial cells. This figure illustrates the spatial correlation between the location of microbial cell and their uptake of ^{13}C-labelled substrate within the soil core. The NanoSIMS images display (**A**) the $^{13}C/^{12}C$ ratio, highlighting areas of ^{13}C enrichment, and (**B**) the N/C ratio, indicative of microbial biomass. The NanoSIMS images were superimposed onto the CLSM image (**C**) that visualizes fluorescence-labelled microbial cells. This correlative images facilitate the direct comparison between microbial locations to regions of high ^{13}C incorporation. Regions of interests (ROI), i.e. microbial cells, were identified based on fluorescence signals (**C**) and N/C ratios (**B**). These ROI were used to extract ^{13}C isotope composition (Fig. 9, 10). ROI are encircled in red to donate ^{13}C enrichment and in green to indicate cells without enrichment, highlights the selective assimilation of ^{13}C-labelled substrate by only some microbial cells.

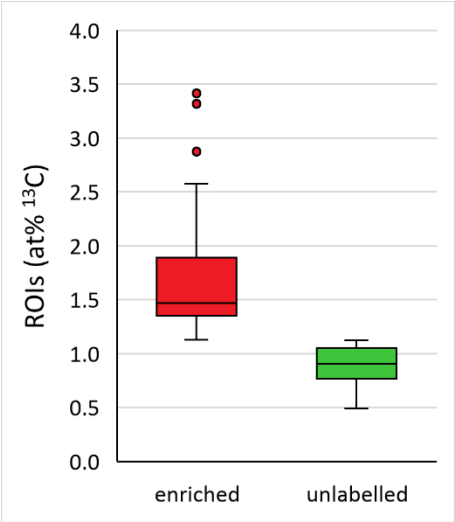


Figure 10: Boxplots depicting the ^{13}C isotopic content (at% ^{13}C) of microbial cells. A total of 78 regions of interest (ROI) were selected from the NanoSIMS image (Fig. 8) and grouped based on their at% ^{13}C into ROI that were ^{13}C-enriched (n=49) and unlabelled (n=29). Natural abundance (background) was 1.10 ± 0.01 (mean ± standard deviation). Enriched cells had on average 1.68 ± 0.54 at% ^{13}C, while unlabelled cells had 0.89 ± 0.18 at% ^{13}C.

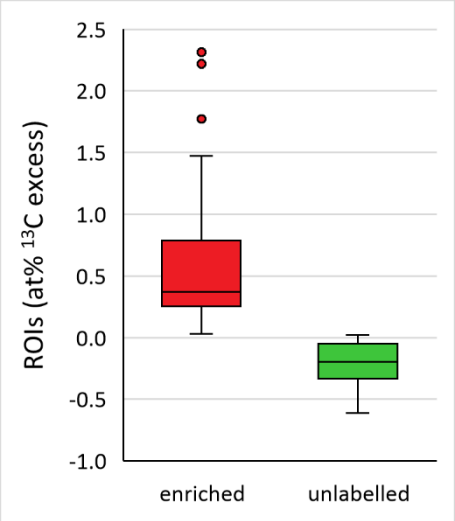


Figure 11: Boxplots depicting the ^{13}C enrichment (at% ^{13}C excess) of microbial cells. A total of 78 regions of interest (ROI) were selected from the NanoSIMS image (Fig. 8) and grouped based on their at% ^{13}C into ROI that were ^{13}C-enriched (n=49) and unlabelled (n=29). The average ^{13}C-enrichment of enriched cells was 0.58 ± 0.54 at% ^{13}C excess.

3. Results & Discussion

In this study, we aimed to set up and test a correlative imaging workflow to link spatial distribution of microbial cells in their native soil environment to their uptake of isotopically labelled substrates. This test is linked to an experiment, in which we introduced ^{13}C-labelled substrate by simulated root exudation into undisturbed soil cores (Wiesenbauer et al., 2024b, submitted). While our previous work focused on the temporal dynamics of microbial activity (substrate respiration, metabolite production) over 18 days after these inputs, the approach developed in this study highlights the spatial distribution of microbes and the released substrate at the endpoint of the experiment. By integrating confocal laser scanning microscopy (CLSM) with nanoscale secondary ion mass spectrometry (NanoSIMS) and scanning electron microscopy (SEM), we were able to visualize and quantify the spatial distribution of substrate-derived ^{13}C and its uptake by microbial cells.

3.1 Visualization of fluorescence-stained microbial cells via CLSM

Using CLSM, we acquired image stacks of varying depths and projected them into a single layer to clearly delineate highly fluorescent spots representing microbial cells (Fig. 4). This approach facilitates the clear differentiation of cells, stained bright green for nucleic acids, from the surrounding soil matrix, where autofluorescence appeared red. We observed a heterogeneous distribution of microbial cells within the structurally preserved soil, characterized by a mix of small colonies and single cells (Fig. 4, S1-S7). Despite the introduction of labile substrate at the center of the soil via the microdialysis membrane, our images did not show an apparent increase in microbial biomass near this substrate input site (Fig. 3, 4, S1-S7). This observation suggests that the additional substrate availability did not uniformly enhance microbial growth as observed in this snapshot 18 days after substrate addition. Correspondingly, phospholipid fatty acids (PLFA) analysis from the same experiment did not indicate an increase in microbial biomass either (Wiesenbauer et al., 2024b, submitted). It is, however, possible that changes in microbial biomass could have occurred outside of this single-time-point observation or were spatially varied, which would make detection more challenging. While the number of CLSM images obtained was sufficient to provide an initial overview, they might not have captured the entire range of spatial variability in microbial response to the introduced substrate. A more extensive sampling strategy and more comprehensive imaging are likely necessary to fully capture the spatially heterogenous microbial processes, particularly in the heterogenous soil environment posed by the undisturbed soil structure.

3.2 Integration of CLSM and NanoSIMS data

Following the identification of microbial cells via CLSM, NanoSIMS imaging was conducted to elucidate the spatial distribution and uptake of ^{13}C-labelled substrate within these cells. To achieve this, it was essential to integrate the fluorescence and NanoSIMS data, to pinpoint the locations where microbial cells coincide with substrate-derived ^{13}C. To demonstrate the practical application of our workflow, we specifically chose one area near the microdialysis membrane, where the ^{13}C-labelled substrate was introduced (Fig. 2, Fig. 4).

However, the alignment of images from different microscopy techniques presented significant challenges, as each imaging technique captured a slightly different projection of the soil surface. In order to ensure precise alignment of NanoSIMS images with the corresponding CLSM image, we used the Si^- secondary ion map obtained by NanoSIMS and SEM images to identify common landmarks, enabling us to accurately superimpose the images (Fig. 8). The Si^- secondary ion map, in conjunction with SEM, provided a clearer visualization of the soil structure, which was obscure in the at% ^{13}C NanoSIMS and CLSM images. We considered both Si^- and AlO^- secondary ion maps for alignment due to their ability to reveal mineral composition (Mueller et al., 2013). However, the Si^- map offered a more accurate depiction of the soil's mineral structure (Fig. 7). This was corroborated by the SEM-EDX analysis, which confirmed the predominance of Si-rich minerals, constituting 24% of the soil, compared to only 7% for Al-rich minerals (Fig. 6b). This meticulous alignment process ensured the accurate overlay of NanoSIMS and CLSM images, allowing for a more detailed interpretation of microbial distribution and activity within the native soil structure.

To facilitate the precise spatial analysis, we selected seventy-eight regions of interest (ROI), i.e., microbial cells, based on the fluorescence signals and the corresponding N/C ratio image (Fig. 9). The fluorescence signals served as initial markers for locating microbial cells in the soil cores (Fig. 4, 8c). Subsequently, by matching these signals with the N/C ratio image, which is typically associated with cellular biomass, we further validated the locations of microbial cells in the superimposed image (Fig. 9b). It is worth noting that P^- (e.g.: phospholipids, nucleic acid, ATP) and S^- (e.g.: biomolecules) secondary ion maps could have been used alongside $^{12}C^{14}N^-$ to verify the location of microbial cells. However, this approach was less effective in our study, likely due to the presence of P in minerals and absence of pronounced S hotspots. The SEM-EDX analysis confirmed that both P and S constituted only 2% of the soil composition each (Fig. 6b).

3.3 Uptake of ^{13}C-labelled artificial root exudate by microbial cells

Having identified seventy-eight ROI as microbial cells, we then analysed whether their location corresponded with the distribution of ^{13}C to assess their involvement in substrate assimilation. NanoSIMS imaging identified areas with elevated at% ^{13}C at microbial cell locations (i.e., ROI), indicating potential assimilation of the substrate-derived ^{13}C (Fig. 9a, 11a). However, given the 18-day period since substrate addition, the possibility of crossfeeding among microbial communities should be considered.

Upon superimposing the at% ^{13}C onto the fluorescence image, we observed a significant heterogeneity in substrate assimilation among the microbial cells (Fig. 9). We categorized the 78 ROI into 49 enriched cells and 29 cells showing no substrate-derived ^{13}C incorporation. The enriched ROI exhibited an average of 1.68 ± 0.54 at% ^{13}C (mean ± standard deviation), in contrast to 0.89 ± 0.18 at% ^{13}C in unlabelled ROI (Fig. 10), with the labelled ROI averaging a ^{13}C-enrichment of 0.58 ± 0.54 at% ^{13}C excess (Fig. 11). Our visualization confirmed the effective diffusion of the substrate into the soil matrix. This observation is supported by our earlier work, which showed a significant fraction of substrate-derived ^{13}C in microbial respiration during and shortly after the artificial root exudation, suggesting the microbial uptake and metabolism of substrate (Wiesenbauer et al., 2024b, submitted).

The observed variations in ^{13}C enrichment across different microbial cells underscore the complex ecological interactions within the soil, suggesting differential assimilation of ^{13}C-labelled substrate and competitive dynamics among soil microbes. This was supported by the analysis of lipid fatty acids conducted at the experiment's endpoint, which revealed varied utilization strategies among microbial groups (Wiesenbauer et al., 2024b, submitted). This was indicated by the uneven enrichment in substrate-derived ^{13}C across different lipid fatty acid biomarker groups, reflecting diverse metabolic responses to the introduced substrate. Interestingly, while the average PLFA enrichment was only 1.07 ± 0.01 at% ^{13}C (mean ± standard deviation) (Wiesenbauer et al., 2024b, submitted), our NanoSIMS measurements identified single cells with enrichment levels as high as 3.4 at% ^{13}C (Fig. 10). Among the 49 labelled ROI, eleven ROI exhibited enrichment greater than 2 at% ^{13}C, and five ROI exceeded 2.5 at% ^{13}C (Fig. 10). These findings underscore the fine-scale heterogeneity in microbial substrate utilization that our imaging approach can capture, enabling the identification of activity hotspots by detecting highly labelled cells. Unlike PLFA isotope analysis, which averages the isotopic signatures across many cells, our method provides a detailed view of the spatial and metabolic diversity within microbial communities.

Further, this variability in substrate assimilation was likely in parts influenced by the structural heterogeneity of the soil, as evidenced by LMD and SEM images (Fig. 2, 5), which displayed differences

in soil particle size and composition, potentially affecting the accessibility of the diffusing substrate to microbes. Our observations suggest the presence of a complex ecological network, where nutrient availability and physical accessibility can dynamically impact microbial processes. These insights provide new perspectives on the spatial dynamics of microbial processes and differential metabolic capabilities (e.g.: substrate assimilation) within the microbial communities.

3.4 Limitations and challenges

While providing new insights into microbial activity, the integrative approach presented here involves inherent limitations and challenges that may impacts its broader application. Our method requires extensive sample preparation, from simulating root exudation to fixing, dehydrating, and impregnating the soil with epoxy resin, all while aiming to preserve the native soil structure. This process risks introducing artifacts that might affect the data interpretation.

Moreover, quantifying the amount of isotopically labelled substrate released into the soil matrix per analysed soil volume poses inherent challenges due to the nature of reverse microdialysis. The diffusive gradients by which substrates are released depends significantly on microbial uptake as well as soil properties (water content, soil composition). Added to this, the potential for cross-feeding among microbial communities can complicate the interpretation of substrate uptake, making it challenging to attribute isotopic signatures to specific microbial groups or interactions.

Additionally, the high costs associated with operating instruments like NanoSIMS, SEM, and CLSM limit the number of samples that can be analysed, necessitating cautious interpretation due to the small number of replicates. To save costs and resources, one might omit SEM imaging if the structural information gained from SEM is not of primary interest. Although SEM was essential in our approach for identifying target spots for NanoSIMS analysis, it may be possible to forgo SEM if the sample permits easy orientation without a detailed electron images, perhaps using just an overview image from light microscope or LMD. Alternatively, one could capture CLSM images of the entire sample and later attempt to locate the specific spot analysed by NanoSIMS using ion maps or secondary electron images from NanoSIMS.

Additionally, NanoSIMS is restricted to measuring only a select few ion species at a time, which limits the chemical information obtained. However, this might potentially be offset by the energy-dispersive X-ray (EDX) of SEM. Although it offers a much coarser resolution than NanoSIMS, EDX covers a wider range of elements, potentially enhancing our understanding of the microbial environment.

4. Conclusion

Our study demonstrates the potential of integrating high-resolution stable isotope imaging via NanoSIMS with fluorescence microscopy (CLSM) and scanning electron microscopy (SEM) for a better understanding of microbial spatial ecology in soil. This multi-imaging approach allows for a unique visualization of the uptake of ^{13}C-labelled substrates by microbes in undisturbed soil cores. By precisely locating microbial cells and correlating their position with isotopic data, our integrative approach provides a comprehensive analysis of substrate distribution and assimilation. By simulating root exudation through minimally invasive reverse microdialysis and observing its assimilation by nearby microbial populations, we effectively bridge the gap between controlled laboratory experiments and the dynamic conditions of natural soil environments. Our spatial analysis complemented previous temporal studies by providing a detailed view of where substrate uptake occurs within the soil. While Wiesenbauer et al. (2024b, submitted) focused on how microbial respiration and metabolite production changed over time in response to substrate addition, our current study added a spatial dimension to this understanding. Our findings suggest that the physical accessibility, shaped by the heterogeneous soil structure, significantly influences microbial uptake of artificial root exudates. The ability to simultaneously visualize substrate assimilation and microbial positioning at the microscale offers a powerful tool for studying the *in-situ* dynamics of microbial activity and nutrient cycling in soils.

Looking ahead, this correlative imaging approach holds potential for applications beyond studying root exudate assimilation. It could be adapted to explore microbial interactions with other types of organic amendments or environmental contaminants. Furthermore, extending this method to include isotopic labelling (e.g. $^{13}CO_2$) of plants could provide insights into the dynamics of carbon and nutrient cycling and the interactions of microbial communities in the plant's rhizosphere. The integrated imaging approach would also be well-suited for combination with water vapor SIP to visualize growing microbial cells in soils through deuterium incorporation (Canarini et al., 2024). Furthermore, integrating this imaging workflow with molecular techniques such as fluorescence *in situ* hybridisation (FISH) could offer a more comprehensive understanding of microbial community structure and function *in situ*.

Our integrative approach allows us to observe a snapshot of microbial dynamics and nutrient cycling under near-natural conditions. This method's ability to minimize disturbance while providing detailed spatial and chemical data offers a powerful framework for future studies aimed at unravelling complex soil-microbe interactions.

Acknowledgements

SEM and other microscopy work was carried out at Core Facility Cell Imaging and Ultrastructure Research, and NanoSIMS imaging at the Large-Instrument Facility for Advanced Isotope Research, both at the University of Vienna. We thank Ilka Wünsche for support with sample polishing, Siegfried Reipert and Daniela Gruber for help in SEM preparation and microscopy.

Supplement figures

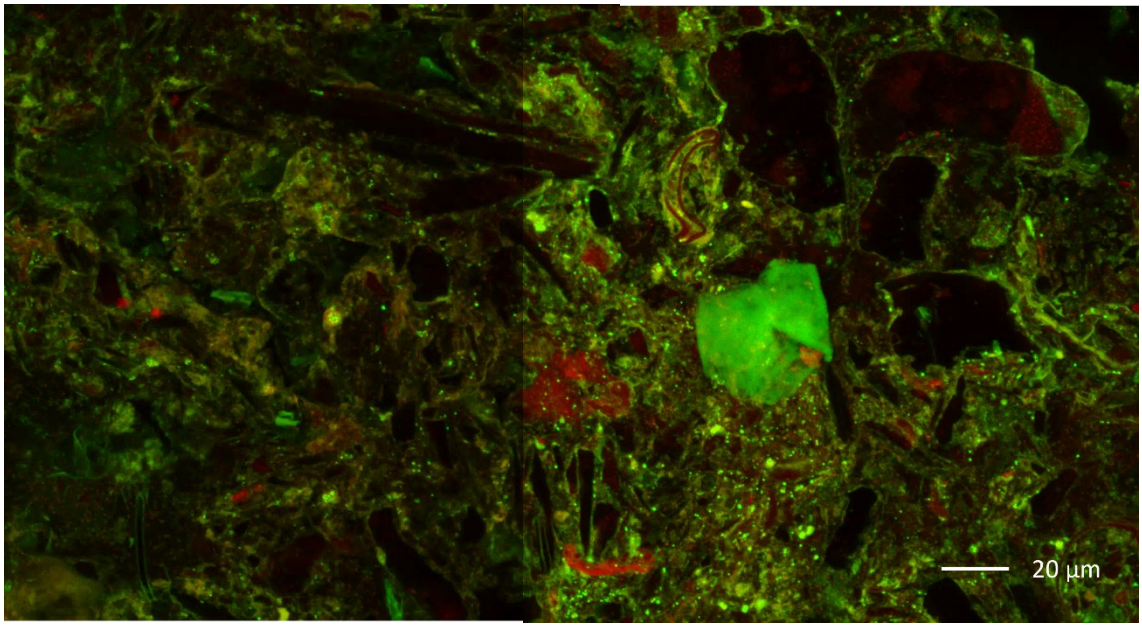


Figure S1. Composite CLSM image of dsGreen stained microbial cells in the soil core that received ^{13}C-labelled substrate. This composite image combines two CLSM images, each 184.5 × 184.5 µm, showcasing microbial cells stained with dsGreen. Red and green fluorescence channels were captured and overlaid to distinguish microbes (green) from organic matter and general background fluorescence (red).

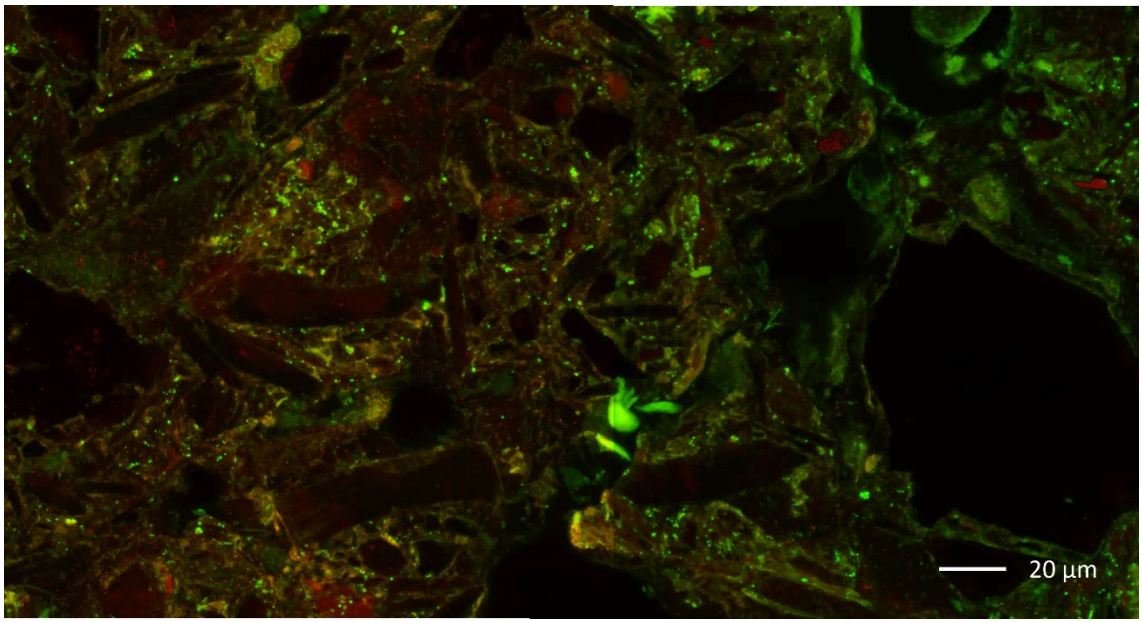


Figure S2. Composite CLSM image of dsGreen stained microbial cells in the soil core that received ^{13}C-labelled substrate. This composite image combines two CLSM images, each 184.5 × 184.5 µm, showcasing microbial cells stained with dsGreen. Red and green fluorescence channels were captured and overlaid to distinguish microbes (green) from organic matter and general background fluorescence (red).

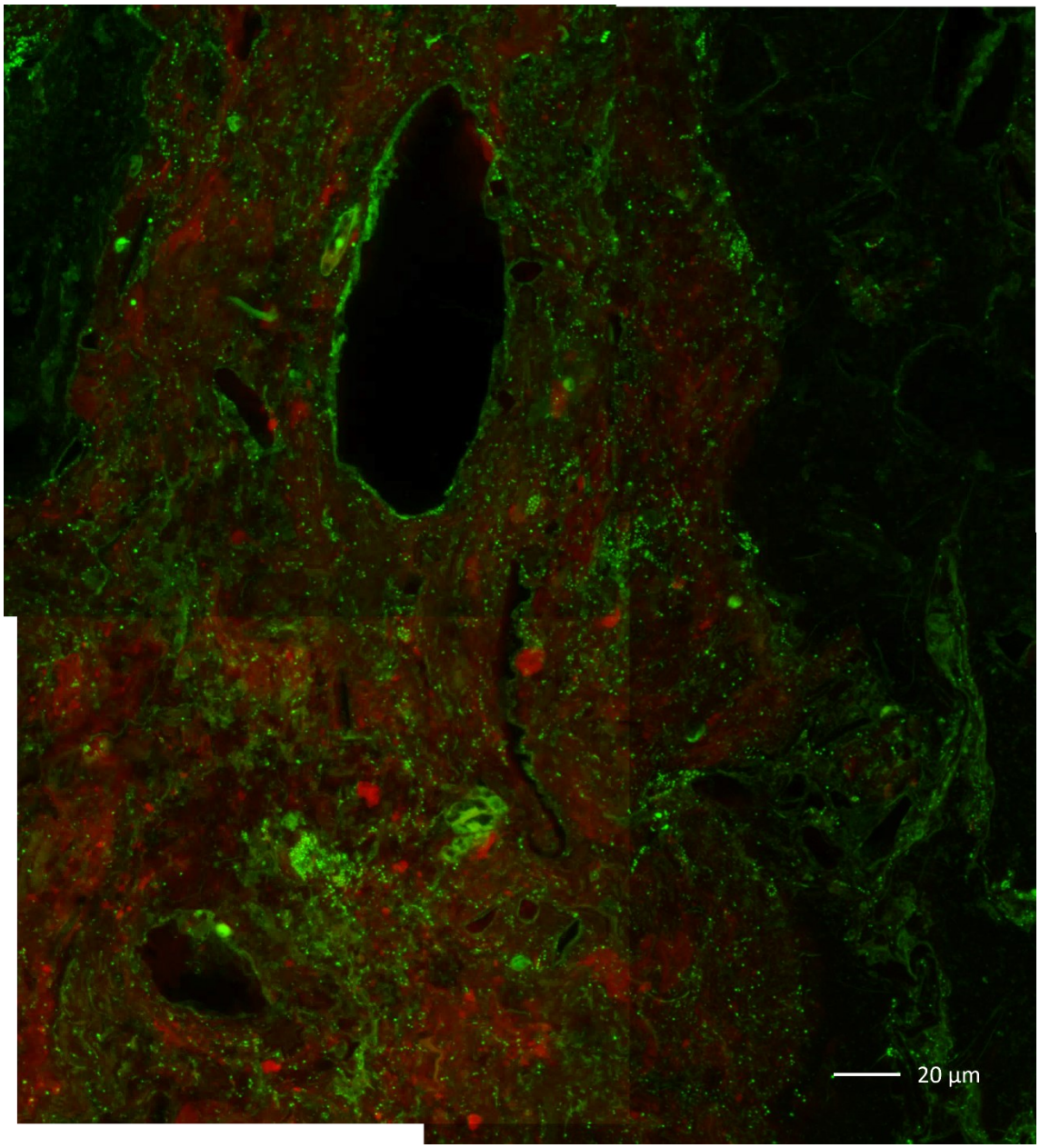


Figure S3. Composite CLSM image of dsGreen stained microbial cells in the soil core that received ^{13}C-labelled substrate. This composite image combines four CLSM images, each 184.5 × 184.5 µm, showcasing microbial cells stained with dsGreen. Red and green fluorescence channels were captured and overlaid to distinguish microbes (green) from organic matter and general background fluorescence (red).

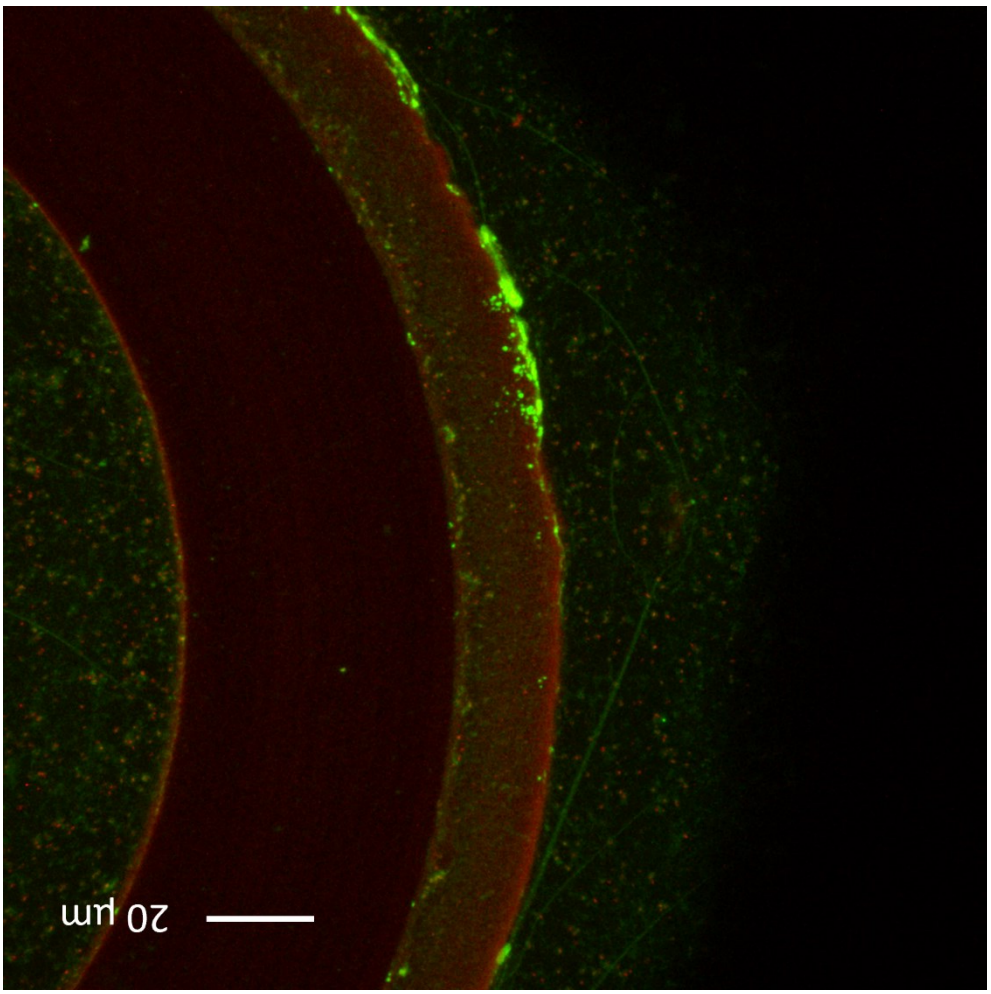


Figure S4. **CLSM image of dsGreen stained microbial cells on microdialysis membrane in the soil core that received ^{13}C-labelled substrate.** This 184.5 × 184.5 µm CLSM image showcases microbial cells stained with dsGreen on the microdialysis membrane. Red and green fluorescence channels were captured and overlaid to distinguish microbes (green) from microdialysis membrane and general background fluorescence (red).

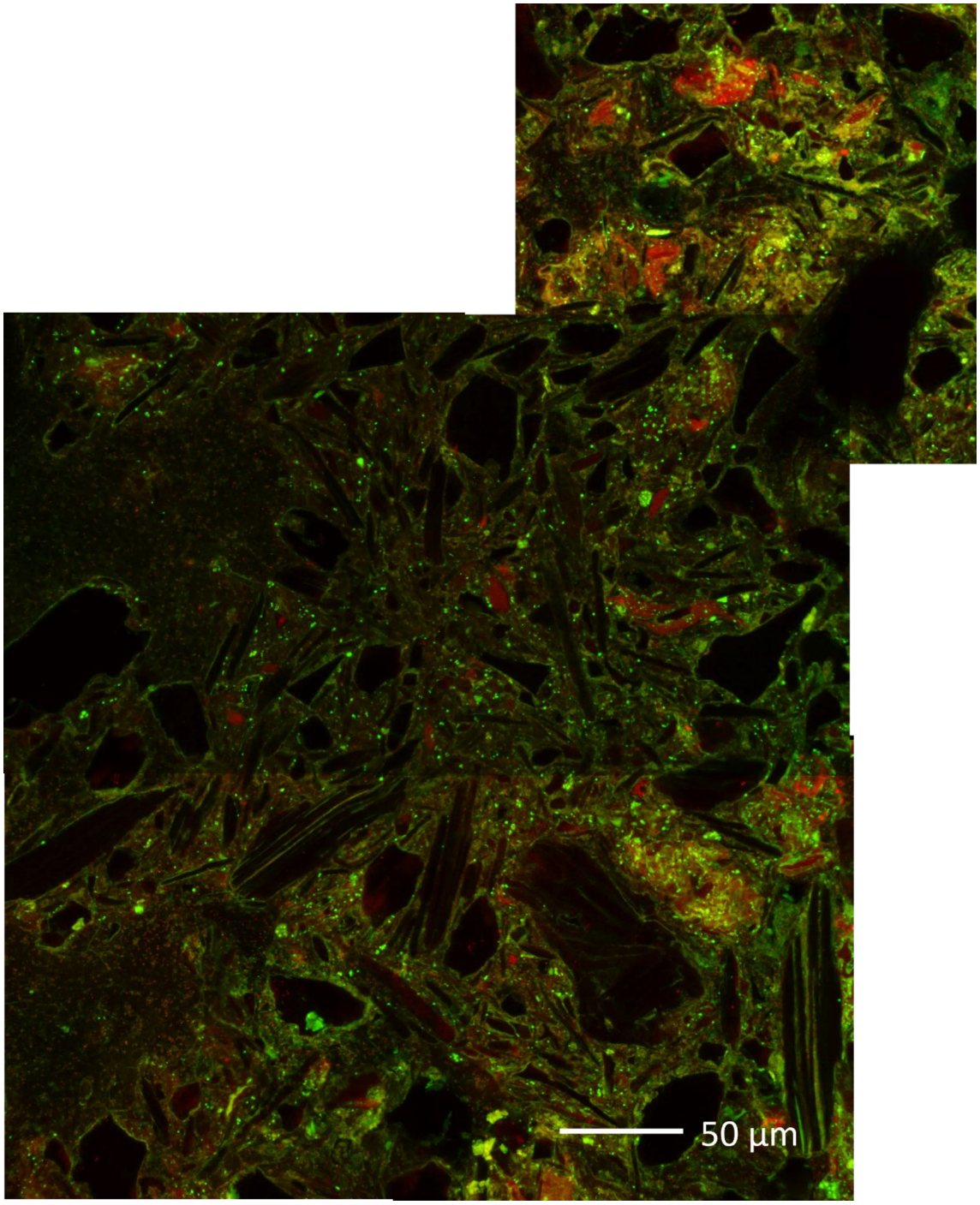


Figure S5. Composite CLSM image of dsGreen stained microbial cells in the soil core that received ^{13}C-labelled substrate. This composite image combines five CLSM images, each 184.5 × 184.5 µm, showcasing microbial cells stained with dsGreen. Red and green fluorescence channels were captured and overlaid to distinguish microbes (green) from organic matter and general background fluorescence (red).

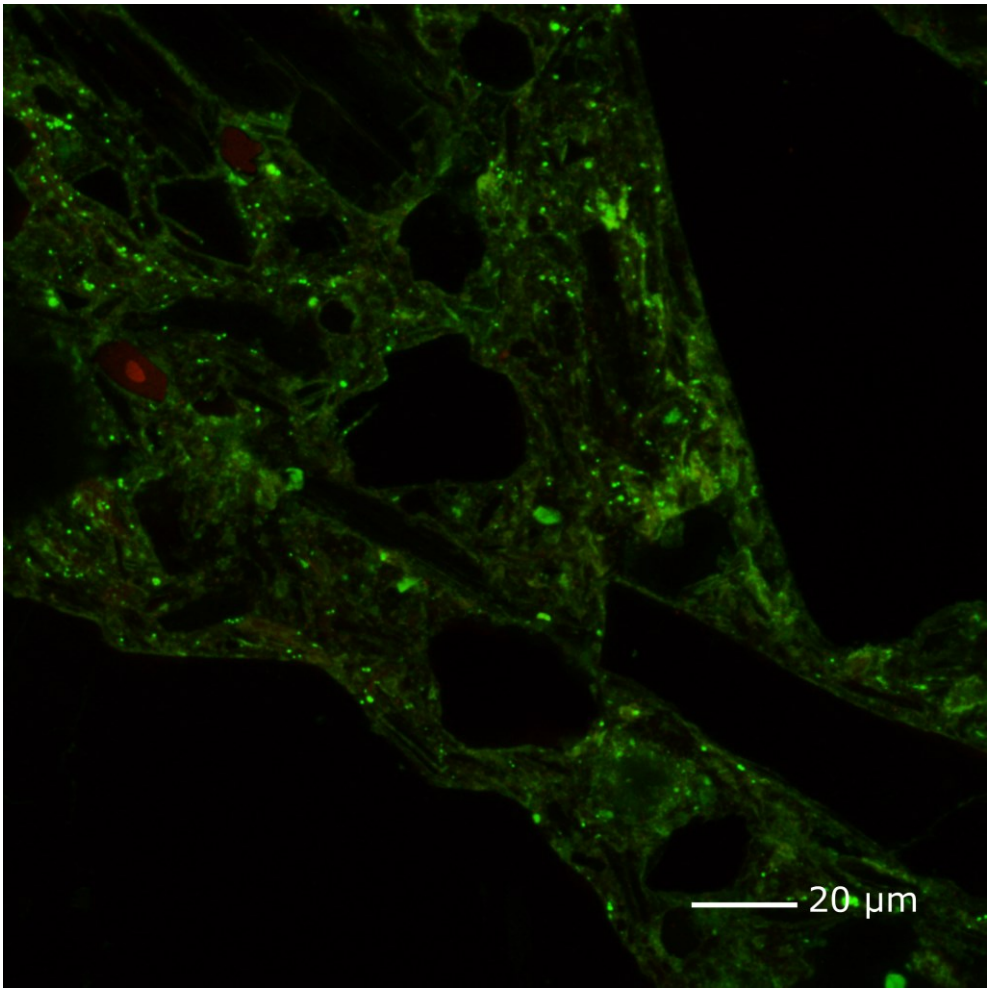


Figure S6. CLSM image of dsGreen stained microbial cells in the soil core that received ^{13}C-labelled substrate. This 184.5 × 184.5 µm CLSM image showcases microbial cells stained with dsGreen. Red and green fluorescence channels were captured and overlaid to distinguish microbes (green) from organic matter and general background fluorescence (red).

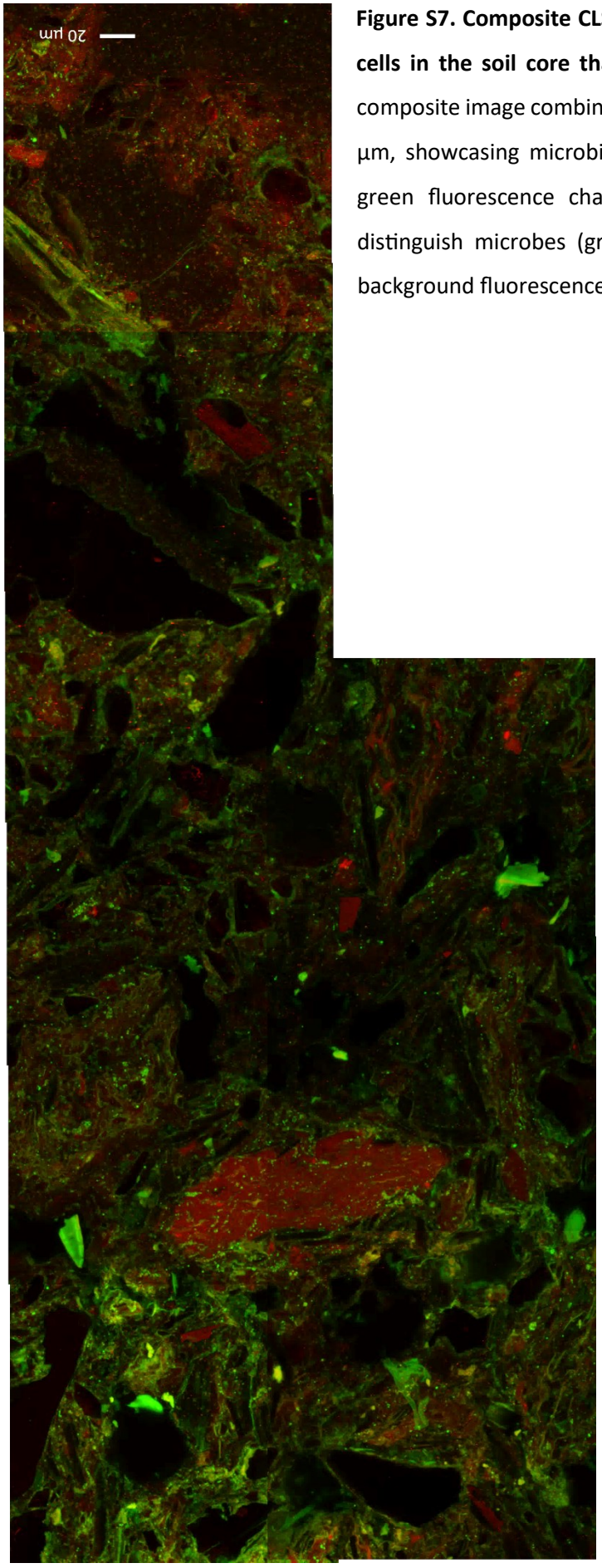


Figure S7. Composite CLSM image of dsGreen stained microbial cells in the soil core that received ^{13}C-labelled substrate. This composite image combines nine CLSM images, each 184.5 × 184.5 µm, showcasing microbial cells stained with dsGreen. Red and green fluorescence channels were captured and overlaid to distinguish microbes (green) from organic matter and general background fluorescence (red).

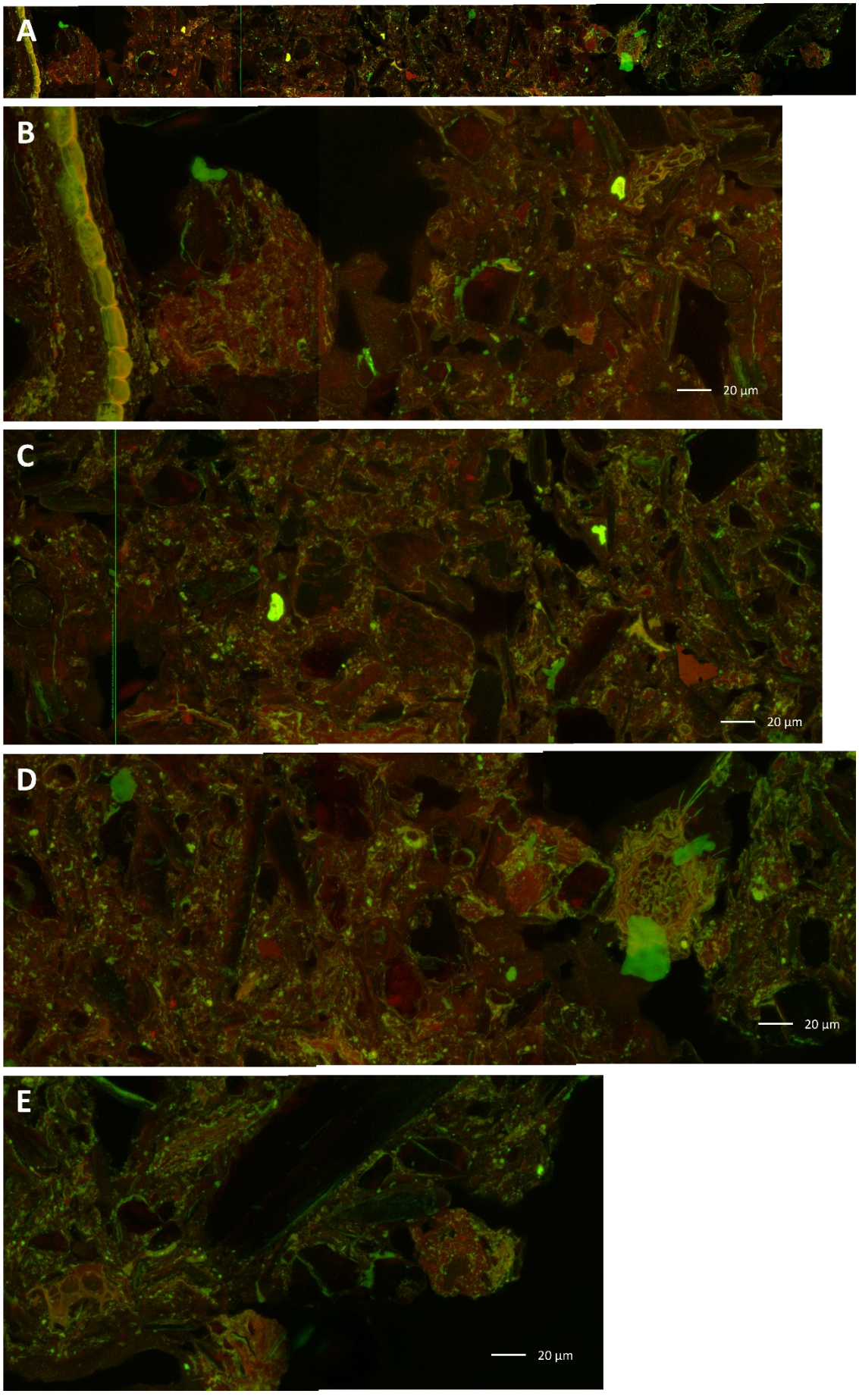

A
B
20 µm
C
20 µm
D
20 µm
E
20 µm

Figure S8. Composite CLSM images of dsGreen stained microbial cells in the control soil core. (**A**) This composite image combines eleven CLSM images, each measuring 184.5 × 184.5 µm, showcasing microbial cells stained with dsGreen. Red and green fluorescence channels were captured and overlaid to distinguish microbes (green) from organic matter and general background fluorescence (red). (**B**) Consists of the first three CLSM images from the left section of the full composite. (**C**) Features the next set of three CLSM images to the right of section B. (**D**) Consist of another set of three CLSM images, following section C. (**E**) Comprises the final two CLSM images at the very right end of the composite image.

References

Bandara, C.D., Schmidt, M., Davoudpour, Y., Stryhanyuk, H., Richnow, H.H., Musat, N., 2021. Microbial Identification, High-Resolution Microscopy and Spectrometry of the Rhizosphere in Its Native Spatial Context. Frontiers in Plant Science 12. doi:10.3389/fpls.2021.668929

Benard, P., Zarebanadkouki, M., Brax, M., Kaltenbach, R., Jerjen, I., Marone, F., Couradeau, E., Felde, V.J.M.N.L., Kaestner, A., Carminati, A., 2019. Microhydrological Niches in Soils: How Mucilage and EPS Alter the Biophysical Properties of the Rhizosphere and Other Biological Hotspots. Vadose Zone Journal 18, 180211. doi:10.2136/vzj2018.12.0211

Blagodatskaya, E., Kuzyakov, Y., 2008. Mechanisms of real and apparent priming effects and their dependence on soil microbial biomass and community structure: Critical review. Biology and Fertility of Soils 45, 115–131. doi:10.1007/s00374-008-0334-y

Canarini, A., Fuchslueger, L., Schnecker, J., Metze, D., Nelson, D.B., Kahmen, A., Watzka, M., Pötsch, E.M., Schaumberger, A., Bahn, M., Richter, A., 2024. Soil fungi remain active and invest in storage compounds during drought independent of future climate conditions. Nature Communications 15, 10410. doi:10.1038/s41467-024-54537-y

Canarini, A., Kaiser, C., Merchant, A., Richter, A., Wanek, W., 2019. Root Exudation of Primary Metabolites: Mechanisms and Their Roles in Plant Responses to Environmental Stimuli. Frontiers in Plant Science 10. doi:10.3389/fpls.2019.00157

Cardinale, M., 2014. Scanning a microhabitat: plant-microbe interactions revealed by confocal laser microscopy. Frontiers in Microbiology 5. doi:10.3389/fmicb.2014.00094

Costa, O.Y.A., Raaijmakers, J.M., Kuramae, E.E., 2018. Microbial Extracellular Polymeric Substances: Ecological Function and Impact on Soil Aggregation. Frontiers in Microbiology 9. doi:10.3389/fmicb.2018.01636

Dijkstra, F.A., Zhu, B., Cheng, W., 2021. Root effects on soil organic carbon: a double-edged sword. New Phytologist 230, 60–65. doi:10.1111/nph.17082

Haichar, F.E.Z., Marol, C., Berge, O., Rangel-Castro, J.I., Prosser, J.I., Balesdent, J., Heulin, T., Achouak, W., 2008. Plant host habitat and root exudates shape soil bacterial community structure. ISME Journal 2, 1221–1230. doi:10.1038/ismej.2008.80

Herrmann, A.M., Ritz, K., Nunan, N., Clode, P.L., Pett-Ridge, J., Kilburn, M.R., Murphy, D.V., O'Donnell, A.G., Stockdale, E.A., 2007. Nano-scale secondary ion mass spectrometry — A new analytical tool in biogeochemistry and soil ecology: A review article. Soil Biology and Biochemistry 39, 1835–1850. doi:10.1016/j.soilbio.2007.03.011

Hinsinger, P., Plassard, C., Tang, C., Jaillard, B., 2003. Origins of root-mediated pH changes in the rhizosphere and their responses to environmental constraints: A review. Plant and Soil 248, 43–59. doi:10.1023/A:1022371130939

Jilling, A., Keiluweit, M., Gutknecht, J.L.M., Grandy, A.S., 2021. Priming mechanisms providing plants and microbes access to mineral-associated organic matter. Soil Biology and Biochemistry 158, 108265. doi:10.1016/j.soilbio.2021.108265

Jones, D.L., Nguyen, C., Finlay, R.D., 2009. Carbon flow in the rhizosphere: carbon trading at the soil–root interface. Plant and Soil 321, 5–33. doi:10.1007/s11104-009-9925-0

Keiluweit, M., Bougoure, J.J., Nico, P.S., Pett-Ridge, J., Weber, P.K., Kleber, M., 2015. Mineral protection of soil carbon counteracted by root exudates. Nature Climate Change 5, 588–595. doi:10.1038/nclimate2580

Khorassani, R., Hettwer, U., Ratzinger, A., Steingrobe, B., Karlovsky, P., Claassen, N., 2011. Citramalic acid and salicylic acid in sugar beet root exudates solubilize soil phosphorus. BMC Plant Biology 11, 121. doi:10.1186/1471-2229-11-121

König, A., Wiesenbauer, J., Gorka, S., Marchand, L., Kitzler, B., Inselsbacher, E., Kaiser, C., 2022. Reverse microdialysis: A window into root exudation hotspots. Soil Biology and Biochemistry 174, 108829. doi:10.1016/j.soilbio.2022.108829

Kuzyakov, Y., Blagodatskaya, E., 2015. Microbial hotspots and hot moments in soil: Concept & review. Soil Biology and Biochemistry 83, 184–199. doi:10.1016/j.soilbio.2015.01.025

Lehmann, A., Zheng, W., Rillig, M.C., 2017. Soil biota contributions to soil aggregation. Nature Ecology & Evolution 1, 1828–1835. doi:10.1038/s41559-017-0344-y

Lippold, E., Schlüter, S., Mueller, C.W., Höschen, C., Harrington, G., Kilian, R., Gocke, M.I., Lehndorff, E., Mikutta, R., Vetterlein, D., 2023. Correlative Imaging of the Rhizosphere–A Multimethod Workflow for Targeted Mapping of Chemical Gradients. Environmental Science & Technology 57, 1538–1549. doi:10.1021/acs.est.2c07340

Moran, J., McGrath, C., 2021. Comparison of Methods for Mapping Rhizosphere Processes in the Context of Their Surrounding Root and Soil Environments. BioTechniques 71, 604–614. doi:10.2144/btn-2021-0021

Mueller, C.W., Weber, P.K., Kilburn, M.R., Hoeschen, C., Kleber, M., Pett-Ridge, J., 2013. Advances in the analysis of biogeochemical interfaces. Nanosims to investigate soil microenvironments, Advances in Agronomy. Elsevier Inc. doi:10.1016/B978-0-12-407685-3.00001-3

Musat, N., Musat, F., Weber, P.K., Pett-Ridge, J., 2016. Tracking microbial interactions with NanoSIMS. Current Opinion in Biotechnology 41, 114–121. doi:10.1016/j.copbio.2016.06.007

Oburger, E., Schmidt, H., 2016. New Methods To Unravel Rhizosphere Processes. Trends in Plant Science 21, 243–255. doi:10.1016/j.tplants.2015.12.005

Philippot, L., Chenu, C., Kappler, A., Rillig, M.C., Fierer, N., 2023. The interplay between microbial communities and soil properties. Nature Reviews Microbiology 1–14. doi:10.1038/s41579-023-00980-5

Reinthaler, D., Harris, E., Pötsch, E.M., Herndl, M., Richter, A., Wachter, H., Bahn, M., 2021. Responses of grassland soil CO2 production and fluxes to drought are shifted in a warmer climate under elevated CO2. Soil Biology and Biochemistry 163, 108436. doi:10.1016/j.soilbio.2021.108436

Richter-Heitmann, T., Eickhorst, T., Knauth, S., Friedrich, M.W., Schmidt, H., 2016. Evaluation of Strategies to Separate Root-Associated Microbial Communities: A Crucial Choice in Rhizobiome Research. Frontiers in Microbiology 7. doi:10.3389/fmicb.2016.00773

Schindelin, J., Arganda-Carreras, I., Frise, E., Kaynig, V., Longair, M., Pietzsch, T., Preibisch, S., Rueden, C., Saalfeld, S., Schmid, B., Tinevez, J.-Y., White, D.J., Hartenstein, V., Eliceiri, K., Tomancak, P., Cardona, A., 2012. Fiji: an open-source platform for biological-image analysis. Nature Methods 9, 676–682. doi:10.1038/nmeth.2019

Schlüter, S., Eickhorst, T., Mueller, C.W., 2019. Correlative Imaging Reveals Holistic View of Soil Microenvironments. Environmental Science & Technology 53, 829–837. doi:10.1021/acs.est.8b05245

Schmidt, H., Nunan, N., Höck, A., Eickhorst, T., Kaiser, C., Woebken, D., Raynaud, X., 2018. Recognizing patterns: Spatial analysis of observed microbial colonization on root surfaces. Frontiers in Environmental Science 6, 1–12. doi:10.3389/fenvs.2018.00061

Uroz, S., Calvaruso, C., Turpault, M.-P., Frey-Klett, P., 2009. Mineral weathering by bacteria: ecology, actors and mechanisms. Trends in Microbiology 17, 378–387. doi:10.1016/j.tim.2009.05.004

Védère, C., Vieublé Gonod, L., Nunan, N., Chenu, C., 2022. Opportunities and limits in imaging microorganisms and their activities in soil microhabitats. Soil Biology and Biochemistry 174, 108807. doi:10.1016/j.soilbio.2022.108807

Wiesenbauer, J., König, A., Gorka, S., Marchand, L., Nunan, N., Kitzler, B., Inselsbacher, E., Kaiser, C., 2024a. A pulse of simulated root exudation alters the composition and temporal dynamics of microbial metabolites in its immediate vicinity. Soil Biology and Biochemistry 189, 109259. doi:10.1016/j.soilbio.2023.109259

Wiesenbauer, J., Gorka, S., Jenab, K., Schuster, R., Kumar, N., Rottensteiner, C., König, A., Kraemer, S., Inselsbacher, E., Kaiser, C., 2024b. Preferential use of organic acids over sugars by soil microbes in simulated root exudation. Soil Biology and Biochemistry, **submitted**.

Witzgall, K., Vidal, A., Schubert, D.I., Höschen, C., Schweizer, S.A., Buegger, F., Pouteau, V., Chenu, C., Mueller, C.W., 2021. Particulate organic matter as a functional soil component for persistent soil organic carbon. Nature Communications 12, 4115. doi:10.1038/s41467-021-24192-8

Zhalnina, K., Louie, K.B., Hao, Z., Mansoori, N., da Rocha, U.N., Shi, S., Cho, H., Karaoz, U., Loqué, D., Bowen, B.P., Firestone, M.K., Northen, T.R., Brodie, E.L., 2018. Dynamic root exudate chemistry and microbial substrate preferences drive patterns in rhizosphere microbial community assembly. Nature Microbiology 3, 470–480. doi:10.1038/s41564-018-0129-3

Chapter 5

Summary and general learnings

Summary

Soil ecosystems are dynamic interfaces that foster complex interactions between plant roots and microbial communities, crucial for biogeochemical cycles such as carbon sequestration and nutrient cycling. Roots exude a range of organic compounds that serve as energy sources for soil microbes (Kuzyakov and Blagodatskaya, 2015; Canarini et al., 2019; Vetterlein et al., 2020), influencing microbial activity and soil chemistry (Brzostek et al., 2013; Drake et al., 2013). However, our understanding of the mechanisms by which microorganisms metabolize these exudates and the subsequent effects on soil organic matter (SOM) dynamics, particularly at root exudation sites, is still limited.

The primary aim of this doctoral thesis was to explore the fine-scale spatiotemporal dynamics of microbial activity at these hotspots and to assess how variations in root exudate composition influence microbial processes across different soil types. Central to our approach was the use of 'reverse' microdialysis to simulate passive root exudation, allowing for precise control over the introduction of organic compounds, i.e. ^{13}C-labelled sugars and organic acids, into the soil and enabling detailed study of the microbial response.

Chapter 2 explored the immediate and lasting impacts of simulated root exudation on microbial activity in a beech forest soil. Utilizing reverse microdialysis, we introduced a mixture of ^{13}C-labelled sugars and organic acids directly into the soil, which allowed us to mimic natural exudation patterns while minimizing physical disturbances. Simultaneously, microdialysis allowed us to collect compounds from the soil solution to analyse the concentration of microbial metabolites and other organic compounds over the course of the 12-day experiment, thereby providing direct evidence of microbial processes at the exudation site. Additionally, microbial responses to introduced substrates were monitored using a combination of respiration measurement and stable isotope tracing to determine substrate-derived and SOM-derived respiration. At the end of the experiment, we extracted phospholipid and neutral-lipid fatty acid (PLFA, NLFA) to track substrate assimilation into microbial groups and to monitor changes in microbial biomass and community composition.

We observed a rapid respiration of added substrate within the first few hours. We hypothesized that the intense substrate respiration led to an oxygen depletion at the microbially active site, prompting a shift to anaerobic metabolic pathways within 24 hours, marked by a production of organic acids (acetate, propionate) and N-compounds (ammonium). By the third day, we observed a noticeable increase in SOM decomposition, indicating a potential priming effect. Additionally, analysis of PLFA and NLFA revealed that all major microbial groups within 5 mm radius of exudation site, i.e. the microdialysis membrane, were ^{13}C-erniched, indicating they had incorporated the substrate.

This study demonstrated that the release of labile C compounds significantly altered microbial respiration and nutrient availability, showcasing a three-stage microbial response characterized by rapid substrate respiration, metabolic shifts, and increased SOM degradation. These sequential responses highlighted the dynamic shifts in microbial metabolism and nutrient availability at the exudation site and advance our understanding of the mechanisms that contribute to rhizosphere priming.

Chapter 3 investigated the microbial responses to root exudation, focussing on how different exudate compositions, i.e. purely sugars, purely organic acids, or their combination, affect microbial activity and soil chemistry across two soil types (forest, meadow). At the start of the experiment, we released the ^{13}C-labelled sugars and/or organic acids into the soil by means of reverse microdialysis for 6-hours. This controlled approach allowed us to elucidate the specific impact of each compound class (sugar vs. organic acid) on the microbial processes at the exudation sites over the 18-day long experiment.

We assessed the microbial activity by measuring respiration, coupled with stable isotope probing (SIP), to differentiate between substrate-derived and SOM-derived respiration. We monitored changes in soil chemistry and microbial metabolites production by analysing changes in concentrations of compounds collected from soil solution by microdialysis. The analysis revealed that organic acids were preferentially metabolized over sugars, with significantly higher respiration rates observed when organic acids were part of the exudate solution. Additionally, the presence of organic acids led to a notable increase in the concentrations of short-chain fatty acids (butyrate, lactate, propionate), particularly during the second half of the simulated exudation pulse. Additionally, organic acids also promoted a rise in cations (potassium, magnesium, calcium), indicative of their role in mobilizing mineral-associated nutrients. Contrastingly, the release of sugars did not produce similar changes, suggesting a limited role in the immediate microbial metabolism observed. PLFA and NLFA analyses at the end of the experiment revealed differential assimilation of the substrate-derived ^{13}C into microbial groups, with distinct responses based on soil type and substrate.

Our findings clearly demonstrated that organic acids, more so than sugars, drive microbial activity and alter soil chemistry at root exudation sites. This results underscores the critical influence of exudate composition in shaping rhizosphere dynamics and nutrient availability.

Chapter 4 established an integrative imaging approach that combines advanced imaging techniques with the simulation of root exudation of ^{13}C-labelled substrates introduced via reverse microdialysis. We utilized several imaging techniques to map the microscale spatial distribution and uptake of substrates by microbial communities within resin-embedded soil cores. We employed confocal laser scanning microscopy (CLSM) to visualize the spatial distribution of fluorescently labelled microbial

cells, and nanoscale secondary ion mass spectrometry (NanoSIMS) to gain detailed isotopic and elemental data, mapping the distribution of ^{13}C along with other essential elements (C, N, Si, Al). Scanning electron microscopy (SEM) further complemented these analyses by offering insights into the soil microstructure surrounding the exudation site.

By integrating CLSM, SEM, and NanoSIMS, we successfully localized regions of interest (ROI) representing microbial cells and tracked the incorporation of substrate-derived ^{13}C by these cells at the conclusion of the 18-day long experiment. By correlating structural data with chemical signatures, this approach enabled the precise identification of microbial cells that assimilated introduced substrate, revealing significant variability in ^{13}C incorporation across different cells. This variability indicated that substrate assimilation was not uniform among all microbes near the exudation site. Instead, this pointed to the selective nature of microbial substrate utilization, a nuanced pattern likely influenced by both microbial traits and the heterogeneous soil environment.

This study demonstrated the value of integrating multiple high-resolution imaging techniques to elucidate microbial function (e.g., root exudate utilization) and its spatial heterogeneity in the rhizosphere.

General learnings

Collectively, these three studies contribute to the better understanding of the nuanced ways in which microbes interact with plant-derived organic compounds and reveal the potential for root exudates to modulate microbial community dynamics and soil carbon cycling. In my doctoral thesis, I was able to identify three overarching learnings.

1. **Microbial preference for organic acids**

   Our findings consistently revealed a microbial preference for organic acids over sugars in the context of simulated root exudation. We observed not only a greater release of organic acids into the soil but also higher rates of substrate-derive respiration associated with the release of organic acids. These higher respiration rates suggested that microbes were removing organic acids from around the microdialysis membrane more quickly, not because of molecular size or charge affecting diffusion, but due to active microbial uptake (König et al., 2022). Consequently, we measured higher release rates of organic acids due to the establishment of concentration gradients along which their passive transport, i.e. diffusion, occurred (König et al., 2022). In contrast, sugars accumulated around the membrane due to low microbial assimilation, thus restricting their release through passive diffusion. These findings challenge the prevailing belief that sugars are the most

favourable and rapidly consumed substrates for soil microbes (Jones and Murphy, 2007; Gunina and Kuzyakov, 2015).

Moreover, our findings offer novel insights into how microbial preferences might impact root exudation dynamics due to feedback mechanisms. The swift microbial uptake of organic acids could facilitate their easier release from roots by affecting the concentration gradients essential for passive root exudation, potentially altering the exudates released into the rhizosphere. This suggests that microbial activity could play a significant role in shaping the composition and quantity of root exudates, indicating its potential importance in regulating nutrient availability at the soil-root interface.

2. Microbes prioritize rapid growth over energy efficiency

Despite sugar metabolism yielding more ATP per molecule, microbes opted for metabolizing organic acid. Organic acids are processed through shorter metabolic pathways that allow for faster rates of ATP production, but at a lower yield (Kreft et al., 2020). By favouring the metabolism of organic acids over sugars, microbes can maximize biomass growth at the expense of ATP yield (Kreft and Bonhoeffer, 2005; Wortel et al., 2018). This strategic trade-off is particularly advantageous in competitive environments like root exudation hotspots, where substrate is in excess and rapid biomass accumulation is crucial (Kuzyakov and Blagodatskaya, 2015). This metabolic adaptation highlights how the microbial community prioritizes rapid growth over energy efficiency to capitalize on the transient nature of root exudation within the rhizosphere.

3. Spatial distribution and temporal dynamics are core drivers of rhizosphere processes

The integration of spatial and temporal data from our experiments provided crucial insights into the mechanisms that govern root-microbe interactions, highlighting the importance of considering spatial and temporal factors when evaluating microbial processes in the rhizosphere.

Spatially, our findings revealed that the proximity to exudation sites influenced microbial uptake of root exudates. Substrate incorporation into lipid fatty acids was predominantly observed within a < 5 mm radius of the exudation site. Our integrated imaging approach (NanoSIMS, CLSM, SEM) revealed a spatially heterogeneous incorporation of ^{13}C-labelled substrate by microbial cells, in which roughly two-thirds of cells near the exudation site assimilated the substrate. However, lipid fatty analysis (PLFA & NLFA) indicated varied ^{13}C enrichment across different microbial groups, suggesting that factors beyond mere proximity to exudation site influenced microbial assimilation of root exudates. Instead, it reflected the diverse microbial response to substrates by different microbial groups.

Temporally, my findings revealed a three-stage microbial response to the release of artificial root exudates. Initially, microbes took up and respired the introduced substrate, predominantly organic acids, potentially leading to a formation of anoxic hotspots due to increased oxygen consumption (Borer et al., 2018). Following this, we observed a production of microbial metabolites, particularly short-chain fatty acids, indicative of shorter incomplete catabolic pathways (e.g. fermentation) that released these intermediates (Kreft et al., 2020). Sugars, however, did not induce metabolite production. Moreover, the addition of organic acids lead to a mobilization of cations due to abiotic interactions with soil minerals (Adeleke et al., 2017). And lastly, after 3 days we observed an increased SOM respiration in one of our experiment. This phased response highlights the dynamic nature of microbial interactions with root exudates.

My doctoral thesis provides new insight into the immediate and delayed microbial responses to root exudation, advancing our understanding of the processes that contribute to rhizosphere priming. Using stable isotope probing, reverse microdialysis, and imaging techniques, I have shed light on the spatial and temporal aspects of microbial activity in response to root exudation. My results highlight the nuanced ways in which microbes interact with root-derived organic compounds and reveal the potential for root exudates to modulate microbial community dynamics and soil carbon and nutrient cycling. My research provides a valuable framework for future studies aimed at investigating the complex interactions that define the rhizosphere.

References

Adeleke, R., Nwangburuka, C., Oboirien, B., 2017. Origins, roles and fate of organic acids in soils: A review. South African Journal of Botany 108, 393–406. doi:10.1016/j.sajb.2016.09.002

Borer, B., Tecon, R., Or, D., 2018. Spatial organization of bacterial populations in response to oxygen and carbon counter-gradients in pore networks. Nature Communications 9, 769. doi:10.1038/s41467-018-03187-y

Brzostek, E.R., Greco, A., Drake, J.E., Finzi, A.C., 2013. Root carbon inputs to the rhizosphere stimulate extracellular enzyme activity and increase nitrogen availability in temperate forest soils. Biogeochemistry 115, 65–76. doi:10.1007/s10533-012-9818-9

Canarini, A., Kaiser, C., Merchant, A., Richter, A., Wanek, W., 2019. Root Exudation of Primary Metabolites: Mechanisms and Their Roles in Plant Responses to Environmental Stimuli. Frontiers in Plant Science 10. doi:10.3389/fpls.2019.00157

Drake, J.E., Darby, B.A., Giasson, M.A., Kramer, M.A., Phillips, R.P., Finzi, A.C., 2013. Stoichiometry constrains microbial response to root exudation-insights from a model and a field experiment in a temperate forest. Biogeosciences 10, 821–838. doi:10.5194/bg-10-821-2013

Gunina, A., Kuzyakov, Y., 2015. Sugars in soil and sweets for microorganisms: Review of origin, content, composition and fate. Soil Biology and Biochemistry 90, 87–100. doi:10.1016/j.soilbio.2015.07.021

Jones, D.L., Murphy, D.V., 2007. Microbial response time to sugar and amino acid additions to soil. Soil Biology and Biochemistry 39, 2178–2182. doi:10.1016/j.soilbio.2007.03.017

König, A., Wiesenbauer, J., Gorka, S., Marchand, L., Kitzler, B., Inselsbacher, E., Kaiser, C., 2022. Reverse microdialysis: A window into root exudation hotspots. Soil Biology and Biochemistry 174, 108829. doi:10.1016/j.soilbio.2022.108829

Kreft, J.-U., Bonhoeffer, S., 2005. The evolution of groups of cooperating bacteria and the growth rate versus yield trade-off. Microbiology 151, 637–641. doi:10.1099/mic.0.27415-0

Kreft, J.U., Griffin, B.M., González-Cabaleiro, R., 2020. Evolutionary causes and consequences of metabolic division of labour: why anaerobes do and aerobes don't. Current Opinion in Biotechnology 62, 80–87. doi:10.1016/j.copbio.2019.08.008

Kuzyakov, Y., Blagodatskaya, E., 2015. Microbial hotspots and hot moments in soil: Concept & review. Soil Biology and Biochemistry 83, 184–199. doi:10.1016/j.soilbio.2015.01.025

Vetterlein, D., Carminati, A., Kögel-Knabner, I., Bienert, G.P., Smalla, K., Oburger, E., Schnepf, A., Banitz, T., Tarkka, M.T., Schlüter, S., 2020. Rhizosphere Spatiotemporal Organization–A Key to Rhizosphere Functions. Frontiers in Agronomy 2, 1–22. doi:10.3389/fagro.2020.00008

Wortel, M.T., Noor, E., Ferris, M., Bruggeman, F.J., Liebermeister, W., 2018. Metabolic enzyme cost explains variable trade-offs between microbial growth rate and yield. PLOS Computational Biology 14, e1006010. doi:10.1371/journal.pcbi.1006010